Design of a free-fall penetrometer for geotechnical characterisation of saturated sediments and its geological application

Doctoral Thesis

Submitted for the doctoral degree in natural sciences at the
Faculty of Geosciences of Bremen University

Zur Erlangung des Doktorgrades der Naturwissenschaften im Fachbereich
Geowissenschaften der Universität Bremen

by
vorgelegt von

Sylvia Stegmann

Bremen, September 2007

Abstract

Cone Penetration Testing (CPT) is a versatile, time efficient method to characterise sediment strength and pore pressure in offshore settings and on land. The majority of the penetrometers rely on heavy trucks or rigs to provide the necessary force to push the CPT probe into the ground. This laborious process usually deforms or otherwise affects the uppermost deposits, whose physical properties are in turn vital to understand processes related to scour, burial of mines, cable or pipeline laying, silting of water ways and harbours, or sediment transport and remobilisation. Owing to the shortcomings of heavy seagoing CPT gear, this thesis aimed to develop and use a cable-led marine penetrometer lance which profiles the uppermost sediments in a less destructive manner.

The study summarises the development and deployment of a marine cone penetrometer system. It consists of an instrument for shallow-water application (200 m) and, based on the experience of the first, a second version operable down to 4000 m water depth. Design and construction of the instruments occurred at the Research Centre Ocean Margins, Bremen University (RCOM) in close and productive collaboration between Achim Kopf, Matthias Lange and myself during the first year. After an initial phase of researching for sensors and components, I contributed to the design. After construction, a total of 338 CPT experiments (both with the shallow-water [SW] and deep-water [DW] device) were carried out to date. From the wealth of deployments, 300 of them were performed by me while 204 raw data sets were processed by me over the course of this thesis (mostly 2nd and 3rd year). The CPT deployments were initially dedicated largely to instrument testing, and later focused on geological application.

A total of ten manuscripts, on six of which I am lead author, were submitted for publication and are contained in this thesis. Five of them serve as a proof-of-concept of the two CPT lances, which are operable on winches as well as in free drop. Two of these texts, one each on the SW- and DW-instrument, are rather generic in nature and introduce the instrument design and its benefit to a broader scientific community. A third and fourth paper summarise the initial results from various deployments in different modes of operation, comprising both short-term CPT profiling and mid-term deployments to also study pore pressure response. The fifth paper provides a comprehensive systematic comparison of velocity-controlled CPT deployments and, after having built an adapter for our lance, hydraulically pushed constant-rate deployments. From 38 selected data sets, the strain-rate effects of the dynamic tests were assessed and, based on earlier empirical solutions from the CPT literature, corrected for. Overwhelmingly, the results with the RCOM lance agree well

with those from the pushed tests, and further help to accentuate them. Within the spectrum of velocities tested (35 – 135 cm/s), it is found that the faster the rate of initial penetration is chosen, the larger the discrepancy between the deviations caused by layering and variations in physical properties of the sediments. This observation may be vital when carrying out CPT experiments in geomaterials where lithological variability is small, because it helps identifying features otherwise undetectable by pushed profiling at the standard rate of 2 cm/s.

Another five manuscripts summarise the geological application of the CPT devices. The tests were performed in geological environments as diverse as the Baltic Sea, Lake Lucerne, an active mud volcano in Azerbaijan, and the Cretan Sea in the Eastern Mediterranean. Regardless of the regional scenario, some overarching consistent results were obtained during the CPT deployments. As an outstanding finding, three types of characteristic pore pressure signals are recorded by CPT lance when deployed in "free-fall" mode on a cable. In granular, normally consolidated material, a pore pressure spike upon impact is usually followed by an exponential decay back to ambient values (if sufficient time is allowed for dissipation). Alternatively, a second pattern often met is a negative (i.e. sub-hydrostatic) pressure spike followed by an increase in pressure to ambient pore pressure values. The sub-hydrostatic signal is caused by displacement of pore fluid by the profiling CPT instrument, which results in flow away from the probe. This second pattern is restricted to coarse-grained deposits with high permeability. The third characteristic signal generally shows supra-hydrostatic pressures upon impact and during profiling, but then climbs to even higher pressures with time. Graphs like this are found in sediments of variable grain size distribution and are related to fluid overpressures. Interestingly, the third type is observed in clays as well as silt- or sand-bearing deposits, and appears no matter what the cause of the excess pore pressure is. In the various field studies, very similar pore pressure curves are seen although the reason for the overpressures were glacial loading (and potentially EQ tremor; Lake Lucerne), presence of microbial gas (Baltic Sea), hydrocarbon formation in folded and faulted shales of the Maykopian Formation (Azerbaijan, Greater Caucasus), or neo-tectonic movement and landsliding (Cretan Sea).

In summary, this study has shown that velocity-controlled "free-fall" CPT lances are an efficient, user-friendly means to characterise geotechnically shallow sub-bottom deposits. They obtain reproducible results that can be linked with standard pushed tests, but have the added advantage of producing more pronounced excursions in cone resistance and sleeve friction as well as characteristic pore pressure responses indicative of geological conditions.

Zusammenfassung

Cone **P**enetration **T**ests (CPT) stellen eine vielseitig einsetzbare, zeitgünstige Methode zur geotechnischen Charakterisierung der Sedimentfestigkeit und des Porendrucks an Land und im Wasser dar. Die Mehrzahl der Penetrometer basiert hierbei auf LKWs oder schweren Metallrahmen als notwendiges Widerlager, um die CPT-Sonde in den Untergrund zu drücken. Dieser arbeitsaufwendige Prozess führt generell zur Deformation und Beeinträchtigung der obersten Sedimentlagen, deren physikalische Zustandsgrößen umgekehrt wichtig sind, um Prozesse wie Auskolkung, Versandung von Minen, Verlegung von Kabeln oder Pipelines, Verschlickung von Wasserstrassen und Häfen sowie Sedimenttransport und –remobilisierung zu verstehen. Aufgrund der Nachteile der schweren CPT-Rahmen für marine Tests hatte diese Doktorarbeit zum Ziel, eine drahtgeführte marine Penetrometerlanze zu entwickeln, die die obersten Sedimente möglichst ungestört profiliert.

Die vorliegende Studie beinhaltet die Entwicklung und Anwendung eines marinen Penetrometer-Systems. Dieses besteht aus einem Instrument für den flachmarinen Bereich (Wassertiefen bis 200 m) und, aufbauend auf den Erfahrungen mit dieser Lanze, eine zweite Lanze, die bis in 4000 m Wassertiefe einsetzbar ist. Das Design und die Konstruktion beider Geräte fanden am DFG-Forschungszentrum Ozeanränder der Universität Bremen (RCOM) in enger Kooperation zwischen Achim Kopf, Matthias Lange und mir im ersten Projektjahr statt. Neben einer umfassenden Marktanalyse geeigneter Sensoren und Komponenten arbeitete ich in der Initialphase am Entwurf mit. Nach dessen Umsetzung wurden bis heute insgesamt 338 CPT-Experimente (sowohl Flach- als auch Tiefwasserlanze) durchgeführt. Von dieser Vielzahl an Geräteeinsätzen führte ich 300 persönlich durch und arbeitete bei 204 von ihnen an der Aufbereitung der Rohdaten im Verlauf der Dissertation (vornehmlich 2. und 3. Projektjahr).

Insgesamt zehn Manuskripte, auf derer sechs ich Erstautorin bin, kamen zur Einreichung und sind in der vorliegenden Dissertation enthalten. Fünf Manuskripte dienten primär als Nachweis des Funktionsverhaltens der beiden CPT-Instrumente, die an Seilwinden und Kränen oder im freien Fall eingesetzt werden können. Zwei der Publikationen, je eine zur Flach- und Tiefwasserlanze, sind generischer Natur und stellen die Geräte und ihre Vorzüge einer breiteren wissenschaftlichen Öffentlichkeit vor. Der dritte und vierte Artikel fassen die ersten vorläufigen Ergebnisse von Tests in unterschiedlichen Operationsmodi zusammen, die sowohl kurze CPT-Einsätze zur Sedimentprofilierung als auch längere Messungen zum Porendruckverhalten beinhalten. Das fünfte Manuskript stellt einen umfassenden systematischen Vergleich der geschwindigkeitskontrollierten CPT-Einsätze mit den

hydraulisch gedrückten Tests mit konstantem Vorschub dar, für die eigens ein Adapter an die Lanze gebaut wurde. An einer Auswahl von 38 CPT-Tests konnten die Effekte der Verformungsrate bei dynamischer Eindringung der Freifall-Lanze ermittelt und, basierend auf früheren empirischen Lösungen aus der CPT-Literatur, herausgerechnet werden. Ergebnis dieser Analyse ist die gute Übereinstimmung der Resultate der RCOM-Lanze mit jenen der gedrückten Tests. Ferner hilft der dynamische CPT-Test, die physikalischen Parameter der quasi-statischen Tests zu akzentuieren. Innerhalb des betrachteten Geschwindigkeits-spektrums (35 – 135 cm/s) zeigt sich, dass eine schnellere Eindringung der Lanze auch zu stärkerer Ausprägung der Signale führt, dergestalt, dass die Diskrepanz beim Auftreffen auf Lagen unterschiedlicher Materialeigenschaften bei den beiden Operationsmodi entsprechend zunimmt. Diese Erkenntnis ist insbesondere in Sedimenten nutzbar, die sich in ihrem physikalischen Verhalten nur geringfügig unterscheiden, und wo durch den dynamischen CPT-Test eine Variabilität herausgearbeitet werden kann, die sich der gedrückten Methode bei 2 cm/s entzieht.

Weitere fünf Fachartikel befassen sich mit den Ergebnissen der geologischen Anwendung der CPT-Lanzen. Die Experimente wurden in stark unterschiedlichen Szenarien wie der Ostsee, dem Vierwaldstädter See, in einem aktiven Schlammvulkan Aserbaidschans sowie in der Kreta-See im Östlichen Mittelmeer durchgeführt. Ungeachtet der regionalen Unterschiede lassen sich übergreifend einige Charakteristika in allen CPT-Einsätzen beobachten. Das herausragende Resultat der “Freifall”-Einsätze am Draht war, dass drei Kurvenverläufe mit jeweils typischen Porendrucksignalen auftreten. In granularen, normalkonsolidierten Sedimenten tritt beim Eindringen der CPT-Lanze ein Porendruckanstieg auf, der dann mit der Zeit exponentiell auf ein Hintergrundniveau abfällt (sofern man genügend Abklingzeit einräumt). Alternativ dazu zeigt die zweite Typkurve zunächst negative (i.e. sub-hydrostatische) Drücke an, die dann umgekehrt auf das Niveau des Umgebungsporendrucks ansteigen. Das subhydrostatische Signal wird durch die Verdrängung des Porenwassers beim Einschlag und Durchörtern der Sedimente durch die Lanze hervorgerufen, bei der Flüssigkeit von der CPT-Sonde wegfließt. Dieser zweite Kurvenverlauf ist in grobkörnigen Ablagerungen hoher Permeabilität anzutreffen. Das dritte charakteristische Porendrucksignal zeigt zuerst supra-hydrostatische Werte während des Profilierens, steigt aber anschließend zu noch höheren Drücken an. Graphen dieser Form finden sich in unterschiedlich körnigen Sedimenten und werden mit Porenüberdrücken erklärt. Interessanterweise trifft man diese Überdrücke in Tonen, aber auch in schluff- und sandhaltigen Lagen an; die Ursache des Überdruckes kann dabei recht unterschiedlich sein. In den verschiedenen Feldstudien im

Rahmen dieser Dissertation fanden sich sehr ähnliche Porendruckverläufe, obwohl die hohen Porendrücke durch frühere glaziale Beladung (und Seismizität; Vierwaldstädter See), das Vorkommen mikrobiellen Methans (Ostsee), Kohlenwasserstoffbildung in Tonschiefern der Maykop-Formation (Aserbaidschan, Hoher Kaukasus), oder neotektonische Bewegungen und Hangrutschungen (Kreta-See) herrühren.

Zusammenfassend zeigt die vorliegende Studie, dass geschwindigkeitskontrollierte Freifall-CPT-Tests eine effiziente, nutzerfreundliche Methode zur geotechnischen Charakterisierung oberflächennaher Sedimente darstellen. Die Experimente liefern reproduzierbare Resultate, die mit gedrückten Standard-CPT-Tests korrelieren, haben aber den Bonus, dass sie Ausschläge im Spitzenwiderstand oder der Mantelreibung akzentuieren und mittels charakteristischer Porendrucksignale geologische Zustandsformen identifizieren helfen.

Content

1. Introduction

1.1. Motivation

The *in situ* investigation of geotechnical parameters of marine sediments is of fundamental importance for engineering as well as scientific research relating to numerous aspects of offshore construction and sediment stability processes. Most of these applications are based on the profound knowledge of the sediment physical properties. Stability of sediments is given by the strength acting between the solid particles (cohesion), which is controlled by the mineralogy, the state of consolidation and the pore pressure within the voids of the solid particle's skeleton. Cone Penetration Testing (CPT) provides one of the most efficient means to comprehensively characterise the mechanical properties of sediments *in situ*, as one profile collects parameters such as cone resistance q_c (as a measure for [bearing] strength), sleeve friction f_s (as a measure for cohesion) and pore pressure u in various positions along the cone. The *in situ* parameters complement laboratory-based sedimentological data and constitute an essential contribution to the understanding of the mechanical behaviour of sediments, controlling numerous geological processes (e.g. slope failure, liquefaction). Inspired by this crucial geotechnical contribution in sedimentological scientific work, the aim of this thesis was to design and construct a seagoing cone penetrometer for geotechnical *in situ* investigation of superficial marine sediments in terms of geological processes based on the stability of sediments. Given that many of the existing cone penetrometer systems rely on heavy rigs that destroy the uppermost, soft layers, the key objective was the development of a slim, less-destructive instrument. Since there are also rather different ramifications for shallow and deep water, both a lightweight shallow-water probe and a sturdier deep-water probe were deployed. Both instruments aimed for user-friendly deployment from research vessels and small boats over a range of winch speeds, or even free drop. Both devices are equipped with an industrial used standard piezocone, manufactured by the Dutch company GEOMIL, which measures cone resistance q_c, sleeve friction f_s and pore pressure u. Regarding the influence of the geometry of the cone, the standard used geometry facilitates (a) a potential comparison with further standard devices and (b) to use the correlations and interpretations based on the Cone Penetration Testing standard ISSMFE (International Reference Test Procedure for Cone Penetration; see Lunne et al. 1997, their Appendix A).

1.2. Outline

This thesis incorporates 10 manuscripts, which are organised in various chapters. The order of the manuscripts is not chronological, but reflects the progression, which was obtained when running through the complete process of design, construction and testing in various geological environments.

The first chapter containing the scientific rationale (*Chapter 1.1*) and outline of the thesis (*Chapter 1.2*) is followed by a review in *Chapter 2.* It includes a summary of cone penetration testing (i) giving a brief historical background of this method (*Chapter 2.1*), (ii) describing the measured parameters and theoretical concepts, which depict the interrelationship between the response of penetrated material and the measured and derived parameters (*Chapter 2.2*), and (iii) illustrating the relevance of CPT testing for geological application (*Chapter 2.3*).

Chapter 3 focuses on the design and technical specification of the developed free-fall CPT instruments, whereas *Chapters 3.1* and *3.2* relate to the shallow-water and the deep-water version and *Chapter 3.3* illuminates improvements to date (compared to the initial state). In the two manuscripts (*Chapter 3.1* and *3.2*) the introduction of the instrument design outweighs the geology of the test sites.

Chapter 4 concentrates on the proof of the concept of the new marine FF-CPT (*Chapters 4.1* and *4.2*). In *Chapter 4.3,* standard pushed and velocity-controlled free-drop tests are compared in a field study. The influence of the penetration rate is an essential aspect in CPT testing and is controversially debated in the CPT community. Consequently, this chapter critically illuminates the concept of free-fall testing compared to standard constant-rate tests.

Chapter 5 summarises geological applications of the SW-FF-CPT and the DW-FF-CPT. Geotechnical FF-CPT investigations were performed in landslide studies in Lake Lucerne (*Chapters 5.1* and *5.2*) and in the Cretan Sea (Eastern Mediterranean Sea) (*Chapter 5.3*). Results of pore pressure measurements regarding gassy fine-grained sediments in the Baltic Sea and muddy sediments in the crater of the mud volcano Dashgil (Azerbaijan) are presented in *Chapters 5.4* and *5.5*, respectively.

Chapter 6 serves as a summary recapitulating and accentuating the main aspects of the thesis. Discussion of each aspect is included in each manuscript.

Chapter 7 comprises an appendix-like summary of the work load of this thesis. *Chapter 7.1* provides an overview of all FF-CPT tests during the course of this thesis (28 months after the first prototype was built), which also shows how many CPT deployment were performed and post-processed by the candidate. *Chapter 7.2* describes the role of the candidate in each manuscript published or submitted.

The thesis concludes with a *Literature* and an *Acknowledgments* section. The Literature section is related to Chapter 1 – 3.

The CPT nomenclature is kept consistent during the chapters. Published manuscripts are included as they are printed (i.e. in their published PDF format including the journal's/book's page numbering). Given the various journals and editorial conventions the spelling of this thesis switches between BE and AE, and the citation mode, albeit consistent for each manuscript, is not uniform over the thesis.

2. Cone Penetration Testing

Cone **P**enetration **T**est (CPT) instruments can be considered as one of the most useful tools for *in situ* site characterisation and soil exploration in geotechnical engineering as well as science. The principle of the CPT measurement is *per se* very simple as a cone penetrates the ground and measures the force acting on its tip (cone resistance) and on a sliding cylinder behind it (sleeve friction). Additional to the strength of the sediment, a piezocone penetrometer measures pore pressure u at defined locations. CPT systems can be divided into mechanical cone penetrometers, electrical cone penetrometers and piezocone penetrometers. An electrical cone penetrometer, which is supplemented with a pore pressure sensor, is named CPTU.

As a result of the popularity of this *in situ* testing device, there is a great demand of accurate correlations between measured cone parameters quantities (e.g. cone resistance, sleeve friction, pore pressure) and geotechnical (i.e. physical) properties (such as undrained shear strength or permeability) of the profiled material.

This chapter is focused on a

i) brief historical background of the cone penetration method (a detailed review is given in Lunne et al. [1997]),

ii) description of the measured and derived parameters, and

iii) introduction of the theoretical and laboratory analysis describing the interrelationship between measured CPT parameters and the soil response due to penetration and its geotechnical properties.

2.1. Historical Background

Cone penetrometers were first of all used for *in situ* determination of the stiffness of the penetrated material (soil or sediment; here: sediment). In the Roman era, the number of slaves, which were required to push a certain rod into the ground, was used as a measure for the strength of the ground (Song et al. 1999). This crude method to quantify the strength can be considered as a forerunner of cone penetrometer devices, standing out today for an effective ground probing instrument. The first cone penetrometer tests, as we know them today, were carried out with a mechanical cone penetrometer by the Dutch engineer Barentsen in the 1940ies (Lunne et al. 1997). The principle of this so-called Dutch cone based on a gas pipe with an inner diameter of 19 mm and a steel rod, which could move vertically (up and down) freely inside the pipe (Figure 1a). A 10 cm² cone with a 60° apex angle was attached to

the steel rod and both, the pipe and the rod, were manually pushed stepwise into the ground, therefore reaching a remarkable penetration depth of up to 12 metres. The penetration resistance was measured by a manometer. This instrument represents the first version that evaluates pile bearing capacity.

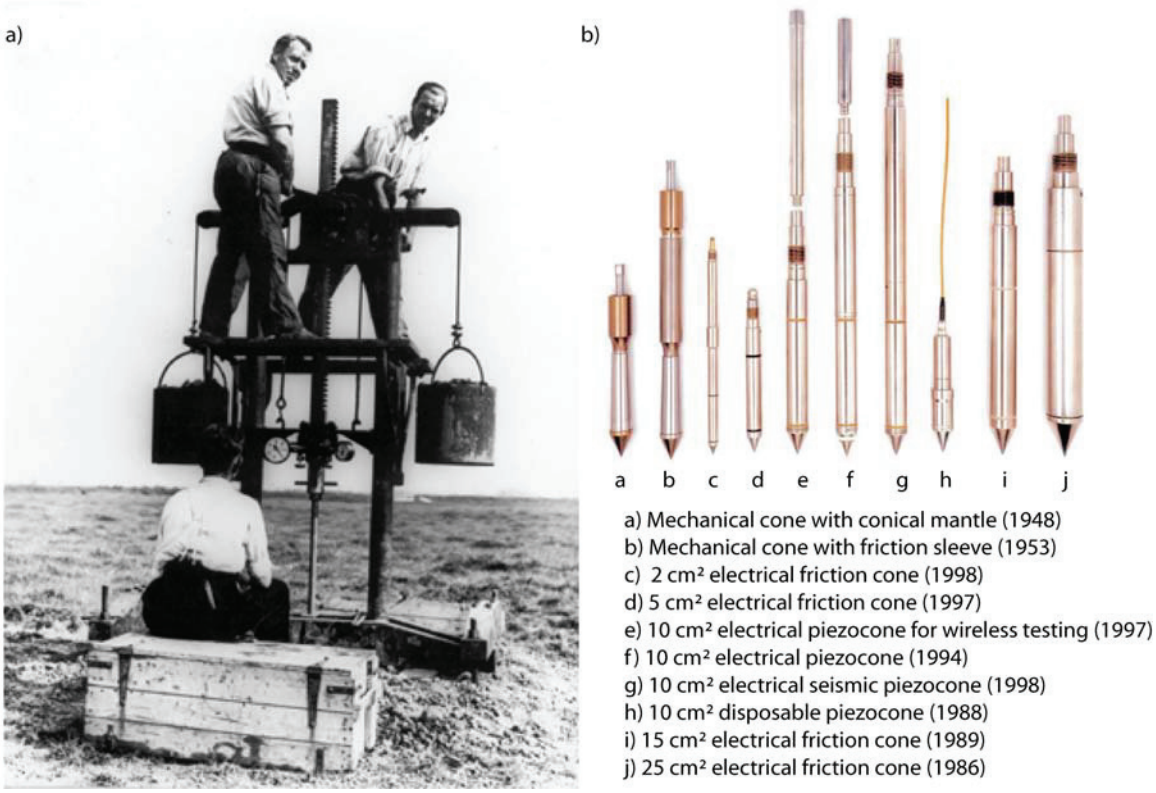

Figure 1 Historical development of CPT cones: **(a)** A Dutch cone penetrometer system, which was used in the 1940s (courtesy of Delft Geotechnics, taken from Lunne et al. 1997); **(b)** Various CPT probes over time (source: www.conepenetration.com/online-book/introd).

A decade later, the Dutch device was parlayed with an "adhesion jacket" behind the cone by Begemann, which additionally measured the local skin friction. Begemann was the first to postulate, that the friction ratio (ratio between the sleeve friction and the cone resistance) can be used for a classification of the profiled soil layers in terms of soil type (e.g. clay, silt, sand). Although further principles of mode of operation, mainly hydraulic penetrometers (e.g. Sanglerat, 1972), have been developed, mechanical cone penetrometers are still widely used (see Figure 1b, cones [a] and [b]). The first electrical cone penetrometer, where the signals were transmitted to the penetrating probe in the ground via a cable inside the hollow penetrometer rods, was developed in Berlin at the Deutsche Forschungsgesellschaft für Bodenmechanik (Degebo) during the 2nd World War (Lunne et al. 1997). Providing continuous testing with a constant (i.e. defined) penetration rate, elimination of uncertainty given by friction of the inner rod and the outer rods of the mechanical penetrometer and the higher accuracy of the much more sensitive load cells describe the main improvement of

electrical cones in contrast to mechanical ones. In 1965, the company Fugro developed an electrical cone, whose geometry formed the basis for the International Reference Test Procedure (ISSMEFE 1989; Lunne et al. 1997). Among other things, it was established, that "standard" CPT deployments were to be carried out at a constant rate of 2 cm/s. In addition to the determination of penetration resistance, pore pressure measurements were performed with piezocones, which were deployed adjacent to CPT profiles. In 1974, the first piezocone developed by the Norwegian Geotechnical Institute (Lunne et al. 1997) was presented. The first published combined measurements of cone resistance and pore pressure were carried out in sensitive Canadian clays by Roy et al. (1980). In the progressing development of cone penetrometers they were fitted with different sensors, measuring physical and geotechnical parameters such as density, salinity, and conductivity. A detailed overview is given in Burns and Mayne (1998a).

An appropriate improvement took place in the 1970ies, when on-shore devices have been modified for seagoing use (e.g. Dayal 1978; Schultheiss 1990). Depending on the penetration depth, two different principles of instruments were developed. To reach deep penetration (tens of meters), rigs are required, which have to be lowered to the seafloor and then push the cone by hydraulic force with constant velocity into the sediment (e.g. Ruiter and Fox 1975; Ferguson et al. 1977). To the contrary, lance-shaped free-fall cone penetrometers were lowered on a cable or freely dropped, running through the water column and penetrating the sediment with their own momentum gained through their acceleration and weight (e.g. Dayal et al. 1973). The non-constant penetration velocity and depth is determined by the cone's momentum and the stiffness and cohesion of the sediments. Penetrating only superficial sediment down to 10 meters maximum, the free-fall devices do not disturb the uppermost soft layers as heavily as the rigs. Hence, artefacts in CPT results from consolidation by the rig are avoided. A more comprehensive summary of off-shore cone penetrometers and their differences is given in Chapter 4.3.

The actual standard geometry of a cone available for on- as well as off-shore CPT application consists of a 60° cone with a 10 cm² base area and a 150 cm² friction sleeve located above the cone. In addition, 15 cm² cone penetrometers (diameter = 43.7 mm, sleeve area = 225 cm²) are used, especially in case of incorporation of additional sensors (e.g. pore pressure sensor) into the probe (Figure 2a). For offshore seabed tests, 15 cm^2 cones are preferred. The influence of the different geometry of the 10 cm² (standard) and the 15 cm² cone can be neglected, as in practice cone penetrometers range in cross section from 5 cm² to 15 cm² give very similar corrected cone resistance data (Lunne et al. 1997).

2.2. Cone Penetration Parameters

Generally, tip and sleeve readings and pore pressure measurements during insertion of a cone penetrometer into the sediment produce a profile of measured geotechnical properties (Figure 2b). The tip as well as the sleeve of a penetrometer is equipped with strain gauges to measure stresses exerted by the sediment during penetration. Cone resistance q_c is defined as the force acting on the cone tip divided by the area of the cone, and sleeve friction f_s results in the force acting on the friction sleeve divided by the area of the sleeve (Figure 2a, b). Pressure transducers detect the ambient pore pressure u during measurement on a port on the cone tip (u_1 position), on the cone shoulder (u_2 position) and/or behind the friction sleeve (u_3 position) (Figure 2b). The position of the pressure port has a significant influence on the values and is outlined below.

The measured cone parameters underlie a certain variability, which is generally caused by the heterogeneity and diversity of the sediment and a certain degree of error in testing procedures. Inherent sediment variability is given by natural, often superimposed geological processes, whereas measurement error is based on inaccuracies of the measurement system and variations in equipment geometries. During penetration, the cone causes a material to deform elastically, plastically or fail within a spatial volume in the vicinity of the penetrometer during insertion of the instrument. This means the measurements are not absolute point measurements, but represent the extent and the characteristics of the failure zone, which again depend on physical properties of the material (e.g. stiffness, plasticity, consolidation, density, water content). In general, firm materials are compressed upon penetration of the instrument, while pore fluids either cause high excess values (low permeability sediments) or get displaced (high permeability in loose sands), the latter resulting occasionally in sub-hydrostatic values. In soft, fine-grained sediments, clay fraction particles migrate radially from the axis of the penetration path and may get suspended by the fluids (pore water) when stress is induced by insertion of the cone (Kim and Tumay 2004). The effects described here are more pronounced in dynamic (free-fall) CPT deployments than in constant rate tests (2 cm/s).

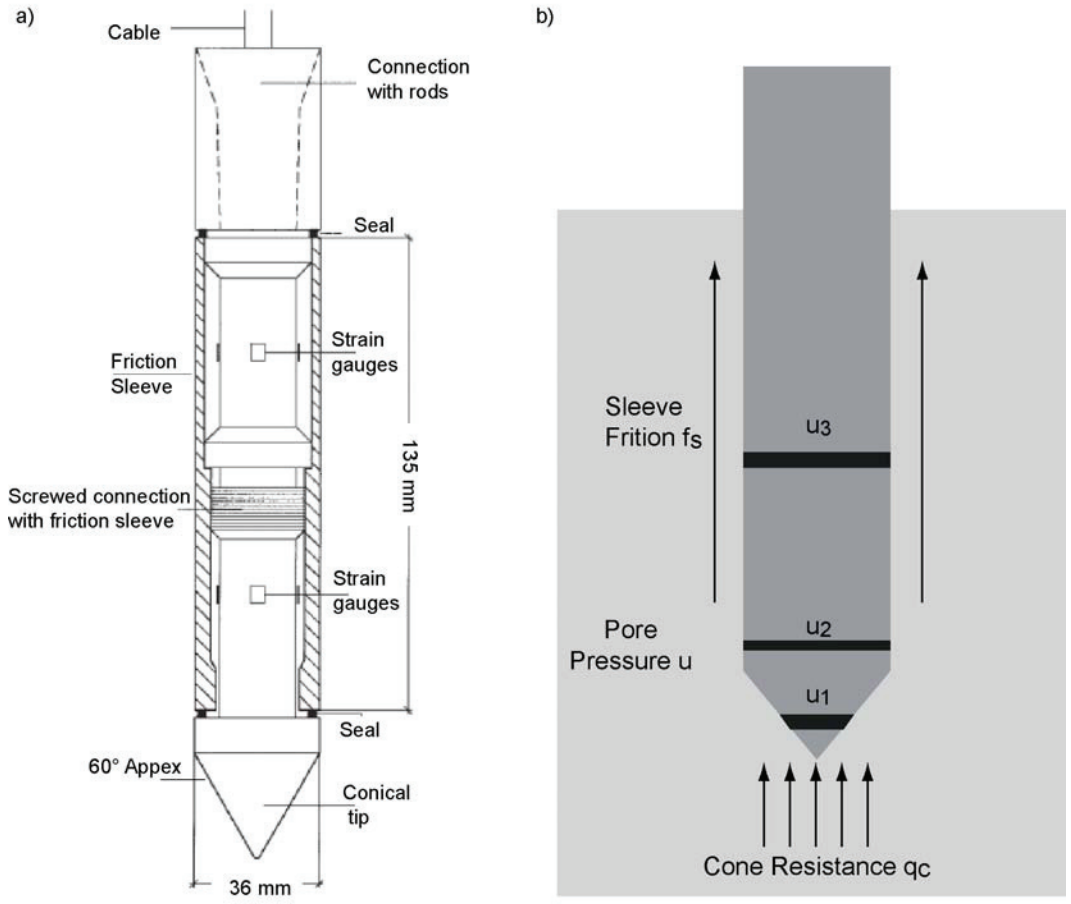

Figure 2 (a) Schematic sketch of an electrical 15 cm² subtraction cone (10 cm² cone diameter = 36.4 mm) and **(b)** its measured parameters (not to scale). In a subtraction cone the two strain gauges are connected. Under compression the sleeve friciton load cell records the sum of both strain gauges. The sleeve friction is obtained from the difference between the friction and cone resistance strain gauge. The main advantage of the subtraction cone is the overall robustness (Lunne et al. 1997).

Cone resistance

One of the major challenges in cone penetration testing is the establishment of a systematic relationship between q_c (and f_s for that matter) and sediment physical properties such as bearing capacity or undrained shear strength. In general, penetrometrists either (a) correlate cone resistance q_c with a given set of sedimentary physical properties, which can be used to calculate cone resistance for geotechnical and geological application (e.g. liquefaction, slope stability), and/or (b) carry out back-calculation of sediment physical properties from measured cone resistance (e.g. undrained shear strength). To reduce the variations of the input strength, which can produce large deviations in the calculation of cone resistance, theoretical solutions are used. A large number of theoretical analyses have been carried out, but none of them is rigorous (Yu and Mitchell 1998). All those models are generally confronted with large deformations and a non-linear behaviour of the sediment (e.g. Kiousis et al. 1988, Yu et al. 2000). The failure zone due to penetration of a cone can

commonly divided into a plastically deforming region and, at some distance, an elastically deforming region, whereas along the lance-sediment interface intense shearing remoulds the material (e.g. Teh and Houlsby 1991; Silva et al. 2006). The extent of this failure zone depends mainly on shear strength and the shear modulus of the sediment (Teh and Houlsby 1991). A variety of theoretical solutions for cone penetration have been proposed in the past approaching the penetration problem with different theories. These include: i) the bearing capacity theory (Terzaghi 1946), ii) the cavity expansion theory (Bishop 1945), and iii) the strain path method (Baligh 1985).

For the bearing capacity theory (i), the cone resistance is assumed to be equal to the collapse load of a deep foundation in the soil (Yu and Mitchell 1998). The extension of this theory to penetrometer analysis assumes a failure mechanism. Chari and Abdel-Gawad (1981) summarise theoretical failure analysis by Meyerhof (1961), Terzaghi (1946) and Durgunoglu and Mitchell (1973) (Figure 3).

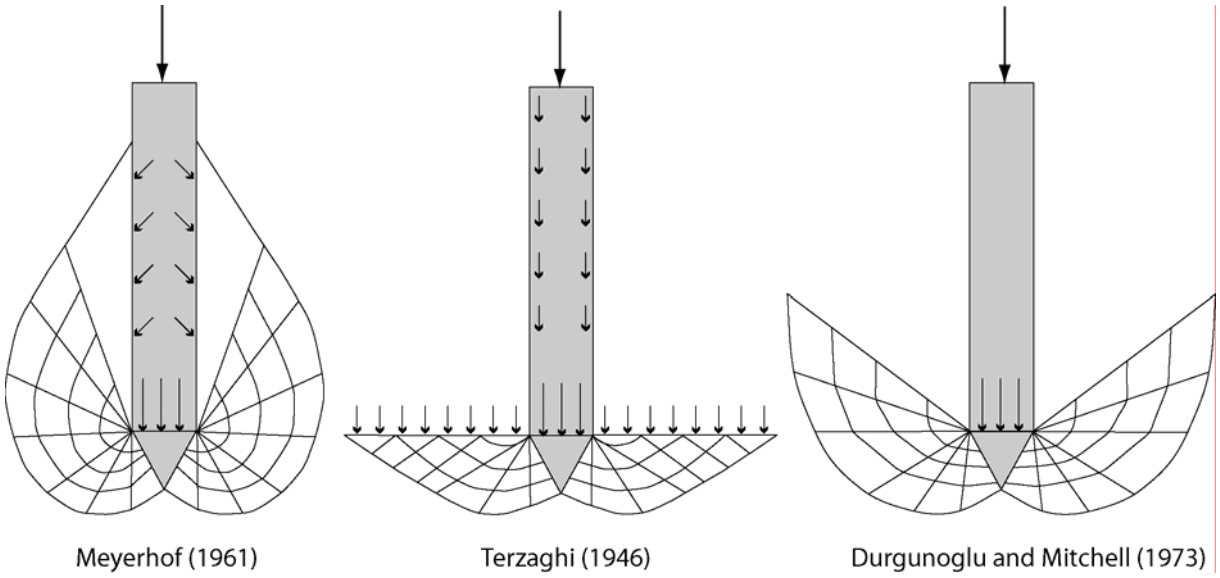

Figure 3 Different kinds of failure mechanisms referring to the bearing capacity theory (modified by Chari and Abdel-Gawad [1981]).

The limitations of this theory are in the neglect of the material stiffness and the compressibility as well as the ignorance of the influence of the penetration process on the initial stress regime around the cone shaft (Yu and Mitchell 1998). Consequently, this theory is usually adapted to shallow penetration, which involves a mechanism where the displaced material can escape as an entity to the surface. In deep penetration, however, the displacement is controlled by elastic deformation of the material (Teh and Houlsby 1991). Satisfying the latter, the cavity expansion method (ii) is used regarding the force required to produce a

(deep) hole in an elastic-plastic medium, which is equal to expanding a cavity of the same volume under the same conditions (e.g. Salgado et al. 1997; Yu and Mitchell 1998). Thus, elastic and plastic sediment deformation during cone penetration is taken into account as well as the influence of the penetration process on the initial stress regime and the effect of stress around the tip, in turn influencing q_c (Yu and Mitchell 1998). Prior to this, Yu and Mitchell (1998) demonstrated that preponderant cavity expansion solutions give the closest agreement between predicted and measured resistance values. The strain path method (iii) is an improvement of the cavity expansion theory, as the latter does not model the strain paths correctly (Baligh 1986a). Baligh (1986a) suggested the application of the strain path method to account for the complex deformation history of the sediment during cone penetration.

These theoretical approaches were used to interpret the strength of fine-grained, cohesive sediments based on CPT/CPTU data. The *in situ* undrained shear strength depends on sediment failure, anisotropy, stress history and strain rate. Regarding the non-linear stress-strain behaviour due to cone penetration, no single value for undrained shear strength exists. Nevertheless, theoretical analysis describes the relationship between cone resistance and s_u as follows:

$$q_c = N_c \times s_u + \sigma_o ,$$

with the theoretical cone factor N_c , and the total pressure σ_o (see Lunne et al 1997). Depending on the theory used, σ_o may be σ_{vo}, σ_{ho}, or σ_{mean} (Lunne et al. 1997). A lot of solutions for the cone factor are given in a summary by Lunne et al. (1997; see their Table 5.5). As theoretical solutions simplify the complex phenomenon of cone penetration, they have to be verified from actual field and laboratory-based data, which estimate s_u from CPT data using the following equation:

$$s_u = \frac{q_c - \sigma_{vo}}{N_k} ,$$

with the empirical cone factor N_k and the total stress σ_{vo}. Depending on the sediment, N_k ranges between 11 and 19 for normally consolidated marine clay (Kleven 1986), and averages 17 for non-fissured, overconsolidated clays (Kjekstad 1978). The relationship between s_u and q_c is modified with CPTU employing the cone resistance corrected for pore pressure effects:

$$s_u = \frac{q_t - \sigma_{vo}}{N_{kt}} .$$

The corrected cone resistance is represented by $q_t = q_c + (1-a) \times u_2$, with u_2 = the measured pore pressure and a = area ratio of the cone, which is defined as the ratio between the cross-sectional area of the strain gauge and the cross-sectional area of the cone. In CPT

nomenclature ($q_t - \sigma_{vo}$) is named as the net cone resistance q_{net}. Depending on the plasticity N_{kt} ranges between 10 or less and 20 for normally consolidated clays (see Table 3 in Karakouzian et al. 2003). Often used values are N_{kt} = 10, 12, 15 (e.g. Baltzer et. al. 1994; Sultan et al. 2007a).

Numerous geotechnical sediment parameters of (e.g. deformability [expressed by constrained modulus, elastic modulus, shear modulus], stress history) may be derived from cone resistance, but they are not further considered in this thesis.

Sleeve Friction

The frictional (i.e. cohesive) force exerted by the sediment onto the friction sleeve of a CPT cone during penetration defined as sleeve friction f_s. Similar to cone resistance, it is measured using electrical strain gauges mounted onto the stainless steel core of the CPT probe. The friction sleeve is similar to cone geometry subject to CPT standards and has a defined area depending on the diameter of the cone (for 10 cm^2 cone = 150 cm^2 and for 15 cm^2 cone = 225 cm^2). Different arrangements of the CPT strain gauges are used:
(i) cone resistance and sleeve friction are detected by individual, independent strain gauges during compression while the instrument penetrates,
(ii) sleeve strain gauge measures in tension while cone is recorded by a compressional strain gauge, and
(iii) cone strain gauge and the sleeve strain gauge are connected to the same stainless steel core to record q_c and f_s (Figure 2a above). The sleeve friction is finally obtained by the difference in load of the friction sleeve and the cone resistance strain gauge (Lunne et al. 1997).

Configuration (iii) is referred to as the "subtraction cone", which has been demonstrated to be more robust. Sleeve friction f_s is used for soil classification, one of the most important issues in CPT profiling. The friction ratio, F, calculated by dividing sleeve friction by the net cone resistance (q_{net}), is believed to provide a first-order description of the soil type as a repeatable index for the mechanical behaviour of its *in situ* properties adjacent to the CPT probe (Douglas and Olsen 1981). A tentative application of that first-order soil classification was undertaken with data obtained with the SW-FF-CPT in fine-grained harbour deposits and brackish sediments (see Chapter 4.2 below). Recent studies have shown that the measurement of sleeve friction f_s is less accurate and less reliable than that of cone resistance in spite of corrections for pore pressure effect (Lunne et al. 1997). Consequently, f_s is of subordinate importance in comparison to cone resistance q_c and pore pressure u, which both are viewed as

the key parameters in CPT studies (see Lunne et al. 1997). In this thesis, sleeve friction was measured in each profile, but its interpretation was omitted for the above reasons on most occasions.

Pore Pressure

Pore pressure is simply the pressure of the fluids in the voids between the solid grains of the sediment matrix. It should be noted that only saturated matrices will be here considered as they are most relevant for marine sediments. In any marine geological environment realm the surrounding pressure is measured and defined as the pore pressure consisting of a hydrostatic component u_o resulting from the thickness of the water column, and an excess pore pressure component Δu in the sediment due to loading (e.g. Fang et al. 1993; Strout and Tjelta 2005):

$$u = u_o + \Delta u \, .$$

Excess pore pressure u can be consequently estimated to be zero, if hydrostatic conditions occur in the sediment (Figure 4a). Non-hydrostatic pore pressure (= excess pore pressure) provides direct evidence for advection of pore fluids in the sediment, glacial, tectonic, sedimentary or anthropogenic loading, or dynamic processes such as earthquake tremor (Maltman 1994). The geo-mechanical role of excess pore pressure will be discussed in Chapter 2.3.

An insertion of any kind of probe into a sediment causes changes in the stress and pore pressure regimes surrounding the penetrometer. The total magnitude of measured pore pressure during penetration tests consists of the hydrostatic component u_0, the excess pore pressure due to changes of the normal stress $\Delta\sigma_n$ resulting from the displacement of material by the insertion of the probe, and on excess pore pressure due to changes in the shear stress, caused by the shear deformation of the soil adjacent to the cone body:

$$U = u_o + \Delta\sigma_n + \Delta\sigma_{shear} \, ,$$

(e.g. Burns and Mayne 1998b) (Figure 4b). Both $\Delta\sigma_n$ and $\Delta\sigma_{shear}$ comprise a stress component induced by the profiling CPT lance and another component of pre-existing (excess) pore pressure in the geosystem. The zone of the influence of the normal stress is considered as a function of the stiffness, as expressed by the rigidity index I_r (see below). In field measurements, pore pressure is defined as a total magnitude response of $\Delta\sigma_n$ and $\Delta\sigma_{shear}$ and can be only distinguished in an analytical way (Burns and Mayne 1998b).

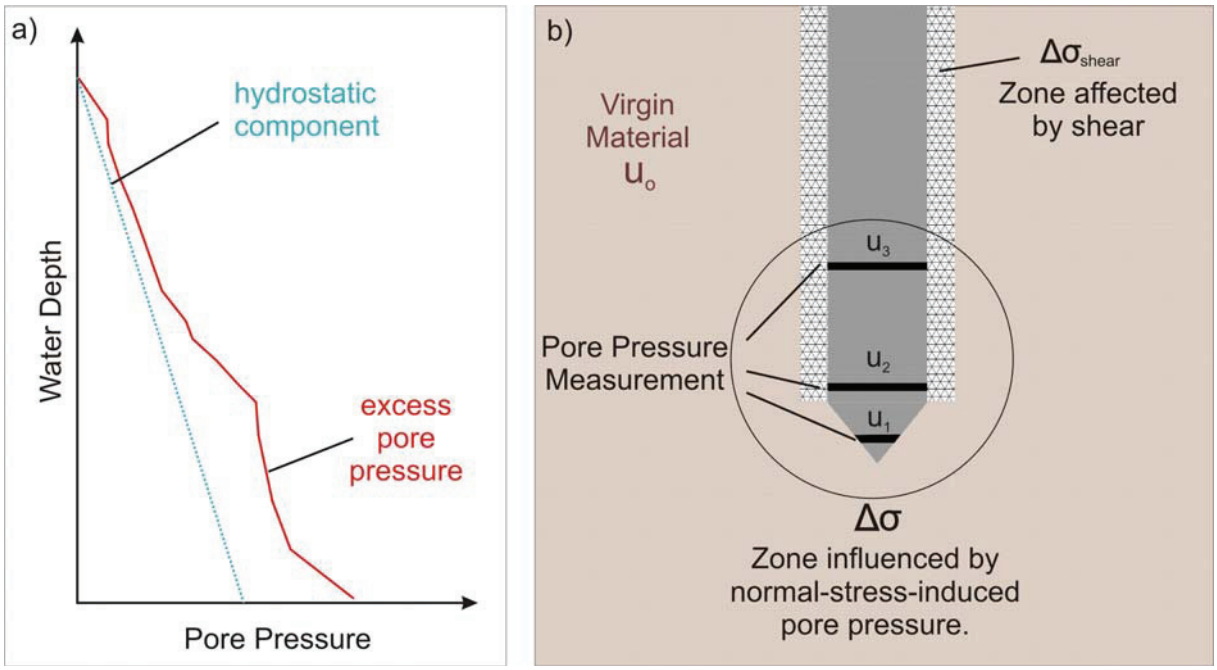

Figure 4 Measured pore pressure and its components: **(a)** hydrostatic and excess pore pressure in marine sediments; **(b)** soil-mechanical components of pore pressure during insertion of the probe (modified by Burns and Mayne 2002)

Considering a measured pore pressure signal, it can be divided into two different parts that contain different geotechnical as well as geological information. The first part of the signal is characterised by a pressure pulse associated with probe insertion and the sediment properties followed by an evolution of the insertion pore pressure over the time, which formed by the insertion response depends on *in situ* permeability (e.g. Bennett et al. 1985). When the instrument is halted over a long period of time, the induced pore pressure will approach its ambient conditions, which is the final component of pore pressure evolution. The duration, which is needed for the complete decay of the insertion pore pressure as a function of the permeability of the sediment varies between days and months (e.g. Becker et al. 1997). The dissipation decay may record two different signals (Fang et al. 1993). Burns and Mayne (1998b) assume that the dissipation of the shear-induced pressure occurs more rapidly than that of the cone-induced pore pressure, as the volume of sediment affected by the frontal impact (i.e. normal stress) is much larger than that affected by the sliding probe (i.e. shear stress). Dissipation tests performed in soft, fine-grained silts and clays show a monotonous decrease of pore pressure (similar to observations in the laboratory one-dimensional consolidation tests). In contrast, dissipation tests in heavily overconsolidated fine-grained sediments often reflect dilatory pore pressure response with an increase in pore water pressure followed by a decrease and a return to hydrostatic values (e.g. Burns and Mayne 1998b, 2002).

Similar to the cone resistance, many analytical approaches have been developed to describe the changes in pore pressure during and after an insertion of a probe (=dissipation) into sediment. This also includes the same theoretical solutions as mentioned in the context of cone resistance (see above). An overview of the historical development of piezocone dissipation modelling until the 1990ies is given in Burns and Mayne (1998b, their Table 1). The theoretical analysis of dissipation of pore pressure based on the consolidation theory was used to predict the coefficient of horizontal consolidation C_h, from time taken for 50% of the maximum insertion pore pressure U_{imax} to dissipate (t_{50}) (Bennett et al. 1985):

$$C_h = \frac{r^2 \times T_{50}}{t_{50}},$$

where r is the radius of the probe and T_{50} is a dimensionless time factor. Calculating C_h, the permeability k can be determined as follows:

$$k = \frac{C_h \times y_w}{D},$$

with D = constrained modulus and y_w = unit weight of water.

As the failure zone during penetration is a function of the stiffness expressed by the rigidity index $I_r = G/s_u$ (see above), Bennett et al. 1985 suggest an empirical relationship for soft marine sediments between U_{imax} and undrained shear strength as

$$s_u = \frac{U_{i\max}}{6}.$$

Based on the theoretical solution, when the soil is modelled as an elastic, perfectly plastic material, it follows:

$$U_{i\max} = s_u \times \ln\left(\frac{G}{s_u}\right),$$

with G being the elastic shear modulus (Randolph et al. 1979).

An essential aspect of pore pressure measurement with cone penetrometers is the position of the pressure port (Figure 2b). Due to changes in normal stress during penetration (Figure 4b), the largest effect on the magnitude of pore pressure is under beneath the cone, whereas the relative changes in shear stress are small (<20%; see Baligh 1986b). It has been long known that the pore pressure measured at the cone (u_1) is higher than measured behind the cone (u_2) or along the shaft (u_3; Figure 2b) (Lunne et al. 1997; Sully et al. 1999). Song and Voyiadjis (2005) described in detail the pore pressure behaviour taken at the different locations during penetration tests in a calibration chamber (33% kaolin - 67% fine-grained sand) with a constant penetration rate of 2 cm/s. The pore pressure responses for the u_1 and u_2

position show a similar trend with an initial increase followed by the decay to steady-state (constant equilibrium conditions such as stabilised pore water flow and stress-strain conditions) (Song and Voyiadjis 2005). In contrast, the u_3 pressure signal is characterised by an initial fluctuation with an increase followed by a decrease before it increases again to reach the steady-state. The absolute values of the steady state condition at the end of the penetration process are higher the closer the pore pressure is measured near the tip. The decrease of the signal is assumed to be linked with a dilative behaviour of the specimen caused by lightly overconsolidated conditions (OCR = 1.5). In addition to the pore pressure signal and its absolute magnitude, the position of the pore pressure port influences also the dissipation behaviour. In lightly over-consolidated (Song and Voyiadjis 2005) as well as normally consolidated (Sully et al. 1999) specimens, the induced pore pressure measured at u_1 dissipates more rapidly than that in u_2 position.

2.3. Geological Application of Cone Penetration Testing

Cone Penetration Testing provides measurements to determine the strength (q_c), cohesion (f_s) and the pore pressure (u) of profiled sediments. Considering the geotechnical aspect of them, both they seem to be controlling factors for (saturated) sediment behaviour and stability. Saturated sediments can be considered as a two-phase-system, where the voids between the solid particles are filled with fluid (Figure 5a). Depending on the cohesion forces acting between the grains, the skeleton of the solids is characterised by certain strength, which is largely a function of mineralogical composition. On the other hand, the forces of the pore water (i.e. pore pressure) are counteracting the binding forces between the particles, and hence lower the strength. This relationship is expressed in the principle of effective stress (σ') presented by Terzaghi (1946):

$$\sigma' = \sigma - u \,,$$

where σ = total stress and u = pore pressure. Relating to the stability of (saturated) sediments and modifying the Mohr-Coulomb relationship with respect to effective stress, it can be expressed as follows (Terzaghi 1946; Hubbert and Rubey 1959):

$$\tau = c' + \sigma'_n \times \tan\Phi \,.$$

The equation implies that overpressuring weakens the sediment as the fluid is sustaining an extra part of the stresses acting against the granular skeleton. As a consequence, both the overall, and the interparticle friction (σ'_n x tanΦ) are reduced. This means that it is the effective stress rather than the total stress, which controls deformation and stability of sediments. The occurrence of overpressuring is often combined with fine-grained, cohesive

sediments characterised by low permeability and linked with geological processes such as tectonic deformation, mineral dehydration, decomposition of gas hydrates, hydrocarbon formation and high sedimentation rate. In these scenarios, the expulsion of the pore fluid is not in equilibrium with the reduction of the pore space by consolidation (Figure 5b) (e.g. Schultheiss 1990; Maltman 1994). Generally, the reduction in effective stress (and strength) by overpressure is a crucial factor in all scenarios of sediment deformation and mass wasting (Hampton et al. 1996; Mienert 2004). This fact underlines the necessity of pore pressure measurement, which is only *in situ* possible. Going back to cone penetration testing, these devices establish synchronous and continuous *in situ* measurements of both (strength and pore pressure), which are vital to study different kind of potential failure mechanisms of sediments.

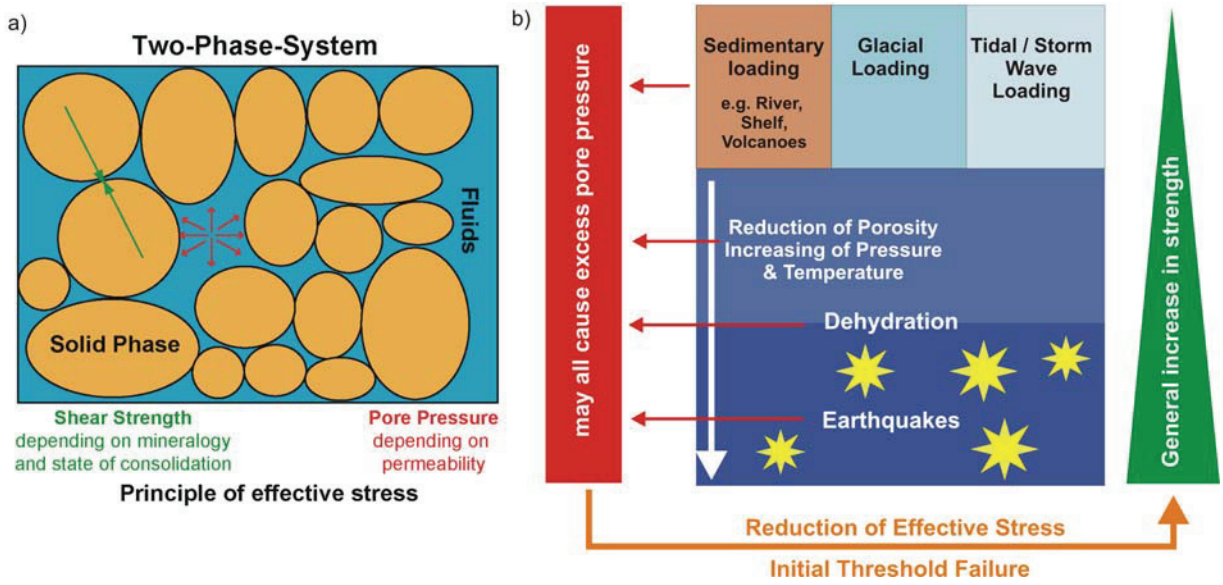

Figure 5 Principle of effective stress: **(a)** micro-scale view on forces acting in water-saturated sediments, and **(b)** geological processes influencing effective stress.

Cone penetration is also a very suitable method for landslide studies as it is possible to identify failed and non-failed sediment bodies by their *in situ* physical properties (e.g. Mahmoud et al. 2000). Remoulded sediment for example is characterised by a lower cone resistance and sleeve friction (e.g. Sultan et al. 2007b). In intact sediments adjacent to failed sediments, the shear surface can be detected by a decrease of the measured strength, because failure almost always occurs in the weakest material. Determining different pore pressure regimes is also critical to figure out the role of pore pressure in failure and may further serve to reconstruct historical events (e.g. Stegmann et al. 2007). A further application may be the study of the dynamics of superficial sediments in terms of liquefaction. Such a kind of fluidisation is associated with a build up in the pore pressure due to loading rather than pore

water advection. If the pore pressure exceeds the confining (i.e. effective) stress, the particle skeleton is supported by the fluid and the sediment. Another aspect is long-term pore pressure measurement. As the pore pressure regime is influenced by various processes (such as tidal effects [e.g. Jeng and Cha 2003], dehydration [Moore and Vrolijk 1990], consolidation), which are characterised by different geo-dynamic processes, pore pressure observations on different time-scales are a crucial contribute to geo-mechanical studies. Therefore the piezocone has to be arrested for a defined duration in the sediment to collected ambient data.

3. Design and Construction of a FF-CPT Instrument

The most evident advantage of free-fall devices for geotechnical exploration of submarine sediments is their time- and cost-efficiency. As a result, a free-fall cone penetrometer system (FF-CPT system) was developed. The FF-CPT system consists of two instruments, operable in shallow water depth (up to 200 m) and deep water depth (up to 4000 m). Technical specifications and description of the shallow-water (SW-)FF-CPT is given in Chapter 3.1. The deep-water (DW-)FF-CPT and initial data of its first application in the Cretan Sea are described in Chapter 3.2. Finally, Chapter 3.3 and Chapter 3.4 contains the description of the testing procedures and refinements, which have been undertaken based on experience gathered during ca. 28 months testing.

3.1. Shallow-water CPT Concept and Design of a modular, marine Free-fall CPT instrument – A time- and cost-efficient device for *in situ* geotechnical characterization of marine sediments

Stegmann, S., Villinger, H., and Kopf, A., Sea Technology, 47, 2, 27-33, published in 2006.

Concept and Design of a modular, marine Free-fall CPT instrument

A time- and cost-efficient device for in situ *geotechnical characterization of marine sediments*

By Sylvia Stegmann
Research Scientist
Dr. Heinrich Villinger
Professor
Dr. Achim Kopf
Professor

DFG-Research Centre Ocean Margins
University of Bremen, Bremen, Germany

Increasing human impact on near-coast areas and towards the continental shelves and slopes require a profound knowledge of the uppermost seafloor sediments. Not only natural disasters such as storm surges, landslides and tsunamis, but also anthropogenic effects such as static or dynamic loading of the seafloor by offshore construction represent an economical and environmental threat to society. As a consequence, the physical properties of seawater-saturated soils appear to be the key parameters in the assessment of sediment stability.
Marine sediments can be considered as a two-phase-system, mineral particles and fluids (water, gas), the latter occupying the voids between the first. Pore volume generally decreases with increasing stress onto the sediment. The lower pore volume of the sediment, the stronger the cohesion between particles, which translates to higher shear strength. The mechanical behaviour of any sediment is controlled by the equilibrium between the force on the solids (normal stress) and the counteracting pore pressure, which is given by the incompressible, less dense fluids. It has long been known that the mechanical stability of soil is a function of mineralogical strength and excess pore pressures, the latter of which may overbear the normal stress and cohesion, hence causing failure, liquefaction, or hydro-fracture. Especially clay mineral-rich soils with their low intrinsic frictional strength and low permeability represent zones of fluid overpressures and potential weakness.

Cone Penetration Testing

Cone **P**enetration **T**ests (CPT) are a neat way to collect a variety of the abovementioned sediment physical parameters *in situ* with a single device. These include sediment strength (derived from the resistance of the cone and the sleeve of the probe during penetration), pore pressure (in up to three positions, u_1 - u_3), temperature, tilt, and deceleration. The heart of the system is a sensor-equipped, conical probe which penetrates the sediment. The two commonly accepted standard sizes are 10 cm^2 and 15 cm^2 probes.

From the primary CPT data set, secondary parameters can be derived. The main aim of standard CPTesting is to profile the penetrated sedimentary succession at a rate of 2 cm s^{-1}. Given the wealth of existing data, Robertson (1) established a first-order soil classification based on the friction ratio (= sleeve friction/cone resistance) corrected for pore pressure effects. The frictional resistance of the soil to penetration of the lance may also be used to derive undrained sediment strength using empirical equations (based on laboratory soil mechanical testing). For details refer to the fundamental overview on CPTs by Lunne (2). The pore pressure, which is measured near the tip (u_1), beneath (u_2) and/or above (u_3) the sleeve may serve as an indication for sediment permeability. Insertion of the probe results in a displacement of the sediment, which generates an artificial pore pressure response. The dissipation of this artefact is a measure of permeability, with the t_{50} parameter being accepted as the half decay of the initial peak (3). When allowing for further decay towards ambient values, the measured pore pressure (with hydrostatic pressure subtracted) serves as a transient stress-strain indicator.

Since the early 1970s, the concept of CPTs has become of increasing importance in the characterization of soils in the marine realm. It is usually distinguished between static, dynamic and fall cone penetrometer. Static and dynamic cone penetrometers are pushed in the sediment with constant hydraulic force provided by trucks (onshore) or huge seabed rigs (offshore). In contrast, the less common fall cone penetrometers are lowered on a cable and penetrate the sediment under their own momentum gained during descent. Despite the disadvantage of generally lower total penetration depths, we have re-visited the concept of a free-fall instrument, because it provides a more time- and cost-efficient investigation of the upper marine soft sediment layers.

Instrument Design and Performance

The newly developed lance is an easy-to-use, lightweight free-fall CPT (FFCPT) instrument for shallow marine application (200 m water depth). The probe consists of an industrial 15 cm^2 piezocone and a water-proof housing containing a microprocessor, volatile

memory, battery, and accelerometer (Fig.1). Strain gauges inside the probe measure the cone resistance and sleeve friction by subtraction. A single pore pressure port (u_2) is equipped with an absolute 10 MPa pressure sensor. An inclinometer is used installed to monitor the penetration angle at +/-30° relative to vertical, while temperature is monitored via a thermistor. An accelerometer provides information about the descent velocities and deceleration behavior of the instrument upon penetration. Its data enable the user to calculate penetration depth during multiple deployments by integration. The aluminium pressure housing tolerates 2 MPa confining pressure (ca. 200 m water depth) and hosts the power supply and microprocessor. Frequency of data acquisition is variable, and is has usually been set to 40 Hz during our tests. Binary data are temporarily stored on a Micro Flash Card and then downloaded to a PC. The two non-volatile battery packs available provide performance times of about six and twelve hours, respectively.

Fig. 1 Design of the marine free-fall cone penetration test instrument: **(a)** schematic, **(b)** the instrument during deployment with a portable winch, **(c)** the instrument during deployment from R/V Planet in long and short (inset) mode.

Our instrument is designed for both pogo-style measurements from moving platforms as well as mid-term deployments from a crane, winch, anchored vessel, or tied to a buoy. The length of the lance varies from 1.5 m (short mode) up to a max. 6.5 m (long mode). The extension is accomplished by adding 1m-long metal rods and internal extension data/power cables within them. The weight of the instrument thus ranges from ca. 45 kg (1.5 m) to max. 110 kg (6.5 m). If deep penetration is desired, modular weight pieces (15 kg each) can be mounted to the pressure housing at the top of the instrument, then reaching a max. 170 kg. This construction

allows us variable testing methods depending on the platform, geological setting and the scientific question. The light-weight version can be handled almost effortlessly by an individual. Even the 6.5m-long instrument can be deployed from relatively small boats by two people, recovery is facilitated by a portable 4x4 car winch powered by a battery. However, the easiest way to operate the device is by a regular winch and deep-sea cable on research vessels, either over the side or the A-frame.

The autonomous instrument has been used for long-term dissipation overnight. Here, the lance can be left deployed over the desired period, e.g. connected to a buoy or other mooring. If on a positioned platform, step-like measurements can be carried out at certain depth intervals, with pore pressure dissipation monitored for 10s of minutes to hours at many levels of the depth profile. Until now, the FF-CPT has been deployed from bridges, small pontoons and boats at lacustrine (Lake Lucerne, Switzerland) and estuarine sites (Weser estuary, NW Germany), and from larger vessels in the North and Baltic Seas (e.g., RV *Planet*).

FF-CPT Results

Initial tests have been successfully carried out in muddy, gas-rich to stiff, coarse-grained sediments in lakes, estuaries, and on the marine shelf (North Sea) (for an example of a test protocol see Fig. 2). Depending on the sediment and on the deployment velocity (winch speeds of 17 cm s^{-1} to free drop), the penetration depth ranges between 0.5 m (fine-grained sand) and 5 m (silty clay). In the fine-grained sands, mounting of weight pieces results in an increase of penetration depth of ca. 20 cm per 15 kg weight. Pore pressure response was not affected by the additional weight during impact.

In general, our results attest similar cone and sleeve resistance, and hence friction ratios as in standard CPTests, when comparing our sediment grain size analyses with the CPT results. Soil classification following Robertson's chart (1) is applicable at low to moderate winch speeds, while high penetration rates (>80 cm s^{-1}) and free-drop fail to provide meaningful results. We suggest that additional high velocity testing is required to empirically adjust the classification for our instrument.

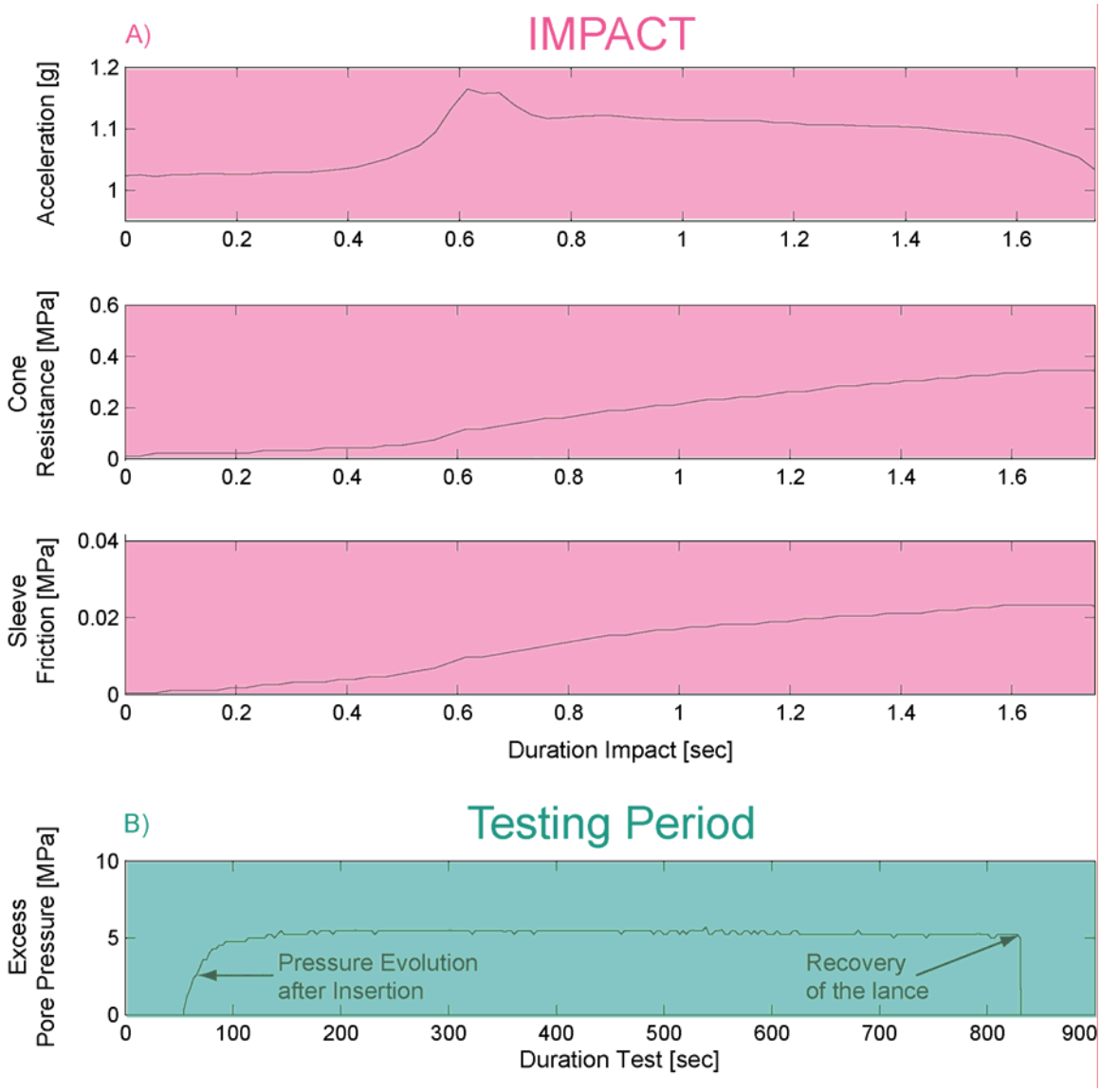

Fig. 2 Primary parameters versus time from a test in the North Sea. Excess pore pressure rises to values above five kilopascals shortly after insertion of the instrument, and does not show significant decay over the 15 minutes of testing.

Pore pressures generally rise during impact, but often show rapid decays towards ambient values during our dissipation tests. We followed two different strategies during our longer tests aiming at pore pressure evolution: full penetration of the probe and dissipation times of several hours (Fig. 3a), and stepwise depth profiling and arresting the instrument at each level for about 10 mins (Fig. 3b). As an example for strategy (A) , a 2 hr.-long dissipation test in Bremerhaven mud is presented. The pore pressure evolution in Bremerhaven is characterized by a build-up soon after insertion (> 12 kPa), followed by a decay to half that value (t_{50}) after approximately one hour. Strategy (B) was followed during measurements in glacial and post-glacial clayey sediments of Lake Lucerne, Switzerland. Interestingly, we observe a different behavior in the Holocene clays down to 340 cm penetration depth, and in the late glacial clays underneath. In the hangingwall, pore pressure evolution during each measuring increment is

characterized by an initial increase when lowering the instrument followed by a decay in the subsequent 10 minutes. In contrast, the late glacial clays show a significant pore pressure drop when inserting the probe further, which in turn is followed by a continuous rise in pore pressure over the 10 min. period. We attribute this change in pore pressure signal to overpressure in the footwall section, most likely due to the presence of gas.

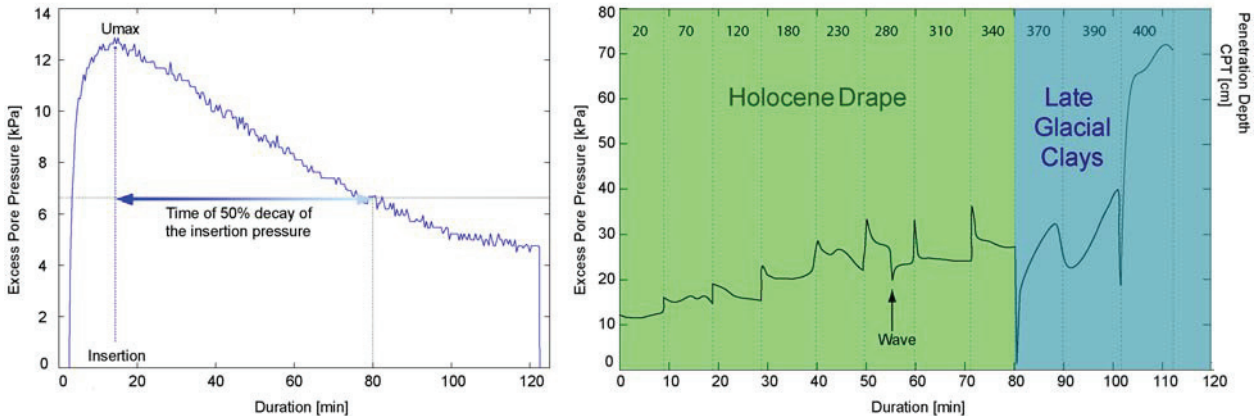

Fig. 3 Results from pore pressure dissipation tests in clayey sediments. The left chart shows full penetration and two-hour decay in Wilhelmshaven, Germany, The right chart shows step-wise deployment and 10 minute intervals of pore pressure decay in lacustrine clays in Lake Lucerne, Switzerland.

In summary, our initial tests have been demonstrated that the new FF-CPT instrument represents a flexible, cost-efficient way to carry out *in situ* geotechnical sediment characterization. Data are in general agreement with standard industry CPTesting, however, the device offers new opportunities for longer term deployments or use from small platforms and boats.

Applications

We envisage our FF-CPT instrument to be a valuable addition to pushed industry CPT experiments. The light-weight, modular design of the probe makes it a good companion when approaching different scientific questions such as the stability of sediments, the temporal evolution of fluid mud in estuaries and harbors, the collection of *in situ* geotechnical data for construction and cable laying, the assessment of tidal forcing/re-suspension, the liquefaction potential of marine soils, and the ground-truthing of geophysical data. Our data indicate that this new FF-CPT represents a time- as well as cost-efficient way for sediment characterization. Modifications to the instrument are straightforward in case larger penetration depth, longer deployments, or different ranges of the sensors are required.

References

For a comprehensive list of references, please contact author Sylvia Stegmann at stegmann@uni-bremen.de. For more information, email oceanbiz@sea-technology.com.

Acknowledgments

M. Lange is acknowledged for valuable suggestions and immense help with construction, programming, and testing of the FF-CPT. Our colleagues V. Berhorst (Geomil, Netherlands), B. Heesemann, and N. Kaul provided valuable discussion. S. Potthoff (Wilhelmshaven), F. Anselmetti and M. Strasser (Lake Lucerne), and T. Wever (North Sea) shared time for assisting CPTesting during their campaigns. Funding for this research was provided by the German Science Foundation (DFG) to Research Centre Ocean Margins, Bremen.

About the authors:

Sylvia Stegmann has developed two CPT free-fall instruments during the course of her PhD thesis. They comprise a shallow water probe presented in this paper, and a deep-water instrument (4000 m) to extend the measurements to the continental slope. Stegmann's research is dedicated to pore pressure measurements *in situ* and in the laboratory.

Dr. Heinrich Villinger is the head of the marine technology and sensors section at the University of Bremen. He is a geophysicist with a focus on marine heat flow and deep-sea instrumentation. As a member of the Integrated Ocean Drilling Program Scientific Measurement Panel, Villinger has years of experience in cutting-edge downhole tool technology.

Dr. Achim Kopf leads the Marine Geotechnics section at RCOM Bremen. His research objectives include sediment deformation, natural hazards, and long-term monitoring of subduction zone processes. Kopf develops equipment for geotechnical laboratory testing and seagoing expeditions and observatories.

Reference List:

(1) Robertson, P.K., (1990). Soil classification using the cone penetration test. Canadian Geotechnical Journal, 27, pp. 151-158.
(2) Lunne T., Robertson P.K. & Powell, J.J.M., (1997). Cone Penetrating Testing in Geotechnical Practice, Spon Press, London, pp. 312
(3) Bennett R.H., Li H., Valent P.J., Lipkin J. & Esrig, M.I., (1985). In-Situ Undrained Strengths and Permeabilities Derived from Piezometer Measurements. Strenght Testing of Marine Sediments: Laboratory and In-Situ Measurements, ASTM STP 883, R.C. Chany & Demars K.R. (Ed.). American Society for Testing and Materials, Philadelphia, pp. 83 – 100.

3.2. Marine deep-water Free-fall CPT measurements for landslide characterisation off Crete, Greece (Eastern Mediterranean) - PART 1: a new 4000 m cone penetrometer

Stegmann, S., and Kopf, A., In: Lykousis, V., Sakellariou, D., and Locat, J. (Eds.), Submarine Mass Movements and their Consequences, 3rd International Symposium, Springer, Netherlands, 171-177, published in 2007.

Marine deep-water Free-fall CPT measurements for landslide characterisation off Crete, Greece (Eastern Mediterranean Sea) - *PART 1: a new 4000m Cone penetrometer*

S. Stegmann, A. Kopf

Research Centre Ocean Margins, Bremen University, Leobener Strasse, 28359 Bremen, Germany

Abstract

The *in situ* measurement of seafloor physical properties such as pore pressure, shear strength or compressibility poses a challenge to engineers, in particular in the marine realm. We present the design and first use of a marine, deep-water free-fall instrument for cone penetration testing (CPT). The probe can be operated in up to 4000 m water depth to measure cone resistance, sleeve friction, deceleration, temperature and tilt as well as pore pressure in u_1 and u_3 position. In this paper we discuss the advantages and disadvantages of the current prototype design, and dwell on the differences between quasi-static versus dynamic cone penetration testing.

KEYWORDS: CPT, FREE-FALL INSTRUMENT, SHEAR RESISTANCE, PORE PRESSURE

1. Introduction

Mechanical properties of seafloor sediments (e.g. undrained shear strength, compressibility and permeability) are influenced by a variety of characteristics such as grain-size distribution, bulk density, effective-stress history and *in situ* pore pressure. All of these properties are typically non-linear functions of the strain history that must be evaluated for each scenario and measurement technique. Likewise, there are differences in measurement techniques, if it comes to cone penetration tests for geotechnical soil characterisation. The two principal techniques are quasi-static (i.e. pushed) cone penetration tests and dynamic (i.e. free drop) tests (e.g. Stoll and Sun, 2005). While industry favours the first where the probe is jacked into the soil at a constant rate of 2 cm/s (see summary in Lunne et al., 1997), several workers have started to develop instruments for marine application which are lowered in free drop, or at high winch speeds into the seafloor (Christian et al., 1993; Osler et al., 2006). The results of penetrometer tests show that there can be a wide spread in the penetration resistance that is measured depending on the degree of sediment inhomogeneity and the rate of

penetration (Lunne et al., 1997; Sultan et al., 2007a, b; Stegmann et al., 2007). Moreover the dilative response of sediments appears to further complicate matters because of the sudden, large changes in shear strength and pore pressure that may occur. All the above findings suggest that further development of seagoing penetrometers for geotechnical characterisation of the uppermost seabed sediments is an emerging need.

One parameter, which is rather difficult to measure *in situ* is pore pressure (e.g. Fang et al., 1993, Strout and Tjelta, 2005), mainly because the stress field is disturbed once a probe is lowered to carry out the measurement. A tremendous engineering effort for several decades in both industry (see www.fugro.com) and academia (e.g. Davis et al, 1991; Christian et al., 1993; Meunier et al., 2004; Wright, 2004) was undertaken to develop seagoing tools operable in several hundred meters of water depth. Different designs have been constructed in order to meet regional or budget requirements. One common example is a rig, where a CPT probe is pushed hydraulically into the sediment at 2 cm/s, following ASTM Standard No. D3441. The deployment of these systems represents a huge technological and logistical challenge, and results in several tens of meters of penetration depth (e.g. Fugro, Penfeld [Meunier et al., 2004]). The disadvantage, however, is the destruction of the uppermost sediments by additional loading of the instrument. For that purpose, other groups developed lance-shaped free-fall instruments (FF-CPT) that penetrate several meters into the sediment by its own weight, providing a time and cost efficient tool for exploration (e.g. Christian et al., 1993; Osler et al., 2006). This paper describes a new marine free-fall penetrometer for deep-water applications (4000 m maximum water depth), which was recently designed at the Research Center Ocean Margins, Bremen, Germany. It completes an already established free-fall shallow-water instrument (Stegmann et al. 2006a, b), which is limited to 200 m water depth.

2. Instrument Design and Measurement Methodology

The 380 cm long deep-water (DW) free-fall instrument is equipped with a standard 15 cm^2 CPT piezocone (Geomil) with strain gauges inside the probe to measure cone resistance q_c (25 MPa range) and sleeve friction f_s (0.25 MPa range) (Fig. 1). The instrument has two pore pressure ports, which are located at the cone (u_1) and 80 cm above the cone (u_3, following the CPT nomenclature); both ports are connected to high-resolution (10 Pa) differential pressure transducers (Validyne DP215, ±82 kPa range) via stainless steel tubing to a sea bottom water reference port. An absolute pore pressure sensor measures hydrostatic pressure (i.e. water depth) down to 4 km water depth. To prevent the entrapment of gas inside the tubing, especially during the initial phase of deployment when the instrument is lowered

through the water column, valves are used to bleed the gas from the tubing. The pressure sensors are protected by valves in case high excess pore pressures are encountered. Temperature sensors and 2 bi-axial acceleration sensors are also connected to the Tiger Basics microcontroller (>40 Hz operating frequency).

The DW-CPT may either be run self-contained on batteries and equipped with a flash card, or could be run with a Seabird Electronics (SBE36) telemetric system, which powers the microcontroller, sensors, and valves (Fig. 1). The telemetry provides real-time data acquisition as well as control of the instrument via an attached PC with custom-programmed LabView control software. The autonomous mode is utilised for long-term observation of the dissipation behaviour of pore pressure by disconnecting the deployed lance from the winch and recovering it after several hours. The raw data protocol was implemented for time, acceleration, absolute pore pressure (hydrostatic pressure), cone resistance, sleeve friction and differential pore pressures (u_1, u_3). Using the vertical component of acceleration, penetration velocity (1st integration) and depth (2nd integration) can be derived.

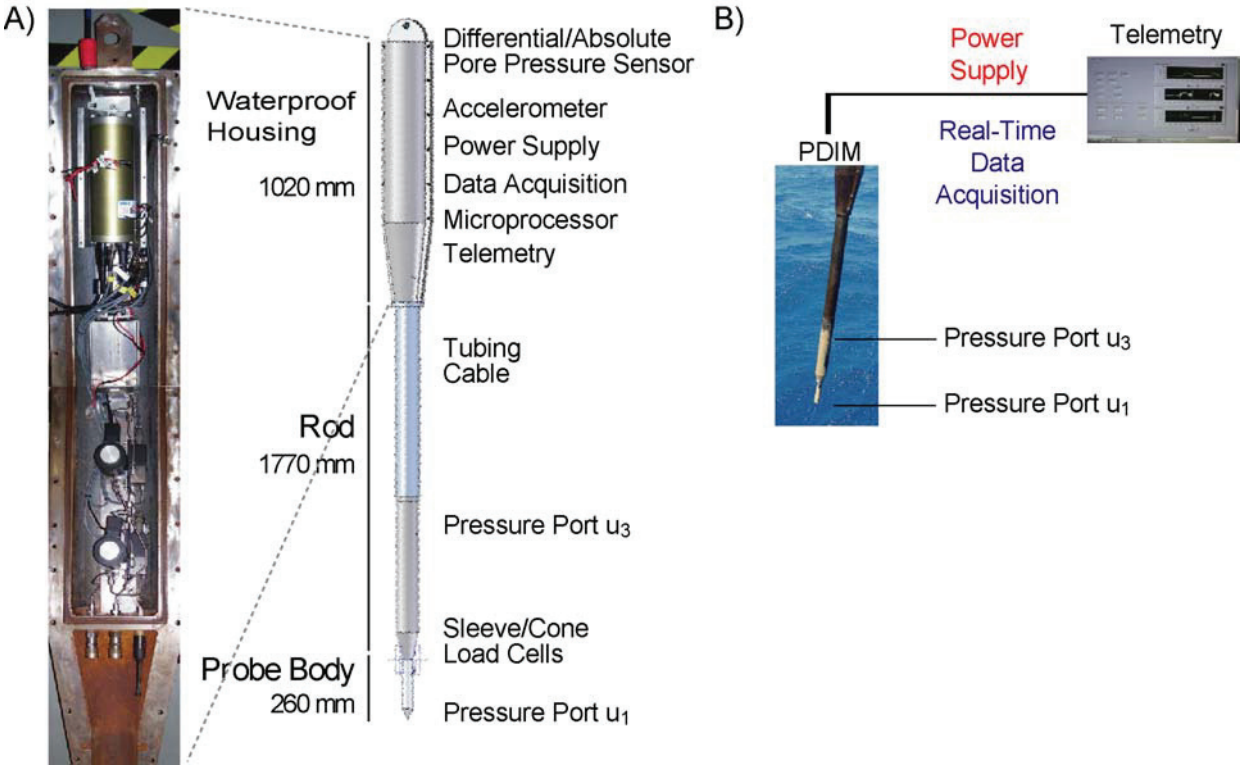

Figure 1: Photograph and schematic sketch of the deep-water lance **(a)** and its configuration **(b).**

During cruise P336 in the Cretan Sea, the instrument was lowered on a cable at an average rate of 1.5 m/s through the water column until it penetrates the seafloor and underlying sediment. The lance remained embedded in the sediment after insertion for 10 minutes to

observe the dissipation of the pore pressure. This can be quantitatively expressed as T_{50} value (the time needed for a 50% decay of the maximum pore pressure), and serves as a first-order indicator of permeability (e.g. Bennett et al., 1985). Penetration velocity and depth was derived from the y-component of the acceleration sensor. After the lance was recovered through the water column, sediment stuck to the cone was measured and used as a control for the calculated penetration depth. Regarding water depth, most of the measurements were carried out in pogo-style. CPT data have been filtered (low-pass) using custom-made Matlab routines.

3. Results

We here summarise the results from a total of 40 CPT deployments we carried out during cruise P336 with RV *Poseidon*. 35 of the deployments were done with the prototype deep water instrument, while 5 were carried out with the shallow water device in the upper slope area. Since this paper is dedicated mostly to the new DW FF-CPT, we summarise only data from that instrument.

Figure 2 represents a typical data protocol, including penetration velocity, sleeve friction f_s, cone resistance q_c and pore pressure data obtained by ports u_1 and u_3 collected in undisturbed sediments at the northern Cretan margin. It can be seen that the values are largely synchronous, with q_c and f_s being followed with minor delay at port u_1, and a somewhat larger delay at port u_3 (Fig. 2d). The delay reflects some compliance of the pressure sensors, however, can be largely related to the insertion progress. CPT measurements were carried out with an initial penetration velocity between 1.1 m/s and 1.8 m/s, which was controlled by winch speed (max. 2 m/s) and influenced by external conditions (waves, swell). Absolute penetration depth of the complete CPT data set (2^{nd} integration of acceleration) ranged between 0.6 m and 1.6 m with 1 m in average. In nearly all measurements the tilt of the penetrated lance did not exceed ±9°. Unfortunately, the CPT cone failed during the campaign, so that the strength parameters (q_c, f_s) could not be measured in each location. Consequently, we focus mainly on differential pore pressure signal at u_1 and u_3 position (Fig. 1). Regarding the u_1-signal vs. time, pore pressure evolution reflects different physical properties (Fig. 3).

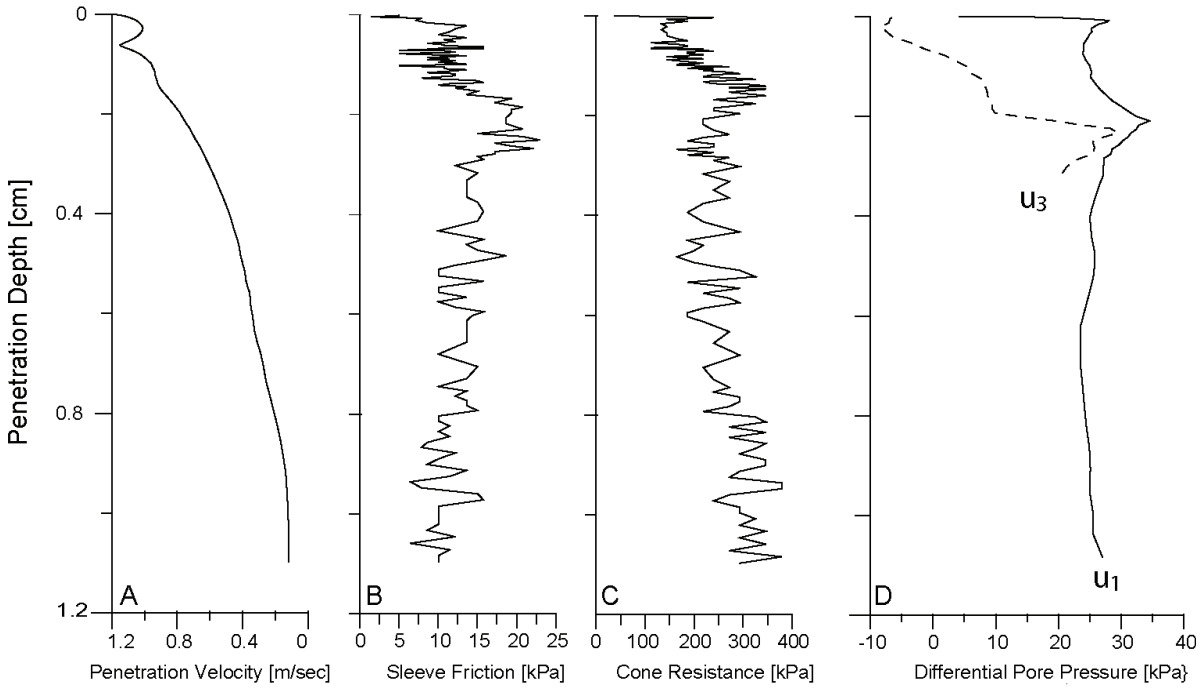

Figure 2: Typical penetration protocol showing **(a)** penetration velocity, **(b)** sleeve friction, **(c)** cone resistance, and **(d)** differential pore pressure at the port position u_1 and u_3 taken at the Cretan slope.

During penetration the signal is generally characterised by an insertion maximum followed by a sudden drop (possibly, but not necessarily, to sub-hydrostatic values) (see the red part in Fig. 3). With the halt of the lance, pore pressure rises again and later asymptotically dissipates towards equilibrium (Fig. 3). If we regard all our test results, the difference between the maximum and the minimum of the drop ranged between 7 and 145 kPa. By comparing the pore pressure profile during penetration with cored sediments (see Kopf et al., this issue, section 4.3), the excess pore pressure peak, which varied between 13 to >82 kPa, coincides with an increase in sedimentary strength. Moreover, this higher strength is accompanied by decreasing sediment permeability (influencing the magnitude of the pore pressure drop) and larger T_{50} values during pore pressure decay. In order to overcome a potential bias resulting from the impact of the probe, we used the second excursion maximum in the pore pressure curve when calculating T_{50} (following Burns and Mayne, 1998).

There are two shortcomings in our DW CPT instrument. First, several measurements exceeded the upper limit of the differential pore pressure sensor during insertion, maybe as a result of the stiffness of the sediment. This means that we may have potential errors in case the second pore pressure maximum still exceeded 82 kPa. Second, the lower portion of the instrument (Fig. 1) seems too sturdy to allow deep penetration. As a consequence, we obtained only u_3 signals in 80% of the deployments. The insertion signal at u_3 was significant lower than at u_1 (i.e. 9.5-52 kPa), which maybe resulted from the different shear resistance

along the sturdier portion of the lance during penetration. The lower values of u_3 represented the shear-induced pore pressure, whereas the high u_1 signal is generated by compression in the vicinity of the tip (see discussion in Song and Voyiadjis, 2005).

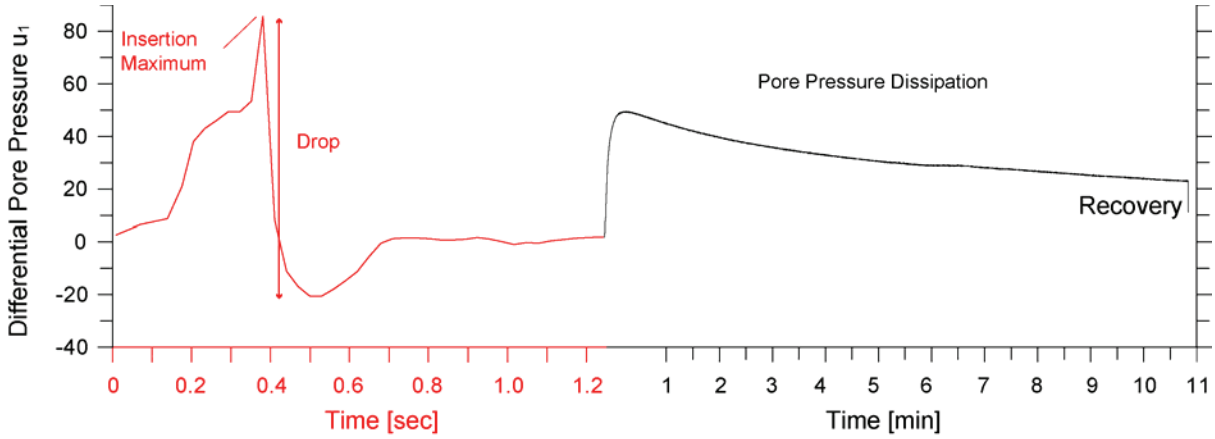

Figure 3: Typical pore pressure response measured in u_1 position during the insertion (red portion of graph) and within the 10 minutes of the lance remaining stuck in the sediment (black portion of graph). Please note the different time scales on the x-axis.

4. Discussion

Compared to the shallow-water CPT device (e.g. Stegmann et al., 2006a, b, 2007), there are still a number of shortcomings in the proto-type deep-water FFCPT design. First, the differential pressure sensors need to accommodate for higher excess pore pressure ranges, since they repeatedly maxed out when inundated surface sediments were hit (current range ±82 kPa differential pressure). However, this can easily be achieved by replacement of the diaphragm and recalibration of the Validyne DP215 transducers. Second, the overall layout of the lower part of the instrument is too sturdy and hampers deep penetration. We are currently building a new instrument where the lower portion is as narrow as the actual 15 cm^2 probe (Geomil). On the positive side, we observe consistent results with the shallow-water and deep-water FF-CPT instruments. With either probe, both q_c and pore pressure allow us to make a distinction between undisturbed vs. remobilised sediments off Crete, which is consistent with what is expected based on the seismic reflection profiles. Still, given the overall volume of mass wasting deposits at the Cretan slope (see Kopf et al., this volume), the most emerging need for improvement is a larger penetration depth, especially given that some amalgamated, remobilised deposits may be covered by background sediment again. This can be achieved by either designing a smaller diameter tool, increase total weight, or a combination of the two.

On the pro-side, we feel confident that the free-fall probe will provide us with interesting *in situ* soil physical properties. The instrument fell down on the seafloor only four times, while all other measurements led to stable positioning, even if penetration was as low as 0.6 m. We are particularly optimistic that the high impact velocities help to accentuate changes in physical parameters. This has been found earlier in controlled laboratory tests as well as seagoing deployments in the Gulf of Mexico. Here, Stoll et al. (2006) used a quasi-static instrument called STATPEN and a freely-falling dynamic instrument called PROBOS. Typically, the STATPEN results show a gradual, more or less uniform increase in cone resistance whereas the PROBOS record contains many large peaks of high penetration resistance suggesting an inhomogeneous sediment structure that is not obvious from the quasi-static test results (Stoll et al., 2006; their Fig. 6). No matter how different the absolute values of cone resistance, etc. were, the curves of both instruments agreed in principal (i.e. in stiffer layers, q_c increased with either probe, the PROBOS exceeding that of the STATPEN by a factor of 10!). When comparing the two types of test it should be remembered that the STATPEN penetrates the sediment at a constant rate of 2 cm/s. In contrast the PROBOS penetrates at a variable but much higher rate ranging from 400-600 cm/s at first contact decreasing to zero at maximum depth of penetration. The latter correlates well with impact velocities of 110-180 cm/s of the new RCOM free-fall DW-CPT described in this paper. We hence assume that our typical test protocols (Fig. 2) equally help to underline changes in grain size, density, or shear strength. For further discussion on this penetration-rate or strain-rate effect, see Dayal and Allen (1973) and Stoll et al. (2006).

In an effort to explain the differences between static vs. dynamic data acquisition, we postulate that the sediment must contain lenses or thin layers of coarser, more granular sediment that exhibits a dilative response when penetrated at a high rate. This can be seen when the pore pressure data are regarded, where subhydrostatic excursions are not uncommon. They are believed to results from displacement of pore fluid when the probe penetrates at high rate. Examples include the Gulf of Mexico (Stoll et al., 2006), the Baltic Sea (Seifert, unpublished data), or the Cretan Sea (Kopf et al., this volume). Each of these studies further demonstrate that the *in situ* strength measured with the FF-CPT agrees well with laboratory-derived values using the fall cone apparatus or vane shear device. Similar results were published earlier by Johnson et al. (1988), or in recent work concerning the stability of slope sediments in lakes by Stegmann et al. (2007) and Strasser et al. (2007).

5. Acknowledgements

We thank Master Michael Schneider and his crew for the help on deck and excellent manoeuvring during CPT deployments during cruise P336 with RV *Poseidon*. We also thank Matthias Lange at RCOM Bremen for technical support when building the DW-CPT. The manuscript benefited from constructive reviews and suggestions by Katrin Huhn and Nabil Sultan. Funding for this work was received by DFG through RCOM Bremen (project C8). This is RCOM publication #500.

6. References

Bennett, R.H., Li, H., Valent, P.J., Lipikin, J., Esrig, M.I., 1985. In-Situ Undrained Shear Strengths and Permeabilities Derived from Piezometer Measurements, Strength Testing of Marine Seidments: Laboratory and In-Situ Measurements, ASTM STP 883, R.C. Chany, K.R., Demars, ASTM Philadelphia, p.83-100.

Burns, S.E., Mayne, P.W., 1998. *Penetrometers for Soil Permeability and Chemical Detection*. School of Civil and Environmental Engineering, Georgia Institute of Technology, Report No. GIT-CEEGEO-98-1

Christian, H.A., Heffler, D.E., Davis, E.E., 1993. Lancelot – an *in situ* piezometer for soft marine sediments. Deep-Sea Research, 40/7, p.1509-1520.

Davis, E.E., Horel, G.C., MacDonald, R.D., 1991. Pore Pressure and Permeabilities Measured in Marine Sediments With a Tethered Probe. J. Geophys. Res., 96, B4, p.5975-5984.

Dayal, U., Allen, J. H., 1973. Instrumented Impact Cone Penetrometer. Can. Geotech. J. ,10, p.397-409

Fang, W.W., Langseth, M.G., Schultheiss, P.J., 1993. Analysis and Application of *in situ* Pore Pressure Measurements in Marine Sediments. J. Geophys. Res., 98, p.7921-7938.

Johnson, G. W., Hamilton, T. K., Ebelhar, R.J., Mueller, J.L., Pelletier, J.H., 1988. Comparison of In-situ Vane, Cone Penetrometer, and Laboratory Test Results for Gulf of Mexico Deepwater Clays. In: Richards, A.F. (ed.), ASTM Spec. Tech. Publ. 1014, *Vane Shear Strength Testing in Soils, Field and Laboratory Studies*, p.293-305.

Meunier, J., Sultan, N. Jegou, P., Harmegnies, F., 2004. First Test of Penfeld: a New Seabed Penetrometer. Proc. 14th Int. Offshore Polar Eng. Conference, Toulon, France, May 23-28, p.338-344.

Osler, J., Furlong, A., Christian, H., Lamplugh, M., 2006. The integration of the Free Fall Cone Penetrometer (FFCPT) with the Moving Vessel Profiler (MVP) for the rapid assessment of seabed characteristics. Canadian Hydrographic Conference, The Westin Nova Scotian, Halifax, N.S., p.11.

Song, C.R., Voyiadjis, G.Z., 2005. Pore pressure response of saturated soils around a penetrating object. Computers and Geotechnics, 32, p.37-46.

Stegmann, S., Villinger, H., Kopf, A., 2006a. Design of a modular, marine free- fall cone penetrometer. Sea Technology, 47/02, p.27-33.

Stegmann, S., Moerz, T., Kopf, A., 2006b. Initial Results of a new Free Fall-Cone Penetrometer (FF-CPT) for geotechnical *in situ* characterisation of soft marine sediments. Norwegian Journal of Geology, 86/3, p.199-208.

Stegmann, S., Strasser, M., Anselmetti, F.S., Kopf, A., 2007. Geotechnical in situ characterization of subaquatic slopes: The role of pore pressure transients versus frictional strength in landslide initiation. Geophys. Res. Lett., 34, L07607, doi:10.1029/2006GL029122.

Stoll, R.D., Sun, Y.-F., 2005. Using Static and Dynamic Penetrometers to Measure Sea Bed Properties. Office of Naval Research, Science & Technology, Ocean Battlespace Sensing (32), Coastal Geosciences Annual Reports FY05: 1-5, also available at http://www.onr.navy.mil/obs/321/docs/cg/04/cgstoll.pdf

Stoll, R.D., Sun, Y.-F., Bitte, I., 2006. Seafloor properties from penetrometer tests. IEEE J. Ocean Eng., http://www.onr.navy.mil/obs/reports/docs/05/cgstoll.pdf

Strasser, M., Stegmann, S., Bussmann, F., Anselmetti, F.S., Rick, B., Kopf, A., 2007. Quantifying subaqueous slope stability during seismic shaking: Lake Lucerne as model for ocean margins: Marine Geology, in press.

Strout, J.M., Tjelta, T.I., 2005. In situ pore pressure: What is their significance and how can they be reliably measured? Mar. Petrol. Geol., 22, p.275-285.

Sultan, N., Voisset, M., Maresset, B., Marsset, T., Cauquil, E., Colliat, J.-L., 2007. Potential role of compressional structures in generating submarine slope failures in the Niger Delta. Mar. Geol., 237/3-4, p.169-190.

Wright, I., 2004. Geotechnical Investigations Using Mini-Cone Penetrometer Testing. Sea Technology, 45/7, p.49-52.

3.3. Testing and processing procedures of the FF-CPT

In this chapter, the deployment techniques used as well as the data flow and processing routines will briefly be explained, because they hardly found their way into the manuscripts above (Chapters 3.1, 3.2).

Concerning the mode of deployment, the diversity of this thesis and the requirements in the various settings forced us to use (or build) a number of platforms. In short, they included:

a) Pier/harbour: Free-drop or controlled lowering of the FF-CPT by hand;
b) Pier/harbour: Velocity-controlled deployment by 4 x 4 car winch;
c) Streams/rivers: Use bridge rather than pier, deployment as in a) and b);
d) Lake Hemelingen shore: Use huge crane for velocity-controlled deployment;
e) Lake Hemelingen pontoon: Utilise hydraulic stamp in a load frame by building an aluminium adapter that connects the CPT instrument to the stamp;
f) Lake Lucerne boat: Deployment as in a);
g) Lake Lucerne pontoon: Lower instrument stepwise for a couple of decimetres each time with the 4 x 4 car winch;
h) Marine expeditions: Use ship's winch or crane for deployment, either just the wire (SW-CPT) or the "single conductor cable" to monitor seafloor performance via a telemetric system.

In the majority of the studies, we used either the 4 x 4 car winch (scenarios a, b, c, f) or available cranes/winches (scenarios d, g, h) for instrument recovery. Only on occasion, we relied on the hydraulic load frame (pushed tests at 2 cm/s; see Chapter 4.3 below) or man power (scenario a).

Once the testing is completed, both the SW- and the DW-CPT have to be opened to access the data storage chip. While the SW-instrument is completely self-contained and has to be run "blindly", the DW-instrument has a telemetric system (Seabird Electronics SBE36) to transmit a low-frequency sub-set of the data in real time to the ship. This way the quality of the test (e.g. tilt of the probe, state of pore pressure dissipation, etc.) can be checked during the deep water deployments. For details, refer to Chapter 3.2 above.

After retrieval of the storage media, raw data are downloaded to a PC via a card reader. Initial binary data are converted to ASCII format by a Labview routine. Customised Matlab routines, which were programmed at RCOM Bremen for the CPT application, split the complete data set into individual profiles. This way each CPT parameter (q_c, f_s, pore pressure [u_1, u_2 and u_3] temperature, tilt) plus all the other values monitored (battery power; time;

acceleration sensors; additional tiltmeter) get separated and can then be plotted versus time (i.e. duration of the test). Also, during this step data are converted from voltage in the raw data into absolute values in units of each sensor. For quality control, the data file contains the status of the power supply during testing.

Cone parameters are processed with a low-pass filter and then visualised in overview plots, again using Matlab routines. Thereafter, the information from the accelerometers is integrated once to obtain velocity information during deployment, and then a second time to get the absolute depth of penetration. For this latter step in data processing, it is crucial to pick the exact time of impact of the CPT device on the sediment-water interface; otherwise depth estimates may be erroneous and may lead to discongruencies when comparing several deployments or relating the CPT data to reference cores.

3.4. Refinements of the FF-CPT system

Over the course of 36 months (i.e. this thesis), a total of 338 CPT deployments were carried out with either the SW- or DW-CPT lance (see Chapter 7.1 for details). Given the experience gained, some modifications were undertaken or are underway to improve the performance concerning both the geometry of the instrument and the sensors contained. In this chapter, the current state-of-technology of the two RCOM instruments is described:

Geometry of the SW-FF-CPT and DW-FF-CPT

- The initially large diameter (100 mm) of the rod behind the *GEOMIL* CPT probe of the DW-FF-CPT was chosen for stability and to host the *Swagelok* connectors between the u_3 pore pressure port and the hydraulic tubing. The sturdiness of this design proofed to be useful when the lance struck the (to us unknown) concrete floor plate in the harbour of Warnemünde (expedition NEST06 on RV *Planet*) three times without any damage whatsoever. On the other hand, deployments of the DW-FF-CPT in fine- to medium-grained sediments (e.g. Cretan Sea) demonstrated that the geometry of the strong frontal portion of the lance hinders or disables deep penetration (see Fig. 6, left). As a consequence, the instrument was provided with a thinner (46 mm) and longer (2000 mm) frontal part to reach higher penetration depth with a total length of 5.8 m (Fig. 6, right). As a positive outcome, significantly larger penetration depths (> 4m in some places; see Fig. 6) were reached in the Ligurian Sea, where sediments comprised comparable stiffness to those studied in the Cretan Sea. However, the slim design was severely damaged twice when hitting a gravel layer.

- To achieve higher penetration rates and deeper total penetration of the DW-FF-CPT, our deployments suggest that the weight of the instrument seems to have more profound influence than its momentum owing to the velocity. We hence consider to have modular weight sets manufactured that may be attached to the new stainless steel cylindrical housing in case deeper penetration is desired.
- The design of the SW-FF-CPT with the cylindrical housing at the head of the instrument and the modular system of weight pieces and extension rods containing data cables was found to perform excellently during many different deployments. Similar to that design, the geometry of the "sandwich"-type (meanwhile rusty) pressure housing of the current DW-instrument will be replaced by a stainless steel cylinder. This also involves the modification of the underwater connector at the outside of the pressure housing, which is presently adapted for charging the battery and downloading the data without opening the housing.
- During the initial testing phase with the SW-FF-CPT, we once lost the frontal 6 m of the instrument (CPT probe and 5 extension rods) owing to material wear and failure at the junction between the the rods and the conical connector to the pressure housing. We then modified this "adapter" by adding a sturdier, 30 cm long cylinder that supports the uppermost rod and connecting thread.

Sensor and data logging technology of the SW-FF-CPT and DW-FF-CPT

- Initially a CPT cone with a standard range of measurement (100 MPa for cone resistance and 1 MPa for sleeve friction, see Table 1) was chosen for the SW-FF-CPT. As many deployments illustrate that it is possible to penetrate mainly fine-grained superficial sediments (there is no chance to penetrate coarse-grained sediment), the measured cone resistance did never exceed 10 MPa. Based on this experience, the cones for the DW-FF-CPT were manufactured by *GEOMIL* with a lower total range (i.e. 25 MPa). This represents the maximum reduction of the range, as otherwise the mechanical stability of the strain gauges would be too small. The same improvement has to be undertaken for the SW-FF-CPT to provide a more sensitive cone in the near future.
- In order to accommodate the different initial velocities, ranging from several hundred cm/s in free drop to 2 cm/s when lowered on a winch or pushed by an hydraulic piston, four acceleration sensors with different measurement ranges were installed into the shallow-water CPT to avoid measurements exceeding the limits of the sensors and also to provide maximum accuracy for each velocity during the various deployments (for details, see Table 1). The careful analysis of the accelerometer data (e.g. artefacts from movement

of the ship/wire) has to result in the full understanding that ensures a reliable calculation of penetration velocity and depth at any point during the CPT experiment. For instance, in the field study in Lake Hemelingen, some oscillation in the accelerometer data of the 5g sensor was observed, which produces uncertainties in the integration. One possible solution to illuminate and eliminate this problem is to establish or exclude whether the swinging response is related to frinch effects (e.g. movement of the winch due to waves). Another possible test is the measurement of the response due to the dynamic shear modulus of sediments, i.e. if "damped oscillation" is observed (see discussion in Stoll and Akal [1999]), or it is related to the sensor configuration.

- The sampling frequency of the shallow-water FF-CPT was monitored over many tests, where the sampling rate varied between 28 and 111 Hz as a consequence of the saving procedure of the microcontroller (Tiger Basics DL7000). This means that spatial resolution may vary between 0.03 and 0.1 m depending on the penetration rate. We are currently exploring if sampling frequency, and thus higher spatial resolution, can easily be improved by replacing the existing microprocessor (currently used in both the SW- and DW-instruments) with a different one.

Table 1 Actual technical specification of the sensors in the SW-FF-CPT and DW-FF-CPT.

	SHALLOW-WATER LANCE (200 m water depth)			
	Type	**Range**	**Accuracy**	**Operating Temperature**
CPT Subtraction Cone 15 cm²				
Cone Resistance	Geomil 15cm² Subtraction Cone	100 MPa	0.25 % FS	- 10°C - + 40°C
Sleeve Friction	Geomil 15cm² Subtraction Cone	1 MPa	0.5 % FS	- 10°C - + 40°C
Absolute Pressure Sensor	Geomil 15cm² Subtraction Cone	2 MPa	0.4 % FS	- 10°C - + 40°C
Inclinometer	Geomil 15cm² Subtraction Cone	0-30°	2° FS	- 10°C - + 40°C
Acceleration				
Analog Devices	ADXL103	+/- 1.7 g	0.5% FS	
Vernier	Low-g	+/- 5 g	0.05 g	
Analog Devices	ADXL321	+/- 18 g	0.2% FS	
Freescale Semiconductor	MMA3202	+/- 100 g	1% FS	
Microcontroller	Tiger DL7000			
Power Supply		12 V		

	DEEP-WATER LANCE (4000 m water depth)			
	Type	**Range**	**Accuracy**	**Operating Temperature**
CPT Subtraction Cone 15 cm²				
Cone Resistance	Geomil 15cm² Subtraction Cone	25 MPa	0.25 % FS	- 10°C - + 40°C
Sleeve Friction	Geomil 15cm² Subtraction Cone	0.25 MPa	0.5 % FS	- 10°C - + 40°C
Differential Pressure Sensor	Validyne P55D	+/- 220 kPa	+/- 0.25 % FS	
Absolute Pressure Sensor	Wika ECO1	400 kPa	<0.5% FS	
Acceleration				
Analog Devices	ADXL103	+/- 1.7 g	0.5% FS	
Analog Devices	ADXL321	+/- 18 g	0.2% FS	
Freescale Semiconductor	MMA3202	+/- 100 g	1% FS	
Microcontroller	Tiger DL7000			
Power Supply		12 V		

Figure 6 Photographs of the DW-FF-CPT instrument after deployments taken during cruise Pos336 (RV *Poseidon*) in spring 2006 and M73/1 (RV *Meteor*) in summer 2007. Please note difference in instrument geometry and significantly deeper penetration in case of the Meteor-deployment at the Ligurian continental slope.

4. Proof of Concept

The first deployments of the SW-FF-CPT were carried out in different easily accessible locations close to Bremen. They include harbour sites at Wilhelmshaven and Bremerhaven, a small stream near the University campus (Kuhgraben) and Lake Hemelingen, where a crane was readily available for us. With the infrastructure of the locations (bridge, pier, pontoon), we deployed the lance either by a winch (crane, 4x4 car winch) or let it sink by its own weight, and also used the winch or man power to recover it. The primary intention of these experiments was to test the performance of the sensors and to play with the variable options given by the modular design of the instrument (weight, length, speed of penetration). Essential results of velocity-controlled and free-drop deployments, where the instrument was arrested for minutes to hours in the sediment, are summarised in Chapters 4.1 and 4.2. These chapters purposefully neglect geological aspects.

In Chapter 4.3, results from pushed and free-drop CPT deployments with different penetration velocities are compared, which is a crucial point for the discussion about the use of free-fall devices versus constant rate instruments. Therefore this chapter stands out as a contribution to support the concept of free-fall devices.

4.1. A new modular marine free-fall CPT

Stegmann, S., Villinger, H., and Kopf, A., In: Dahlin, H., Flemming, N.C., Marchand, P., and Petersson, S.E., European Operational Oceanography: Present and Future, Proc. of the 4th International Conference on EuroGOOS 6-9 June 2005, Brest, France, 854. published in 2006.

A new modular marine free-fall CPT

Stegmann, S[1)]., Kopf, A.[1)], Villinger, H[2)].

1) Research Centre Ocean Margins, University Bremen, Postfach 330440, 28344 Bremen, Germany
2) Departement of Geoscience,University Bremen, Postfach 330440, 28344 Bremen, Germany

Abstract

Cone Penetration Tests (CPT) are a standard method for the *in situ* characterisation of shallow sub-seafloor sediments. Hence we have developed an easy-to-use, lightweight free-fall CPT (FFCPT) lance for shallow marine application (200 m water depth). The lance consists of an industrial 15 cm^2 piezocone measuring pore pressure, temperature, tilt, tip resistance and sleeve friction. The lance may be optionally equipped with extension rods (0.5 m – 6.5 m total length) to control penetration depth. A pressure case (200 m) hosts a microprocessor, volatile memory, battery, and accelerometer, and may be loaded with additional weights (up to 90 kg) for tests in indurated sediment.

Initial deployments have been successfully carried out in muddy to coarse-grained sediments. The results attest similar friction ratios as in standard CPT tests, with the maximum penetration having exceeded 4 m sub-seafloor depth (as a function of the weight added). Our main focus was pore pressure, which generally rises during impact (between 10 and 50 kPa in excess of hydrostatic pressure). However, even medium-grained sediments often show rapid decays towards ambient values during dissipation tests (30 min. to 5 hrs.).

Keywords: Cone penetration test, Pore pressure, Friction, Sediment, *in situ* measurement

1. Introduction

Since the early 1920s, CPT measurements have become a widely accepted means to characterise the geomechanical properties of soft to indurated sediments in onshore and offshore settings. The principle of the testing procedure is vertical profiling using a lance equipped with a standard cone (usually 10 or 15 cm^2 in diameter), which is pushed into the sediment at a constant rate of 2 cm/s (e.g., Lunne et al., 1997). The cone can be equipped with various sensors, most often measuring tip and sleeve resistance (as a function of sediment stiffness), pore pressure (to be monitored in different positions, u_1-u_3), temperature and tilt. The two parameters of major interest are friction ratio (i.e., the ration between sleeve friction and tip resistance) and pore pressure, since both of them control sediment strength and

effective stress state. As a consequence, CPTs are efficient devices in tasks such as cable or pipeline laying, slope stability concerns, navigability of harbours/estuaries, or ground-truthing of geophysical data.

One of the most difficult environments in standard CPT sediment characterisation are marine realms because the penetration force is not easily provided. In shallow water, pontoons may be used to host onshore devices (CPTs mounted on trucks, etc.), however, in deeper water, heavy rigs have to be lowered to the seafloor in order to provide an inert abutment to push the lance-shaped device into the sediment. For this purpose, an easy-to-handle, lightweight CPT free-fall device was designed, which offer the possibility for cost- and time-effective *in situ* measurement in quasi un-disturbed sediments, as there is no need for rigs put down on the sea floor.

2. Instrument Design and Method

The free-fall instrument developed at RCOM Bremen is characterised by its modular design concerning length and weight (see Fig. 1A). It hence may be handled by two people from very small platforms, but could also be used on large vessels using a winch. The lance consists of an industrial 15 cm^2 piezocone (with pore pressure in u_2 position, temperature, tilt sensors, as well as the capability to measure tip and sleeve resistance) and a pressure case containing a microprocessor, volatile memory, battery, and accelerometer. As a result, the device works completely autonomous. Data are sampled and recorded at variable frequency, the upper limit being 20 Hz. The FFCPT may be optionally equipped with additional weights (up to 90 kg) and extension rods (0.5 m – 6.5 m total length; see Fig. 1B) to control penetration depth. The modular design allows us *in situ*-profiling of sediments by repeated testing at the same site. Each added weight increases penetration by a couple of cm to dm, so that each horizon can be monitored regarding its frictional response, temperature, and – most importantly – pore pressure decay after insertion of the probe. Penetration depth is further controlled by the speed the probe is entering the sediment (namely controlled rate using a winch vs. free fall). Our initial results indicate that the device is a worthwhile cost- and time-efficient alternative to conventional CPT systems.

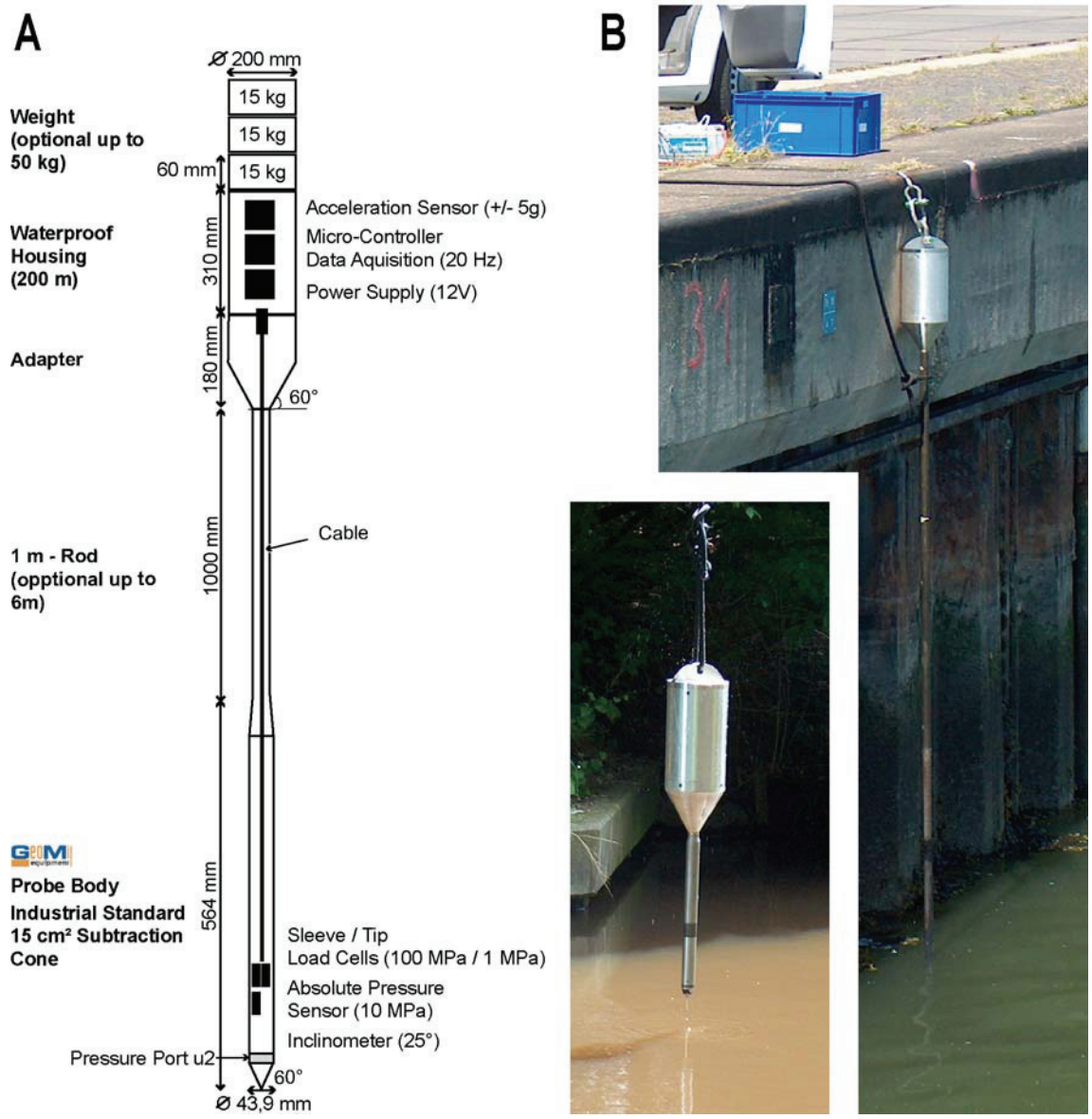

Figure 1 (A) Schematic diagram of FFCPT; **(B)** Photographs of FFCPT in the longer (5 m) and shorter (no extension rod; see inset) configuration prior to deployment.

3. Results and Discussion

Initial FFCPT measurements focused on pore pressure response of the sediment rather than sediment profiling or mechanical resistance. The data presented here represent preliminary results of our initial measurements at sites located in marine to brackish settings at the North German coast and adjacent estuaries/streams. In those settings, water depth varied between 1 m and 12 m. They include the ports of Bremerhaven, Wilhelmshaven, and Kuhgraben near Bremen. In addition to CPT tests with various total lengths and weights of the lance, we were taking sediment samples for laboratory analyses such as density, porosity, and grain size distribution. A more complete data set, showing detailed analyses of data quality and temporal/spatial resolution during penetration, is given in Stegmann et al. (2006).

3.1 Sediment strength and composition

Shear strength *sensu stricto* is not measured directly with a CPT, but estimated from the resistance of the tip and sleeve of the device during penetration. Our main goal was not only to relate the FFCPT data to the sediment itself, but to standard (i.e. pushed) CPT tests published in the literature (see summary in Lunne et al., 1997).

In the uppermost decimetres, we found tip resistance to reach values up to 1 MPa, which is higher than what is known from standard tests. This result was most profound when inserting in free-fall mode and can be attributed to the high force upon insertion. Below ca. 50 cm, our absolute insertion pressures agree well with those in pushed tests (see compilation by Lunne et al., 1997, and references therein). However, if we regard the friction ratio (i.e. tip resistance being normalised against sleeve friction), our data are in good agreement with standard CPT tests. Friction ratio ranges from 1 to 9%, with the lower values typically corresponding to sands and their high tip resistance. This assumption was confirmed by grain size analyses using a Beckman Coulter LS200 laser particle size analyser. The Kuhgraben samples are dominated by sand (ca. 62%) and with clay contents around 5%, while the mud from the other sites comprise clayey silt with sand contents of 20 % and 32%, respectively.
In principle, the resistance of the sediment upon penetration combined with maximum sampling frequency (20 Hz) and known terminating depth, sediment profiling is possible by integration of the acceleration data. In practice, however, a more appropriate way is coring near the testing location to recover sediment for laboratory testing.

3.2 Pore pressure measurements

The pressure of the fluid between sediment particles has a profound effect on the stress state, and hence stability, of the material. Its transient increase due to tides, geodynamics (e.g. tectonic loading, rapid sedimentation) and human construction is an important factor in hazard research. Generally, fine-grained sediments show high fluid pressures owing to their low permeability and poor drainage (Maltman, 1994; Strout & Tjelta, 2005). As a consequence, pore pressure monitoring was our main objective during the FFCPT deployments. Figure 2 shows pore pressure records from four tests with variable duration (0.5 – 6 hrs.). It can be seen that even in the finer grained settings (clayey silt; see previous chapter), the induced pore pressure decreases significantly within hours. In the Wilhelmshaven test (Fig. 2A), this decay is overprinted during rising tide during the Bremerhaven test. The absolute initial pore pressures (assuming the harbor sediments to exhibit hydrostatic stress state) measured range between 30-50 kPa. In contrast, the initial pore pressure peak in the silty sands of Kuhgraben was ca. 10 kPa in excess of hydrostatic

(see Fig. 2B). Moreover, the sands show a more rapid pressure decay due to their higher permeability as well as a lower water head.

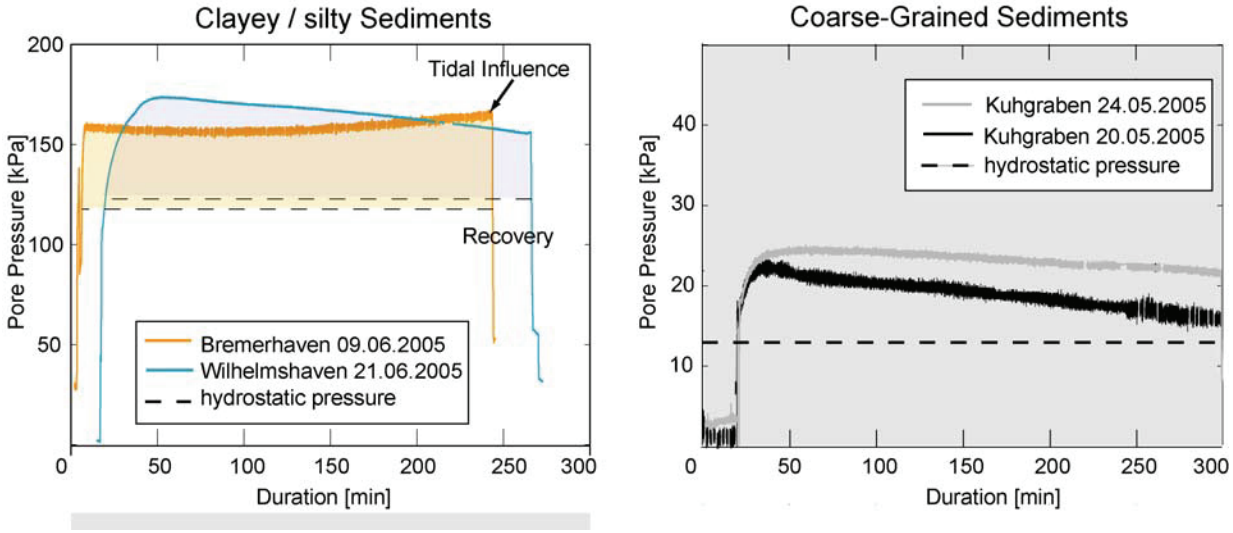

Figure 2 Pore pressure data from various FFCPT deployments with hydrostatic pressure at the seafloor for reference (dashed lines): (A) Fine-grained sediments; (B) Coarse-grained sediments. Note different scale of y-axes!

In conclusion, we present data from our first successful multiple deployments of a new FFCPT in unconsolidated sediments of variable grain size. *In situ* friction measurements agree with those from standard CPT tests in the literature (Lunne et al., 1997). Pore pressure curves indicate moderately fast decay rates of induced pore pressure, shedding light on the possible stress response of those sediments. Our device is time- and cost-efficient, and – in its lightweight configuration - may be used from small platforms and without a winch or crane.

Acknowledgements

M. Lange is acknowledged for valuable suggestions and immense help with construction, programming, and testing of the FFCPT. Our colleagues V. Berhorst, B. Heesemann, N. Kaul, and T. Mörz provided valuable discussion. S. Potthoff is also thanked for supporting the Wilhelmshaven tests. Funding for this research was provided by the German Science Foundation (DFG) to the Research Centre Ocean Margins. This is RCOM publication # 0323.

References

Lunne, T., P.K. Robertson, and J.J.M. Powell (1997). Cone Penetrating Testing In Geotechnical Practice, Spon Press, pp. 312

Maltman, A. (ed.) (1994). The Geological Deformation of Sediments, Champman & Hall London, pp. 362.

Stegmann, S., Villinger H. and A. Kopf. (2006). Concept and Design of a modular, marine Free-fall CPT system - A time- and cost-efficient device for *in situ* geotechnical characterisation of marine sediments, Sea Technology, in press.

Strout, J. M., and T.I., Tjelta (2005). "In situ pore pressures: What is their significance and how can they be reliably measured?" Marine and Petroleum Geology 22, 275-285.

4.2. Initial Results of a new Free Fall-Cone Penetrometer (FF-CPT) for geotechnical *in situ* characterisation of soft marine sediments

Stegmann, S., Mörz, T., and Kopf, A., Norwegian Journal of Geology, 86, 3, 199-208. published in 2006.

Initial Results of a new Free Fall-Cone Penetrometer (FF-CPT) for geotechnical *in situ* characterisation of soft marine sediments

Sylvia Stegmann, Tobias Mörz & Achim Kopf

Stegmann, S., Mörz, T. & Kopf, A.: Initial Results of a new Free Fall-Cone Penetrometer (FF-CPT) for geotechnical in situ characterisation of soft marine sediments. *Norwegian Journal of Geology*, Vol. 86, pp. 199-208. Trondheim 2006. ISSN 029-196X.

Two of the most crucial sediment physical parameters controlling slope stability and trigger mechanism of mass movements are shear strength and excess pore pressure. Since both of them require in situ measurement, Cone Penetration Testing (CPT) is an ideal method to characterise *in situ*. While standard CPT tests penetrate of sediments at constant rate, a new free fall cone penetrometer (FF-CPT) for shallow-water application down to 200 m water depth has been developed. Its modular, lightweight design allows us to operate from small platforms to research vessels. The length (0.5 m – 6.5 m) and the weight (40 kg – 170 kg) of the device can be adapted according to the geological setting and main scientific interests. Here we present our initial results as a "proof-of-concept". In five locations with variable sediment composition, the lance was deployed with different penetration velocities ranging from 30 cm/s to free drop in different weight- and length-modi. Based on the primary data (acceleration, cone resistance, sleeve friction, pore pressure), we mainly focus on dissipation of insertion pore pressure and a first-order sediment classification. The results show an influence of the different penetration velocities on pore pressure regarding to its evolution over the time and on the magnitudal strength parameters. Finally, our preliminary data suggest that the time- and cost-effective use of our marine FF-CPT is an appropriate alternative to standard CPT measurements.

S. Stegmann, T. Mörz & A. Kopf, Research Centre Ocean Margins, University Bremen, Leobener Strasse/MARUM Building, 28359 Bremen, Germany. email: stegmann@uni-bremen.de

Introduction

Marine sediments consist of a skeleton of mineral grains and pore space, which is usually occupied by aqueous and gaseous fluids (Maltman 1994). The stability of the sediment is controlled by the forces between the grains (cohesion) and the pressure of the fluids in the pores (Strout & Tjelta 2005). While the first depends on the mineralogy of the grains, the latter is a function of physical properties such as water content, state of consolidation, or grain size distribution. Variability in one or more sediment physical properties may result in instability and failure. Geological processes, which are capable of causing pore pressure increase and weakening of the sedimentary framework include tectonic deformation, earthquakes, rapid sediment accumulation, gas-hydrate melting or tidal/storm wave loading (e.g. Hampton et al. 1996; Locat & Lee 2002). In this context, Cone Penetration Tests (CPT) represent a widely used, time efficient method for the *in situ* characterisation of the physical properties of the sediments and their variability. (Chari et al. 1978; Konrad 1987; Bennett et al 1989; Lunne et al. 1997; Christian et al. 1993; Wright 2004). Standard probes measure the cone and sleeve resistance (as a first order estimate of sediment strength), pore pressure in defined locations (u_1, u_2, u_3), tilt, and temperature (Lunne et al. 1997). Apart from this set of primary data, a number of secondary physical-sedimentary parameters can be calculated. If the insertion pressure and velocity profile during penetration of the probe are known, undrained shear strength (Esrig et al. 1977) and consolidation ratio (Bennett et al. 1985) may be derived. As a consequence, CPT tests play a significant role in the assessment of the underground in offshore construction, and the stability of subsurface sediments deposited on continental shelves and slopes. In this paper we present the initial results of a recently developed FF-CPT device for soft sediments. In contrast to industrial CPT procedures, where the probe is pushed hydraulically at a constant rate (2 cm/s), our lightweight, cable-controlled lance may be universally deployed. Its modular design, with optionally added weights (up to 60 kg) and extension rods (0.5 m–6.5 m total length) allows us to control the maximum penetration depth and tackle various scientific questions. In this manuscript, we provide a "proof of concept" and illustrate how we vary weights, extension rods, and winch speed to accommodate for various settings (soft vs. indurated sediment) and deployment platforms (free-fall mode vs. crane or winch). In addition, long-term testing records of pore pressure dissipation after insertion may help us to assess whether

intrinsic sediment strength or excess pore pressures are likely to trigger shallow submarine mass movements.

Instrument design, theoretical background, and methods

Design of the FF-CPT

A marine free-fall FF-CPT has recently been developed for 200 m water depth at the Research Centre Ocean Margin (RCOM) at the University of Bremen (Fig.1). We use the term "free-fall" to distinguish between our gravity-driven deployment style and the hydraulically pushed standard CPT tests. However, most of the deployments are carried out with controlled speed using a winch, while very rarely, we deploy in free drop (i.e. only when the underground is known to be free of rocks, etc.).

Our instrument consists of an industrial standard 15 cm^2 cone penetrometer manufactured by GEOMIL (Netherlands), which is equipped with an absolute pore pressure sensor (2 MPa), an inclinometer (25°), and a temperature sensor. Load cells measure the sediment resistance acting on the cone during penetration. The force acting on the cone, divided by the cone base area (Fig. 1a) produces the cone resistance q_c. The force acting on the sleeve friction in relation to the surface of the sleeve area (Fig. 1a) is defined as the sleeve friction f_s (Lunne et al. 1997). The sleeve friction load cell records the sum of the cone resistance and the sleeve friction. This principle defines a subtraction cone, which is used in our device. Sleeve friction is obtained from the difference in load between the friction and cone resistance load cells (Lunne et al. 1997). The tilt sensor in the lowermost part of the lance provides information on the angle of penetration. A waterproof housing at the upper end of the lance, fitted with micro controller and data-acquisition, an acceleration sensor and the power supply, provides autonomous FF-CPT measurements even on very small vessels and research platforms (Fig. 1b). Concerning weight and the length, our lance is characterised by a modular design. Depending on the sediment strength the lance can be mounted optionally with extension rods (up to 6 1-m-pieces) and weights (up to 4 x 15 kg-pieces). In the short mode, the FF-CPT weighs about 40 kg (Fig. 1c), whereas the

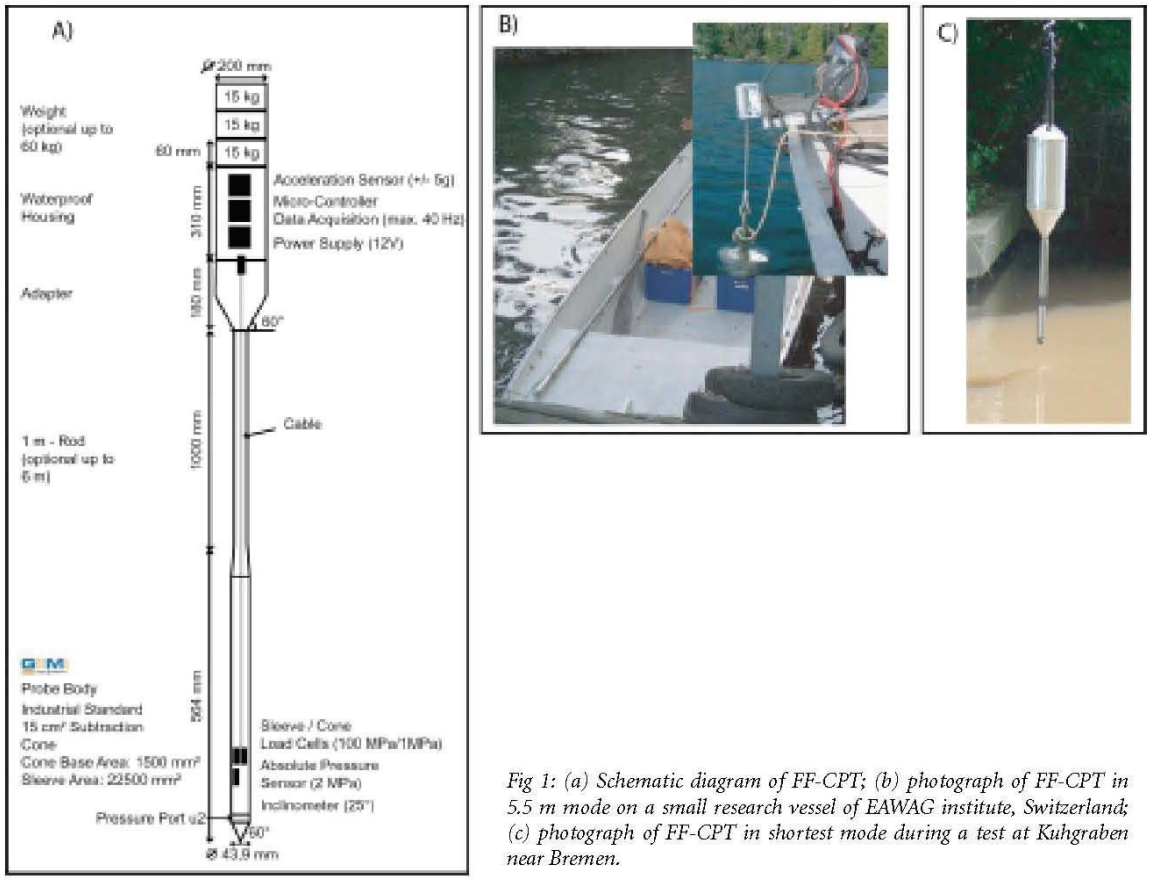

Fig 1: (a) Schematic diagram of FF-CPT; (b) photograph of FF-CPT in 5.5 m mode on a small research vessel of EAWAG institute, Switzerland; (c) photograph of FF-CPT in shortest mode during a test at Kuhgraben near Bremen.

weight totals approximately 170 kg if all extension rods and extra weights are mounted. In short to moderate mode, the FF-CPT can be deployed by two people from small platforms; recovery is aided by a standard 4x4 car winch. In this way, we ensure maximum flexibility in the use of our lance depending on different scientific questions. For further description of the design and the application of the FF-CPT see Stegmann et al. (2006).

Testing methods and data handling with the FF-CPT

Variation of the penetration velocity and the weight is useful for controlling the penetration depth. As can be seen from Figure 1, variable penetration is achieved by three factors:

(i) Length of the frontal part of the lance,
(ii) Weights added to the head of the lance, and
(iii) Penetration velocity.

While the first two parameters have to be set prior to the test (see Fig. 1b, c), the velocity is varied during the test. So far, we have tested at velocities ranging from free drop (ca. 600 cm/s) to various winch speeds upon penetration (30-200 cm/s). However, lower velocities are possible, and we have also conducted tests in clayey mud where the probe is placed at the sediment-water interface and then sinks in by its own weight (estimated rates ca. 1 cm/s in cohesive mud). In any case, velocity is decreasing with increasing penetration depth (and cohesion along the lance's surface), and has to be integrated in order to provide exact depth profiling. Almost 30 years of standard CPT testing (chiefly industrial) provide a sound base for the interpretation of data acquired during tests with non-linear penetration velocity (our FF-CPT device). The immense amount of data, predominantly collected onshore, is compiled in a fundamental and widespread overview by Lunne et al. (1997).

Measured and derived physical properties of FF-CPT tests

Primary parameters

The crucial geotechnical parameters measured in FF-CPT tests are cone resistance (q_c), sleeve friction (f_s), acceleration, and pore pressure (u). In contrast to standard CPT tests where the lance is pushed by hydraulic force at a constant velocity of 2 cm/s, penetration velocity varies with depth both in free-fall mode and when lowered using a winch. This change in penetration velocity has profound effects on the primary parameters and is a subject of this paper. Also, the terminal depth (TD) of penetration of the FF-CPT is not a simple function of time (as in the pushed tests), but a complex deceleration path caused by the sedimentary succession encountered. The built-in acceleration sensor is used to reconstruct the penetration velocity and to assign depth to the data. As an additional control of total insertion depth, we measure the length along which material is stuck to the lance. However, this can only be done during individual tests, but not when running multiple penetration experiments (pogo-style deployment). Prior to individual measurements, calibration of the probe is performed in air as well as in the water column to monitor its potential offset. Before testing, the pore water port and filter element are filled/saturated to minimise artefacts in pressure measurement. Depending on the penetration velocity and on the duration of the test, an adequate frequency for data acquisition is chosen (up to a maximum 40 Hz). From the main parameters of FF-CPT experiments, both cone resistance and sleeve friction are strongly rate-dependent. As we are measuring in saturated sediments, the pore pressure is the sum of hydrostatic pressure and excess pore pressure (Maltman, 1994). Assuming that the pore fluid is in conjunction with the hydrostatic system at our test sites, we subtract the hydrostatic pressure of the water column plus penetration depth from the measured pressure data and obtain the excess pore pressure induced upon insertion of the lance.

Secondary paramaters

There are a number of secondary parameters which can be easily derived from the sensor data. These include both empirical, CPT-specific measures such as the friction ratio, but also well established parameters such as undrained shear strength or permeability. The main aim of estimating sediment strength by measuring cone resistance and sleeve friction is a first order sediment classification, whereby cone resistance is a measure of the stiffness of the sediment (Lunne et al. 1997). It should be noted here that this strength parameter is not a measure for static resistance, but records the dynamic resistance depending on the penetration rate. In cohesive sediments, this increase of penetration velocity results in an increase in cone and sleeve resistance (Dayal & Allen 1975a). The increase of q_c is described as a logarithmic increase with penetration velocity (for 0.13 cm/s < v > 81 cm/s). In non-cohesive, granular sediments, this relationship is less pronounced, or absent (Dayal & Allen, 1975b). To identify several soil types, the ratio between f and q (also known as friction ratio) is generally used, where greater values correspond to fine-grained sediments, and vice versa (Fellenius & Eslami 2000). The first soil classification chart for electrical penetrometer measurements was published by Douglas & Olsen (1981). Robertson (1990) used a similar method (plotting friction ratio vs. cone resistance), but recalculated the effect of pore pressure on

cone resistance, as expressed in the corrected cone resistance q_t (Robertson 1990):

$$q_t = q_c + u_2 (1-a)$$

where: q_t = cone resistance corrected for pore water pressure
q_c = measured cone resistance
u_2 = penetration pore pressure measured on cone shoulder
a = ratio between shoulder area (cone base) unaffected by the pore water pressure to the total shoulder area, here: 0.6

Robertson's classification chart includes 12 different soil types based on grain size composition, amount of organic matter, stiffness and overconsolidation ratio (Robertson, 1990). For standard CPT tests the corrected cone resistance q_t can be used to estimate the undrained shear strength of the sediment (s_u). It is represented by the ratio between the sum of q_t and the cone factor Nc, which is a function of sediment rigidity and *in situ* stress state. Lunne et al. (1997) give an overview of several theoretical solutions for the factor N_c, which ranges in natural systems from 10 – 18. Esrig et al. (1977) suggest the empirical relationship for moderately to highly sensitive marine sediments:

$$S_u = U_{imax}/6,$$

where: S_u = undrained shear strength
U_{imax} = maximum excess pore pressure.

As our tests have been carried out with different, non-linear velocities, we use this relationship to determine the undrained shear strength.

Complementary Laboratory Testing

Sediment samples have been analysed in the laboratory to get reference data for the interpretation and quality assessment of the *in situ* FF-CPT data.

Grain Size Distribution

A Beckman Coulter LS200 laser particle counter was used for grain size distribution analysis. It is capable of measuring particles between 0.37 and 2000 µm, so that the fraction coarser than 2 mm has to be separated by sieving prior to the measurement. The vessel for the sample (50-2000 mg) is moved relative to the 750 nm-laser during the measurement. Each analysis monitors 92 grain size categories controlled by a multi-element sensor. The data are presented in Table 2 and serve as a reference for the interpretation of the FF-CPT results.

Vane Shear Testing

Vane shear tests were conducted using a viscosimeter device manufactured by Haase, Germany, equipped with a miniature vane. The device is motor-driven and measures the torque and rotation angle of the vane. Shear strength values are optioned from the torque measurements and the known vane geometry following standard procedures. (e.g., DIN 18130, BS1377). Values are used for comparison with the undrained shear strength as derived from FF-CPT parameters.

Results and discussion

The test sites chosen for our initial FF-CPT testing mostly lie in the vicinity (100 km radius) of the city of Bremen for convenience's sake. The only exceptions were two short cruises with multiple deployments in "normal" as well as gas-rich muds in the Mecklenburg and Eckernförde Bights, Baltic Sea (Table 1). The two main criteria for their selection was (i) knowledge of the local deposits, and (ii) some variation in fluid char-

Table 1.

Location	Water depth (m)	Deployment	Weight (kg)	Length (m)	Penetration depth (m)	Number of individual tests	Duration of dissipitation (min)
Kuhgraben	1	controlled (50cm/s) - free drop	40 - 70	0.5	0.1 - 0.5	5	10 - 300
Hemelinger See	6	controlled (70-130 cm/s)	125 - 170	3.5	1.3 - 2.0	2	25
Wilhelmshaven	9	controlled (30cm/s)	100	5.5	2.5	1	240
Osthafen	11	controlled (30cm/s) - free drop	160	5.5	5.5 - 5.9	2	30
Baltic Sea (Mecklenburg Bight/Eckernförde Bight)	20 - 30	controlled (50 cm/s-200 cm/s)	90 - 140	2.5 - 3.5	1.9 - 2.8	3	5 - 90

Table 1: Location, water depth, and FF-CPT testing mode (velocity, added weight and length of lance, number of individual tests, duration).

ging for the pore pressure tests. With the sites selected, we cover the full range of clay-rich mud through sandy silts, some of which are normally consolidated while others are organic-rich harbour muds (e.g. Wilhelmshaven) or soupy material from pockmark fields (Eckernförde). Details about the geological setting are not so important for this paper, but the local names are given throughout for clarity (please refer to Tables 1, 2 for sites, testing procedures, etc.).

FF-CPT measurements

Initially our FF-CPT tests were aimed to study the effect of variable weight of the lance on total depth of penetration. Figure 2 provides an example of a series of tests in short mode (Fig. 1c) with variable weight and in free drop versus controlled winch speed of 50 cm/s. It can be seen that for the relatively coarse-grained sediment (Kuhgraben), each added 15 kg weight amounts to an extra 20 cm penetration.

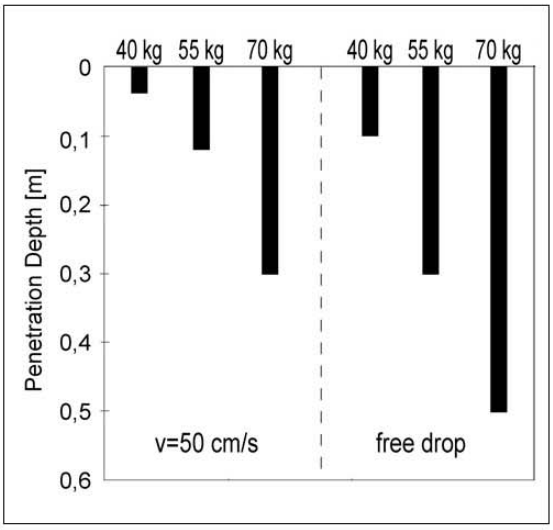

Fig 2: Example of varying penetration depth as a function of different deployment mode (winch vs. free-fall) and total weight. See also Table 1.

Figure 3 exemplifies the results of a FF-CPT test in silty mud (Mecklenburg Bight, Baltic Sea, see Table 1), mainly dedicated to the penetration behaviour and the records of the different sensors. The penetrometer was launched with a speed of 200 cm/s. Acceleration (Fig. 3a), or better: decelaration, is used to obtain penetration velocity and total depth of penetration by integration. It can be seen that the initial insertion velocity of ca. 200 m/s decreases rapidly to about half that value within the uppermost 35 cm below the sea floor (cm bsf; Fig. 3a). Penetration speed then drops less rapidly for the stiffer underlying muds before the probe comes to a complete halt at 220 cm bsf. Both cone resistance qc (Fig. 3b) and sleeve friction f_s (Fig. 3c) show an increase in the upper part of the penetrated sediment, with the maximum cone resistance being >500 kPa. Figure 3d shows the "excess pore pressure" evolution upon and during penetration, with the hydrostatic pressure (P_{hyd}) having been subtracted from the total pressure readings. Again, the strongest deviation of the curve is observed at 35-40 cm bsf, suggesting that a discontinuity is met. When comparing all sensors at this depth level, it can be seen that values near 7 m/s^2 as well as profound increases in cone resistance and sleeve friction point towards a harder horizon (Figs. 3a-c). In contrast, the initial pore pressure increase induced by the impact of the FF-CPT suddenly ceases, reaching even negative pressures for a fraction of a second (Fig. 3d, 35-40 cm depth). This observation is consistent with other tests at high insertion speed in coarser-grained sediments (e.g. Kuhgraben; see below).

To gain insights into the evolution of excess pore pressure dissipation after impact of the FF-CPT, the complete data record has to be embraced. Figures 4 and 5 provide examples of pressure behaviour at various scales and modes. This is merely to shed light on the influ-

Table 2.

Location	Mean Grain Size (% clay/silt/sand)	Penetration Depth (m)	Max. excess pore pressure after insertion (kPa)	Undrained Shear strength (kPa) (in situ with CPT derived by Esrig (1977)	Undrained Shear Strength (kPa) (Vane Shear)
Kuhgraben	10/55/35	0.1 - 0.5	15	2.5	3.1
Hemelinger See	10/62/28	1.3 - 2.0	20/40	~3.5	
Wilhelmshaven	12/59/29	2.5	34.5	5.7	
Osthafen	14/73/13	5.5 - 5.9	16	2.6	2.5
Baltic Sea	14/81/5	1.9 - 2.8	43/60	7/10	

Table 2: Location, grain size distribution, excess pore pressure after insertion, and undrained shear strength from vane shear and CPT testing, based on the empirical relationship by Esrig et al. (1977).

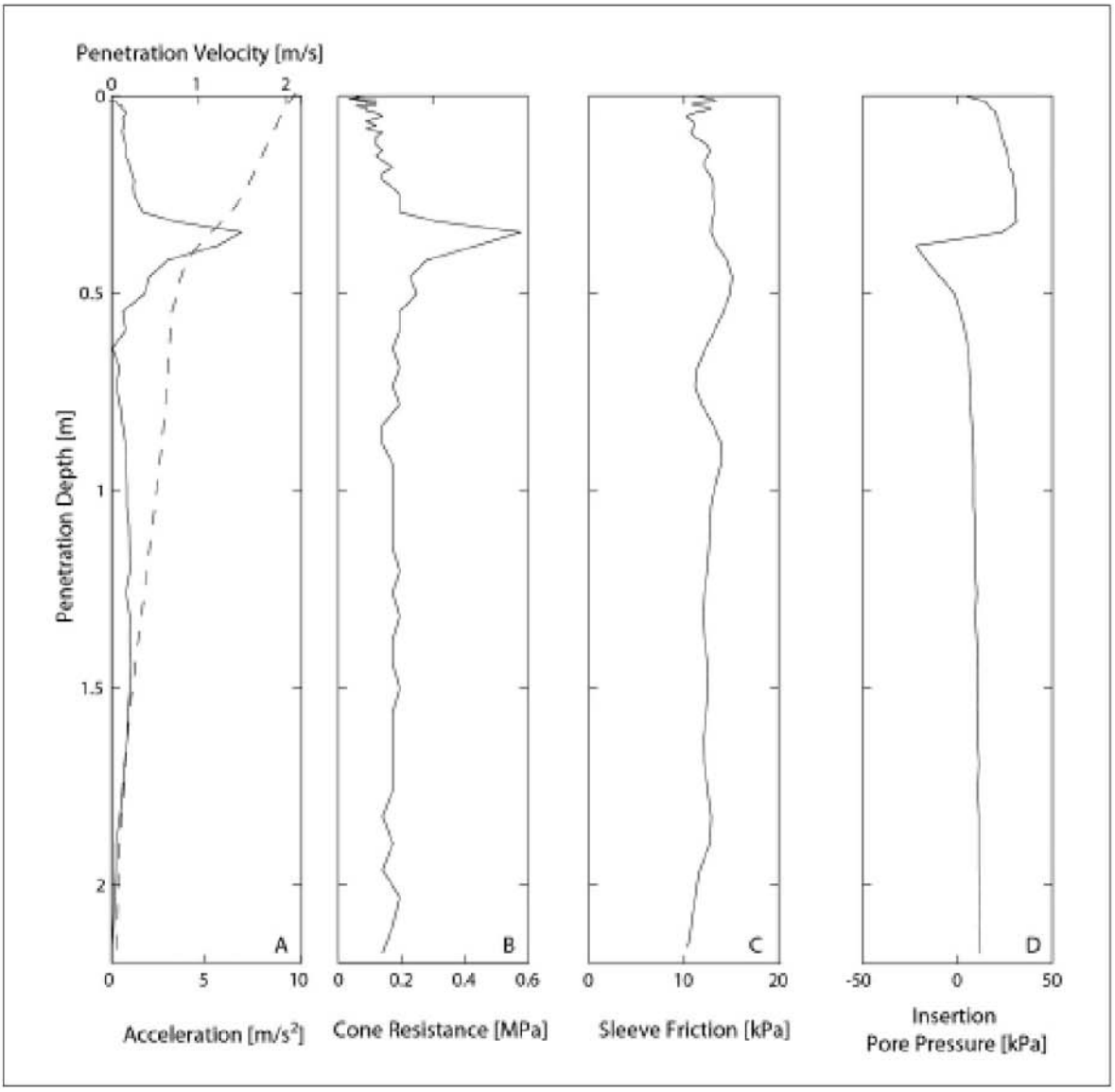

Fig 3: Diagram showing a set of parameters measured with the CPT in clayey mud in the Baltic Sea: (a) Acceleration (overlain by penetration velocity, as derived from deceleration), (b) cone resistance, (c) sleeve friction, and (d) insertion pore pressure. For details, see text and Table 1.

ence of the sediment composition, impact velocity, and different evolution of the pressure signal with time. In Figure 4, we compare the finer grained end of our suite of samples (Osthafen, Baltic Sea), while Figure 5 focuses on the coarser grained end members at Hemelinger See and Kuhgraben. Figure 4a illustrates the induced excess pore pressure evolution caused by the impact of the FF-CPT into Osthafen muds at variable rates (30 cm/s vs. free drop [according to the P_{hyd} data with time, this amounts to ca. 600 cm/s]). It can be seen that pressure increase is more inert at high insertion rate, with the excess pore pressure still increasing after 25 minutes past insertion. In contrast, moderate deployment velocity causes a distinct pore pressure maximum of about 16 kPa after less than 5 minutes, followed by an equally rapid decay to about half that value 10 minutes later (t_{50} value). We attribute this fact to a pressure pulse (or wave) of fluids being displaced and driven away from the probe in case of rapid deployment. In general, we acknowledge this effect to be more profound in coarser-grained sediments. If we disregard the artificial overpressures and compare sediments with naturally high fluid pressures of the Baltic Sea, we observe striking similarities. Figure 4b compares slow deployments (50 cm/s winch speed) into the mud from Mecklenburg Bight (regular deposition) and the Eckernförde Bight

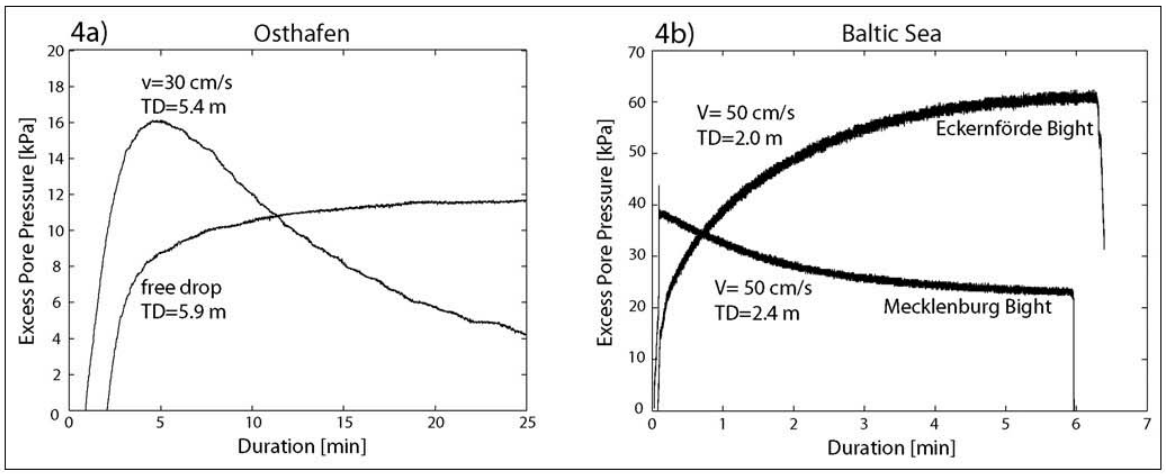

Fig 4: Pore pressure evolution during FF-CPT tests in some of our test sites. (a) Pressure response to FF-CPT insertion at 30 cm/s and free-drop (ca. 600 cm/s) into muds at Osthafen; (b) Pressure response of "normal" mud (Mecklenburg) and gassy mud of a pockmark field (Eckernförde) in the Baltic Sea, both from deployments at winch speeds of 50 cm/s. Note the different behaviour during as well as after insertion. All plots show "excess" pore pressure values along the y-axes since hydrostatic pressure was subtracted. TD means terminal depth. See text for details.

(gas-charged mud in a pockmark area). At the Mecklenburg site, a maximum pore pressure peak is reached almost immediately (ca. 44 kPa), which is followed by an exponential decay with time. In the pockmark area, however, no such peak is seen; instead, excess pore pressure is constantly increasing with time until reaching a plateau at about 60-65 kPa after 6 minutes (Fig. 4b). We interpret the latter value close to the ambient pore pressures in the gas-charged mud. However, *in situ* pore pressures at the Mecklenburg site are at best one third of those at Eckernförde, because the decay has not reached the background plateau value. Taken the observations of Figures 4a and 4b together, we can state that the FF-CPT is capable of detecting different pore pressure responses, no matter whether they are caused by deployment artefacts or natural processes.

When looking at the results of tests into the coarser grained deposits of e.g., Hemelinger See and Kuhgraben (Fig. 5), we observe a somewhat different pore pressure response than in the finer muds (Fig. 4). The first objective was to shed light on the influence of both insertion speed and total weight of the probe, as illustrated by the data from four tests in Hemelinger See (Fig. 5a). In all cases, we observe a distinct pore pressure peak upon insertion, which is rapidly followed by a drop by several kPa. Only after 1-3 minutes, pore pressure signals pick up again and rise steadily (Fig. 5a). Regardless of the total weight of the probe, it is seen that the slower deployment (dashed curves) results in a more accentuated pressure drop, but also a higher total pore pressure reading. Maximum excess pore pressures of the slow deployments exceed that with roughly twice the insertion speed by 3-8 kPa (or ca. 10-50%; see period from 5-25 mins. in Fig. 5a). The net pore pressure drop after the insertion pore pressure peak is also higher in the slow deployments (8 [125 kg] and 13 kPa [170 kg], respectively) than in their fast counterparts (6 [125 kg] and 4 kPa [170 kg], respectively). In addition to the insertion velocity, the total weight has a profound impact on both cone resistance (not shown) and excess pore pressure. In exactly the same location, doubling the speed of deployment causes almost exactly doubling of the pressure readings on the path of the curves where pore pressure build-up occurs (5-25 mins, Fig. 5a). This quasi-systematic behaviour is beneficial when relating FF-CPT data to results from standard CPT tests (see discussion below).

If the insertion velocity is increased even further, we also expect the "trough" after the initial pore pressure peak to develop more profoundly. This behaviour was already seen in the Baltic Sea mud where penetration of a silt layer caused negative excess pressures (i.e. displacement of water) after the initial increase (see Fig. 3d., 35-40 cm depth). This trend is even more profound when slightly coarser Kuhgraben sediments (Table 2) are penetrated at speeds as high as 600 cm/s (=free drop). Figure 5b shows two of the free drop tests with different total weights of the FF-CPT in comparison to a controlled deployment at 50 cm/s winch speed. A blow-up of the initial portion of each of these tests confirm the already known pore pressure response. The slow deployment causes a steady pressure increase with only ca. 5 kPa in excess of P_{hyd}. In contrast, the pore pressure evolution after free-drop deployment shows immediate negative pressures of down to –70 kPa, which become positive within less than a second and then climb to max. excess pressures of approximately 10 kPa. As a function of the difference in total weight,

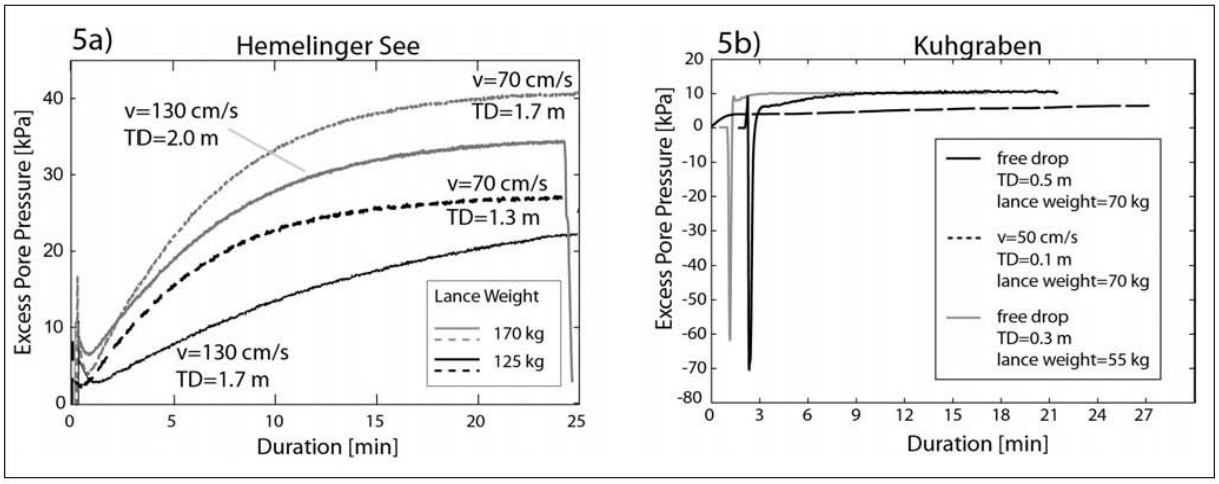

Fig 5: Pore pressure evolution at test sites Hemelinger See and Kuhgraben. (a) Comparison of four tests at Hemelinger See in sandy and clayey silt, with variable deployment rate (70 and 130 cm/s) and weight (125 and 170 kg totally) of the FF-CPT. Dashed lines represent the lower insertion speed in each mode. Note the pressure drop immediately after insertion, which is followed by an increase with time; (b) Comparison of three tests at Kuhgraben sandy and clayey silt, showing the profound difference in pore pressure response between low winch speed (50 cm/s) and free drop (upper two curves). All plots show "excess" pore pressure values along the y-axes since hydrostatic pressure was subtracted. TD means terminal depth. See text for details.

there are slight variations in the two free-drop tests. With the FF-CPT weighing 55 kg, we see a net pressure drop of 62 kPa, while the net decrease is 79 kPa in the 70 kg configuration (Fig. 5b). Similar to what was said above, this somewhat predictable behaviour is beneficial for the interpretation of FF-CPT tests when related to pushed CPT tests (see below).

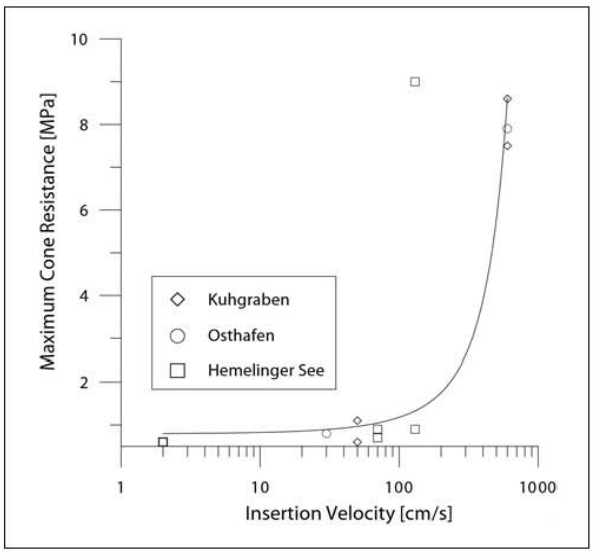

Fig 6: Cone resistance versus insertion velocity for eleven FF-CPT tests in clayey and sandy silt at our test sites. Please note the log-linear relationship in our data sets. The dashed line at 81 cm/s marks the insertion velocity highlighted by Dayal and Allen (1975b); see text for discussion.

Another way of assessing the effect of the insertion velocity on data acquired is to study variations in cone resistance. Figure 6 summarises tests at various velocities at the Hemelinger See, Kuhgraben and Osthafen sites. Without paying too much attention to the slight variations in sediment composition (see Table 2), we observe a log-linear relationship between q_t and insertion speed in these silt-dominated deposits. We will further follow that route by carrying out more tests at each site with different insertion speeds.

Geotechnical Parameters derived from FF-CPT Results

As already introduced above, CPT tests can be used for soil classification purposes when a couple of prerequisites are met. According to Robertson (1990), cone penetration testing allows to distinguish between 12 sediment classes. Plotting the friction ratio versus the corrected tip resistance q_t, and implementing these data into the above mentioned Robertson chart, we can identify the majority of our tested sediments in the fields "clay", "sensitive fine-grained soil", "silty clay to clay", and "clayey silt to silty clay" (Fig. 7). This agrees well with results from particle size analyses according to which most specimens have clay/silt contents of > 80% and ca. 95% as well as high contents of organic matter (see Table 2).

If we look at FF-CPT tests run at higher insertion velocities (100 cm/s and above), however, we observe significant disagreement between the anticipated value obtained at lower velocity (see large symbols in Fig. 7). For instance, both Osthafen clayey silt and Kuhgraben

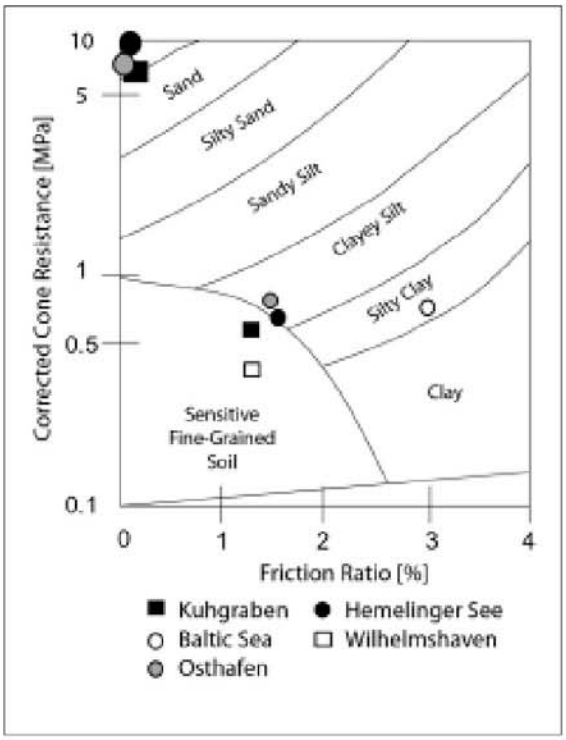

Fig 7: First-order sediment classification (based on Robertson's chart [1990], modified) of deployments at Wilhelmshaven, Osthafen, Hemelinger See, Mecklenburg Bight (Baltic Sea) and Kuhgraben. For those sites where fast (v = >81 cm/s) were carried out, results are shown as large symbols (see inset: Legend). For details, see discussion in text and Figure 6.

and Hemelinger See clayey and sandy silts show very high cone resistance values, and hence plot in the field of pure sand. This implies that for the more rapid of our deployments, a reliable soil classification is severely hindered. It can be seen that the higher the velocity, the more data shift towards the upper left portion of the diagram (Fig. 7). We conclude that friction ratios may get less reliable when penetration velocity is high, because qc is up to 4-fold higher than in the deeper section when momentum has been lost (see Fig. 3b,c). As outlined above, the force measured during penetration of the FF-CPT probe can be translated into undrained shear strength under certain assumptions (see discussion in Esrig et al., 1977). In our experiments, the insertion pressure ranged from 15 kPa to 60 kPa for the total of 13 tests conducted so far (see Table 1 for details). Based on the FF-CPT experiments, undrained shear strength was calculated for all five locations (Table 2). The finer-grained sediments in Osthafen, Wilhelmshaven, and the Baltic Sea are characterised by a relatively wide range of shear strengths from 2.6 kPa to 10 kPa. This may be explained by the different degree of consolidation, which is also mirrored by the difference in total penetration depth (1.9 m - 5.5 m). However, vane shear tests of the Osthafen mud, which were carried out on the surface of a split gravity core, gained 2.5 kPa. The coarser materials show undrained shear strengths of 3.5 kPa (Hemelinger See) and 2.5 kPa (Kuhgraben; see Table 2). Vane shear tests on the latter material were carried out as a reference measurement, and lie higher (3.1 kPa). We conclude that the elevated permeability of the Kuhgraben sandy silt allows water to dissipate very rapidly during FF-CPT impact, so that the insertion pressure monitored at u_2 is biased by negative pore pressures, and thus underestimates the total pressure upon impact.

Conclusions

- We can show that our new FF-CPT device may be used for time-effective *in situ* measurements from nearly any platform in the estuarine or marine realm (Fig. 1).
- Given the modular design of our FF-CPT, we are able to specifically address certain depth levels and hence may perform step-like dissipation tests with the probe to examine different sedimentary layers (see Stegmann et al. 2006, p.29). This includes long-term dissipation tests as well as deployments at variable penetration velocities or weights (Figs. 4-5).
- From the FF-CPT tests carried out so far in clayey and sandy silt, we obtain a log-linear relationship between cone resistance at the probe and insertion velocity. This may allow us to compare FF-CPT data with results from pushed standard CPT tests within certain limitations.
- Comparing the published soil classification charts (e.g., Robertson 1990) with our FF-CPT data and grain-size analysis, *in situ* classification of the tested sediments agrees well with the laboratory measurements (Fig. 6 and Table 2).
- Pore pressure and sediment strength should show a positive correlation in FF-CPT tests, because a certain degree of consolidation/stiffness is required to allow the build-up of a significant pore pressure artefact. Our results of combined FF-CPT, grain size and vane shear analyses indicate that clay content alone does not necessarily result in lower permeability and more rapid pore pressure build-up. In fact, the opposite is suggested when data from Osthafen and Kuhgraben mud are compared. While the first does not exceed excess pressures of 4 kPa (min. dissipation value) to 16 kPa (max.), the latter covers a range from –50 kPa (initial fluid displacement) to 10 kPa in excess of hydrostatic pressure.
- More generally, we can state that the FF-CPT is capable of detecting different pore pressure responses in marine (or estuarine) sediments, no matter whether they are caused by deployment artefacts or

natural processes. This way the device is powerful in distinguishing between the influence of pore water overpressures on the one hand, and weak strength (from q and f) on the other hand as potential triggers of slope instability.

- The correlation of the pore pressure signal and shear strength (for CPT and laboratory tests) is ambiguous, most likely because of the large number of variables such as insertion velocity, total weight etc. during FF-CPT deployment. More testing will be carried out to analyse the influence of the variable parameter of our dynamic measurements.

Acknowledgements: M. Lange is acknowledged for valuable suggestions and immense help with construction, programming, and testing of the FF-CPT. M. Lange and A. Seifert assisted with measurements in the Baltic Sea, for which we thank them sincerely. Our colleagues V. Berhorst (Geomil, Netherlands), H. Villinger, B. Heesemann, N. Kaul provided valuable discussion. S. Kreiter, A. Seifert, G. von Halem and J.B. Struut helped with laboratory testing. B. Buck, A. Schröder, S. Spahic, M. Geisen (Osthafen), S. Potthoff (Wilhelmshaven), and T. Wever and R. Lühder (Baltic Sea) have been extremely supportive during various parts of our experiments. The manuscript benefited from the valuable, detailed suggestions by Jim Strout and an anonymous referee, as well as the superb editorial handling by Anders Solheim. Funding for this research was provided by the German Science Foundation (DFG) to the Research Centre Ocean Margins. This is RCOM publication no. 0398.

References

Bennett, R.H., L. Huon, P.J. Valent, J. Lipkin & M.I. Esrig, M.I 1985: In situ undrained shear strengths and permeabilities derived from piezometer measurements. *In* R.C. Chaney, R.C. & Demars, K.R. (Eds.), Strength Testing of Marine Sediments: Laboratory and In Situ Measurements. *American Society for Testing and Materials*, 88-100.

Bennett, R. H., Li. H., Burns, J.T., Perscival, C.M. & Lipkin, J. 1989: Application of Piezometer Probes to Determine Engeineering Properties and Geological Processes in Marine Sediments. *Applied Clay Science* 4, 337-355.

Chari, T.R., Smith W.G. & Zielinski, A. 1978: Use Of Free Fall Penetrometer In Sea Floor Engineering. In Oceans '78 "The ocean challenge"; *Fourth annual combined conference sponsored by the Marine Technology Society and the Institute of Electrical and Electronics Engineers*, 686-687.

Christian, H.A., Heffler D.E. & Davis, E.E 1993: Lancelot - an in situ piezometer for soft marine sediments. *Deep-Sea Research I* 40, 1509-1520.

Dayal, U. & Allen, J.H. 1975a. The Effect of Penetration Rate on the Strength of Remolded Clay and Sand Samples. *Canadian Geotechnical Journal* 12, 336-348.

Dayal, U. & Allen, J.H. 1975b. A note on friction ratio. *Canadian Geotechnical Journal* 12, 524-526.

Douglas, B.J. & Olsen, R.S. 1981: Soil classification using electric cone penetrometer. American Society of Civil Engineers (ASCE). *Proceedings of Seminar on Cone Penetration Testing and Experience, St. Louis*, 209-227.

Esrig, M.I., R.C. Kirby & Bea, R.G. 1977. Initial development of a general effective stress method for the prediction of axial capacity for driven piles in clay. *Proc. 9th Offshore Technology Conference*, 495-501.

Fellenius, B.H. & Eslami A. 2000: Soil profile interpreted from CPTu data, "Year 2000 Geotechnics" Geotechnical Engineering Conference, Asian Institute of Technology, Bankok, Thailand, 18 pp.

Hampton, M.A., Lee, H.J. & Locat, J. 1996: Submarine Landslides. *Reviews of Geophysics* 34, 33-59.

Konrad, J.-M. 1987: Piezo-friction-cone penetrometer testing in soft clays. *Canadian Geotechnical Journal* 24, 645-652.

Locat, J. & Lee, H.J. 2002: Submarine landslides: advances and challenges. *Canadian Geotechnical Journal* 39, 193-212.

Lunne, T., P.K. Robertson & Powell, J.J.M. 1997: Cone Penetrating Testing. In Geotechnical Practice. Spon Press, 312 pp.

Maltman, A. (Ed.) 1994: The Geological Deformation of Sediments. Champman & Hall London, 362. pp.

Robertson, P.K. 1990: Soil classification using the cone penetration test. *Canadian Geotechnical Journal* 27, 151-158.

Stegmann, S., Villinger, H. & Kopf, A. 2006: Design of a Modular, Marine Free-Fall Cone Penetrometer. *Sea Technology* 47, 27-33.

Strout, J. M. & Tjelta, T.I. 2005: In situ pore pressures: What is their significance and how can they be reliably measured? *Marine and Petroleum Geology* 22, 275-285.

Wright, I., 2004: Geotechnical Investigations Using Mini-Cone Penetrometer Testing. *Sea Technology* 45, 49-52.

4.3. Response of stratified, water-saturated sediments to pushed and free-fall Cone Penetration Test: A comparative field study and a review

Stegmann, S., and Kopf, A., Submitted to Canadian Geotechnical Journal

Response of stratified, water-saturated sediments to pushed and free-fall Cone Penetration Tests: A comparative field study and a review

Stegmann, S.*, Kopf, A.

Research Centre Ocean Margins, University Bremen, P.O. Box 330440, 28334 Bremen, Germany

* corresponding author: stegmann@uni-bremen.de

Abstract

We here present a paper that provides (i) a brief summary of cone penetration testing (CPT) devices for quasi-static and dynamic geotechnical characterisation of sediments, and (ii) results of a systematic study of layered, water-saturated sediments using a cone penetrometer at various modes of deployment. The instrument used is a standard 15 cm^2 piezocone mounted to a modular CPTU (u_2) instrument for shallow marine application. The instrument was deployed in the Weser estuary (Germany) at constant rate (pushed hydraulically at ca. 0.02 m/s) as well as in velocity-controlled, quasi-free fall mode at various winch speeds (0.3, 0.65, 1.35 m/s). Results indicate that regardless of the mode of deployment, the CPTU identifies 4 distinct lithological intervals. At each winch speed chosen, repeated measurements attest a good reproducibility of results. Excursions in both cone resistance and pore pressure appear more accentuated in the "free-fall" tests when compared to the pushed tests, and are most pronounced at the highest winch speed chosen. Although our new data agree well with earlier dynamic tests, it is impossible to establish a systematic relationship between the strain-rate effects and the measured CPT parameters, most likely because of the variability in deployment dynamics and small-scale sedimentological diversity.

Keywords: CPT, field study, penetration rate, strain-rate, dynamic cone resistance

1. Introduction

Cone penetrometers for marine application

The application of soil mechanics and the measurement of physical parameters of seafloor sediments are of emerging importance for engineering as well as scientific research, covering numerous aspects such as (1) off-shore construction (facilities for coastal protection, foundations for mining and drilling platforms, underwater pipelines, cables and tubes, man-

made islands, manned and unmanned installations), (2) sediment stability (submarine slopes, sedimentary transport, silting of harbours, deepening of navigation channels, scour around foundation), (3) deployment and burial of mines, and (4) mooring and anchoring devices in marine sediments. Most of these applications require detailed information about the strength of the seafloor deposits, which can be obtained either by laboratory testing (e.g vane shear probe, fall cone penetrometer, ring shear device, direct shear apparatus) on cored sediments or by *in situ* measurements. In contrast to coring, where sediment may be deformed by the sampling procedure and by removal out of its *in situ* conditions, a variability of measurement techniques have been developed for direct seafloor measurement to estimate soil strength and bearing capacity. In the context of penetration tests the terms 'soil strength' and 'bearing capacity' are linked as the bearing capacity is understood as the pressure, which may cause shear failure in the surrounding sediment of a penetrating object (Terzaghi, 1946).

Cone penetration tests provide one of the most efficient means to comprehensively characterise the non-linear mechanical properties of (surface) sediments (e.g. Yu et al. 2000). During deployment, parameters such as cone resistance q_c (as a measure for bearing strength), sleeve friction f_s (as a measure for cohesion of the soil), pore pressure u in various positions (u_1 through u_3, usually measured in excess of hydrostatic pressure; see Lunne et al., 1997), temperature, deceleration, and tilt are collected. The majority of the sensors are hosted in the 10 cm^2 or 15 cm^2 piezocone, which generally measures only about 30 cm in length. These cones are mounted to metal rods, coils, or free-fall lances. While the first are pushed at a constant rate of 2 cm/s (quasi-static mode) into the sediment, the latter can be deployed at any rate (usually depending on the speed of a winch or crane) up to free drop. For these dynamic modes of deployment, it is critical to accommodate tilt sensors (to check on quality of the measurement, i.e. did the probe penetrate vertically into the sea bottom?) and accelerometers (by measuring deceleration, penetration velocity and depth can be calculated) in the instrument.

In this paper we review the similarities and differences between previous quasi-static and dynamic CPT experiments, and compare them with new data from a series of tests in seawater-saturated, stratified sediments in the Weser estuary, Germany. These tests were carried out with a new, modular free-fall CPTU lance (for details, refer to Stegmann et al., 2006a) which was either pushed hydraulically or deployed from a crane at various penetration rates. The rates chosen, ranging from 0.3 m/s over 0.65 m/s to 1.35 m/s, were selected in order to cover the spectrum of winch speeds usually met on research vessels and other industry platforms.

2. Cone Penetration Testing – a review

Cone penetrometers are one of the most popular geotechnical method used for *in situ* determination of the stiffness of the penetrated material (soil/sediment) on land. In the Roman era, the number of slaves, which were required to push a certain rod into the ground, was used as a measure for the strength of the ground (Song et al. 1999). This crude method to quantify the strength can be considered as a forerunner of cone penetrometer devices, standing out today for an effective ground probing instrument. The first electric cone penetrometer, where the signals were transmitted to the penetrating probe in the ground via a cable inside the hollow penetrometer rods, was developed in Berlin at the Deutsche Forschungsgesellschaft für Bodenmechanik (Degebo) during the 2nd World War (Lunne et al. 1997). An appropriate improvement took place in the 70ies of the last century, when on-shore devices have been modified for seagoing tools to measure the geotechnical strength of sediments *in situ* (Dayal 1978). In the following a brief summary of marine *in situ* sedimentary strength characterisation devices is given, which broadly can be subdivided into two classes:

(1) shallow penetration *in situ* testing, and

(2) deep penetration *in situ* testing.

The first group of instruments concentrates on the properties of superficial sediments (upper 15 meters) and includes (a) vane shear testing (e.g. Fenske, 1957; Taylor and Demars, 1970; Richards et al., 1971), (b) dilatometer testing (e.g. Powell and Uglow, 1988), (c) T-bar testing (Randolph et al., 1998), (d) plate bearing testing (e.g. Harrison and Richardson, 1967), (e) static cone penetration testing (e.g. Johnson and Beard, 1985; Meunier et al., 2004; Wright, 2004), and (f) dynamic cone penetration testing (see references below). Static cone penetration tests have their origin in on-shore CPT experiments, which are a standard engineering procedure to measure soil properties. Static cone penetration has become an industrial standard measurement (see the very comprehensive summary for testing and data interpretation of cone penetration testing given by Lunne et al. [1997]). Following the convention, the cone has an area of 10 cm^2 or 15 cm^2 with an apex of 60°. The friction sleeve has a surface area of 150 cm^2 or 225 cm^2. The penetration rate is 2 cm/s. Most often, the quasi-static "pushed" CPT experiments rely on an abutment such as a truck, metal rig, or equally heavy gear. This is required in order to reach penetration depths significantly higher than 10 m sub-bottom depth (group 2, see above).

The adaption of this measurement principle for the sub-aquatic and marine realm requires huge rigs equipped with a hydraulic system to be lowered and placed on the seafloor, where the penetrometer is pushed by hydraulic force into the sediment (e.g. *Penfeld Penetrometer*

[IFREMER], Meunier et al., 2004). The principle of rigged penetrometers is also frequently used for deep penetration *in situ* testing, oftentimes supplemented with wire line modules. The Dutch company FUGRO developed two versions of penetrometer rigs (e.g. *Seacalf* [1972]), which are operable in water depths exceeding 6000 m and reaching a penetration depth of 50 m (de Ruiter and Fox, 1975). In collaboration with McClelland Engineers and the Norwegian Geotechnical Institute (NGI), a further version of penetrometer rig *Stingray* was developed, where a cone penetrometer is inserted into a whole drilling rod (Ferguson et al. 1977; McNeilan and Bugno, 1985). If only surface sediment physical properties are of interest, shallow penetrometers are a more time- and cost-efficient choice, and – more importantly – they do not influence the stress regime of the tested sediments by loading due to the rig's weight (cf. class 1; see above). Since the 1970s free-fall devices for dynamic penetration tests were constructed. A free-fall device is here defined as an instrument, which penetrates the sediment with its own force, given by the initial acceleration and its weight. The lance is moving downwards through the water column – either in free drop by gravitational force or lowered on a cable, which determines the velocity. In either case, the device hits the sediment with v_o (initial velocity) – and penetrates the sediment as a function of its momentum, controlled by the weight, the initial velocity and deceleration (given by the sediment's stiffness, cohesion, grain size distribution, etc.). This dynamic penetration is completely different process in comparison to static penetration tests, where an external force (hydraulic system) guarantees a more or less constant penetration rate. The analysis of free-fall penetrometer data includes the calculation of the absolute penetration depth by dual integration of the monitored acceleration. This method was also used earlier to study the falling behaviour of gravity corers (Preslan, 1969; Villinger et al., 1999).

Free-fall penetrometers can be classified into two categories:

- Penetrometers instrumented solely with accelerometers, such as the e**X**pendable **B**ottom **P**enetrometer (XBP), STING, PROBOS, etc. (e.g. Scott, 1967; Noorany, 1971; Ingram, 1982; Beard, 1985; Stoll and Akal, 1999; Sponner et al., 2004; Stoll, 2004; Stoll and Sun, 2005; Stoll et al., 2007);
- Penetrometers instrumented additionally with strain gauges measuring cone resistance and sleeve friction or pressure sensors, as used in (piezo-) cone penetration tests (Dayal and Allen, 1973; Davis et al. 1991; Christian et al., 1993; Harvey et al. 1997; Furlong et al. 2004; Stegmann et al. 2006a, 2006b, in press, Melton et al., in press).

In the first case the deceleration is considered as a measure for the stiffness of the penetrated material. Data are used to classify different sediment types (Stoll and Akal, 1999) by the

degree and/or pattern of deceleration, and can further be used to relate them to the undrained shear strength s_u (Stoll, 2004).

Penetrometers fitted with (standard) CPT piezocones (second case, see above) profile the sediment more comprehensively measuring a larger number of parameters (cone resistance q_c, sleeve friction f_s, pore pressure u, acceleration, tilt, temperature), which additionally serve a detailed data interpretation and re-calculation of measurement effects. Especially pore pressure measurement primarily serves the purpose to correct the cone resistance experienced by the instrument for effective stresses; in other words, pore pressure magnitude has to be subtracted from the actual cone resistance given it counteracts the binding force of the instrument.

With respect to the (i) variable initial penetration velocity and the (ii) non-linear penetration rate during the dynamic penetration, the measured response is linked with the deceleration controlled by the bearing capacity and (undrained) shear behaviour of the sediment. Generally, shear strain depending on deformation of granular (non-cohesive) sediments may cause volumetric changes and hence compaction or dilatancy. Both compaction and dilation may in turn cause changes in pore pressure transients and consequently in intergranular effective normal stress and shear strength. The effect of these processes therefore depends on the strain rate and on the permeability of the sediment. In loose fine-grained sediments shear deformation tends to cause an increase in pore pressure linked with a decrease in shear strength, which describes the process of weakening. If pore pressure equals or exceeds the strength, liquefaction occurs. In dense fine-grained material the pore pressure drops dramatically upon impact, whereas the shear strength of the sediments increases.

The insertion of a probe or a penetrometer into sediment generates a shear strain response with transient pore pressure fluctuation depending on (i) the shape of the instrument, (ii) the permeability of the sediment, and (iii) the penetration rate. Stoll (2004) reported that in the case of free-fall penetration of small diameter probes (e.g. XBP, PROBOS, STING) with an initial velocity of 600 cm/s into granular medium, the measured penetration resistance increases by a factor of 15 in comparison with quasi-static penetration tests. Furthermore, undrained shear strength in cohesive sediments related to cone resistance for the same case is generally in the range of 2 to 4 times the strength due to quasi-static loading.

As a summary Clayton et al. (1985) provide a comprehensive overview of the influence and complex interaction of soil conditions on dynamic penetration resistance:

- Void ratio: Decreasing void ratio increases penetration resistance (e.g. Terzaghi and Peck, 1948);

- Average particle size: Increasing particle size gives increased penetration resistance: fine-grained soils at low effective stress levels may liquefy (e.g. Clayton and Dikran, 1982);
- Coefficient of uniformity: Uniform soils exhibit lower penetration resistance;
- Porewater Pressure: Dense fine-grained soils dilate with increasing penetration resistance, while very loose fine-grained soils may liquefy (e.g. Terzaghi and Peck, 1948; de Mello, 1971; Clayton and Dikran, 1982; Clayton et al., 1983);
- Particle angularity: Increased angularity gives increased penetration resistance (e.g. Holubec and D'Appolonia (1973);
- Cementation: Cementation increases penetration resistance and lowers permeability;
- Current stress levels: Increased vertical stress gives increased penetration resistance: increased horizontal stresses increase penetration resistance (e.g. de Mello, 1971; Dikran and Clayton, 1982).

The influence of the penetration rate on the response of cohesive sediments has been studied in several theoretically and laboratory studies. The most comprehensive summary, which combines deployments with mechanical cones, electrical cones and piezocones, has been provided by Lunne et al. (1997; see their Table 5.22). Some of the results of these earlier projects are highly controversial. For instance, a number of workers measures a considerable effect of rate dependency on cone resistance (e.g. Jezequel, 1969; Dayal and Allen, 1975; Roy et al., 1982; Kim and Tumay, 2004). Others, however, claim that no appreciable effect is seen despite a change in velocity of 5–20 mm/s (Konrad, 1987) or 2–100 mm/s (Juran and Tumay, 1989), both having used piezocones similar to the one deployed in this study (see Ch. 3 below). We will hence revisit some of the results from these earlier studies here, mainly dwelling on those where similar materials were tested.

Analog laboratory tests have been carried out to study the effect of penetration rate on the measured cone parameters (e.g. Dayal and Allen, 1975; Kim and Tumay, 2004). All these experiments generally demonstrate an increase of pore pressure as well as cone resistance with increasing penetration rate (at different velocities ranging over several orders of magnitude). Based on laboratory tests in a mixture of pottery clay (clayey silt), Dayal and Allen (1975) measured the strain effect doing rate-dependent penetration tests with a standard piezocone. The experiments were performed in mixtures of variable stiffness (s_u = 3 kPa, 46 kPa, 51 kPa and 80 kPa). In the very soft mixture (s_u = 3 kPa), the increase of maximum cone resistance for each of the three rate step (0.13 to 1.28 cm/s [~order of magnitude]; 1.28 to 13.9 cm/s [~order of magnitude]; 13.9 to 81.14 cm/s [~ factor 6]) ranged from 33 kPa to

71 kPa (215%), from 71 kPa to 162 kPa (ca. 230% increase), and finally from 162 kPa to 167 kPa (no significant increase), respectively. In summary, the rate-effect decreased with increasing stiffness of the specimen. Pore pressure was not determined so that the relationship relies purely on q_c rather than q_t (see above). Based on these results, the relationship between cone resistance and penetration rate was empirically expressed as a logarithmic relationship between the ratio of the dynamic cone resistance and the cone resistance in the same specimen at lowest penetration velocity and the logarithm of the ratio between the penetration velocity and the lowest penetration velocity used (Dayal and Allen 1975).

In a more recent paper, Kim and Tumay (2004) specified during their rate-dependent tests (constant velocities of 0.3, 0.6 and 2 cm/s) what the contribution of the consolidation state of the specimen (67 % fine sand/33% kaolin mixtures with OCR = 1 and 10) is. Additionally to a significant increase in measured pore pressure (here for position u_2) between 0.6 cm/s and 2 cm/s in normally consolidated (NC) as well as overconsolidated (OC) sediments, the observed drop is higher in normally consolidated (0.064 MPa [0.3] / 0.081 MPa [0.6 cm/s] / 0.523 MPa [2 cm/s]) than in OC specimens (0.053 MPa [0.6 cm/s] / 0.243 MPa [2 cm/s]). Also the decay of the pore pressure signal (= time of dissipation) generally increased with the increase of the rate, whereas the dissipation in normally consolidated material took longer than in over-consolidated specimens. The significant increase of pore pressure between 0.6 and 2 cm/s (see above) assumes that a penetration rate of 2 cm/s in normally as well as overconsolidated sediments generates more pronounced undrained conditions (when compared to the lower rates). This is in accordance with earlier work by Campanella et al. (1982) who attest that penetration is essentially undrained down to deployment velocities of 2 mm/s (i.e. one order of magnitude lower than for the standard CPT experiments. Similar to the pore pressure response, cone resistance (corrected cone resistance q_t, where $q_t = q_c + (1-a)\, u_2$, with a = area ratio of the cone) shows clearly a rate-dependent increase (1.12 MPa [0.3 m/s], 1.23 MPa [0.6 m/s], 1.34 MPa [2 cm/s]) in NC sediment (Kim and Tumay, 2004). Comparing the rate-dependent cone resistance responses for NC (with effective stress = 262 kPa) and OC (with effective stress = 26 kPa) specimens, there is an apparent decrease with increasing effective stress.

Roy et al. (1982) carried out a comprehensive *in situ* study, whose initial testing at the St. Alban test site date back to 1970. In the so-called St. Alban clays, the authors observed a non-linear relationship between measured cone resistance and penetration rate (v = 0.01, 0.1, 0.25, 0.5, 1, 2, 4 cm/s) with a complete increase of cone resistance of 20% from 0.25 to 4 cm/s. An increase of only 3% of q_c between 1 and 4 cm/s indicates a relatively small influence of the

rate effect for penetration velocities higher than 1 cm/s. Between 0.01 and 0.1 cm/s the cone resistance decreases with increasing penetration rate. This inverse response was also observed by Bemben and Myers (1974) at a penetration rate of 0.3 cm/s, who suggested the increase of q_c to be associated with drained conditions at low strain rates. Regarding pore pressure response, Roy et al. (1982) observed no significant rate effect during their measurements. Similarly, Juran and Tumay (1989) observed no appreciable difference when doing *in situ* tests in clay and sand. These workers used similar deployment velocities ranging from 0.2 to 10 cm/s, but measured a 4-fold increase in u over the velocity spectrum tested. Other researchers, however, found the rate-dependent increase in q_c to be significant. In a study covering similar penetration rates than we did here, May (1987) carried out constant rate tests from 2.5 cm/s to 3.21 m/s. In the lower range of the velocity spectrum (0.25-23.8 cm/s) q_c seemed fairly constant while at higher rates (23.8 cm/s through 3.21 m/s), an increase of up to 40% was measured. Surprisingly, the author does not observe a simultaneous increase in pore pressure in the normally consolidated kaolin tested.

In a comparative study on dense fine sand in the laboratory and *in situ*, Te Kamp (1982) observed a positive correlation between the increase in penetration rate (velocity spectrum: 0.003 to 10 cm/s) and increasing values for both cone resistance and sleeve friction. When the rate was changed by one order of magnitude (0.2 to 2 cm/s), q_c at the low rate was 80-90% of q_c at the higher speed. This rate-effect could not be reproduced in the laboratory experiments on the same material (Te Kamp, 1982).

In contrast to research on sediments in natural settings and, more often, in the laboratory, there is a growing number of numerical studies on cone penetration testing (e.g. Kiousis et al., 1988; Abu-Farsakh et al., 1998; Markauskas et al., 2002; Susila and Hryciw, 2003; Silva et al., 2006). Based on cavity expansion finite element models, Silva et al. (2006) simulated a piezocone test in artificial clay (kaolin, Boston blue clay) with varying values of overconsolidation ratio (OCR = 1, 2, 4, 8, 32) and examined the effect of constant penetration rate (v = 0.0001, 0.001, 0.01, 0.1, 1, 10, 100 mm/s) on the stress and pore pressure distribution. Permeability of the generated soils is held constant, which means that consolidation characteristics due to penetration are linked solely to variations in soil strength and stiffness. Regarding the excess pore pressure u, the simulation evidences that (a) a decrease of the penetration rate is reflected in a decrease of excess pore pressure, (b) excess pore pressure is influenced by the consolidation state as higher excess pore pressure is generated in softer clay (lower OCR), and (c) the dissipation curves after slow penetration (drained case) lag behind those following fast penetration (undrained case) as a result of the

different rate-dependent radial distribution of excess pore pressure (Silva et al., 2006). Shearing in OC sediments results in dilation (negative pore pressure response), which acts against the positive pore pressure due to increasing total stress generated by the impact of the piezoprobe.

We will revisit the abovementioned relationships when discussing our results from pushed and velocity-dependent "free-fall" CPT deployments.

3. Method in this study

Velocity controlled free-fall and pushed cone penetration tests were carried out in stratified sediments to study the influence of penetration rate on cone parameters under non-laboratory conditions. The free-fall cone penetrometer used was designed and constructed at the RCOM, University Bremen, Germany (Figure 1a). The key advantage of this instrument when compared to others is its modular design. Depending on the desired penetration depth, extension rods (1m each) and stainless steel weights (15 kg each) may be mounted to its base and head, respectively. A detailed description of the device is given in Stegmann et al. (2006a) and is supplemented here by technical information of the progressive refinement in Table 1.

Table 1: Technical specifications of the modular free-fall CPTU. See also Stegmann et al. (2006a).

	SHALLOW-WATER LANCE (200m water depth)			
	Type	**Range**	**Accuracy**	**Resolution**
CPT Subtraction Cone 15 cm²				
Cone Resistance	Geomil 15cm² Subtraction Cone	100 MPa	0.25 % FS	0.003%
Sleeve Friction	Geomil 15cm² Subtraction Cone	1 MPa	0.5 % FS	0.003%
Absolute Pressure Sensor	Geomil 15cm² Subtraction Cone	2 MPa	0.4 % FS	0.003%
Inclinometer	Geomil 15cm² Subtraction Cone	0-30°	2° FS	
Acceleration				
Analog Devices	ADXL103	+/- 1.7 g	0.5% FS	
Vernier	Low-g	+/- 5 g	0.05 g	
Analog Devices	ADXL321	+/- 18 g	0.2% FS	
Freescale Semiconductor	MMA3202	+/- 100 g	1% FS	
Microcontroller	Tiger DL7000			
Power Supply		12 V		

For the deployments in the free-fall mode, the instrument was equipped with 4 x 15 kg weight pieces and elongated with two 1m-rods. It was lowered by a crane (Figure 1b) at three different velocities (v1 = 135 cm/s, v2 = 60 cm/s, v3 = 30 cm/s). For each velocity step, the instrument was arrested in the sediment for 10 mins., 30 mins. and 60 mins. after penetration and complete halt of the instrument. A total of 32 deployments were carried out to get a comparable data pool for scientific analysis.

Continuous profiling at a rate of 2 cm/s was maintained by a hydraulic piston to which the device was mounted. The piston is part of a larger pontoon in Lake Hemelingen, Weser estuary. Given the setup and travel distance of the hydraulic piston, the CPT device was elongated using seven 1m-rods, then reaching a total length of 8.6 m (Figure 1c). Six deployments were carried out at constant rate to obtain a reproducible data set. Five of these tests were carried out with 7 extension rods while the sixth was done with only 6 rods, largely to ensure the piezocone halted within the cored interval (see below).

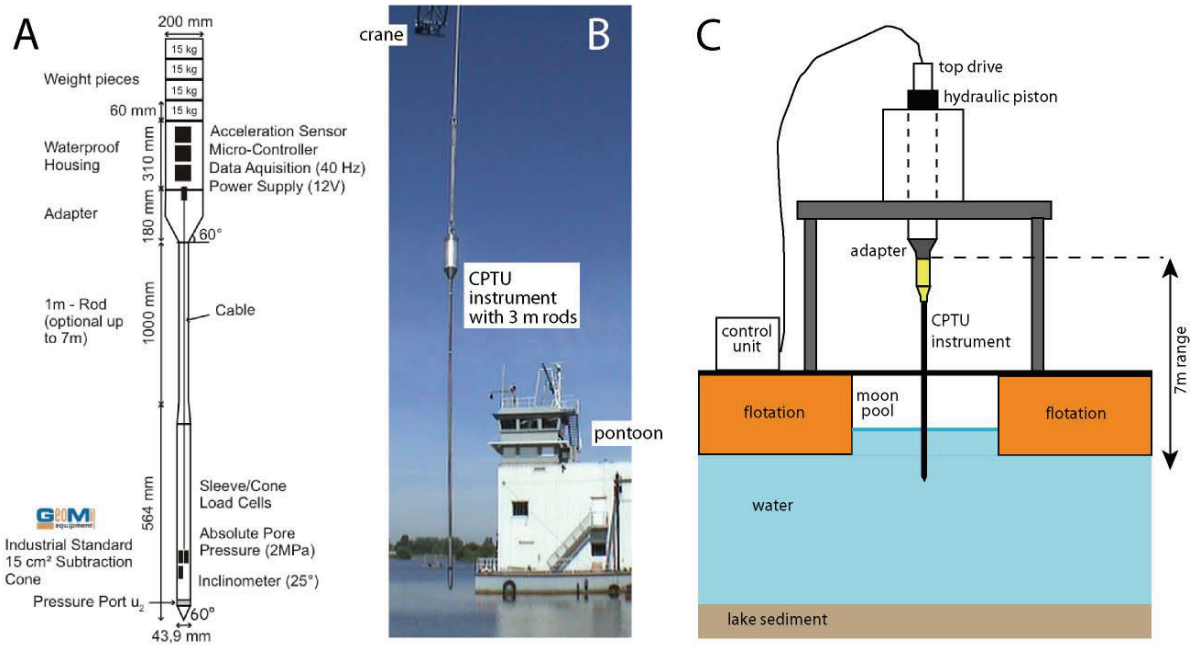

Figure 1: Schematic sketch of the free-fall CPT **(a)**, lowered on the crane for free fall tests **(b)** and fixed on a stamp (not to scale) for quasi-static testing **(c)** in Lake Hemelingen pontoon (shown in background of Figure b).

For the pushed tests, reliable control on penetration rate existed from the hydraulic drive of the piston. In the "free-fall" mode, the speed of the crane's winch can be easily read from the increase in hydrostatic pressure prior to the impact into the sediment. The initial penetration velocity in the sediment as well as the total penetration depth were then calculated by the 1st and 2nd integration of the data obtained by the accelerometer. Pore pressure profiling was helpful to pick the exact starting point of penetration. Deployments with an inclination more than 9° (following ASTM standard D3441, Lunne et al. 1997) were not considered in this study.

4. Geological setting and sediment physical properties reconnaissance study

The velocity-controlled cone penetration tests were carried out in Lake Hemelingen, a bayou of the river Weser near Bremen in the northwestern part of Germany. The location was chosen for two reasons. First, Lake Hemelingen is well studied and layered sediments of variable composition, showing clay mineral-rich soft mud, silt, and sandy layers in the uppermost meter of the sedimentary succession. Second, the lake hosts the testing facilities of the company ATLAS Elektronik, among which are a crane and a pontoon with a hydraulic load frame overarching a moon pool (Fig. 1b, c).

For this CPT study, we first carried out a reconnaissance study of the sediments to be penetrated. Cored sediments (92 cm depth) were taken with the lightweight gravity corer for laboratory measurements of sedimentological and physical properties. Apart from the visual core description, we carried out grain size distribution (Atterberg settling technique) and water content measurement (oven drying). Measurement of undrained shear strength was carried out with a dynamic laboratory method, the Fall Cone Penetrometer, based on the calculation given by Wood (1985) with the cone factor 0.85. In addition, bulk density using the gamma ray attenuation method was performed on a GEOTEK Multi Sensor Core Logger [MSCL]. The combination of sedimentological and geotechnical analyses allow us to distinguish between four different lithological units (Figure 2):

(i) The upper 30 cm were characterised by barely consolidated, muddy sediments (up to 53 % silt) with a water content of 304 % and a porosity of 80 %. The low bulk density of 1.3 g/cm^3 complies with a low undrained shear strength between 3.9 kPa and 4.8 kPa.

(ii) The second layer shows an increase in fine-grained sand and decrease in water content and porosity (46%) between 28 cm and 52 cm. The sediment is stiffer, reaching an undrained shear strength of maximum 52 kPa and an average density of 2 g/cm^3.

(iii) Between 52 cm and 80 cm light-brown silty and clayey sediments dominate layer 3, whereas the clay content increases with depth. Organic material is also more abundant. Undrained shear strength and bulk density range between 18 kPa and 40 kPa and 1.3 g/cm^3 and 1.9 g/cm^3, respectively.

(iv) The fourth layer between 80 cm and 92 cm comprises a stiff silty clay (50% clay content) with an undrained shear strength between 73 and 76 kPa. The water content decreases here to 135%.

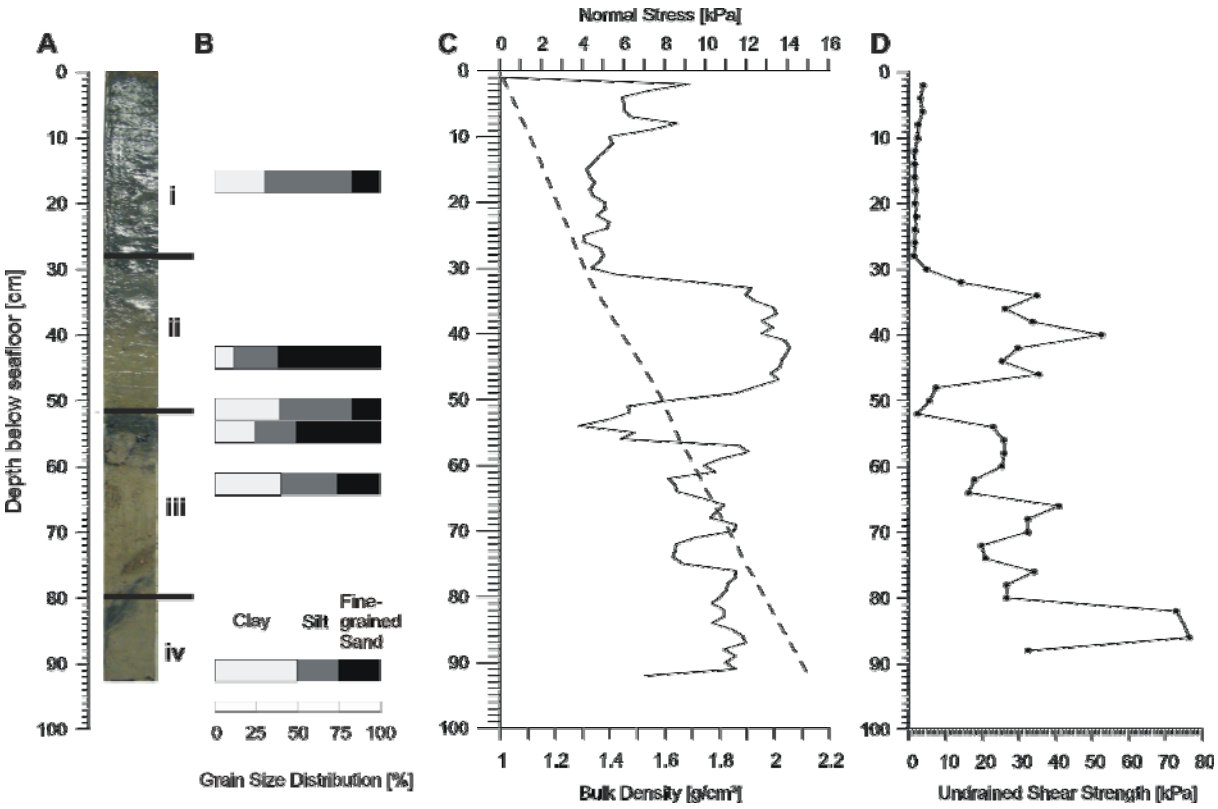

Figure 2: Sedimentological and physical properties measured on a core, which was taken with the lightweight gravity corer at the position where the free-fall cone penetration tests were carried out in Lake Hemelingen: Lithology **(A)**, Grain size distribution **(B)**, bulk density and effective stress σ', derived from the density data **(C)**, undrained shear strength s_u determined with the laboratory Fall Cone Penetrometer **(D)**. The combination of the complete data set shows four sedimentological and physical distinct sections (i – iv) (see description in the text).

To evaluate the consolidation behaviour of the sediments uni-axial oedometer tests with progressive loading from 5 kPa to 1.2 MPa was at 90 cm core depth using the overconsolidation ratio OCR = σ'_0 / σ', with the pre-consolidation stress σ'_0 and the overburden effective stress σ'. The deepest section (90 cm) appear lightly overconsolidated expressed with an OCR = 3.

5. Results

5.1 Pushed penetration tests

We here describe the results from quasi-static (i.e. constant rate) and velocity-controlled, dynamic tests separately. The pushed tests were carried out through the moon pool of the pontoon at Lake Hemelingen. Given the setup of the load frame and hydraulic piston, we achieved a total penetration of max. 1.91 m using the 7 extension rods (see above and Fig. 1c). A typical test protocol showing cone resistance versus depth is given in Figure 3. It can be seen that in the uppermost portion, hardly any measurable resistance was recognised by the strain gauges. This interval (almost 1 m in thickness) is a layer of fluid mud, which we also failed to preserve in the sediment core taken in the vicinity.

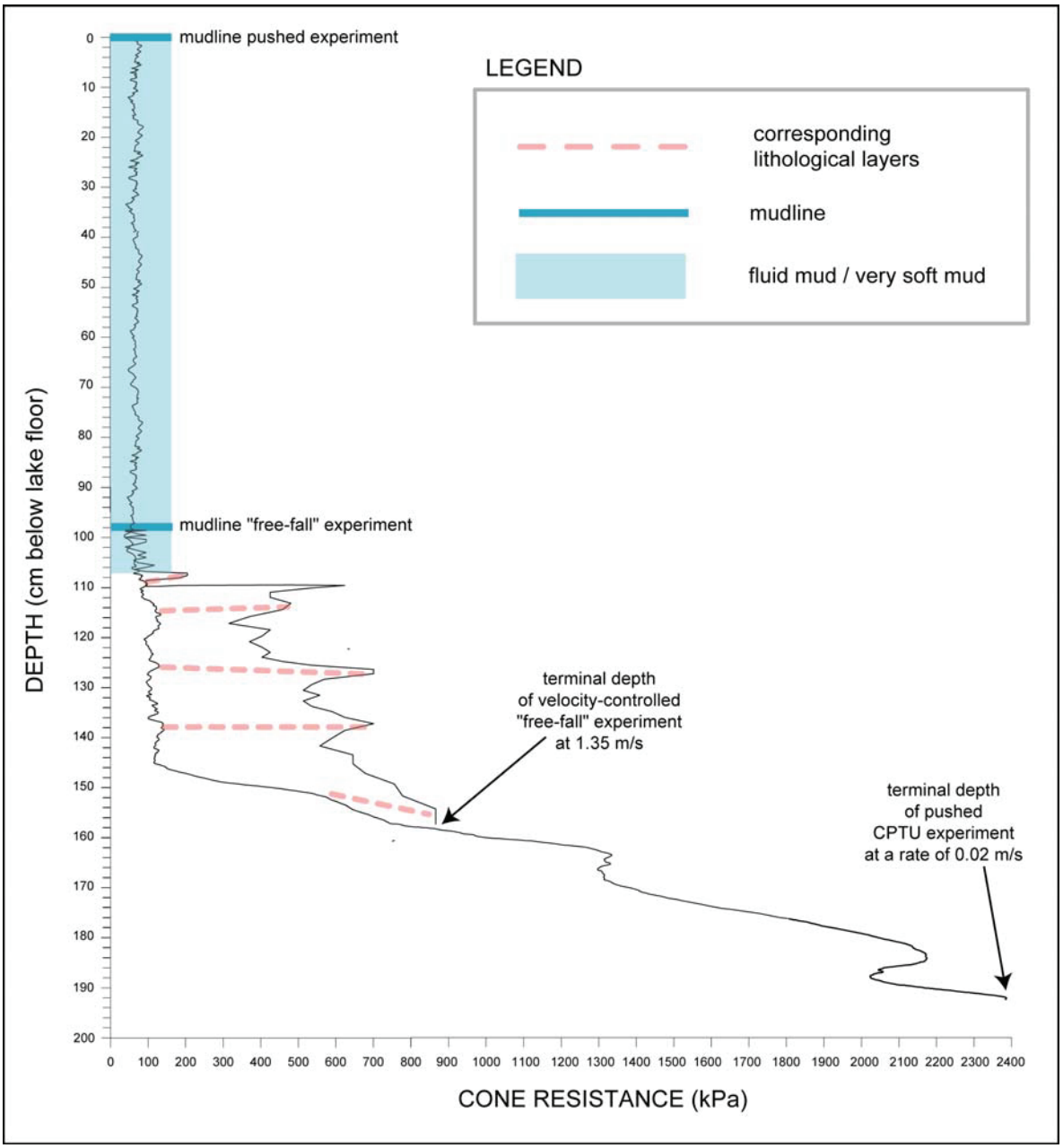

Figure 3: Results from a pushed and "free-fall" (1.35 m/s) CPTU tests where cone resistance is plotted versus depth. A schematic diagram of the sediment core taken adjacent to the test site is given for reference; numbers 1 through 4 refer to the lithological units explained in Figure 2.

Besides the visual evidence of the fluid mud suspension at the extension rods after CPT instrument recovery, a subtle wiggle was recorded by the most sensitive of our accelerometers (1.8 g and 5 g) (for specifications, see Table 1). Below that layer, soft mud causes the cone resistance to increase to values around 50 kPa-100 kPa (Fig. 3). In about 1.1 m below lake level, a first peak is seen. Cone resistance q_c reaches ca. 100 kPa in this interval. Further below, an interval of variable cone resistance between 1.2 m and 1.5 m sub-bottom depth is a second plateau is penetrated down to 2.35 m (Fig. 3). In this zone, q_c again ranges somewhat short of 200 kPa, before a sudden increase is measured. In the final part of the test from 1.5

through 1.91 m sub-bottom depth, a steep, stepwise increase in resistance indicates that some indurated riverine sediments are penetrated. Three distinct steps at approximately 600, 1350, and 2100 kPa can be identified, which indicate an increase in grain size rather than state of consolidation given the short distance of penetration. After a final drop in resistance back to ca. 1940 kPa at 1.84 m depth, the piston reached its termination and the test was stopped at 1.91 m below lake level (Fig. 3). Please note that given the low excess pore pressures and total vertical stresses in Lake Hemelingen, we do not correct q_c (see discussion in Lunne et al., 1997).

5.2 Free-fall penetration tests

A total of 32 "free-fall" deployments were carried out over a period of four weeks (Table 2). These tests can be grouped into three sets: 10 tests at the fast winch speed ($v1_{mean}$=1.35m/s), 13 tests at moderate winch speed ($v2_{mean}$=0.75 m/s), and 9 tests at slow winch speeds ($v3_{mean}$=0.27 m/s). The majority of these tests were carried out with an u_2 piezocone. The mean winch speed velocity (change of hydrostatic pressure measured with the pressure sensor over the time running through the water column) was used to confirm the crane's velocity and to compare it with the initial velocity v_0 derived from the acceleration data (1st integration). The difference between the lowering velocity and the initial velocity v_0 can be considered as a quality check of the derived v_0. The mean inclination for all velocity classes ranged between 0.3° and 1°, which is very satisfying. Only three deployments failed or the inclination exceeded 9°; those were not considered further. The mean average sampling frequency was 44 Hz, which leads to a spatial resolution of 0.03 to 0.1 m depending on the penetration velocity. As derived from the acceleration (2nd integration), total penetration depth reached up to 1.5 m and 1.2 m for the v1 and v2 class. Lower winch speed (v3) resulted in an average 0.5 m of penetration, with only two tests reaching lithological unit iv.

Table 2: Overview of all free-fall CPT deployments summarised for the three velocity classes v1, v2 and v3 (see text for further explanation).

Velocity Class	Deployments	Mean Lowering Velocity [m/s]			Initial velocity v_o [m/s]	Difference between $v_{measured}$ and $v_{derived}$	Penetration Depth [m]			Inclination [°]			Number of Failures	Resolution [cm]
		min	*max*	*mean*	*mean*		*min*	*max*	*mean*	*min*	*max*	*mean*		
v1	10	1.17	1.35	1.32	1.35	0.05	0.5	1.5	0.735	0.2	2.3	0.5	1	0.03
v2	13	0.46	0.86	0.64	0.75	0.15	0.25	1.2	0.65	0.1	6.1	1.0	1	0.02
v3	9	0.16	0.36	0.25	0.27	0.10	0.2	0.9	0.492	0.2	0.6	0.3	2	0.10

A summary plot of a selection of three tests from each winch-speed group is given in Figure 4. It can be seen from those examples that the CPTU tests profile the sedimentary succession in a systematic, coherent manner. In each group, both cone resistance (Figs. 4a, c, e) and pore pressure (Figs. 4b, d, f) show very little deviation in the uppermost part where soft mud dominates. Below that interval, an increase in both parameters is generally observed. This increase is more pronounced in the moderate and fast experiments, but is usually recognisable also in the slow penetrations (Figs. 4a, b). The deeper lithological units 3 and 4 were only reached by two of the low-speed experiments so that data from the lower portion are scarce. Pore pressure trends observed with penetration depth are indicative of the lithologies. Namely during the increase in grain size when profiling from unit i into unit ii, pore pressure increases first and then drops through unit ii before it rises again deeper in the section (Figs. 4d, f).

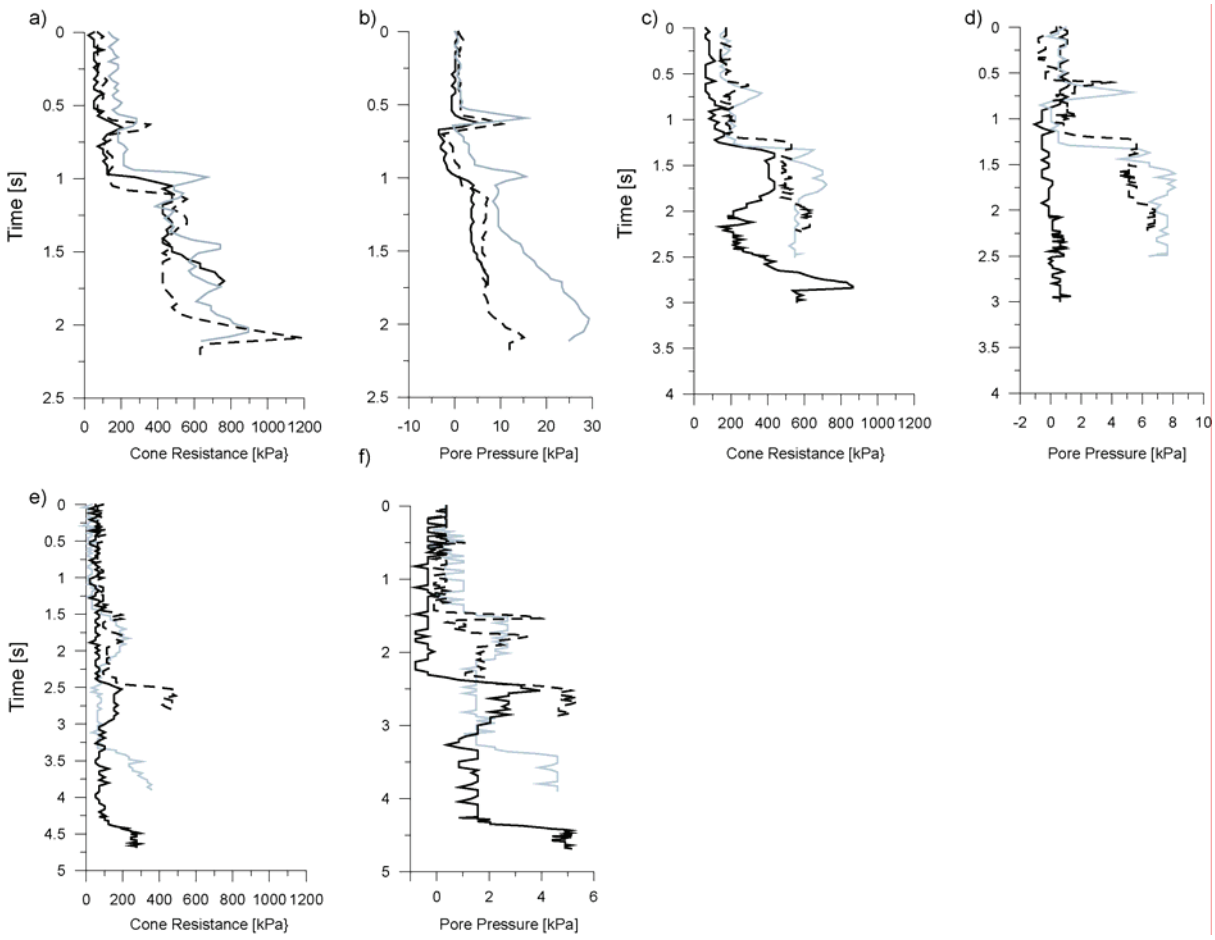

Figure 4: Results from velocity-controlled "free-fall" CPTU deployments. Cone resistance and pore pressure (the latter normalised for hydrostatic pressure) are given vs. time for the three groups of winch speeds: **(a-b)** 1.3-1.4 m/s; **(c-d)** 0.6-0.7 m/s; **(e-f)** 0.25-0.35 m/s.

The decrease in pore pressure after penetration of unit ii indicates a typical dilatant response, which previously has been attributed to displacement of fluids. In contrast, pore pressure

signals in the deeper units iii and iv trend towards higher supra-hydrostatic values, which coincide with the indurated, lightly overconsolidated sediments there.

This is also reflected in Figure 5 where the average cone resistance is plotted for each of the four geological features given in Figure 2. For all velocity classes, the muddy sediments exhibit an average cone resistance between 50 kPa and 100 kPa. The first increase of fine-grained sand corresponding to the upper limit of lithological unit ii is reflected by an increase of cone resistance ranging for v_1 between 120 and 320 kPa, for v_2 between 80 and 200 kPa and for v_3 between 100 and 250 kPa.

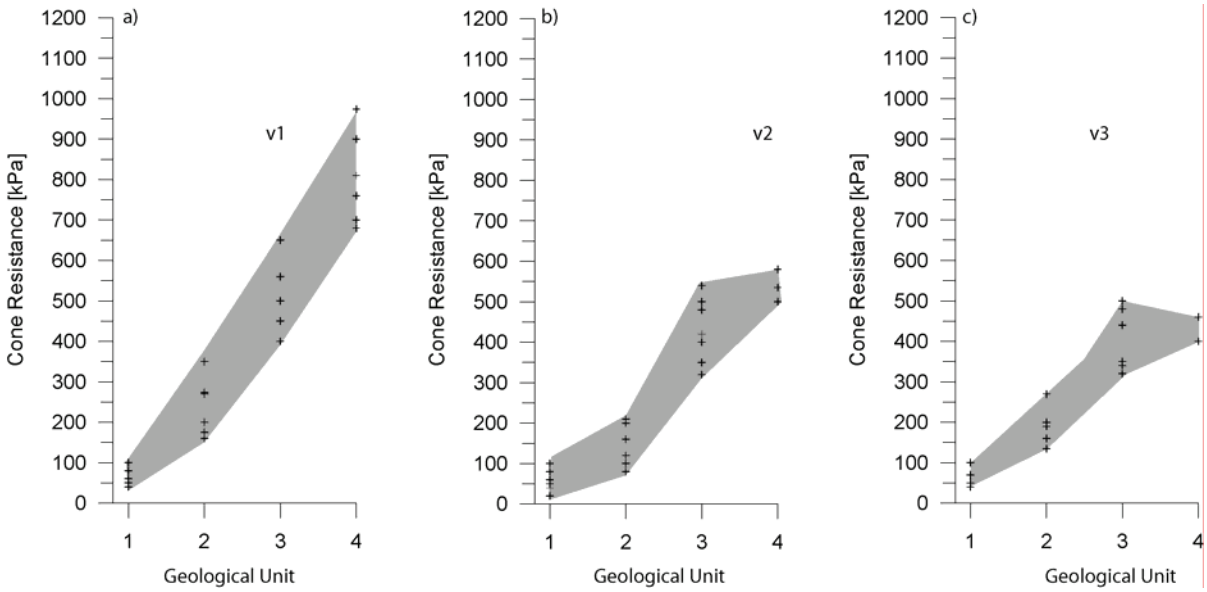

Figure 5: Cone resistance versus units i through iv taken from the 32 free-fall experiments carried out. Shaded corridors indicate variability of results. Velocities v1 **(a)**, v2 **(b)** and v3 **(c)** refer to the dynamic CPTU deployments; pushed tests at v_{pushed} are shown for reference.

Figure 5 neatly demonstrates that, regardless of small-scale variations, the free-fall instrument provides the user with comparable results over the winch speed spectrum tested. The variability at each level can be attributed to both slight changes in winch speed and small-scale geological variations. As a result, the curves for 1.35 m/s show the steepest gradient of all experiments; even in the intermediate depth interval (units ii and iii), they show an increase rather than a plateau (as observed for the low and moderate winch speeds; Fig. 5). For a critical review of the testing procedures including potential errors it has to be referred to the discussion (Ch. 6). In each scenario, values for intervals ii and iii are fairly similar and plot approximately between the low cone resistance of the soft mud (unit i) and the high cone resistance encountered in the indurated silty sands (unit iv). It can further be seen that with increasing rate of penetration, the overall gradient of the corridor is getting steeper. The v1

tests climb to maximum values of almost 1 MPa while those at moderate to low winch speed reach only ca. 600 and 450 kPa, respectively (Figs. 5 a-c).

Table 3: Undrained shear strength data (as mean average values for the respective velocities) derived from corrected cone resistance q_t, excess pore pressure u, and vertical stress σ_v based on dynamic (v_1, v_2, v_3) and pushed (v_{pushed}) CPTU experiments (see also caption of Fig. 5 for further explanation).

	Undrained Shear Strength [kPa]											
Geological Section	**v1**			**v2**			**v3**			**quasi-static test with 2 cm/s**		
	N_k=10	N_k=12	N_K=15	N_k=10	N_k=12	N_K=15	N_k=10	N_k=12	N_K=15	N_k=10	N_k=12	N_K=15
i	7.5	6.3	3.9	6.0	5.0	4.0	5.9	4.9	3.9	7.9	6.0	5.3
ii	23.3	18.1	15.5	13.6	11.3	9.1	15.5	14.9	10.3	11.9	9.9	7.9
iii	48.1	40.1	32.1	49.9	36.6	29.3	38.8	32.4	25.9	14.4	12.0	9.6
iv	86.9	72.4	59.9	57.9	48.3	38.6	51.6	43.0	34.4	59.2	49.4	39.5

When pore pressure and vertical stress are known, cone resistance data may be easily transferred to undrained shear strength (s_u) using an equation by Lunne et al. (1997), where $s_u = (q_t - \sigma_{vo}) / N_{kt}$, with q_t being cone resistance corrected for u_2 (i.e. excess pore pressure; see above), σ_{vo} = total vertical stress, and N_{kt} =10, 12 and 15 having been used as values for the cone factor. N_{kt} relates empirically to cone resistance and back-calculation from lab-based undrained shear strength and corrected cone resistance (Karakouzian et al., 2003). Vertical stress is calculated using penetration depth and bulk density of the sediment, as measured with the MSCL (see Fig. 2 and Ch. 4 above). Potential errors may result from i) the estimation of penetration depth and the corresponding vertical stress, ii) the influence of penetration rate on the pore pressure pulse, and iii) the assumptions concerning the factor N_k.

Our results are given for both N_k=10, 12 and 15. For fine-grained sediments, the cone factor $N_{kt,}$ (derived from plasticity and stiffness) ranges between 8 and 30 (see summary Lunne et al. 1997, Ch. 5.4.2.1). As the most often used values are $N_{kt,}$=10-15, and given further that these values are associated with the underconsolidated to soft, normally consolidated sediments ($N_{kt,}$=10-12) and firm to lightly overconsolidated sediments ($N_{kt,}$=12-15), we selected them for the good agreement with our sediment core (Fig. 2). Since the majority of our tests as well as of the profiled length in our CPTU deployments is in normally consolidated material, we consider N_k=10 more appropriate. However, the wealth of our CPTU data give overlapping data for the N_k values in question and can conveniently compared in Table 3. It is seen here that for the slow tests, the difference between the three factors does not affect the softer units, and causes the sandy unit iv to average around 34.4 kPa (N_k=15) and 51.6 kPa (N_k=10; see Tab. 3). In contrast, the fast tests show a less pronounced variation. In unit i, all values plot well below 10 kPa regardless of the cone factor (Tab. 3). For units ii and iii, the range of s_u

values increases, and in unit iv there is a wide bracket of values from 34-60 kPa (N_k=15) to 43-72 kPa (N_k=12) and 51-87 kPa (N_k=10; see Tab. 3). As anticipated, the intermediate velocity tests plot somewhere between the two other velocities (Tab. 3). If all data in Table 3 are compared, it is clear that the variability in strength caused by the cone correlation factor has a less profound effect on s_u than that by the impact velocity (see discussion, Ch. 6.2 below).

6. Discussion

We have split the discussion of our results into two sections. First, we want to critically review our testing procedures and illuminate possible shortcomings of the CPT instrument design, potential errors, and compare the data to field- and laboratory-based results from earlier work. Second, we will focus of the rate-dependency of CPT results and their ramifications on data interpretation. In this section we will discuss the pros and cons of rapid CPTU experiments when compared to standard constant rate tests, drawing special attention to the effects of sediment physical properties governing the data set acquired by the profiling probe.

6.1 General observations

In general, our results provide a comprehensive and consistent set of mechanical properties of the shallow sediments at Lake Hemelingen (e.g. Figs. 3, 4). The tests at constant rates show systematically a much smaller cone resistance and excess pore pressure excursion when compared to the "free-fall" experiments (e.g. Fig. 3). Namely for q_c, the factor between the pushed (0.02 m/s) and fastest "free-fall" test (v1 = 1.35 m/s) is approximately between 4 to 7 in the upper section and 1.8 in the stiffer sediment (e.g. Fig. 3) and resembles that determined by Stoll et al. (2007) when they compared STATPEN and PROBOS experiments (factor 2-7; see their Fig. 6). However, the slowest tests carried out at v3 (0.3 m/s winch speed) were possibly chosen too conservatively. First, we do not see significant differences in q_c, f_s or pore pressure when compared to v2, where we roughly doubled the speed. Second, 3 out of 9 tests were unstable and the lance fell over (2-times after a while so that only pore pressure dissipation was affected). Given the low total penetration achieved at impact velocity v_1, our instrument is probably too top-heavy. As for the overall accuracy and potential errors in our data, we have to shed light on a number of factors:

First, there is naturally some inaccuracy of any *in vivo* testing procedure (i.e. controlled tests in natural, more or less homogenous settings). This clearly applies to the stratified sediments

in Lake Hemelingen, because there may be slight variations in layer thickness and lateral extent. Lake Hemelingen represents a former slip-off slope where deposition of medium-grained deposits in the meandering river Weser took place. However, the possible variability in thickness of both the silty and sandy units (ii-iv) as well as the unconsolidated muddy cover (unit i) cannot be quantified. It is suggested from our results that the variability in the coarser units is negligible (at least for all the different "free-fall" tests, but that the thickness of the top layer of soft mud may have varied by a few decimetres. This is negligible for the various tests at v_1, v_2 and v_3 because of their vicinity, but at the location of the constant rate tests there is evidence from the test protocols that the soft mud is at least 0.8 to 1 m thick. Unfortunately, the architecture of the hydraulic load frame inside the pontoon does not allow the use to take a gravity core for reference. It has to doubted, however, that it would be possible to recover the soft material anyway. This immediately relates to second potential source of error: The calculation of penetration depth. In the gooey material, we cannot be certain when exactly the strain gauges show the first subtle excursion relative to their overall noise (estimated to be ± 3 kPa according to the manufacturer GEOMIL [Table 1]). As a consequence, the mudline may have been picked too late (i.e. deep) and the overall penetration depth may have got underestimated. On the other hand, however, we used the deviation of the pressure signal from its linear hydrostatic path to control impact, so that we are confident the error in our data is miniscule. Additional errors as a result of winch movement, where it is impossible to hold a constant rate within an error margin of ±0.1 m/s (see also discussion in Villinger et al. [1999]). These variations (and errors) may have been either direction (faster as well as slower), however, we tried to grab the impact velocity as a function of both the crane's tensiometer and the increase in hydrostatic pressure when lowering the instrument in the water column. One significant shortcoming of the CPTU instrument built at RCOM Bremen is the considerable variability of the rate the microcontroller (Tiger-Basic DL7000) is recording. As a result of the mode of data storage, individual data are collected in a buffer and are then written to the Smart Media disk once a threshold value is exceeded. This process of writing delays the further data collection so that the overall sampling rate decreases significantly during that (admittedly short) period. In our experiments, this storage procedure caused variations in temporal resolution. The nominal 40 Hz sampling rate were often exceeded, however, at times sampling rate was as low as 28 Hz. Maximum values were 111 Hz, while the average sampling rate was 44 Hz (i.e. slightly better than according to the manufacturer's specifications). Depending on the mode of deployment, spatial resolution varied between less than 1 cm (low penetration velocity) and more than 5 cm (high

penetration shortly after impact of the probe, disadvantageous storage intervals). The latter resolution is poor and may result in the researcher missing some thin laminae and layers of only a few cm in thickness. On a more general level, the variability in temporal (and hence spatial) resolution of the micro-controller is highly unsatisfactory and will be improved by replacement with another data logger.

On the pro-side, the comparison of our laboratory-based data and *in situ* measurements shows fairly good agreement. If we compare the shear strength data measured on the sediment core (Fig. 2) and those derived from the CPTU tests (Tab. 3), we observe an admissible agreement. In the case of the constant rate experiments, the absolute values in the field appear to slightly underestimate those taken on core material in the geotechnical laboratory. For the "free-fall" deployments, fall cone penetrometer data on the split core resemble s_u data derived from *in situ* CPTU deployments, with the latter plotting somewhat higher (Fig. 2 and Tab. 3). When ignoring some of the excursions in the profiles as well as some variability within the CPTU data set, there is good agreement achieved. Below the soft mud, core data increase to a plateau around 30 kPa, while values up to 24 kPa are also reached in the CPTU tests (see Tab. 3, unit ii). Similarly, unit iii shows values around 30 kPa in the core, and slightly elevated values in the *in situ* tests (ca. 38-48 kPa at N_k=10; Tab. 3). For the firm sandy silt layer (unit iv), s_u from the sediment core (>50 to ca. 80 kPa; Fig. 2) coincide with values between 51 and 87 kPa (for at N_k=10; Tab. 3) during "free-fall" tests. This observation is also in fairly good accordance with earlier studies. In a succession of marine clay and sand, Karakouzian et al. (2003) found matching curves for shear strength using a vane shear on cored material and CPT deployments (see their Fig. 6). An even better agreement was achieved when *in situ* vane shear data, CPTU data and results from vane shear tests on cored sediment were compared in Lake Lucerne slope sediments (see Stegmann et al., 2007; their Fig. 3). Given that these latter CPTU deployments were equally carried out using a winch, these observations are supportive of cone penetration testing at variable rates. Details concerning the rate-dependency of the results will be discussed in the next chapter.

6.2 Influence of penetration velocity

As outlined above in some detail, the main aim of this field study in non-homogenous, water-saturated sediment was to find answers to a series of questions concerning the influence of impact velocity the penetration rate on the measured CPTU parameters. Related questions included:

- How does dynamic testing with its rapid exponential decay of impact velocity with depth affect the CPTU results?
- How do sedimentary (e.g. grain size) and physical (e.g. state of consolidation, shear strength) properties influence the velocity effect?
- Is it possible to re-calculate the influence of rate-dependency? Is there any systematic relationship between v and measured q_c or u? If yes, what kind of relationship (e.g. linear, exponential) can be established?

A large number of theoretical and laboratory studies have been performed concerning these questions (see Ch. 2 above, and – for a more comprehensive overview – refer to Lunne et al., 1997, their Table 5.22). Unfortunately, many of these series of laboratory and *in situ* experiments focused on penetration tests in homogenous sediments with defined physical properties (e.g. grain size distribution, state of consolidation, stiffness/shear strength). In many natural settings, however, such conditions are rarely met, so that the results of those workers are of limited use. In order to ensure that our results are discussed in the appropriate context, from here on only studies reporting data from *in situ* CPT(U) tests will be regarded. These include studies by Roy et al. (1982), Te Kamp (1982), Lacasse and Lunne (1982), Juran and Tumay (1989). A summary table of the findings by a large number of these authors is given in Table 4. We emphasize data from those just mentioned and acknowledge that there is a wide scatter in their results. Following Lunne et al. (1997), we first normalised the highly variable experimental conditions (namely the wide range of velocities above and below the standard rate of 2 cm/s) by dividing the highest through the lowest velocity. We did the same for the range of values for q_c, that way getting two ratios (see Table 4, columns 3 and 4). If those two ratios are divided against each other one more time, an arbitrary and dimensionless factor can be calculated (Table 4, right column), which is helpful for comparison.

Without going into unnecessary detail, it can be safely stated that the studies cited cover a huge spectrum of deployment rates. While much work was dedicated to the lower end of the spectrum with penetration similar or slower than standard pushed tests (e.g. 0.0001 – 100 mm/s [Silva et al., 2006], 0.06 – 2.1 mm/s [Ladanyi and Eden, 1969], 3 – 20 mm/s [Kim and Tumay, 2004], and 1 – 40 mm/s [Roy et al., 1982]), other workers covered the faster range. Those include both fast constant-rate tests (e.g., up to 81 cm/s [Dayal and Allen, 1975], up to 20 cm/s [Vivatrat, 1978], and up to 321 cm/s [May, 1987]) and "free-fall" tests at high impact velocities (e.g. up to 400-600 cm/s [Stoll et al., 2007], or 130 cm/s [Stegmann et al., 2006b]. In the following, we will relate the rate-dependent increase of q_c from the minimum to the maximum penetration velocity from some of those earlier studies (Table 4) to our data.

Table 4: Selected results on rate-dependent CPT experiments by a variety of authors (left column). Columns 3 and 4 summarise the ratios of penetration rates and cone resistance from the fastest and slowest deployment in each publication. Right column introduces an arbitrary ratio between columns 3 and 4 to illustrate the absence of a systematic relationship. * = mean average value in column 4 was used for calculation. See text for discussion.

Reference	Lithology	R(Dv) = ratio between highest and lowest penetration velocity	R(qc) = ratio between cone resistance measured at the highest and lowest velocity	Arbitrary ratio R(Dv) / R(qc) *
Jezequel 1969	soft clay	10	1.4	7.1
	stiff clay	10	0.81	12.3
	silt	10	0.88	11.4
	loose, saturated sand	10	0.94	10.6
Ladanyi and Eden 1969	sensitive clay	10	1.075	9.3
Marsland 1974	fissured clay	200	1.3	154
Bemben and Myers 1974	varved clay	1000	1.5	667
Dayal and Allen 1975	soft clay (tao = 34 kPa)	623	5	125
	medium stiff clay (tao = 46 kPa)	623	1.6	389
	medium stiff clay (tao = 51 kPa)	623	1.4	445
	stiff clay (tao = 80 kPa)	623	1.08	577
Vivatrat 1978	NC Boston blue & EABPL clays	10	1.1	9.1
Lacasse and Lunne 1982	clay	10	1.08	9.3
Lunne et al. 1986	till	10	1.15	8.7
May 1987	NC kaolin	12	1.4	8.6
Juran and Tumay 1989	clay	50	1	50
	sand	50	1	50
Kim and Tumay 2004	NC/OC specimens (67% fine-grained sand, 33% kaolin)	7	1.1	6.4

Comparing the measured cone resistance of the quasi-static tests (2 cm/s) in the Lake Hemelingen pontoon and the free-fall test with 135 cm/s, there is a factor of 4 to 7 in the upper section (corresponding to units i, ii and iii), and a factor of approximately 1.8 in the stiffer section (unit iv). Some uncertainties of correlation are given by geological variability, which has been discussed before in Chapter 6.1. Regarding the "free-fall" tests by themselves, the increase of q_c from max. velocity (135 cm/s) to the lowest velocity (35 cm/s; i.e. factor ~ 4) causes q_c to increase by a factor of about 1.4 on average (for details, see Ch. 5 above). For the various lithologies, the increase is 1.3- (unit i: muddy ooze), 1.5- (unit ii: clayey fine-grained sand), 1.2- (unit iii: silt, fine-grained sand) and 1.6-fold (unit iv: sligthly overconsolidated clayey silt). Compared to the pushed, standard rate test at 2 cm/s, the factor increases to values around 4 for many of the lithologies penetrated (see Fig. 3). In fact, with

the exception of the lowermost unit iv, where $q_{c(135)}$ / $q_{c(2)}$ is only ca. 1.4 (600 kPa vs. 850 kPa; see lowermost dashed line in Fig. 3), all other units show $q_{c(2)}$ being only one quarter of $q_{c(135)}$. We assume that the smaller factor of ca. 1.4 in unit iv can be explained by the low penetration rates deeper the section, because here the probe already lost much of its momentum. However, it is very difficult to quantify the rate-effect on one hand and the tendency for dynamic tests to "pronounce" lithological changes in the CPT record on the other hand. Obviously the influence of penetration rate is also reflected in undrained shear strength, which is derived from cone resistance and given as a mean average for each geological section (see Table 3). Regarding v3 (35 cm/s) and v1 tests (135 cm/s impact velocity), undrained shear strength s_u increased by a factor 1.4 on average due to increase of penetration velocity. This observation does agree with the data from PROBOS deployments carried out by Stoll et al. (2007; see their Fig. 7), where results from sandy Gulf of Mexico sediments scatter around the strain-rate vs. velocity graph based on data by Dayal and Allen (1975). If we plot our data as ratios of v1, v2 and v3 relative to v_{pushed} into the same diagram, it can be seen that dynamic deployments by Stoll et al. (2007) and us plot along the same corridor, which overlaps with the Dayal and Allen (1975) graph (Fig. 6a). The different strain-rate factors found for each penetration velocity can be used to relate the dynamic q_c results to those from pushed tests. If we return to the comparison between PROBOS and STAPEN, the STATPEN results typically show a gradual, more or less uniform increase in q_c whereas the PROBOS record contains many large peaks of high penetration resistance suggesting an inhomogeneous sediment structure that is not obvious from the quasi-static test results (Stoll et al., 2007; their Fig. 6). No matter how different the absolute values of cone resistance were, the curves of both instruments agreed in principal (i.e. in stiffer layers, q_c increased with either probe, the PROBOS exceeding that of the STATPEN by a factor of 10). This is exactly what is found in Figure 3 albeit our data show less pronunciation, largely because of the lower impact rates (35-135 cm/s by the RCOM CPT device vs. 400-600 cm/s by the PROBOS).

When "correcting" our absolute CPT parameter values using the strain-rate factor obtained from Dayal and Allen's (1975) equation (see Fig. 6a), we can assess the effects of dynamic penetration. Unlike Stoll et al. (2007), who did not take their data further than what is shown in Figure 6a, we have processed the "free-fall" deployments using the velocity decrease during downward profiling to obtain a strain-rate factor (hereafter SRF) for each point in depth. A typical example is given in Figure 6b. We compare the upper portion of one of our constant rate (2 cm/s) tests (black curve) with a dynamic deployment at v3 (35 cm/s initial

velocity; purple curve). In the uppermost mud package (16 cm thick), deceleration is negligible so that SRF is 2.24. During penetration through a stiffer layer (q_c = ca. 200 kPa at about 25 cm depth; Fig. 6b), the velocity of the probe decreased to ca. 15 cm/s (i.e. SRF 1.69).

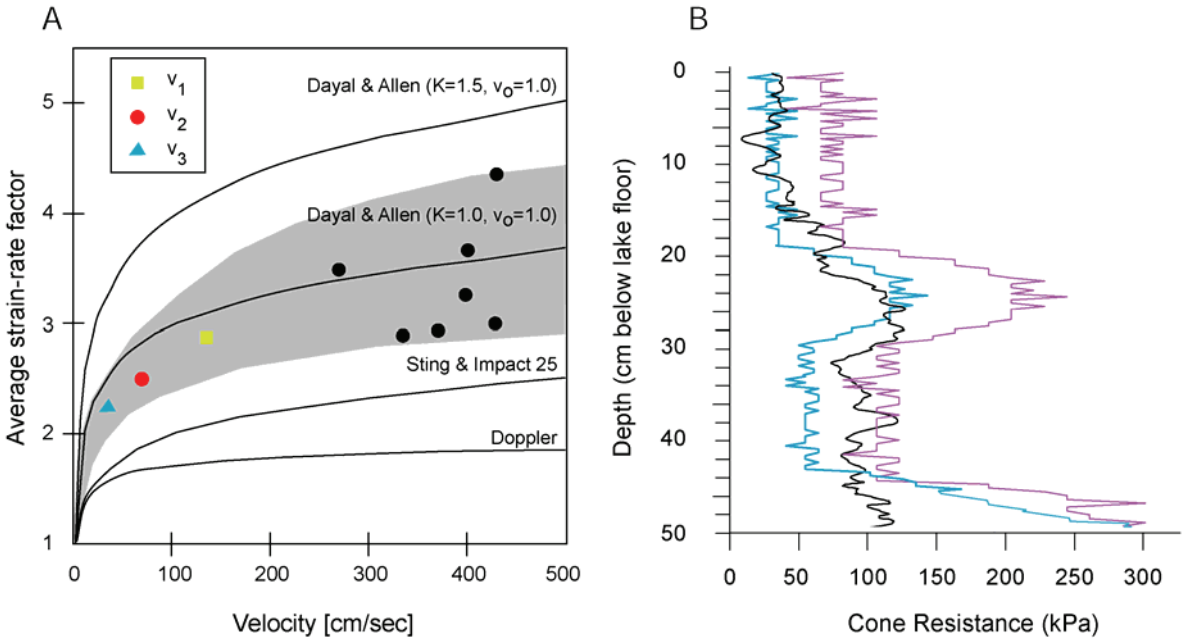

Figure 6: (a) Various forms of the strain-rate factor versus penetration velocity, as compiled by Stoll et al. (2007). Curves relate either to data by those authors (lowermost graphs) or are based on an equation by Dayal and Allen (1975) where the strain-rate factor = 1 + K log[$v_{dynamic}/v_{pushed}$], with K being the soil viscosity coefficient. Crosses represent data from CPT deployments into sands in the Gulf of Mexico (Stoll et al., 2007); coloured symbols represent deployment velocities used in this study. **(b)** Example how the strain-rate factors, as calculated from Dayal and Allen (1975), can be used to relate the dynamic test results (here: v3 deployment at 35 cm/s; purple curve) to the constant rate data (2 cm/s; black curve) at the same location. The blue curve represents the v_3 data divided by the strain-rate factor calculated for the dynamically decreasing penetration velocity during the experiment.

Below that layer, velocity steadily decreases until the instrument comes to a complete halt; here, SRF equals 1 and the "corrected" blue graph meets the raw data (purple; Fig. 6b). This result, which is reproducible at v1 and v2 in the majority of our deployments, attests that the equation postulated by Dayal and Allen (1975) is well applicable at fast penetration rates (ca. 20 cm/s and higher), but tends to overestimate SRF for the lower penetration rates (near the origin of Fig. 6a). As a consequence, correction of dynamic tests at slow rates (5 – 20 cm/s) cause the CPT parameters to be lower than what is measured during standard 2 cm/s experiments. At the very low end of the velocity spectrum, SRF approaches 1, and the measured and "corrected" values diverge even further until the two dynamic curves meet again at terminal depth (see Fig. 6b, purple and blue graphs). If we finally come back to the arbitrary ratio determined from the relative changes in penetration velocity and q_c increase (right column in Table 4), we observe two things. First, there is considerable scatter in the

ratio over more than two orders of magnitude (i.e. 6.4 through 667; Tab. 4). Second, a similar factor is not easily to be calculated for the results by Stoll et al. (2007) or our experiments, mostly because of the highly variable penetration velocity, even during the same deployment. Nonetheless, the wealth of data compiled here may serve to attest that dynamic CPT parameters cannot be placed into a systematic context. Regardless of some differences caused by the various instrument configurations in the papers cited, the main reason for this conclusion are most likely geological small-scale variations in sediment physical properties. Hence, absolute data measured should only be treated as an approximation. That acknowledged, the rapid, quasi-free fall tests may well represent an efficient means of geotechnical characterisation of shallow sub-seafloor deposits.

Literature

Abu-Farsakh, M.Y., Voyiadjis, G.Z., and Tumay, M.T., 1998. Numerical Analysis of the Miniature Piezocone Penetration Test (PCPT) in Cohesive Soils. International Journal for Numerical and Analytical Methods in Geomechanics, 22, 791-818.

Beard, R.M., 1985. Expendable Bottom Penetrometer for Deep Ocean Sediment Measurements. Strength Testing of Marine Sediments: Laboratory and In-Situ Measurements, ASTM, STP 883, R.C. Chaney and K.R. Demars (Eds.), *American Society for Testing and Materials*, Philadelphia, 101-124.

Bemben, S.M., and Myers, D.A., 1974. The influence of rate of penetration on static cone resistance values in Connecticut River Valley varved clay. Procs. Europ. Symposium on Penetration Testing, Stockholm, 2/2, 33-34.

Campanella, R.G., Gillespie, D., and Robertson, P.K., 1982. Pore pressure during cone penetration testing., *Procs. 2nd European Symposium on Penetration Testing*, ESOPT-II, Amsterdam (Balkema Pub.) 1, 507-512.

Christian, H.A., Heffler, D.E., and Davis, E.E., 1993. Lancelot – an in situ piezometer for soft marine sediments. Deep-Sea Research I, 40/7, 1509-1520.

Clayton, C.R.I., and Dikran, S.S., 1982. Pore water pressures generated during dynamic penetration testing. *Proc. 2nd Eur. Symp. On Penetration Testing*, Amsterdam (Balkema Pub.) 1, 245-250.

Clayton, C.R.I., Dikran, S.S., and Milititsky, J., 1983. The S.P.T. and foundation settlements: recent developments. *Highway Engineering*, 30/ 6, 2-7.

Clayton, C.R.I., Hababa, M.B., and Simons, N.E., 1985. Dynamic penetration resistance and the prediction of the compressibility of a fine-grained sand – a laboratory study. *Geotechnique*, 35/1, 19-31.

Davis, E.E., Horel, G.C., McDonald, R.D., Villinger, H., Bennett, R.H., and Li, H., 1991. Pore pressure and Permeabilities Measured in Marine Sediments With a Tethered Probe. Journal of Geophysical Research, 96/B4, 5975-5984.

Dayal, U., Allen, J.H., and Jones, J.M., 1973. Marine Impact Cone Penetrometer. *Proc. Conf. Int. Ocean '73*, Düsseldorf, West Germany, 912-923.

Dayal, U., and Allen, J.H., 1975. The effect of Penetration Rate on the Strength of Remolded Clay and Sand Samples. *Can. Geotech. J.,* 12, 336-348.

Dayal, U., 1978. Recent Trends in Underwater In-Situ Soil Testing. IEEE Journal of Oceanic Engineering, OE-3/4, 176-186.

de Mello, V.F.B., 1971. The standard penetration test - state of the art, *Proc. 4th PanAm. Conf. Soil Mech. Foundation Engineering,* Puerto Rico 1, 1-86.

Fenske, C.W., 1957. Deep vane tests in Gulf og Mexico. Proc. Symp. On Vane Shear Testing of Soils, ASTM STP 193, *American Society for Testing and Materials*, 16-25.

Ferguson, G.H., McClelland, B., and Bell, W.D., 1977. Seafloor cone penetrometer for deep penetration measurement of ocean sediment strength. In: Proc. 9th Offshore Technol. Conf. OTC 2787, 471-480.

Furlong, A., Osler, J., Christian, H, Cunningham, D., and Pecknold, S., 2006. The Moving Vessel Profiler (MVP) – a Rapid Environmental Assessment Tool for the collection of water column profiles and sediment classification. *Proc. UDT-Pacific Conference*, 2-13.

Harrison, W., and Richardson, A.M., 1967. Plate load test on sandy marine sediments, Lower Chesapeake Bay. In: Marine Geotechnique. Urbana, IL: Univ. Of Illinois Press. 274-290.

Harvey, F.E., Rudolph, D.L., and Frape, S.K., 1997. Measurement of hydraulic properties in deep lake sediments using a tethered pore pressure probe: Applications in the Hamilton Harbour, western Lake Ontario. Water Resour. Res., 33/8, 1917-1928.

Holubec, I. and D'Appolonia, E., 1973. Effect of particle shape on the engineering properties of granular soils. Proc. Symp. *Eualuarion of* Relative Density. In ASTM Spec. Tech. Publ. STP 523, 304-318.

Ingram, C., 1982. Expendable penetrometer for seafloor classification. Geo-Marine Letters, 2, 239-241.

Jezequel, J.F., 1969. "Les penetrometre statiques. Influence du mode d'emploi sur la resistance de pointe." Laboratoire Central des Ponts et Chaussees, Bulletin de Liaison, 36, 151-160.

Johnson, B.A., and Beard, R.M., 1985. A Lightweight 12-m Cone Penetrometer. Strength Testing of Marine Sediments: Laboratory and In-Situ Measurements, ASTM, STP 883, R.C. Chaney and K.R. Demars, Eds., American Society for Testing and Materials, Philadelphia, 125-139.

Juran, I., and Tumay, M.T., 1989. Soil stratification Using the Dual Pore-Pressure Piezocone Test. Transportation Research Record, No.1235, 68-78.

Karakouzian, M., B.B. Avar, N. Hudyma, and J.A. Moss, 2003. Field measurements of shear strength of an underconsolidated marine clay, Engineering Geology, 67, 233-242.

Kim, D.-K. and Tumay, M.T., 2004. Miniature Piezocone Test Results in Cohesive Soils. *The Electronical Journal of Geotechnical Engineering*, 9/E, Ppr0441.

Kiousis, P.D., Voyiadjis, G.Z., and Tumay, M.T., 1988. A large Strain Theory and its Application in the Analysis of the Cone Penetration Mechanism. International Journal for Numerical and Analytical Methods in Geomechanics, 12, 45-60.

Konrad, J.M., 1987. Piezo-friction-cone penetrometer testing in soft clays. *Canadian Geotechnical Journal*, 24, 645-652.

Lacasse, S., and Lunne, T., 1982. Penetration test in two Norwegian clays. Procs. of the 2nd European Symposium on Penetration Testing, ESOPT-II, Amsterdam, Balkema Pub., Rotterdam, 661-690.

Ladanyi, B., and Eden, W.J., 1969. Use of the deep penetration test in sensitive clays. Procs. of the 7th International Conference on Soil Mechanics and Foundation Engineering, Mexico, 1, 225-230.

Lunne, T., Eidsmoen, T., Powell, J.J.M., and Quaterman, R.S.T., 1986. Piezocone testing in overconsolidated clays. Procs. of the 39th Canadian Geotechnical Conference, Ottawa, Preprint Volume, Canadian Civil Geotechnical Society, 209-218.

Lunne, T., P.K. Robertson, and J.J.M. Powell, 1997. Cone Penetrating Testing in Geotechnical Practice, Spon Press, 312 pp.

Markauskas, D., Kacianauskas, R., Suksta, M., and Gediminas, V., 2002. Modelling the ConePenetration Test by the Finite Element Method. Foundations of Civil and Environmental Engineering, 2, 125-140.

Marsland, A., 1974. "Comparison of the results from static penetration tests and large in situ plate tests in London clay." Procs. of the European Symposium on Penetration Testing, ESOPT, Stockholm, 2.2, Balkema Pub., Rotterdam, 245-252.

May, R.E., 1987. *A study of the piezocone penetrometer in normally consolidated clay*. Ph.D. thesis, Exeter College, 243 pp.

McNeilan, T.W., and Bugno, W.T., 1985. Cone Penetration Test Results in Offshore California Silts. In: Strength Testing of Marine Sediments: Laboratory and In-Situ Measurements, ASTM, STP 883, R.C. Chaney and K.R. Demars (Eds.), American Society for Testing and Materials, Philadelphia, 55-71.

Melton, J.S., Clausner, J.E., Christian, H., and Furlong, A., Use of Dynamic Penetrometer to Determine Fluid Mud Properties. Proceedings of Conference on Dredged Material Management, Cambridge, MA, in press.

Meunier, J., Sultan, N., Jegou, P., and Harmegnies, F., 2004. First Tests of Penfeld : a New Seabed Penetrometer. Proceedings of the 14th (2004) International Offshore and Polar Engineering Conference Toulon, France, May 23-28, 2004, 338-345.

Noorany, I., 1971. Underwater soil sampling and testing – A state-of-the-art review. Symp. on Underwater Soil Sampling Testing and Construction Control, ASTM, STP, 501, American Society for Testing and Materials, 3-41.

Powell, J.J.M, and Uglow, I.M., 1988. The interpretation of the Marchetti dilatometer test in UK clays. Proc. Institution Civil Engineers, Penetration Testing in the UK, Univ. Birmingham, 34, 269-273.

Preslan, W.L., 1969. Accelerometer-monitored coring. Procs. Civil Engineering in the Oceans II, ASCE Conference, Miami Beach (FL), December 10-12, 655-678.

Randolph, M.F., Hefer, P.A., Geise, J., and Watson, P.G., 1998. Improved seabed strength profiling using T-bar penetrometer. Procs. Int. Conf. Offshore Site Investigation and Foundation behaviour. 'New frontiers', Society for Underwater Technology. London, 221-235.

Richards, A.F., McDonald, V.J., Olson, R.E., and Keller, G.H., 1971. In place measurements of deep sea soil shear strength. In: *Symposium on Underwater Soil Sampling, Testing and Construction Control, ASTM STP 501, American Society for Testing and Materials*, 55-68.

Roy, M., M. Tremblay, F. Tavenas, and P. La Rochelle, 1982. Development of pore pressure in quasi-static penetration tests in sensitive clay. Can. Geotech. J., 19, 124-138.

Ruiter, J.D., and Fox, D.A., 1975. Site investigation for North Sea forties fold, Proc. 7th Offshore Technological Conference, OTC 2246, 21-36.

Scott, R.F., 1967. In place measurement of the ocean floor soils by accelerometer, Prco. Conf. on Civil Engineering in the Oceans – I, ASCE (San Francisco, CA), 419-444.

Silva, M.F., White, D.J., and Bolton, M.D., 2006. An analytical study of the effect of penetration rate on piezocone tests in clay. International Journal for Numerical and Analytical Methods in Geomechanics, 30, 501-527.

Song, C.R., Voyiadjis, G.Z., and Tumay, M.T., 1999. Determination of permeability of soil using the multiple piezo-element penetrometer. International Journal for Numerical and Analytical Methods in Geomechanics, 23, 1609-1629.

Spooner, I.S., Williams, P., and Martin, K., 2004. Construction and use of an inexpensive, lightweight free-fall penetrometer: applications to paleolimnological research. Journal of Paleolimnology, 32, 305-310.

Stegmann, S., Kopf, A., and H. Villinger, 2006a. Design of a Modular, Marine Free-Fall Cone Penetrometer, A Time and Cost-Effective Device for In-Situ Geotechnical Characterization of Marine Sediments, Sea Technology 47/2, 27-33.

Stegmann, S., Moerz, T., and Kopf, A., 2006b. Initial Results of a new Free Fall-Cone Penetrometer (FF-CPT) for geotechnical in situ characterisation of soft marine sediments. Norwegian Journal of Geology, 86/3, 199-208.

Stegmann, S., Strasser, Michael, Anselmetti, F., and Kopf, A., 2007. Geophys. Res. Lett., 34, L07607, doi:10.1029/2006GL029122

Stegmann, S., and Kopf, A., in press. Marine Deep-Water Free-Fall CPT Measurements for LandslideCharacterisation off Crete, Greece (Eastern Mediterranean Sea), Part I: A new 4000m Cone Penetrometer. In: Lykousis, V., Sakellariou, D., Locat, J. (Eds.), *Proc. 3rd Symposium in Submarine Mass Movements and Their Consequences,* Kluwer-Springer.

Stoll, R.D., and Akal, T., 1999. XBP-Tool for Rapid Assessment of Seabed Sediment Properties. Sea Technology, 40/2, 47-51.

Stoll, R.D.,2004. Measuring Sea Bed Properties Using Static and Dynamic Penetrometers. Civil Engineering in the Oceans VI, Proceedings of the International Conference, October 20–22, 2004, Baltimore, Maryland, USA. Briggs, J.M., McCormick, M.E. (Eds.), doi:10.1061/40775(182)31

Stoll, R.D., and Sun, Y.-F., 2005. Using Static and Dynamic Penetrometers to Measure Sea Bed Properties. Office of Naval Research, Science & Technology, Ocean Battlespace Sensing (32), Coastal Geosciences Annual Reports FY05: 1-5, also available at http://www.onr.navy.mil/obs/321/docs/cg/04/cgstoll.pdf

Stoll, R.D., Sun, Y.-F., and Bitte, I., 2007. Seafloor properties from Penetrometer Test. IEEE Journal of Oceanic Engineering, 32/1, 57-63.

Susila, E., and Hryciw, R.D., 2003. Large displacement FEM modelling of the cone penetration test (CPT) in normally consolidated sand. International Journal for Numerical and Analytical Methods in Geomechanics, 27, 585-602, DOI:10.1002/nag.287.

Taylor, R.J., and Demars, K.R., 1970. Naval in place sea floor test equipment. Naval Civil Engineering Laboratory, Port Hueneme, CA, Technical Note N-1135, 45.

Te Kamp, W.G.B., 1982. The influence of the rate of penetration on cone resistance 'q_c' in sand. Procs. of the 2nd European Symposium on Penetration Testing, ESOPT-II, Amsterdam, Balkema Pub., Rotterdam, 627-633.

Terzaghi, K., 1946. Theoretical Soil Mechanics., John Wiley And Sons, New York, 510 pp.

Terzaghi, K., and Peck, R.B., 1948. Soil Mechanics in Engineering Practice, John Wiley And Sons, New York, 566 pp.

Villinger, H., Grigel, J., and Heesemann, B., 1999. Acceleration-monitored coring revisited. Geo-Marine Letters, 19, 275-281.

Vivatrat, V., 1978. "Cone penetration in clays." Ph.D. thesis, Massachusetts Institute of Technology, Cambridge, 429 pp.

Wood, D.M., 1985. Some Fall-Cone Tests. Geotechnique, 35/1, 64-68.

Wright, I., 2004. Geotechnical Investigations Using Mini-Cone Penetrometer Testing. Sea Technology, 45, 7, 49-52.

Yu, H.S., Herrmann, L.R., and Boulanger, R.W., 2000. Analysis of steady Cone Penetration in Clay. Journal of Geotechnical and Geoenvironmental Engineering, 127, 7, 594-604.

Acknowledgments

We are grateful to W. Conrades and his team at Atlas Elektronik for providing outstanding support when carrying out the CPT experiments at their site at Lake Hemelingen. Further assistance by M. Lange, H. Hanff, A. Förster, T. Mörz and W. Schunn helped to carry out the tests both in the field and the laboratory. Funding for this study was provided by DFG (German Research Foundation) through RCOM, Univ. Bremen (project C8).

5. Geological Application

In addition to the initial studies near Bremen, both FF-CPT devices were applied to geological settings concerning slope failure processes and pore pressure measurements in fine-grained sediments in different geological settings. Slope stability was studied comprehensively on small-scale, seismicity-induced mass movement in Lake Lucerne, Central Switzerland (*Chapters 5.1, 5.2*), and on a larger scale in the active convergent margin off Crete (Greece), Eastern Mediterranean Sea (*Chapter 5.3*). Providing a data set of *in situ* strength and pore pressure that is complemented by cores, FF-CPT measurements support sedimentary and mapping data to illuminate the controlling factors for failure in each region. In a fourth study SW-FF-CPT tests in fine-grained sediments of the Baltic Sea were carried out to utilise the pore pressure behaviour of cohesive superficial sediments to estimate gas content and overpressuring (*Chapter 5.4*). A fifth campaign provides CPT measurements in an active mud volcano (Dashgil) in Azerbaijan. A series of experiments were performed to get an idea of the stiffness of the material in the crater lake from the flanks to the conduit. Data serve to assess the likelihood of methane-rich eruptions in the near future.

5.1. Geotechnical *in situ* characterization of subaquatic slopes: The role of pore pressure transients versus frictional strength in landslide initiation

Stegmann, S., Strasser, M., Anselmetti, F., and Kopf, A., Geophys. Res. Lett., 34, L07607, doi:10.1029/2006GL029122, published in 2007.

GEOPHYSICAL RESEARCH LETTERS, VOL. 34, L07607, doi:10.1029/2006GL029122, 2007

Geotechnical in situ characterization of subaquatic slopes: The role of pore pressure transients versus frictional strength in landslide initiation

Sylvia Stegmann,[1] Michael Strasser,[2] Flavio Anselmetti,[2] and Achim Kopf[1]

Received 26 December 2006; revised 26 February 2007; accepted 7 March 2007; published 11 April 2007.

[1] Mineralogical composition and pore fluid pressure are the crucial controls for mechanical stability of water-saturated sediments. Their in situ measurements were undertaken in earthquake-triggered slope deposits in Lake Lucerne (Switzerland) in addition to geophysical characterization and laboratory index properties, shear and consolidation experiments on core. Two lithological units were identified: A weak, lightly underconsolidated section of postglacial silty clays overlies overconsolidated fine-grained glacial deposits with coarser components and excess fluid pressure (ca. 2.5× higher than in the hanging wall clay). In the event of an earthquake, hydrofracturing in the overconsolidated section facilitates an upward pore pressure pulse to the base of the softer, less stable unit. Here, excess pore pressure initiates sliding along a failure plane at the lithological boundary, causing the entire postglacial sedimentary section to slip downslope. We propose that many submarine landslides at active and passive continental margins may follow this mechanism of pore pressure-induced failure. **Citation:** Stegmann, S., M. Strasser, F. Anselmetti, and A. Kopf (2007), Geotechnical in situ characterization of subaquatic slopes: The role of pore pressure transients versus frictional strength in landslide initiation, *Geophys. Res. Lett.*, *34*, L07607, doi:10.1029/2006GL029122.

1. Introduction

[2] Measurement of pore fluid pressure as a crucial factor controlling effective strength and mechanical behavior of saturated sediments is a difficult task, because the measurement itself disturbs the hydrologic regime [*Schultheiss*, 1990; *Lee and Elsworth*, 2004]. Otherwise, pore pressure is a fundamental parameter for the understanding of the stability of (saturated) sediments and hazards. The stability of sediment is controlled by shear strength τ at a given normal stress σ_n, where friction coefficient μ is the ratio between the two and pore pressure P lowers effective normal stress ($\tau = [\sigma_n - P]\mu$) [*Hubbert and Rubey*, 1959]. Extensive research concerning the stability of marine sediments has been carried out [e.g., *Biscontin et al.*, 2004; *Sultan et al.*, 2004]. Much of the geotechnical data on landslide sediments were derived in laboratory experiments [e.g., *Ilstad et al.*, 2004], and rather little is known about in situ sediment strength and pore pressure [*Baltzer et al.*, 1994]. Despite the difficulty of in situ pore pressure measurements in marine sediments, however, seagoing piezoprobes measuring pore pressure [e.g., *Davis et al.*, 1991] and additionally sediment strength [*Stegmann et al.*, 2006] have been developed recently. This paper presents results from the study of earthquake-induced subaquatic slope failure in Lake Lucerne (Switzerland) using in situ vane shear and Cone Penetrating Testing (CPT) devices to obtain the key geotechnical parameters. These data help distinguish between the role of pore pressure vs. mineralogically controlled strength and their ramifications for landslide initiation. Furthermore the in situ data complement an extensive geophysical and sedimentary data base [*Strasser et al.*, 2007] and are used for comparison with laboratory-derived pre-consolidation stresses. With the unique, comprehensive set of largely in situ data, we are able to unambiguously distinguish the relative role of fluids vs. sedimentary constituents in failure of slope sediments.

2. Geological Setting

[3] This study focuses on the biggest subaqueous mass movement (Weggis Slide) of perialpine, glacially-overdeepened Lake Lucerne, central Switzerland (Figure 1). A detailed description of the slope and sediment characteristics is given by *Schnellmann et al.* [2005] and *Strasser et al.* [2007]. In summary, the translational tsunamigenic landslide mobilized ~8.5 × 10^6 m^3 of sediment and was triggered by a M~6.2 earthquake that hit the Lucerne area in 1601 A.D. The intact sedimentary succession covering the ~10–15° dipping glacially eroded bedrock adjacent to the prominent 1601 A.D.-failure scar consists at the base of thin (1–3 m thick) glacially deformed, glacio-lacustrine sediments (in this paper assigned to glacial deposits, unit 2), that are overlain by 4–6 m of Late Pleistocene to Holocene fine-grained lacustrine drape deposits (here assigned to postglacial deposits, unit 1). The failure surface of the Weggis Slide, as revealed by high-resolution 3.5 kHz acoustic seismic profiles (Figure 1) and sediment cores coincides with the lithological boundary between the glacial and postglacial deposits.

3. Methods

[4] From a moored platform, an in situ vane shear probe (Genor A/S) and a free-fall cone penetrometer [*Stegmann et al.*, 2006] were deployed. Both devices sank by their own weight into the soft, clay-rich sediment adjacent to the failure scar (Figure 1). Local water depth was 31.5 m (hydrostatic pressure [P_{hyd}] ~309 kPa). In situ vane shear tests were performed at 30- and 50-cm intervals using a

[1] Research Centre Ocean Margin, University of Bremen, Bremen, Germany.
[2] Geological Institute, Eidgenössische Technische Hochschule, Zurich, Switzerland.

0094-8276/07/2006GL029122$05.00

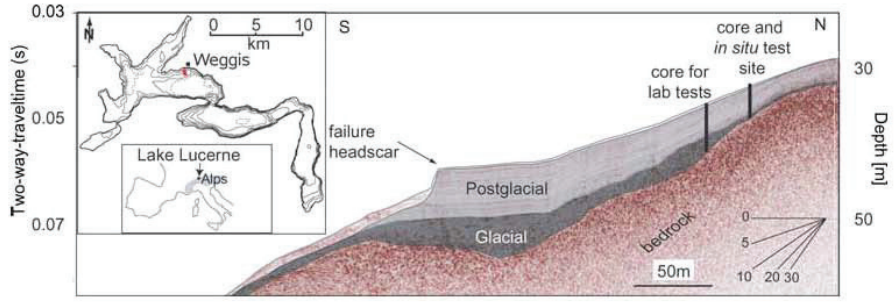

Figure 1. 3.5 kHz seismic reflection profile across the Weggis Slide showing the morphology of the slide and the different lithological units. The black bar marks the location of coring and in situ testing.

6.5 cm diameter vane. Penetration depth of the probe was taken from the wire length. At each target depth the probe was extruded carefully from the casing into the undisturbed sediment and rotated mechanically from the platform at a constant rate of 6°/min until failure occurred. A 15 cm^2 CPT probe mounted to a lance-shaped autonomous instrument was deployed in the same stepwise-fashion. During insertion of the penetrometer, cone resistance q_c, sleeve friction f_s and pore pressure u_2 were measured to determine the stiffness and the excess pore pressure of the sediment. The lance was held at each penetration level for 10 minutes to observe the dissipation of the induced pore pressure signal towards ambient in situ values. Additionally, CPT data were used to estimate undrained shear strength S_u. Depending on the mode of failure, soil anisotropy, strain rate, and stress history, a theoretical relationship between S_u and corrected cone resistance q_t can be used (see summary by *Lunne et al.* [1997]): $S_u = (q_t - \sigma_{vo})/N_k$, where N_k is an empirical cone factor and σ_{vo} is the in situ total vertical stress. N_k averages 15 for normally consolidated clays and 17 for overconsolidated clay [*Lunne et al.*, 1997]. Assuming that the insertion pore pressure is dominated by a pressure pulse associated with the displacement and/or compaction of the sediment, *Esrig et al.* [1977] suggest an empirical relationship for soft saturated sediments between the maximum pore pressure during insertion U_{imax} and S_u: $S_u = U_{imax}/6$. Regarding the relationship between S_u and U_{imax}, we use the maximum pore pressure within the 10 minutes window ignoring the artificial excursion of the pressure signal during impact. This procedure is based on the assumption that at the end of each testing period, pore pressure values are closest to ambient background values. Laboratory measurements were carried out on two sediment cores adjacent to the site where the in situ tests were performed (Figure 1). Sediment bulk density was measured using a multi-sensor core logger (GEOTEK) at ETH Zurich. Grain size analyses were performed using laser diffraction techniques at ~10-cm intervals along the split core. Clasts >2 mm in the glacial sediments were extracted and measured prior to analysis. Every 15 cm S_u was measured on the same split core using a standard laboratory vane shear device. In addition, ring shear and oedometer tests were carried out on the two distinct lithologies, i.e. above (3.5 m core depth) and beneath (6.3 m core depth) the sliding surface. Ring shear tests were conducted using a custom-built Bromhead ring-shear apparatus at RCOM Bremen. Progressive loading increments up to normal stresses of between 100 and 400 kPa were performed corresponding to the in situ normal stress of the tested specimens. After consolidation, the samples were sheared under drained conditions at a rate of 0.001 mm/s until peak strength was reached. On the residual path of each experiment, rate-dependency and frictional behavior of drained shear strength were tested at different rates (0.0005, 0.01 and 0.1 mm/s). The uniaxial compression behavior of the sediments was studied using an oedometer after *Terzaghi* [1925] with progressive loading increments from 5 kPa to 4 MPa effective stress. Experiments on the glacial and postglacial sediments served to evaluate the consolidation behavior, expressed by the overconsolidation ratio $OCR = \sigma'_c/\sigma'_o$, with σ'_c known as the preconsolidation stress *sensu* [*Casagrande*, 1936] and σ'_o as the overburden stress.

4. Results

[5] The combination of in situ and laboratory measurements provide a consistent characterization of the sediment properties immediately upslope of the Weggis Slide scar, and allow us to define two lithological units on the basis of geotechnical data (glacial vs. postglacial). Both types of sediments are dominated by silt and clay (40% and 55%, respectively) with max. 20% sand in the glacial unit (Figure 2a). In the postglacial section, CPT data show a continuous increase of q_c with depth reaching 150 kPa, whereas f_s vary between 0.5 and 2 kPa (Figure 2b). Below 3.8 m both parameters rise abruptly to 318 and 5.2 kPa, respectively, before q_c decreases within the glacial unit to a value of 240 kPa at the bottom of the depth profile (Figure 2b). Pore pressure follows the same trend as q_c and f_s, with higher excess pore pressures in the lower (glacial) unit (Figure 2c). In a typical measurement, a spike in pore pressure in unit 1 is induced upon insertion, followed by a non-linear asymptotic decrease towards background values. Here, pore pressure dissipates to about 70 80% of the insertion value after 10 minutes. In contrast, the underlying glacial unit shows negative pressures upon insertion, which are then followed by an increase in pore pressure during the 10 minutes recording. We interpret this increase to indicate ambient overpressures, which is supported by high values up to 80 kPa above P_{hyd} after 10 minutes. When undrained shear strength based on CPT data is compared to in situ and laboratory vane shear tests, a similar trend is recognized (Figure 3). Depending on the method, S_u in postglacial deposits ranges between 0.5 4.5 kPa (Figure 3a), 3 6.5 kPa (Figure 3b), and 1.5 6.5 kPa (Figure 3c). In the glacial unit, S_u increases up to 16 kPa

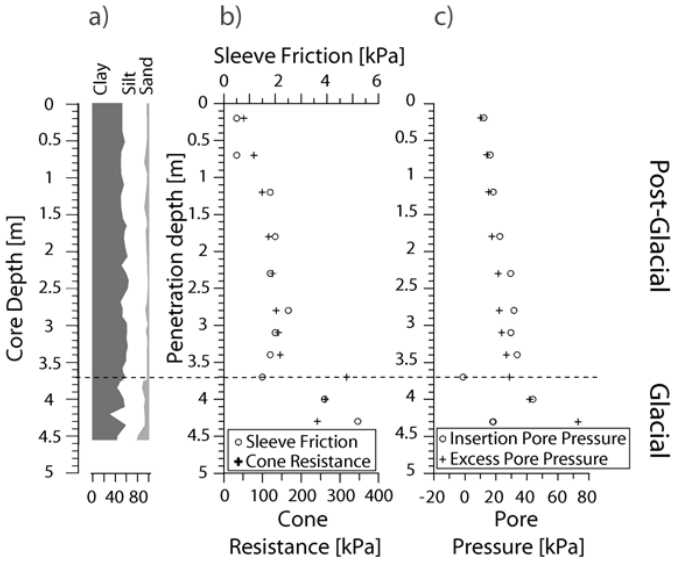

Figure 2. Physical and sedimentary properties along the Weggis slope, measured on a core and in situ. (a) Grain size distribution, (b) in situ CPT cone resistance and sleeve friction, and (c) in situ pore pressure measured during CPT insertion and after 10 minutes.

(Figures 3b and 3c). in situ S_u derived from q_c, agrees well with the lab vane shear (Figures 3b and 3c), whereas in situ measurements using the vane shear probe are significantly lower (<8 kPa in the glacial clay; Figure 3a). The discrepancy between in situ vane shear and CPT data may be partly explained by a general underestimation of the first caused by the pre-disturbance of the sediment by the insertion of the device before shearing and, moreover, by uncertainties when choosing the empirical factor N_k for calculating S_u from CPT data [*Karakouzian et al.*, 2003]. However, an overall increase in strength in the lower unit can be observed regardless of the method. Ring shear tests serve to measure the mineralogically controlled frictional behavior at quasi-infinite strain. Our results show a similar mechanical behavior for glacial and postglacial sediments.

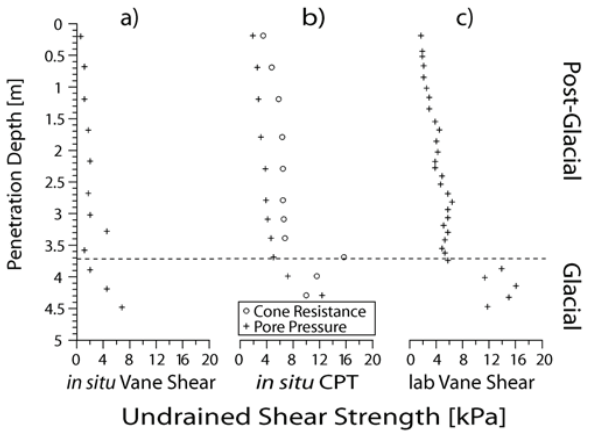

Figure 3. Undrained shear strength based on (a) in situ vane shear probe, (b) in situ CPT, and (c) laboratory vane shear probe.

Peak shear strength ranges between 41 and 143 kPa at 100 and 400 kPa normal stress, leading to friction coefficients of approximately 0.36 0.4 for either lithology, which is typical for silty clay [*Lupini et al.*, 1981; *Logan and Rauenzahn*, 1987; *Brown et al.*, 2003]. Also, both the glacial and postglacial sediments show velocity strengthening behavior when tested at various shear rates. The overall similarity of the ring shear tests suggests that both sediment types are dominated by clay minerals resulting in similar mechanical behavior (Figure 2a). Oedometer tests on samples from above and beneath the sliding surface reveal that the postglacial sediment is very compressible, slightly underconsolidated (OCR = 0.86), and has a pre-consolidation stress of 19 kPa (see Figure S1 of the auxiliary material).[1] Glacial sediments, however, are characterized by a lower compressibility with high pre-consolidation stresses of 100 kPa[a] and overconsolidation (OCR = 1.58), the latter resulting from glacial compaction [see *Strasser et al.*, 2007].

5. Discussion

[6] It has long been known that fault initiation, propagation and slip are a function of fault zone mineralogy and transient pore pressure [*Hubbert and Rubey*, 1959]. Separating the effect of intrinsic sediment friction from that of pore pressure is one of the major targets in marine soil mechanics. Attempts to achieve this goal usually rely on modelling or estimating the excess pore pressure from geophysical data or water release due to mineral dehydration and gas hydrate processes [*Moore and Shipboard Party ODP Leg 156*, 1995; *Brown et al.*, 2001; *Saffer et al.*, 2000]. However, these studies do not include the in situ measurement of pore pressure and are hence hampered by uncertainties. In our study of Lake Lucerne slope deposits, we are

Auxiliary materials are available in the HTML. doi:10.1029/2006GL029122.

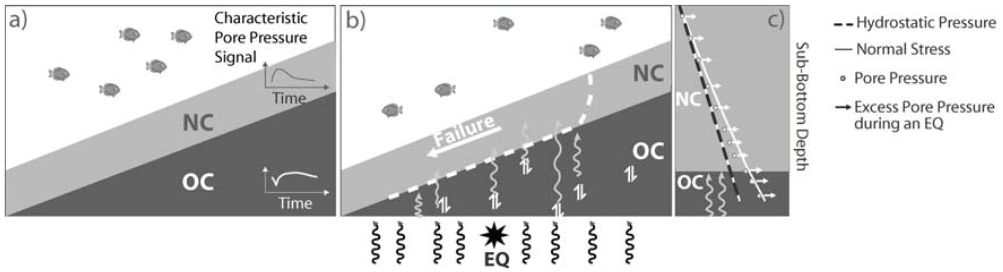

Figure 4. Conceptual model of the forces acting on and within a sedimentary sequence prior and during an earthquake event. Next to the two lithological units, we show diagrams of the typical pore pressure response during CPT tests in those sediments. (a) Pre-failure condition. (b) Failure triggered by an EQ. Wiggly arrows illustrate stress changes from depth and associated pore pressure pulses in the overburden (white wiggly arrows); up-and-down arrows represent hydrofractures. (c) Schematic sketch of effective stress conditions during an EQ, based on actual data (core and CPT). White arrows represent pore pressure increase during an EQ (see discussion).

able to separate the two factors by a suite of in situ and laboratory measurements. On a regional level, our results show a reliable quantitative geotechnical characterization of the undisturbed glacial-to-postglacial succession in the source area of the Weggis Slide, which failed along a planar sliding surface that developed at the lithological boundary between slightly underconsolidated postglacial deposits and overconsolidated glacial deposits. Measured in situ pore pressure can be related to the different states of consolidation (see Figures 1, 2c, and S1), where negative insertion pore pressure in the overconsolidated unit may be generated by dilatant shear behavior with a displacement of fluids during insertion and a following slow increase of pore pressure controlled by the low permeability. We can exclude, that measured negative response is due to suction by pulling back the tool, because the acceleration sensor did not show any movement after insertion. Undrained shear strength, measured and derived with several methods, accentuates the difference in strength and consolidation state between the two lithologies. In contrast, laboratory ring shear frictional properties reveal no significant difference in the mechanical behavior of glacial and postglacial sediments. We conclude that pore pressure (and related lowering of effective stress) rather than the presence of weak mineral phases plays the key role in failure initiation along the Weggis slope. On a broader scale, our results may have important repercussions for triggering of failure processes along marine slopes and continental margins at lowered effective stresses. We condense our result to a model of earthquake-triggered failure initiation along the lithological boundary between two sediment layers with similar intrinsic mechanical behavior, but different consolidation and pore pressure regimes. The underlying overconsolidated sediments have lower permeability and higher shear strength, while their overburden drape is characterized by slightly more permeable, less competent sediments (Figure 4). At constant stress, such a slope is stable (Figure 4a). In case of an earthquake, however, seismic pulses from the poroelastic response to the earthquake-induced strain generate hydrological transients and - possibly - hydrofractures [*Cocco and Rice*, 2002]. A stress pulse may disrupt the overconsolidated glacial clay, thereby transferring excess pore fluid pressures up to less stable Holocene deposits (Figure 4b). This model may be transferred from the micro-scale lacustrine realm to the macro-scale landslide prone active and passive margins. Long-term records of pore pressure along the Nankai Trough [*Davis et al.*, 2006] and Costa Rica subduction zones [*Brown et al.*, 2005] and of water-level oscillations on-shore Oregon [*Brodsky et al.*, 2003] have documented the interaction between seismicity and pore pressure as well as its transfusion over tens of kilometres. At the frontal thrust of the Nankai accretionary prism, *Davis et al.* [2006] have measured up to >100 kPa increase in pore pressure to low-frequency EQs (M3.5 4.4) some 10 s of km away. Given that the 1601 A.D. M 6.2 EQ epicenter is only 15 km from the Weggis site, even a smaller pore pressure pulse may likely have caused values in excess of lithostatic (see arrows in Figure 4c). Hydrofracturing may have been facilitated by the historically documented 4 m-high tsunami waves after the 1601 EQ, which caused cyclic normal stress drops and eventually failure. This mechanism seems similar to large-scale landslides in seismic and/or tectonically active regions, where transient pore pressure pulses as main triggers have been proposed. One of the largest landslides is the Storegga Slide on the Mid-Norwegian shelf (3000 km^3). Considering the pre-failure condition for slope instability (rapid loading of clayey sediments, over-pressuring during glaciation cycles and possible dissociation of gas hydrates) initial failure has been linked to a M > ~7 EQ [*Bryn et al.*, 2005]. Other large mass movements at passive margins are often related to rapid sediment accumulation and overpressures (New Jersey margin; *Dugan and Flemings* [2000]). Slope failure along convergent margins may be associated with tectonic steepening and fluid venting during subduction processes (e.g., slumps and landslides along the Middle American Trench; *von Huene et al.* [2004]). At volcanic margins or islands, both seismicity in the magma chamber and hydrothermal circulation adjacent to it influence the pore pressure regime, making these factors responsible for mega-landslides such as those in La Palma, Canary Island (ca. 5000 km^2; *Masson et al.* [2002]) or the Nuuanu Landslide, Hawaiian Islands (ca. 5000 km^2; *Moore et al.* [1994]).

6. Conclusions

[7] As a general conclusion, we emphasize that despite variability in regional geological processes and regardless of

the scale of the mass wasting event, slope instability is often triggered by variations in pore pressure resulting from underlying processes such as sedimentary, glacial, tidal, storm-wave and tectonic loading, gas hydrate processes, or EQ tremor [*Hampton et al.*, 1996; *Locat*, 2001]. The reliable in situ measurement of pore pressure, ideally over longer periods of time, will be the most promising step towards a more complete understanding of landslide initiation, risk assessment and mitigation.

[8] **Acknowledgments.** We thank Robert Hofmann, Felix Bussmann and Benjamin Dürr from ETH Zürich for their help and enthusiasm during the measurements on Ararat platform in fall 2005. We thank the Limnologic Research Center of Eawag for providing logistic support during the field campagn. Beat Rick is acknowledged for assisting with the in situ vane shear device (Dr. von Moos AG, Zürich). Tobias Mörz and Stefan Kreiter are acknowledged for discussion and help with oedometer testing at RCOM Bremen. We thank Peter Clift for language check and discussion. The manuscript benefited strongly from the constructive comments, ideas and discussion by referees Demian Saffer and Mike Tryon. This study was funded by Swiss National Science Foundation (SNF grant 620-066113) and German Science Foundation (to RCOM Bremen). This is RCOM publication 0467.

References

Baltzer, A., P. Cochonat, and D. J. W. Piper (1994), In situ geotechnical characterisation of sediments on the Nova Scotian slope, eastern Canadian continental margin, *Mar. Geol.*, *120*, 291–308.

Biscontin, G., J. M. Pestana, and F. Nadim (2004), Seismic triggering of submarine slides in soft cohesive soil deposits, *Mar. Geol.*, *203*, 341–354.

Brodsky, E. E., E. Roeloffs, D. Woodcock, I. Gall, and M. Manga (2003), A mechanism for sustained groundwater pressure changes induced by distant earthquakes, *J. Geophys. Res.*, *108*(B8), 2390, doi:10.1029/2002JB002321.

Brown, K. M., D. A. Saffer, and B. A. Bekins (2001), Smectite diagenesis, pore-water freshening, and fluid flow at the toe of the Nankai wedge, *Earth Planet. Sci. Lett.*, *194*, 97–109.

Brown, K. M., A. Kopf, M. Underwood, J. Steurer, and J. L. Weinberger (2003), Frictional and mineralogic properties of sediments entering the western Nankai subduction zone: Implications for state of stress on the subduction thrust, *Earth Planet. Sci. Lett.*, *214*, 589–613.

Brown, K. M., M. D. Tryon, H. R. DeShon, L. M. Dorman, and S. Y. Schwartz (2005), Correlated transient fluid pulsing and seismic tremor in the Costa Rica subduction zone, *Earth Planet. Sci. Lett.*, *238*, 189–203.

Bryn, P., K. Berg, C. F. Forsberg, A. Solheim, and T. J. Kvalstad (2005), Explaining the Storegga slide, *Mar. Pet. Geol.*, *22*, 11–19.

Casagrande, A. (1936), The determination of preconsolidation load and its significance, paper presented at the First International Conference on Soil Mechanics and Foundation Engineering, Cambridge, Mass., 22–26 June.

Cocco, M., and J. R. Rice (2002), Pore pressure and poroelasticity effects in Coulomb stress analysis of earthquake interactions, *J. Geophys. Res.*, *107*(B2), 2030, doi:10.1029/2000JB000138.

Davis, E. E., G. C. Horel, R. D. McDonald, H. Villinger, R. H. Bennett, and H. Li (1991), Pore pressures and permeabilities measured in marine sediments with a tethered probe, *J. Geophys. Res.*, *96*(B4), 5975–5984.

Davis, E. E., K. Becker, K. Wang, K. Obara, Y. Ito, and M. Kinoshita (2006), A discrete episode of seismic and aseismic deformation of the Nankai trough subduction zone accretionary prism and incoming Philippine Sea plate, *Earth Planet. Sci. Lett.*, *242*, 73–84.

Dugan, B., and P. B. Flemings (2000), Overpressure and fluid flow in the New Jersey continental slope: Implications for slope failure and cold seeps, *Science*, *289*, 288–291.

Esrig, M. I., R. C. Kirby, and R. G. Bea (1977), Initial development of a general effective stress method for the prediction of axial capacity for driven piles in clay, paper presented at the 9th Annual Offshore Technology Conference, Houston, Tex., 2–5 May.

Hampton, M. A., H. J. Lee, and J. Locat (1996), Submarine landslides, *Rev. Geophysics*, *34*, 33–59.

Hubbert, M. K., and W. W. Rubey (1959), Role of fluid pressure in the mechanics of overthrust faulting. I: Mechanics of fluid filled porous solids and its applications to overthrust faulting, *Geol. Soc. Am. Bull.*, *70*, 115–166.

Ilstad, T., J. G. Marr, A. Elverhoi, and C. B. Harbitz (2004), Laboratory studies of subaqueous debris flow by measurements of pore-fluid pressure and total stress, *Mar. Geol.*, *213*, 403–414.

Karakouzian, M., B. B. Avar, N. Hudyma, and J. A. Moss (2003), Field measurements of shear strength of an underconsolidated marine clay, *Eng. Geol. Amsterdam*, *67*, 233–242.

Lee, D. S., and D. Elsworth (2004), Indentation of a free-falling sharp penetrometer into poroelastic seabed, *J. Eng. Mech.*, *130*, 170–179.

Locat, J. (2001), Instabilities along ocean margin: A geomorphological and geotechnical perspective, *Mar. Pet. Geol.*, *18*, 503–512.

Logan, J. M., and K. A. Rauenzahn (1987), Frictional dependence of gouge mixtures of quartz and montmorillonite on velocity, composition and fabric, *Tectonophysics*, *44*, 87–108.

Lunne, T., P. K. Robertson, and J. J. M. Powell (1997), *Cone Penetration Testing in Geotechnical Practice*, Taylor and Francis, Philadelphia, Pa.

Lupini, J. F., A. Skinner, and A. E. Vaughan (1981), The drained residual strength of cohesive soils, *Géotechnique*, *31*, 181–213.

Masson, D. G., A. B. Watts, M. J. R. Gee, R. Urgeles, N. C. Mitchell, T. P. Le Bas, and M. Canals (2002), Slope failure on the flanks of the western Canary Islands, *Earth Sci. Rev.*, *57*, 1–35.

Moore, J. C., and Shipboard Party ODP Leg 156 (1995), Abnormal fluid pressures and fault-zone dilation in the Barbados accretionary prism: Evidence from logging while drilling, *Geology*, *23*, 605–608.

Moore, J. G., W. R. Normark, and R. T. Holcomb (1994), Giant Hawaiian underwater landslides, *Science*, *264*, 46–47.

Saffer, D. M., E. A. Silver, A. T. Fischer, H. J. Tobin, and K. Moran (2000), Inferred pore pressures at the Costa Rica subduction zone; implications for dewatering processes, *Earth Planet. Sci. Lett.*, *177*, 193–207.

Schnellmann, M., F. Anselmetti, D. Giardini, and J. A. McKenzie (2005), Mass movement-induced fold-and-thrust belt structures in unconsolidated sediments in Lake Lucerne (Switzerland), *Sedimentology*, *52*, 271–289.

Schultheiss, P. J. (1990), Pore pressures in marine sediments: An overview of measurement techniques and some geological and engineering applications, *Mar. Geophys. Res.*, *12*, 153–168.

Stegmann, S., H. Villinger, and A. Kopf (2006), Design of a modular, marine free-fall cone penetrometer, *Sea Technol.*, *47*(2), 27–33.

Strasser, M., S. Stegmann, F. Bussmann, F. S. Anselmetti, B. Rick, and A. Kopf (2007), Quantifying subaqueous slope stability during seismic shaking: Lake Lucerne as model for ocean margins, *Mar. Geol.*, in press.

Sultan, N., et al. (2004), Triggering mechanism of slope instability processes and sediment failures on continental margins: A geotechnical approach, *Mar. Geol.*, *213*, 291–321.

Terzaghi, K. (1925), *Erbaumechanik auf bodenphysikalischer Grundlage*, 399 pp., Franz Deuticke, Leipzig, Germany.

von Huene, R., C. R. Ranero, and P. Watts (2004), Tsunamigenic slope failure along the Middle America Trench in two tectonic settings, *Mar. Geol.*, *203*, 303–317.

F. Anselmetti and M. Strasser, Geological Institute, ETH Zürich, Universitätstrasse 16, CH-8092 Zurich, Switzerland.

A. Kopf and S. Stegmann, Research Centre Ocean Margin, University of Bremen, P.O. Box 330440, D-28334 Bremen, Germany. (stegmann@uni-bremen.de)

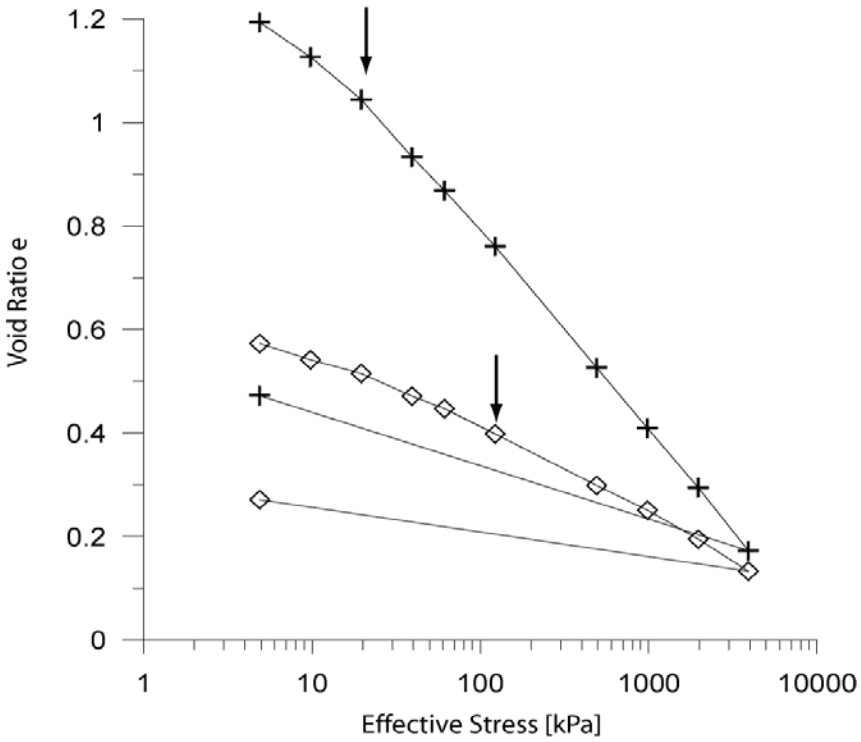

Stegmann et al., Auxiliary Material A

5.2. Quantifying subaqueous slope stability during seismic shaking: Lake Lucerne as a model for ocean margins

Strasser, M., Stegmann, S., Bussmann, F., Anselmetti, F.S., Rick, B., and Kopf, A., Marine Geology, 240, 77-97, published in 2007

ELSEVIER

Marine Geology 240 (2007) 77–97

MARINE GEOLOGY
INTERNATIONAL JOURNAL OF MARINE GEOLOGY, GEOCHEMISTRY AND GEOPHYSICS

www.elsevier.com/locate/margeo

Quantifying subaqueous slope stability during seismic shaking: Lake Lucerne as model for ocean margins

Michael Strasser [a,*], Sylvia Stegmann [b], Felix Bussmann [a], Flavio S. Anselmetti [a], Beat Rick [c], Achim Kopf [b]

[a] *Geological Institute, ETH Zurich, Universitätstrasse 16, CHN, 8092 Zurich, Switzerland*
[b] *Research Centre Ocean Margins (RCOM), University of Bremen, P.O. Box 330440, 28334 Bremen, Germany*
[c] *Dr. von Moos AG, Consulting geologists and engineers, Zurich, Switzerland*

Received 19 October 2006; received in revised form 1 February 2007; accepted 8 February 2007

Abstract

Lakes can be used as model basins to investigate subaqueous slope stability under static and dynamic loading conditions. This study combines geophysical, sedimentological and in situ geotechnical methods with limit equilibrium calculations in order to discuss (i) the geological and sedimentological processes acting on submerged non-deltaic lateral slopes in perialpine, fjord-type Lake Lucerne (Central Switzerland); (ii) their control on physical and geotechnical properties that eventually affect the subaqueous stability conditions and slope failure initiation, and (iii) the quantitative assessment of subaqueous slope stability. Three detailed case studies are presented to describe and quantitatively reconstruct stability conditions of slopes that failed during a well-documented historic earthquake in 1601 A.D. and during a prehistoric Late Holocene earthquake around 2220 cal yr BP (both $M_w > 6$).

Glacio-lacustrine sedimentation dominated by suspension settling from meltwater plumes and slight overconsolidation from ice-grounding during small readvances of a generally retreating glacier lead to a peculiar glacial-to-postglacial lithologic slope succession that eventually was buried by the Holocene sediment drape. During past earthquake shaking, the slopes that were stable under static loading conditions (factor of safety of 1.5 2) failed along planar sliding surfaces that developed at the lithological boundary between fine-grained, thinly-laminated, slightly underconsolidated cyclic plume deposits with low undrained shear strength values above and overconsolidated, glacially-deformed, glacio-lacustrine deposits with excessive formation pore pressure below. Measured in situ shear strength characteristics and sediment geometries were implemented into limit equilibrium models that allow for quantitative reconstruction of critical ground accelerations of past earthquakes in Central Switzerland. Results reveal seismic peak ground acceleration (PGA) of ~0.08 g and ~0.14 g for the historic 1601 A.D. M_w ~6.2 earthquake and the prehistoric, ~2220 cal yr B.P. earthquake, respectively. Additionally, results reveal that stability conditions change over relative short geological time scales because the postglacial sedimentation rate, which mainly controls the static weight of the slope sediment acting on the critical lithological boundary, turns out to be a key parameter in "charging" slopes susceptible to sliding.

Keywords: submarine landslides; slope stability; in situ measurement; sedimentation; limit equilibrium; paleoseismology

1. Introduction

Local instability of submerged sediment-covered slopes are common features in both marine and

* Corresponding author. Tel.: +41 44 632 6975.
E-mail address: strasser@erdw.ethz.ch (M. Strasser).

0025-3227/$ - see front matter © 2007 Elsevier B.V. All rights reserved.
doi:10.1016/j.margeo.2007.02.016

lacustrine environments and may have considerable catastrophic impact on offshore and coastal infrastructure (e.g. Shilts and Clague, 1992; Chapron et al., 1999; Locat and Lee, 2002; Boe et al., 2004; Lee, 2005). They originate from various processes such as erosion, rapid sedimentation, gas release or migration, earthquake shaking, diapirism, glacial and tidal loading, wave action, or clathrate dissociation (Hampton et al., 1996; Locat and Lee, 2002). Some of these geological processes act on the submerged slopes over longer time periods and are considered as causal factors whereas others are of instantaneous nature (e.g. earthquakes) and are thus referred to as short-term trigger mechanisms (Locat and Lee, 2002; Sultan et al., 2004). To understand past slope failure events and to eventually assess subaqueous landslide hazard, it is essential to reconstruct the pre-failure and failure conditions associated with subaquatic landslides (Leroueil et al., 1996), and also to quantitatively distinguish between long-term and short-term trigger processes.

Much of what is known today about subaqueous slope stability and hazard-related issues of underwater mass movements has been established from case studies during international campaigns along continental margins (e.g. Costa-Project (Mienert, 2004; and references therein) and Strataform-Project (Nittrouer, 1999; and references therein); see Locat and Lee (2002) for general summary) or from theoretical approaches using laboratory data or numerical modeling techniques (e.g. Biscontin et al., 2004; Azizian and Popescu, 2006). These studies present major advances in the quantitative assessment of submarine slope stability, but have also shown the challenges in determining in situ physical and geotechnical properties (e.g. shear strength and pore pressure) that are crucial for quantitative slope stability analysis. In the submarine environment, coring and in situ testing tools are expensive and critical subsurface structures along which failure occurred (or might occur in the future) are often located in depths inaccessible by those devices. Therefore, the acquired shallow subsurface data have to be extrapolated to critical depths (e.g. Urgeles et al., 2006) or the stability has to be assessed through normalized approaches (Lee and Edwards, 1986).

This study uses the lacustrine environment as a "model ocean" to quantitatively analyze subaqueous slope stability under static and dynamic loading. Due to their well-constrained boundary conditions, their smaller size and the possibility to be investigated on a complete basinwide scale, mass movements in lacustrine environments offer a series of advantages that make lake studies vital to improve our knowledge on marine processes. The three case studies of seismically-triggered slope failures in perialpine, fjord-type Lake Lucerne (Central Switzerland) presented here allow a quantitative discussion about the relationship between long-term causal factors and short-term trigger mechanisms. Methods developed for oceanographic and geotechnical investigations campaigns were utilized for site characterization. The limited sediment thickness covering the bedrock allows a complete in situ characterization of the slope-covering strata in failed as well as in stable areas. The combined geophysical, sedimentological, in situ geotechnical and limit equilibrium study presents a novel approach for slope stability assessment in the lacustrine environment, but resulting conceptual ideas give also new inputs in the context of larger slope instabilities occurring in particular in fjords or – more generally – on continental margins.

The primary objectives of the study are: (i) to understand the sediment dynamics and their control on the stability conditions along the lateral, non-deltaic slopes of Lake Lucerne; (ii) to quantify the sliding related key-characteristics (morphology, sedimentology, physical properties and in situ geotechnical parameters) of three earthquake-triggered slopes failures; and (iii) to quantitatively reconstruct seismic ground accelerations that affected the slopes at the time of failure.

2. Geological setting/Lake Lucerne

Lake Lucerne is a fjord-type, perialpine lake of glacial origin situated in Central Switzerland (~47°N, 8.5°E; 437 masl.; area=116 km^2; Fig. 1). It consists of seven steep-sided sub-basins with relatively flat basin plains down to 220 m maximum water depth (Bührer and Ambühl, 1996). The substratum of Lake Lucerne is composed from S to N by the Helvetic Nappes, the Subalpine Molasse and the Plateau Molasse which are separated by the Northern Alpine thrust and Subalpine thrust, respectively (Fig. 1). The lake's complex shape and morphology result from efficient glacial erosion along weak zones associated with the regional geology. Past lake levels were slightly lower (~−9 m) and probably increased stepwise related to the growth of two opposing deltas in the outlet region near the city of Lucerne (Kopp, 1938).

This study concentrates on the lateral non-deltaic slopes of the external Chrüztrichter and Vitznau basins (Figs. 1 and 2) that are separated from the major deltas by sills formed by submerged moraines (Hantke, 2003). The three discussed study sites (i.e. the Weggis, St. Niklausen and Chrüztrichter sites) are located north of the Northern Alpine Front in areas with a molassic substratum consisting of sandstones and conglomerates.

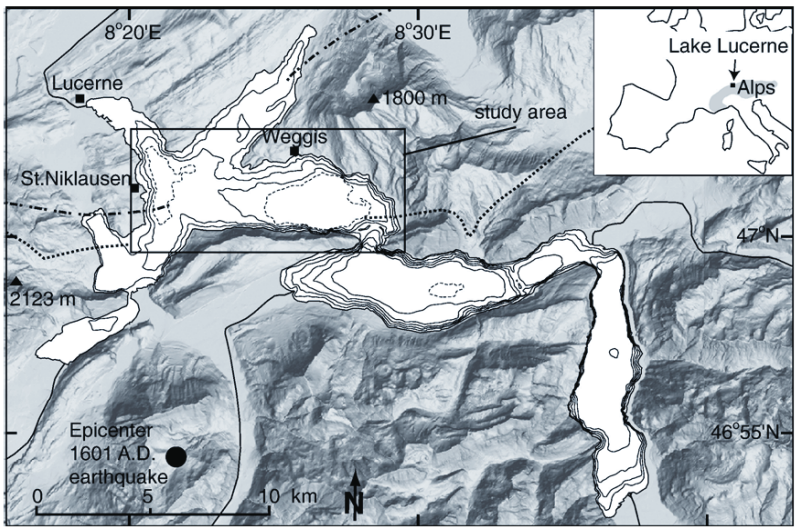

Fig. 1. Overview map of Lake Lucerne and its surroundings (shaded relief from 25 m digital terrain model, Swisstopo) showing the seven steep-sided sub-basins with flat basin plains. Bathymetric contour interval is 40 m. Dotted contour lines represent 20 m intervals and aim to clarify bathymetry. The rectangle indicates the study area and outlines location of subsequent Fig. 2. The dotted and dashed lines mark the Alpine and the Subalpine Front, respectively (see Section 2). Black circle in the SW corner of the map indicates estimated epicentral location of 1601 A.D. M_w ~6.2 Unterwalden earthquake (Schwarz-Zanetti et al., 2003; Gisler et al., 2004).

In the central region of the investigated sub-basins the bedrock is covered with an up to 120 m-thick, mainly glacial and glacio-lacustrine infill (Finckh et al., 1984). The majority of these sediments were deposited in a sub-glacial environment within relatively short time during the end of the last Glacial period. The Late Glacial basin sediments are comprised of thinly-laminated light gray to yellowish mud with frequent intercalated graded turbidite beds. The Holocene sediments consist of 5 to 15 m-thick, faintly laminated grayish to brownish mud with dark layers rich in organic matter and some intercalated graded turbidite beds (Schnellmann et al., 2006). Previous studies identified numerous mass-movement deposits related to a historic M_w 6.2 earthquake occurring in 1601 A.D. (Unterwalden Earthquake; Schwarz-Zanetti et al., 2003; Gisler et al., 2004) in the subsurface of Lake Lucerne (Siegenthaler et al., 1987, Lemcke, 1992; Schnellmann

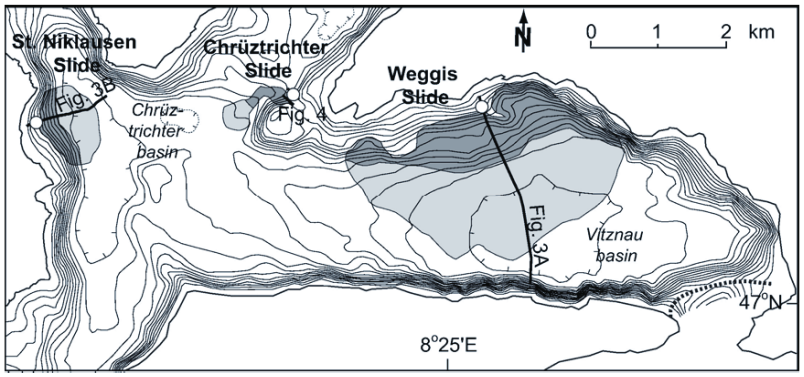

Fig. 2. Bathymetric map of Chrüztrichter and Vitznau basins showing the outline of the Weggis, St. Niklausen and Chrüztrichter Slides (see Fig. 1 for location of the map segment). Slide complexes are marked with grey shadings, whereby dark and light grey indicate erosional and depositional zones, respectively. Contour interval is 10 m. The bold dotted line in the SE corner indicates a major subaqueous sill and corresponds to an intermediate glacier front stage during deglaciation (Hantke, 2003). Bold lines indicate position of 3.5 kHz seismic profiles presented in subsequent figures. Open white circles give position of piston cores and in situ testing sites.

et al., 2002, 2005, 2006). Thirteen synchronous mass movements related to this event triggered a tsunami wave up to 4 m in height and a subsequent seiche wave that lasted for several days (Cysat, 1601; Schnellmann et al., 2002). In the deeper subsurface, five additional event horizons containing seismically-triggered synchronous mass movements were identified that have occurred in the last 15 000 yr. Schnellmann et al. (2006) provide a chronological catalogue of Late Glacial and Holocene mass-movement deposits and related subaqueous landslide scars in the two studied sub-basins. Slope failures are mostly characterized by translational movement and occurred in water depths ranging from 30–100 m. This study focuses on the source areas and on the pre-failure and failure conditions of three well-dated landslides, the deposits and depositional mechanisms of which are well constrained and for which strong seismic shaking was singled out as trigger mechanism (Schnellmann et al., 2005, 2006; Fig. 2).

3. Methods

3.1. Sub-bottom profiling

Closely spaced (~30–50 m grid spacing), single channel high-resolution 3.5 kHz seismic profiles (pinger source) were acquired in 2005 in order to refine the existing basinwide seismic data set (Schnellmann et al., 2006) in the areas of the three study sites. The source/receiver was mounted on a cataraft that was pushed in front of a small vessel. DGPS-positioning with a maximum error of ±2 m guaranteed accurate navigation. The digitally recorded data was processed using both a flat gain and band-pass filtering. Two-way travel time was converted to water depth and sediment thickness using a constant velocity of 1450 ms $^{-1}$. No migration was applied to the data because visual quality and readability is better in the non-migrated data and slope dip errors due to non-migration of the seismic sections are negligible (<2%).

3.2. Coring and laboratory analysis

At each study site, two Kullenberg-type gravity piston cores (Kelts et al., 1986), each 4.5–7 m in length, were recovered in the undisturbed slope-covering sediments adjacent to the failure scars. These cores provide material for both detailed characterization of sedimentological and physical properties, and for further geotechnical analysis on undisturbed samples. Additionally, at each study site 3 short gravity cores with a maximum length of 2 m were recovered along the failed slopes downslope of the failure scar.

The cores were logged in the Limnogeology Laboratory at ETH Zurich using a GEOTEK Multisensor Core Logger (MSCL), which measures Gamma Ray Attenuation bulk density, compressional wave velocity and magnetic susceptibility. Afterwards, cores were split for sedimentological description (macroscopically and using smear slide techniques; Rothwell, 1989; Kelts, 1998). Immediately after splitting, cores were photographed and natural water content measurements were performed by weighing 10 cm^3 of sediment before and after drying in an oven at 105 °C. On the freshly split sediment surface, undrained shear strength was measured perpendicular to bedding at ~15 cm intervals using a pocket vane shear testing device (Eijkelkamp). Atterberg limits were determined according to British Standards 1377 (Institute B.S., 1977) using a Casagrande apparatus. Grain size analysis were performed using laser diffraction techniques (Malvern Mastersizer Hydro 2000S) at ~10 cm intervals along the split core. Gravel clasts >2000 μm in the glacio-lacustrine sediments recovered at the bottom of the cores were removed by sieving prior to analysis, and clast diameters were estimated visually. Additionally, selected samples were analyzed for solid volume using a helium pycnometer device at the Rock Deformation Laboratory at ETH Zurich to derive grain density values. To characterize the consolidation history of the material, one dimensional consolidation tests (oedometer) were performed on two end-member lithologies from undisturbed samples taken from core 4WS05-K5 (Weggis site) at the Research Center Ocean Margins (RCOM), in Bremen. Specimens of 2 cm height and 5 cm in diameter were trimmed out of whole-round core samples and incrementally subjected to normal loads of up to 4 MPa

3.3. In situ geotechnical testing

At the Weggis and St. Niklausen sites (see Fig. 2 for location) in situ geotechnical strength measurements were performed at ~50 cm intervals throughout the sediment profile. Both vane shear tests and Cone Penetration Testing (CPT; with pore pressure measurements) were performed to identify the in situ undrained strength profile. By using two independent methods the strength versus depth profile could be independently confirmed. Additionally, local induced excess pore pressure response could be measured and monitored to approximate the in situ pore pressure distribution.

The in situ vane shear tests were performed using a vane shear probe of 6.5 cm diameter (Geonor A/S) that was lowered in a casing mounted on an anchored platform. At each target depth the probe was extruded

carefully from the casing into the undisturbed sediment and rotated mechanically from the platform at constant rate (6°/min) until failure occurred. In the water saturated, fine-grained sediment, the hereby induced excess pore pressure does not have time to dissipate, thus the measured peak strength is inferred to be the in situ undrained shear strength ($c_{u\ in\ situ}$). The residual strength was then deduced from a consecutive test at the same interval. Only in the lowermost part of the section the measurements might be biased by the presence of gravels that occasionally block the vane shear device during rotation. Calibrating the system in the casing in the water above the lake bottom revealed negligible additional friction of the rotating rod. However, some inaccuracy results from the slight sediment disturbance when the probe is lowered. This results in underestimating the real in situ strength condition. Although the measurements were performed during calm periods with no wind-driven waves on the lake, minor waves from boats could not always be avoided so that early failure due to wave induced vertical movement of the vane shear device during the tests cannot always be excluded, potentially providing a second source for underestimating the actual in situ strength values.

A marine free-fall penetrometer from RCOM Bremen was used to measure strength and pore pressure in situ (Stegmann et al., 2006). The autonomous working tool consists of a standard industrial 15 cm^2 CPT cone and a pressure housing containing the power supply, data acquisition and an acceleration sensor. The tests were performed at the same location and at comparable depth intervals as the vane shear test. The CPT-instrument was lowered carefully from the anchored platform using a 4×4 car winch at the lowest possible rate (average rate ~2 cm/s) into the sediment, rested at each level for 10 min for pore pressure dissipation, and was then lowered to the next level, and so on. Insertion of the probe results in a compaction of the sediment, which generates an artificial excess pore pressure spike followed by pressure decay that approaches ambient values. By monitoring and evaluating the pore pressure dissipation after insertion, qualitative permeability conditions can be estimated (for details see Terzaghi, 1925). Additionally, these measurements provide confirmation that the strains induced during testing result in excess pore pressures and thus undrained loading at the test locations. Undrained shear strength ($c_{u\ in\ situ}$) was derived based on an empirical equation with the measured cone resistance during CPT-lowering using a standard cone factor (N_k), of 15 and 17 for normally consolidated clays and overconsolidated clays, respectively (for details see Lunne et al., 1997). Vane and cone penetration derived undrained shear strength cannot be directly compared because absolute values may differ significantly due to fundamental differences in the mechanical behavior between vane shearing and cone penetration (Lu and Bryant, 1997). Thus, the two independently measured $c_{u\ in\ situ}$ values are only considered for first order comparison of magnitude, but they can be used to identify characteristic strength versus depth trends.

3.4. Slope stability evaluation

2-D limit equilibrium slope stability analysis (for details see e.g. Duncan, 1996) were carried out using the commercially available software package Slide (Rocscience Inc.) that is widely used in geotechnical engineering for slope stability assessments under subaerial conditions, but allows for adaptation to the subaqueous environment. The program uses equal-width slices and allows for input of a slope profile, sub-bottom geometry of layers, their geotechnical properties and a predefined failure surface geometry. Additionally, a pseudostatic acceleration can be used to model the peak ground acceleration generated by earthquakes and to evaluate the seismic slope stability. This parameter assumes that the earthquake acceleration is applied over a significantly long period of time so that the induced stresses can be considered constant (Hampton et al., 1996). Thus, the dynamic response of the sediment cannot be taken into account. The output factor of safety (FS; i.e. the ratio between the resisting shear strength and the sum of all loading forces (mobilized shear stress)) is calculated using a combined General Limit Equilibrium (GLE)/Morgenstern–Price method (Morgenstern and Price, 1965; Fredlund and Krahn, 1977).

Two types of analysis were performed: (i) Deterministic back-analysis of seismically-triggered slope failures, and (ii) probabilistic limit equilibrium slope stability calculations. The back-analysis approach assumes FS=1 at failure and tries to constrain the parameter combinations that could produce instabilities. Contrary to this deterministic method that uses one single constant value for each input parameter, the probabilistic approach considers variability and hence uses a mean and standard deviation value. Here, the input data samples are randomly generated using the Monte Carlo sampling method simulating the uncertainty and variability of each input parameters. FS is calculated for >1000 runs and model outputs reveal mean FS value of the modeled slope and the corresponding probability of failure (i.e. % of all analyses with FS<1).

4. Data and results

Seismic interpretation and bathymetric evaluation allowed three target locations to be identified that are well suited for the purpose of this study (i.e. the Weggis, St. Niklausen and Chrüztrichter sites). They are characterized by (i) clear landslide scars related to known mass-movement events, (ii) undisturbed postglacial drape thickness adjacent to the failure scar <8 m (i.e., can be penetrated with coring and in situ testing probes), and (iii) water depth <40 m for in situ vane shear testing. In this section the analyzed morphological, sedimentological and geotechnical characteristics of this three studied lateral slopes that failed during past earthquakes are presented.

4.1. Case study sites

4.1.1. Weggis Slide

The largest slide in the study area, the Weggis Slide, mobilized ~8.5×10^6 m^3 of sediment and is located on the northern slope of the Vitznau sub-basin (Figs. 2 and 3A). Previous studies by Siegenthaler et al. (1987), Lemcke (1992) and Schnellmann et al. (2002, 2005, 2006) have shown that this landslide is related to the 1601 A.D., M_w ~6.2 earthquake. The slide scar reaches a maximum height of 6 m and extends laterally over more than 6 km in water depths ranging from 30 to 100 m along the relatively gently dipping, 5° to 15° steep lateral slope. In Fig. 3A, the slide scar appears in approximately 35 m water depth in a zone, where the slope inclination increases downwards from <10° to ~15°. In the uppermost part of the eroded slope acoustically chaotic to transparent proximal mass-movement deposits can be identified. The observed bathymetric step in the lower part of the slope is caused by conglomerate banks of subalpine molasse rocks in the substratum. The slide scar cuts through a 4 m-thick, acoustically laminated sedimentary drape (referred to Holocene and Late Glacial deposits in Fig. 3) that overlies a thin seismostratigraphic unit characterized by a high-amplitude chaotic reflection pattern that is hardly distinguishable from the acoustic basement. This observation suggests that bedrock is covered by a few meters of glacial deposits. However, seismic penetration and resolution do not allow for exact mapping of this boundary. The absence of the entire drape clearly points towards a translational sliding mechanism with the glacial deposits acting as a base for the failure surface.

4.1.2. St. Niklausen Slide

Offshore the village of St. Niklausen in the western Chrüztrichter sub-basin (Fig. 2), stacked debris-flow deposits in the basin plain (Fig. 3B) indicate that parts of the slope have repeatedly been active in Late Glacial and Holocene times, with the youngest being the largest event that affects a total mobilized volume of ~1.5×10^6 m^3. St. Niklausen Slide is smaller than the Weggis Slide described above and is of medium size compared to other Lake Lucerne subaqueous mass movements (Schnellmann et al., 2005, 2006). It was dated at 2180–2410 cal yr B.P. (Schnellmann et al., 2006) and is part of a multiple-slide event that was triggered by a major northern alpine earthquake (M_w>6.5; 2220±40 cal yr B.P.; Strasser et al., 2006). A 1.5 km-long and up to 6 m-high slide scar assigned to this 2220 cal yr B.P. slope failure event is located on a steepening-downward slope in 40–50 m water depth (Fig. 4B). Below the failure scar, a 1.6 m-thick post-landslide sedimentary drape covers the ~13° steep slope. Seismic data reveal the same acoustic characteristics as observed on the Weggis slope described above, with slightly more pronounced continuous, parallel high-amplitude reflections in the undisturbed, acoustically laminated drape upslope the failure scar (Fig. 3).

4.1.3. Chrüztrichter Slide

A third subaqueous landslide, triggered by the 1601 A.D. earthquake (Schnellmann et al., 2005), was surveyed in great detail. The relatively small Chrüztrichter Slide (~0.18×10^6 m^3 eroded volume) is located on the northeastern edge of the Chrüztrichter basin and affects an area of 0.3 km^2 from the failure scar to the toe of the deposits. The failure scar lies on a ~13° steep, northward-dipping slope of a small subaqueous mound at 30–40 m water depth. It cuts a ~6 m-thick, acoustically laminated sedimentary drape that overlies acoustic basement in the undisturbed slope environment, both upslope and lateral to the failure scar (Fig. 4).

4.2. Lithostratigraphy

The continuous glacial-to-postglacial sedimentary succession covering the undisturbed lacustrine slope at the three study sites was recovered in 6 piston cores (two at each site) immediately upslope (Weggis/St. Niklausen) or adjacent (Chrüztrichter) to the failure scar (see Figs. 2–4 for location). Figs. 5–7 show the composite plots of all data obtained at the three study sites. The sedimentary succession is very similar at all three sites and shows three distinct lithologic units composed of (from top to bottom): Unit 1 (2.5–4.9 m thick): homogenous to mottled, olive gray, silty clays with abundant organic material. The sediment is mainly of detrital origin with variable amounts of authigenically-

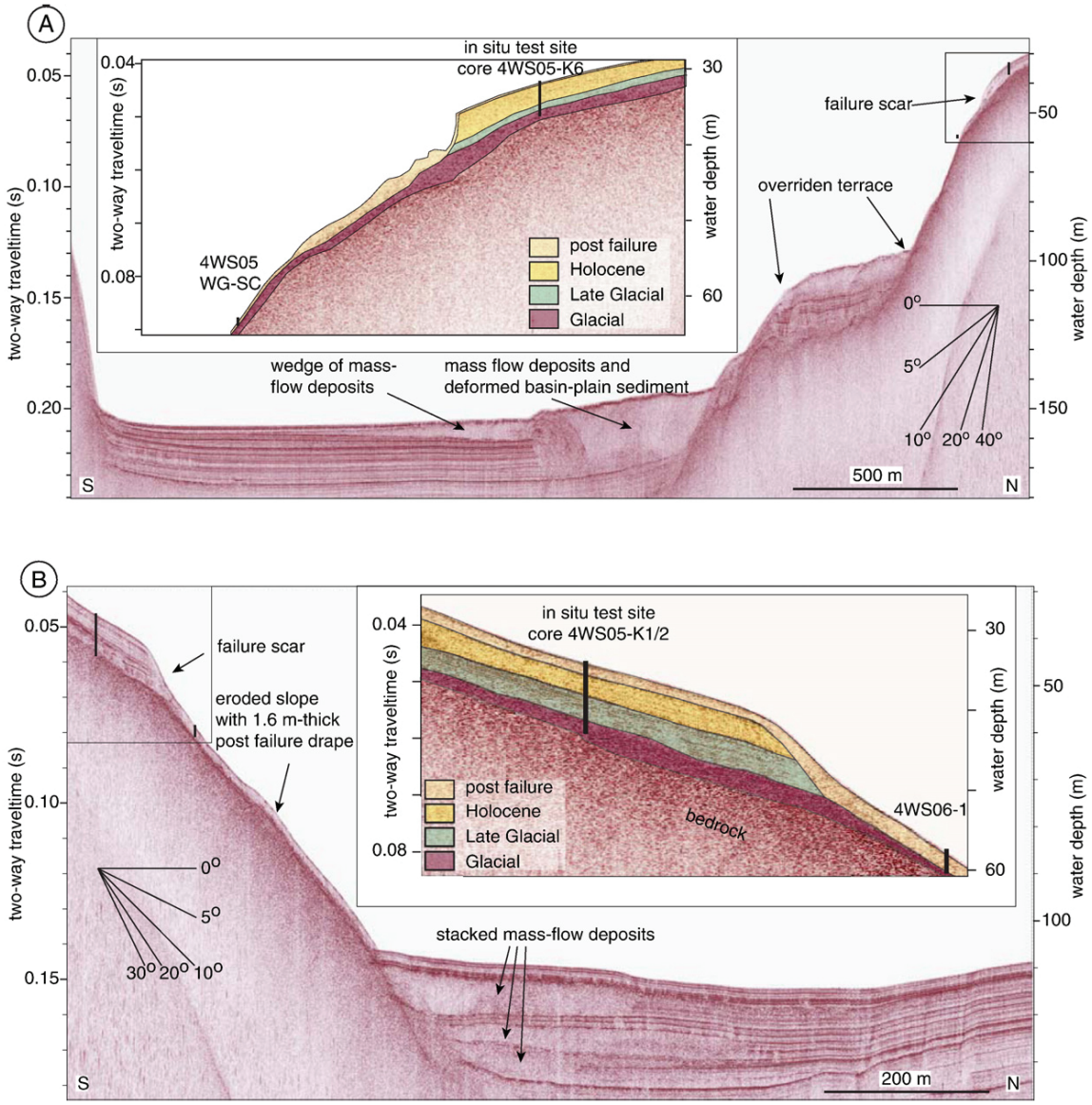

Fig. 3. 3.5 kHz seismic lines illustrating the structure of the Weggis Slide (A) and St. Niklausen Slide (B). See Fig. 2 for location of seismic lines. Inlets show enlarged details of the scars with slope model interpretations of lithological units as cored in reference cores. In the uppermost part of the eroded Weggis slope (A) the acoustically chaotic to transparent unit with an irregular upper surface is interpreted as proximal mass-movement deposit.

produced carbonates and diatoms; Unit 2 (1.2–1.6 m thick): yellowish light gray, thinly-laminated (mm to sub-mm-scale), clays and clayey silts of detrital origin (Fig. 8A); Unit 3 (1–2 m thick) tilted and deformed thinly-laminated yellowish to light gray clayey silts to silty clays with sparse (<20%) sand and medium-sized gravels up to 4 cm in diameter (Fig. 8B) floating in the fine-grained matrix. These angular, poorly sorted gravels show clear glacial striation and cover a wide range of lithologies also including crystalline basement rocks that only outcrop far south of Lake Lucerne. At the base of core 4WS05-K1 (St. Niklausen), a 15 cm-thick diamict deposit with clasts of glacial origin in a poorly sorted, clay–silt–sand matrix was recovered. Although the lowermost part of this core shows coring disturbances, this basal layer can be interpreted as a till deposit.

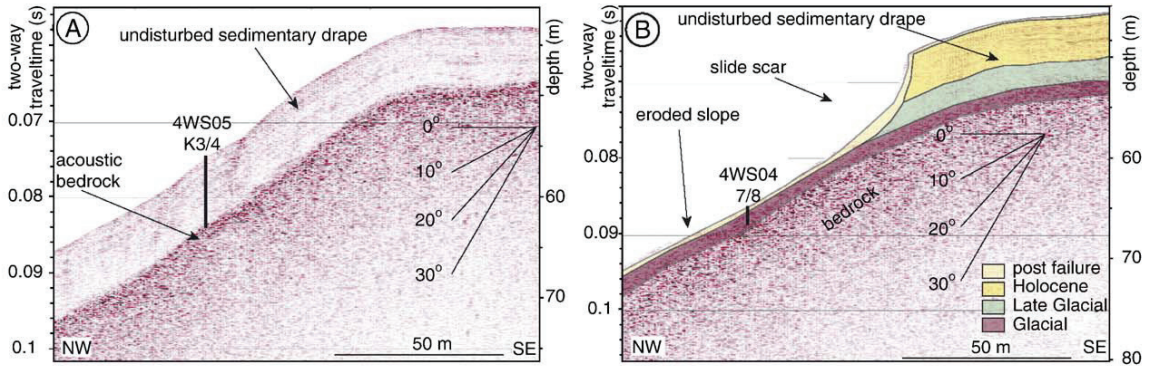

Fig. 4. Two parallel-oriented 3.5 kHz seismic lines across the sub-lacustrine slope in the northeastern edge of Chrüztrichter basin. Distance between the lines is about 80 m. For location see Fig. 2. (A) Profile shows an undisturbed slope characterized by an approximately 6 m-thick continuous sedimentary drape directly overlaying acoustic bedrock and location of cores 4WS05-K3 and K4. (B) Profile displays failure scar of Chrüztrichter Slide with slope model interpretation of lithological units as cored in reference core 4WS05-K4 and short cores 4WS04-7 and 8, which recovered the failure plane of the 1601 A.D. slope failure in core depths of 0.4 m below lake floor. Figure modified after Schnellmann et al. (2005).

Unit 3 can be assigned to the thin seismostratigraphic unit showing high-amplitude, chaotic reflection patterns as observed at the Weggis site (see Section 4.1.1) and is interpreted to represent glacially-deformed glacio-lacustrine deposits (see discussion in Section 5.1.1). Units 1 and 2 can be correlated by seismic stratigraphy, lithological facies and physical properties (mainly magnetic susceptibility and bulk density) to lithologies recovered and dated in sediment cores from the deep basin (Schnellmann et al., 2006; Thevenon et al., submitted for publication) revealing Holocene (<11 500 cal yr B.P.) and Late Glacial (>11 500 cal yr B.P.) ages, respectively. They represent the draping "slope-cover" sediment facies deposited in Lake Lucerne since the glacial retreat from the Swiss Plateau around 17 500 cal yr B.P (Lister, 1988; Wessels, 1998; see discussion in Section 5.1.2). Sedimentation rates in the Late Glacial Unit 2 are similar at the Weggis and Chrüztrichter sites (20 to 21 cm/ka) and slightly higher at the St. Niklausen site (~26 cm/ka). There, the sediments have slightly higher silt contents and few 0.5–2 cm-thick sand layers in the lower part of the postglacial section indicate higher detrital input possibly from a small local creek entering the lake nearby. In contrast, sedimentation rates for the Holocene Unit 1 differ significantly from site to site. At the Weggis site, they are in the same order as during Late Glacial times (~22 cm/ka), while they are clearly higher along the submerged slope offshore St. Niklausen (~36 cm/ka) and reach maximal values at the Chrüztrichter site (42 cm/ka). The difference in sedimentation rate may be caused by small local creeks, currents (Aeschbach-Hertig, 1994) and different amounts of biogenic sedimentation that favors deposition along the St. Niklausen and Chrüztrichter slope.

4.3. Physical properties

Physical property data from all three sites reveal significant contrasts in most measured parameters between the postglacial (Units 1 and 2) and the glacio-lacustrine deposits (Unit 3; Figs. 5–7). Generally, the Holocene section is characterized by downward increasing values of bulk density (ρ_{bulk}) with depth, whereas natural water content and Atterberg limits decrease gradually downsection. Only solid grain densities are more or less constant throughout the section with values of ~2.75 g/cm^3 and ~2.8 g/cm^3 in the Holocene deposits and in the Glacial to Late Glacial material, respectively. At the Weggis site, absolute ρ_{bulk} values increase stepwise at lithological boundaries from 1.3–1.4 g/cm^3 in Unit 1 to 1.45–1.55 g/cm^3 in Unit 2, whereas at the two other sites, ρ_{bulk} values more gradually increase from ~1.3 g/cm^3 in the middle part of the Holocene section to ~1.55 g/cm^3 in the Late Glacial deposits. The boundary between the postglacial and the glacial deposits is characterized by a dramatic increase in ρ_{bulk} of ~0.3 g/cm^3 at Weggis and Chrüztrichter sites. This boundary is further characterized by a significant change in the liquidity index, because natural water contents (w) in the postglacial sediments (decreasing from ~150–175% of dry weight in the uppermost part to ~60–75% in the laminated Late Glacial clays) are higher than the liquid limits (w_L) of these sediments, whereas w values (~40–50%) plot below the respective w_L-values in the glacio-lacustrine deposits of Unit 3. However, at the St. Niklausen site the contrast in physical properties between

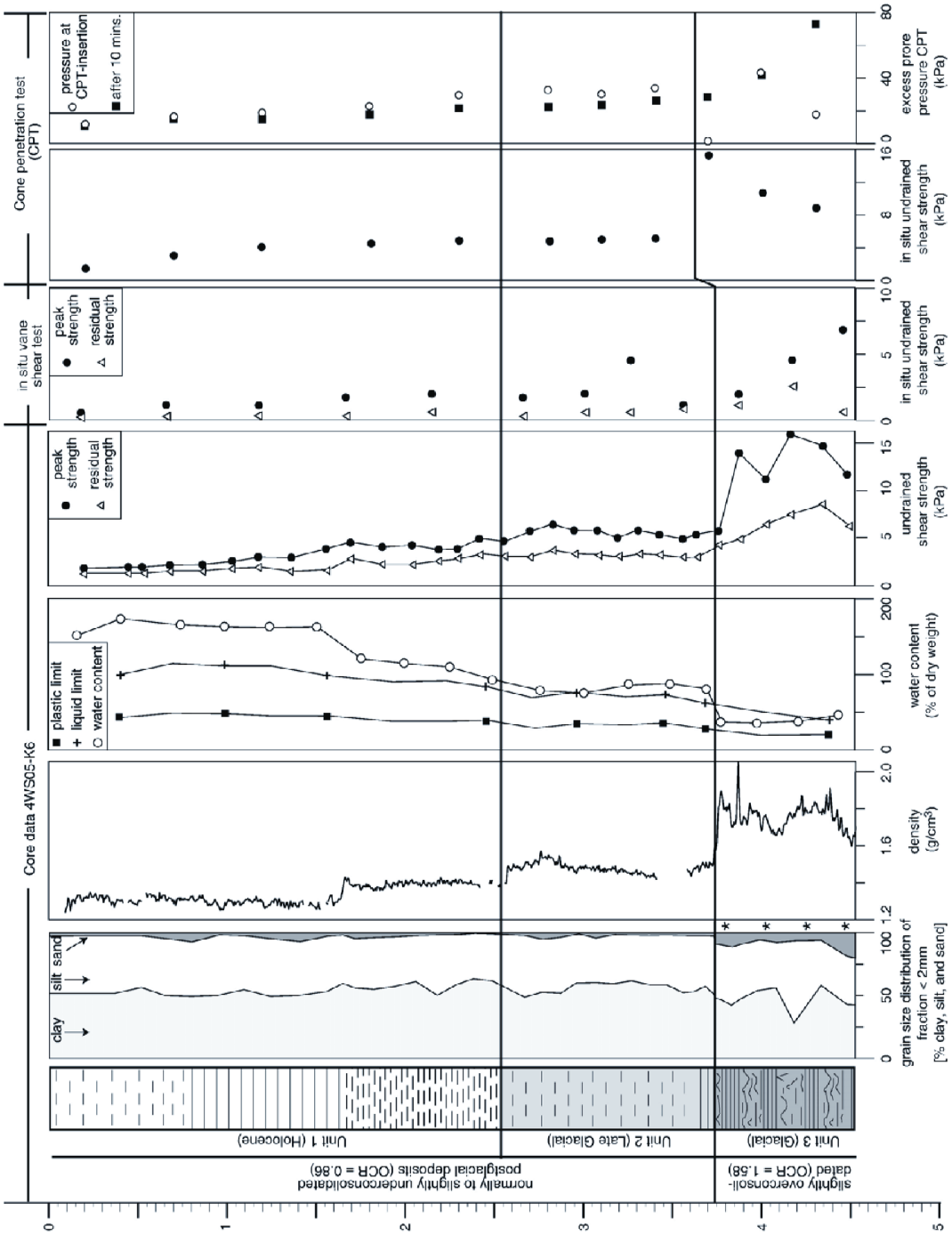

Fig. 5. Data obtained from core 4WS05-K6 and from in situ tests summarizing sedimentological and geotechnical characteristics of the undisturbed continuous glacial-to-postglacial sedimentary succession covering the sub-lacustrine slope offshore Weggis. The site is located immediately upslope the failure scar (see Figs. 2 and 3A for location). Asterisks indicate the presence of material with grain size >2 mm (that are not considered in this plot).

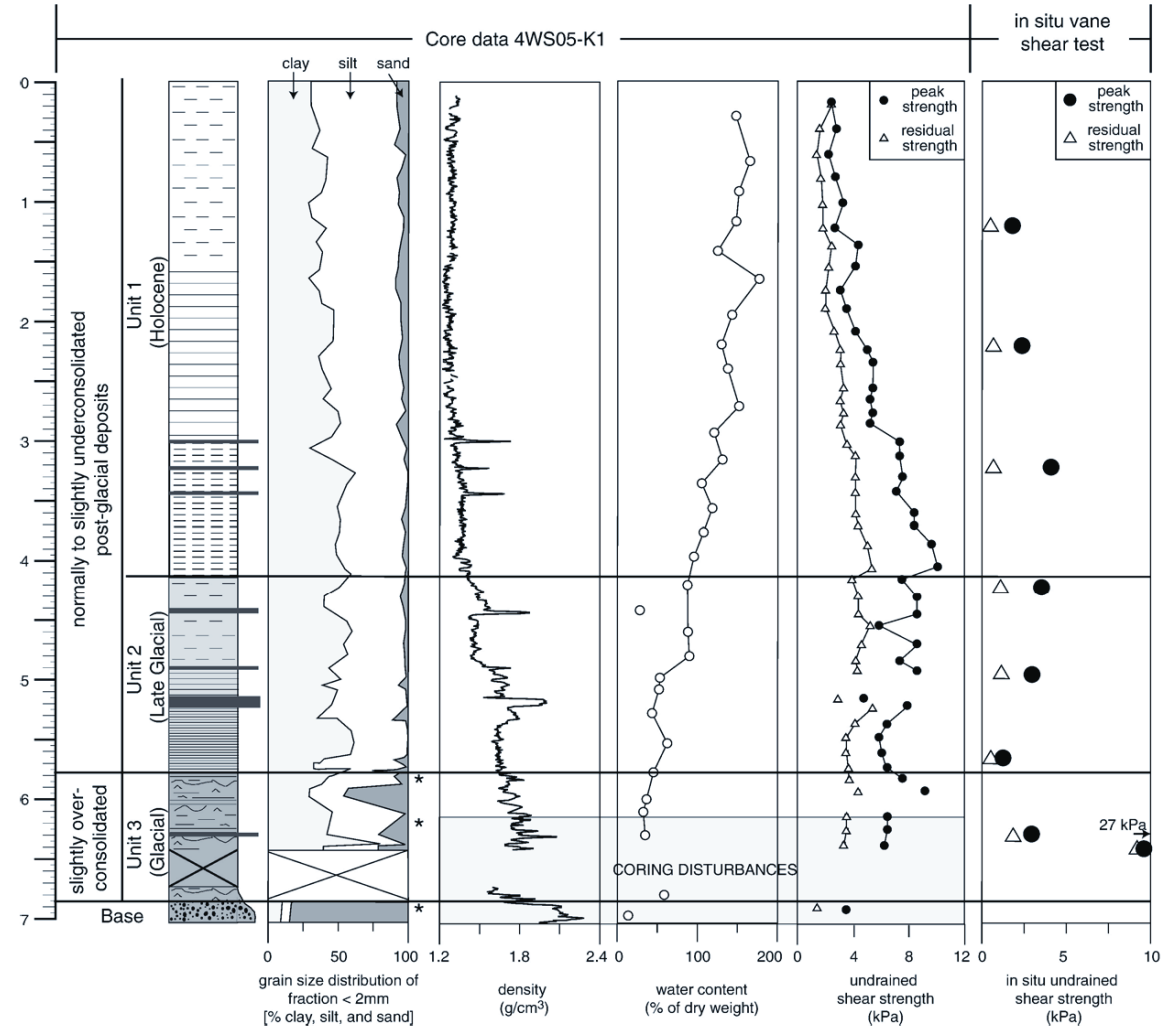

Fig. 6. Data obtained from core 4WS05-K1 and from in situ tests summarizing sedimentological and geotechnical characteristics of the undisturbed continuous glacial-to-postglacial sedimentary succession covering the sub-lacustrine slope offshore St. Niklausen. The site is located immediately upslope the failure scar (see Figs. 2 and 3B for location). Asterisks indicate the presence of material with grain size >2 mm (that are not considered in this plot).

the postglacial sediments and glacial deposits is less pronounced than at the other sites (Fig. 6). This is most likely caused by coring disturbances in the lowermost part of core 4WS05-K1.

At the Weggis site, two samples from immediately above and below the characteristic boundary between Units 2 and 3 were examined with one dimensional consolidation tests (oedometer) to determine the consolidation history and relative permeability of the material. Results reveal that the laminated Late Glacial clays are slightly underconsolidated (OCR=0.86) whereas the glacio-lacustrine deposits of Unit 3 are overconsolidated (OCR=1.58). Both sediment types show low permeability, with the plastic glacial material from Unit 3 being less permeable (hydraulic conductivity (K)=5.35×10^{-10} m/s) than the postglacial sample (K=5.32×10^{-9} m/s) (for details see Stegmann et al., in press).

4.4. Shear strength

Undrained peak (c_u) and residual shear strengths slightly vary with respect to the three different test methods utilized, but all three approaches reveal the

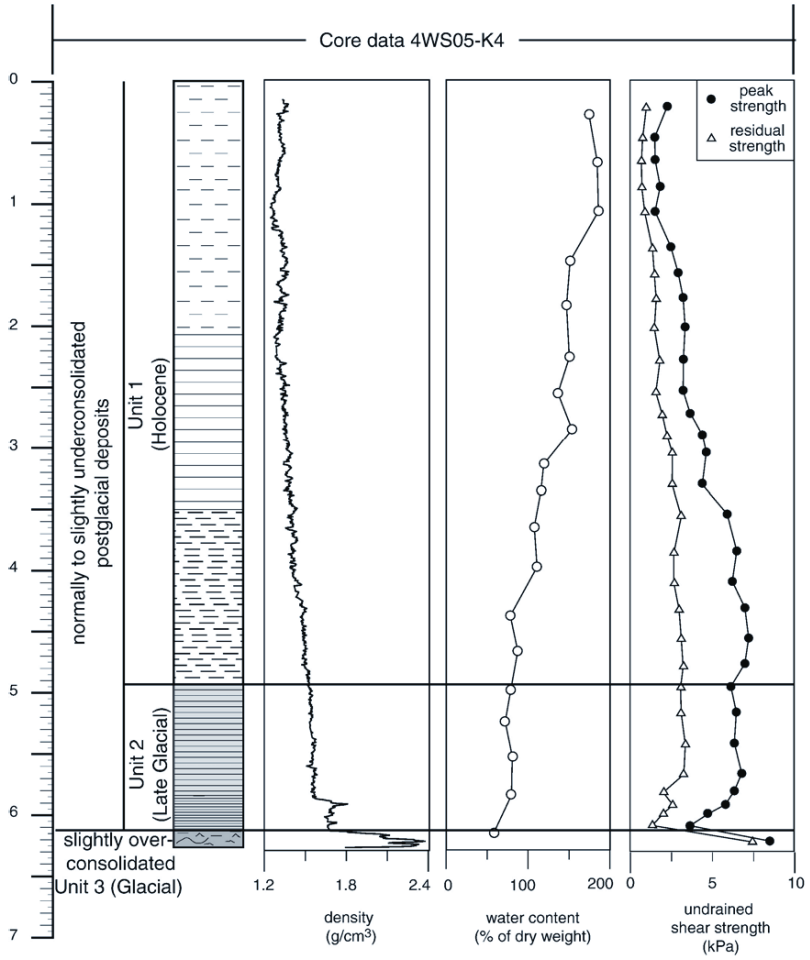

Fig. 7. Data obtained form core 4WS05-K4 summarizing sedimentological and geotechnical characteristics of the undisturbed continuous glacial-to-postglacial sedimentary succession covering the sub-lacustrine slope at the study site in the source area of the Chrüztrichter Slide. The site is located adjacent to the failure scar (see Figs. 2 and 4 for location).

same relative trend (Figs. 5–7): The Holocene Unit 1 is characterized by linearly increasing c_u values with depth, whereas values in the upper part of the Late Glacial Unit 2 are constant and even show a clear downward decrease immediately above the contact with the glacial deposits that again show significantly higher strength values (well pronounced at St. Niklausen and Chrüztrichter sites; Figs. 6 and 7).

Measured $c_{u\ in\ situ}$ values from in situ vane shear tests generally show slightly lower values than those from in situ CPT and laboratory test. This result is interpreted to be caused by disturbances to the material during probe insertion and small waves during the vane shear testing, resulting in slight underestimates of $c_{u\ in\ situ}$ (see Section 3.3). At the Weggis site, $c_{u\ in\ situ}$ values derived from CPT testing and c_u values obtained from laboratory tests correlate well and reveal similar values that increase within the upper 2.5 m (Unit 1) to ~5 kPa. At the St. Niklausen and Chrüztrichter sites, highest laboratory-derived c_u values at the base of the Holocene Unit 1 reach 9 and 7.5 kPa, respectively. In the laminated Late Glacial clays of Unit 2, c_u values vary between 5–8 kPa (laboratory and in situ CPT-test) and 2–5 kPa (in situ vane shear test) but indicate more or less constant strength characteristics in the upper part and a clearly downwards decreasing trend in the lowermost part of the cores. The glacio-lacustrine sediments of Unit 3 show significantly higher strength values, but absolute values derived from the different methods scatter between 3 and 27 kPa. The fact that Unit 3 shows

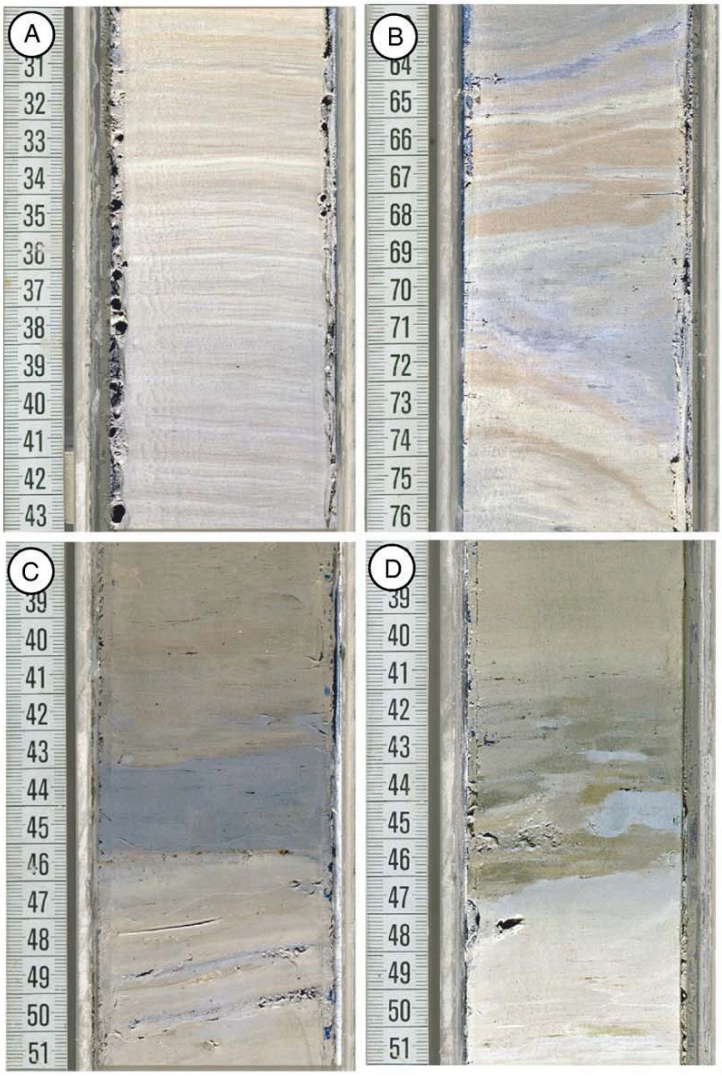

Fig. 8. Core photographs showing: A) thinly-laminated Late Glacial clays (core 4WS05-K6); B) glacially-deformed overconsolidated glacial-lacustrine deposits (core 4WS05-K6); C) 2 cm-thick, grey homogenous silty clay layer between 44 and 46 cm of core 4WS05-WG/SC assigned to the Weggis Slide overlying tilted glacio-lacustrine deposits; and D) sharp and erosive boundary at 46 cm of core 4WS04-7 (i.e. failure plane of Chrüztrichter Slide) between glacially-deformed glacio-lacustrine deposits and post-landslide deposits. Note reworked glacial mud clasts (at 45 cm) at the base of the overlying post-landslide deposits.

some heterogeneity with slightly higher sand content (up to 20%) and presence of gravels (see Section 4.2), vane shear tests might not be perfectly applicable and partly account for the scatter. However, as the bulk sediment in this lower section consists mainly of silty clay with a relative low permeability, undrained loading conditions predominate (Lambe and Whitman, 1979). Thus, the measured undrained strength values are interpreted to adequately represent the strength characteristics in this unit.

4.5. In situ pore pressure (Weggis site)

At the Weggis site, in situ formation pore pressure ($u_{\text{in situ}}$) was estimated after 10 min of monitoring the pressure evolution after CPT insertion at different target depths. Fig. 5 shows measured excess pore pressure values (i.e. absolute measured pressure minus hydrostatic pressure) at CPT insertion and after 10 min. All tests conducted in the postglacial section reveal dissipation curves with a pore pressure spike upon

impact of the probe, followed by a non-linear asymptotic decay. Although ambient excess formation pore pressure cannot be extrapolated from only 10 min of monitoring, the characteristic exponential decay of the dissipation curves points toward equilibrium values slightly above hydrostatic. In the glacio-lacustrine sediments of Unit 3, however, the monitored pore pressure after insertion shows the opposite trend. Insertion pressures are relatively low compared to the postglacial sediments, possibly due to suction and fluid displacement at the tip during insertion or due to a dilatant material response. With time, however, pressure increases significantly. This observation is interpreted to result from considerably elevated formation pore pressure in Unit 3. One test carried out for about 45 min attested that a plateau in pore pressure rise is reached after approximately 25 min.

4.6. Failure plane characteristics

Short gravity cores from the slide-eroded slopes at all three sites recovered tilted and deformed glacio-lacustrine deposits (Unit 3) in 0.36, 0.4 and 1.6 m core depth at the Weggis, Chrüztrichter and St. Niklausen sites, respectively. The upper boundary of the glacial deposits in all cores is sharp and erosive. These boundaries are interpreted as the failure surfaces of the 1601 A.D. and 2220 cal yr B.P earthquake-triggered landslides (Weggis/Chrüztrichter and St. Niklausen Slides, respectively). At the two 1601 A.D. landslide sites, the thickness of overlying post-landslide deposits (Unit 1) reveals sedimentation rates for the last 400 yr of ~1 mm/a, which is consistent with estimated recent sedimentation rates by Lemcke (1992). At St. Niklausen, the 1.6 m thick deposition of post-landslide sedimentary drape on the eroded slope reveals mean sedimentation rates over the last 2220 yr in the order of ~0.75 mm/a. At the Weggis site, a gray, 2 cm-thick, homogenous silty clay layer overlying the failure surface can be related to the Weggis Slide (Fig. 8C). Additionally, reworked glacial mud clasts recovered at the base of post-landslide deposits at the Chrüztrichter and St. Niklausen sites (Fig. 8D) clearly pinpoint the failure surfaces to be related to the glacio-lacustrine Unit 3. However, as observed in the seismic data, there are no evidences for significant erosion of Unit 3 during translational sliding (Figs. 3 and 4). Therefore, combined geophysical subsurface and core data suggests the failure to be located immediately at the top of the glacial Unit 3.

5. Discussion

Results from our study consistently imply that, regardless of regional variations between the sub-basins, initiation and evolution of earthquake-triggered lateral subaqueous slope failures occurred along glide planes that developed at the lithological boundary between overconsolidated, overpressured glacio-lacustrine deposits (Unit 3) and weak, slightly underconsolidated laminated Late Glacial clays (Unit 2). Similarly, it has been reported from other studies in perialpine, fjord-type lakes and fjords that slides also mobilized the slope-covering drape down to glacial deposits comparable to those described here (e.g. *Horgen Slide* and *Oberrieden Slide* in Lake Zurich, Switzerland (Kelts, 1978; Strasser 2006, unpublished data); *Pointe-Du-Fort Slide* in Saguenay Fjord, Canada (Locat et al., 2003); submarine slides in Karmsundet and Skudenesfjorden, Norway (Boe et al., 2000)). It is thus interpreted that the glacial-to-postglacial evolution in sedimentation processes along the lateral slopes in similar settings as Lake Lucerne results in characteristic physical and geotechnical properties that eventually control the stability conditions and that in turn favor subaqueous slope failure initiation at systematic stratigraphic levels.

In the following section, a conceptual slope-sedimentation model since the last glaciation is presented (Fig. 9), and its control on the evolution of the physical properties is discussed. In the subsequent section, the measured geotechnical parameters are implemented into limit equilibrium models in order to quantitatively assess the slope stability condition of the submerged slopes at the time of failure.

5.1. Sedimentation model and its influence on the geotechnical properties

5.1.1. Glacial

The sedimentary facies of the tilted and deformed laminated clayey silts with sparse sand and glacially striated, allochtonous gravels (Unit 3) clearly point towards deposition in a glacio-lacustrine environment and subsequent glacial deformation by ice-grounding and/or ploughing. The fact that the material experienced higher pre-consolidation pressure than the effective overburden stress today (OCR>1) can in this context be interpreted to result from glacial compaction under the additional weight of ice mass acting on the material. Additionally, long-term postglacial secondary compression within the compressible glacio-lacustrine clays and silts (Terzaghi et al., 1996) may also partly explain the observed formation-wide overconsolidation. Other processes that would lead to overconsolidation, such as erosion of previously overlying material or diagenetic cementation, are ruled out, because evidence favoring these processes was neither observed in the seismic data

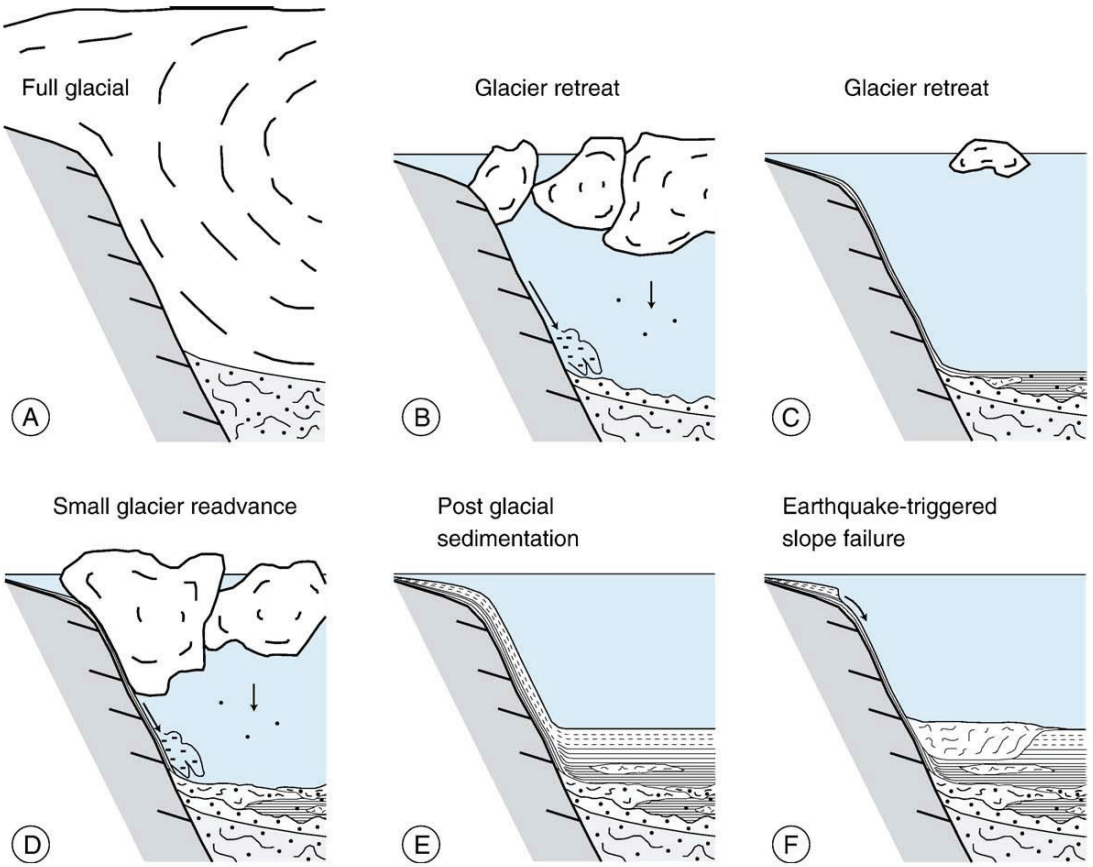

Fig. 9. Conceptual glacial-to-postglacial sedimentation model along lateral non-deltaic slopes in perialpine fjord-type lakes. Schemes (not to scale) are perpendicular to the basin axis and show schematically the depositional and post-depositional processes acting on the submerged slope: (A) Last Glacial Maximum: the basin is fully occupied by the glacier. Glacial bedrock erosion rather than sedimentation occurs along the slopes; (B) Glacial decay results in the formation of a sub-glacial lake (see Section 5.1.1). Glacio-lacustrine deposition occurs focused in the deep basin; along the lateral slope, little sedimentation, erosion, creeping and slumping occurs. (C) Further rapid disintegration of remaining glacial ice back to shallower up-valley parts results in a periglacial setting where a fine veneer of fine-grained sediments also is deposited along the lateral slopes settling out from meltwater plumes. (D) Relatively short-lived periods of colder climate conditions result in minor glacial readvances, during which ploughing and grounding of icebergs along the slope leads to deformation and compaction of the glacio-lacustrine sediment. (E) After the final glacier retreat suspension settling from meltwater plumes and settling from flood-induced over and interflows mixed with authigenic carbonate production occurs during the Late Glacial and Holocene, respectively. Continuous sedimentation "charges" the slopes until external trigger mechanism triggers slope failures. (F) Post-failure situation.

nor in cored material. Glacial compaction and secondary compression also results in reduction of permeability. Therefore, the observed pore fluid overpressures in Unit 3 are interpreted to be a result of the limited drainage capacity in these relative low permeable deposits. The process of overpressuring, however, remains unknown. One possibility is that elevated pore pressures were initially induced during partially undrained glacial compaction and sustained thereafter, although one would rather expect the formation pore pressure to stabilize over such a long time period. Alternatively, and more likely, there could be an influence from a recent local groundwater flow sustaining a positive lateral flux that results in higher pore pressures than expected under hydrostatic conditions.

Because the observed glacial overconsolidation of the deposits is relatively low (OCR=1.58), we exclude that glacial compaction took place during times when the glacier fully occupied the deep basins and the study sites were covered by ~800 m of ice (Florineth and Schluchter, 1998). Therefore, the glacio-lacustrine deposits have to be younger than the Last Glacial Maximum (~24–19 ka B.P; Ivy Ochs et al., 2004). Generally, deglaciation of glacially over-deepened

basins such as Lake Lucerne occurred by stagnation-zone retreat rather than by the retreat of an active glacier front (Lister et al., 1984). Deposition of glacio-lacustrine sediments first takes place in the deep basin of a sub-glacial lake that formed once the buoyancy of the ice body exceeds its weight and the glacier floats up. Further ablation, water contact melting, and calving lead to rapid disintegration of remaining glacial ice back to shallower up-valley parts (e.g. Haeberli and Schlüchter, 1987). Most of the sediment is deposited in the topographic depressions but a thin veneer of fine-grained glacio-lacustrine sediments is also deposited along the lateral slopes settling out of meltwater plumes containing suspended glacial mud (e.g. Mackiewicz et al., 1984; Blass et al., 2003; Anselmetti et al., in press; Fig. 9C). Sand and gravel clasts occasionally are deposited as ice-rafted debris. In this highly dynamic periglacial setting, relatively short-lived periods of colder climate conditions result in minor glacial readvances with higher intensities of ice-calving, during which ploughing and grounding of icebergs along the lateral slopes result in deformation and compaction of the glacio-lacustrine sediment (Fig. 9D).

5.1.2. Post Glacial

After the final glacier retreat (~17 500 cal yr B.P.; Lister, 1988; Wessels, 1998), most of postglacial sedimentation occurs on deltas and is focused in the topographic depressions of the deep basins through underflow processes. However, suspension settling from meltwater plumes that uniformly distribute the fine fraction of the suspended glacial mud over the lake basin also drapes the submerged lateral slopes (Fig. 9C). Cyclic (e.g. seasonal) fluctuations in meltwater discharge result in thinly-laminated and fine-grained draping slope deposits as recovered in the lower part of Unit 2 (Fig. 8A), which potentially could represent proglacial clastic varves (Mackiewicz et al., 1984; Blass et al., 2003; Anselmetti et al., in press). With further glacial retreat into the alpine valley during Late Glacial times, the influence of glacial meltwater plumes on the lacustrine sedimentation is continuously diminished and suspended material entering the lake as under-, inter- and overflows after high precipitation and flood events continuously dilutes the rhythmically laminated Late Glacial clays. With climate amelioration at the Late Glacial to Holocene transition around 11 500 cal yr B.P., sedimentation along the slope is increasingly influenced by both authigenic carbonate and biogenic production as well as detrital input from small local rivers during high discharge events (Sturm and Matter, 1978). This observed change in the sedimentation processes along the lateral slopes reflects the general Late Glacial to Holocene shift in the sedimentary system also recorded in many other perialpine lakes (e.g. Van Rensbergen et al., 1999; Eyles et al., 2000; Beck et al., 2001) and fjords (e.g. Evans et al., 2002; Lysa et al., 2004). It further explains the increased sedimentation rates along the lateral slopes during the Holocene compared to Late Glacial times, as estimated from the core data (see Section 4.2).

The distinct differences in Late Glacial and Holocene sedimentation mechanisms also influence the strength characteristics of the slope-covering material. In the Holocene Unit 1 gradients of undrained shear strength with depth (∇c_u) are constant in the order of ~1.8 kPa/m (Weggis ~1.75 kPa/m, St. Niklausen ~2.0 kPa/m, Chrüztrichter 1.75 kPa/m). Similar Holocene $-\nabla c_u$ values also have been reported from in situ testing results in other Swiss lakes (Gyger et al., 1976). Sediment strength thus correlates with effective stress (ratio c_u/σ'_v ~0.2–0.4) and the characteristic profiles suggest a continuous self weight consolidation associated with a relatively continuous sedimentation rate. In contrast, c_u values in the Late Glacial clays (Unit 2) are constant in the upper part and even reveal negative c_u-gradients at their base, where the lamination of proglacial cyclic plume deposits is well pronounced. This observation suggests a connection between the laminated clays and their unfavorable stability conditions. Indeed, geotechnical investigations of similar Late Glacial varve-deposits in Switzerland and Canada show significant influences of the clay lamination and microstructure on strength characteristics and mechanical behavior (e.g. Quigley and Ogunbadejo, 1972; Plötze et al., 2003). Additionally, the postglacial deposits are characterized by slight formation overpressures, which is interpreted to be related to the relatively high sedimentation rates (20–40 cm/ka) and incomplete drainage of the low permeable sediments. As a consequence, the normal consolidation phenomenon is retarded and the sediment is in an underconsolidated state (Sultan et al., 2004), as measured by consolidation tests (OCR=0.86).

In summary, the depositional and consolidation mechanism of sediments covering the submerged lateral slope of Lake Lucerne created particular sedimentological and geotechnical slope characteristics that control the stability condition and that predefine the eventual failure location. With an external trigger mechanism (i.e. strong seismic shaking) these lithologically inherited conditions result in subaqueous slope failure initiation along the boundary between overconsolidated glacio-lacustrine deposits with overpressured formation pore

pressures (Unit 3) and slightly underconsolidated laminated Late Glacial clays (Unit 2) characterized by low shear strength values at their base. Based on the principle of effective stress, Stegmann et al. (in press) show in detail that, as a result of co-seismic stress fluctuations and stress-transfer upward to the base of the weaker unit, pore pressure exceeds lithostatic load and initiates sliding along a failure plane developing at the boundary between Units 2 and 3.

5.2. Limit equilibrium slope stability analysis

In order to reconstruct slope failure conditions at the study sites and to quantify seismic ground accelerations affecting the slopes at the time of failure, the obtained data were implemented into a limit equilibrium slope stability model that serves to back-analyze the slope failures triggered by the historic 1601 A.D. and the prehistoric 2220 cal yr B.P earthquakes. At both Weggis and St. Niklausen sites, the pre-failure slope geometry was reconstructed as a 3-layer model (Units 1–3) assuming constant sediment thicknesses as recovered in the reference cores immediately upslope of the failure scars and subtracting the uppermost post-landslide deposits as recovered in short cores along the eroded slopes. This assumption is justified by seismic data that show constant sediment thicknesses in undisturbed sections draping the slope adjacent to the slide. The lower model boundary was chosen to be 1 m below the boundary between Units 2 and 3, modeling the thickness of the overconsolidated glacial Unit 3 as indicated in the seismic data (see Section 4.1). Mean ρ_{bulk}, c_u at the layer top and ∇c_u were assigned to each layer according to results from core analysis and in situ testing (Table 1). Based on the observation in the geophysical subsurface data and on the results from in situ and cores analysis, the glide plane along which translational sliding occurred, is interpreted to correspond to the lithological boundary between Unit 2 and Unit 3 (see Sections 4.6 and 5.1). Therefore, a failure plane at the boundary between these to units was predefined in the slope stability analysis.

For all analysis it was assumed that the sediment is subjected to undrained loading conditions because cyclic loading during earthquake shaking is rapid enough that excess pore pressure does not have time to dissipate through the fine-grained medium. The slightly higher sand content in Unit 3 potentially could indicate that loading conditions in the lowermost unit might not fully be undrained. Also, liquefaction induced by pore pressure increase during seismic shaking cannot completely be excluded as potential failure initiation mechanism. However, given the relatively low permeability and predominant fine-grained character of the glacial deposits, undrained loading is interpreted to be the predominant mechanism at the critical depth where failure occurs. Liquefaction as potential failure initiation processes is interpreted to by unlikely because estimations of the susceptibility for liquefaction based on a rough criterion proposed by Andrews and Martin (2000) reveal no critical conditions (i.e. measured clay contents and liquid limits at critical depth in all cores are much higher than critical values of 10% and 32%, respectively). Additional uncertainties in our slope stability analysis arise from the fact that the used pseudostatic modeling approach does not consider the dynamic behavior of the sediment and therefore does not account for potential failure mechanism in addition to the load generated by horizontal seismic acceleration (e.g. degradation of soft clays, accumulation of plastic strains and shear-induced excess pore water pressure with increasing number of cycles (Sultan et al., 2004; Biscontin et al., 2004)). Future investigations on the dynamic behavior of the material under cyclic loading as well as detailed clay mineralogy analysis are required in

Table 1
Geotechnical parameters used for deterministic limit equilibrium back-analysis

	Layer thickness d	Unit weight γ	Undrained shear strength at the top of layer c_u	Undrained shear strength gradient with depth ∇c_u
	(m)	(kN m ^{3})	(kPa)	(kPa m ^{1})
Weggis site at 1601 A.D.				
Layer 1 (Holocene)	2.5	13.25	1	1.75
Layer 2 (Late Glacial)	1.25	14.72	5.4	0
Layer 3 (Glacial)	1	17.7	Varying values	5
St. Niklausen site at 2220 cal yr B.P.				
Layer 1 (Holocene)	2.7	12.8	1	2
Layer 2 (Late Glacial)	1.6	14.72	7.1	0
Layer 3 (Glacial)	1	17.7	Varying values	5

order to better constrain these uncertainties. Therefore, our pseudostatic limit equilibrium model used here only represents a first order estimation of quantifying seismic ground accelerations that affected the Lake Lucerne slopes during past earthquakes.

Sensitivity analysis of the model used in this study revealed that the impact of c_u at the depth of failure and the horizontal acceleration a_H is several-fold higher in comparison with the other parameters for the chosen slope geometry and failure plane location. Absolute c_u values slightly vary with respect to the three different measurement methods and therefore add uncertainties in the back-calculated critical pseudostatic seismic ground acceleration. The back-analysis was therefore carried out with varying values of c_u at the top of Unit 3 and results are presented as contour plots showing the factor of safety (FS) as a function of both c_u at the depth of failure and a_H (Fig. 10).

For the Weggis site, measured c_u values at the top of Unit 3 vary between 3 and 6 kPa as measured with the different independent methods, whereas they are slightly higher at the St. Niklausen site. Results of deterministic stability analysis using these c_u ranges reveal that both slopes are stable under static loading condition (i.e. a_H=0) with FS ranging between 1.1 to 1.7 and 1.3 to >2, respectively. As discussed above, the lower values estimated from in situ vane shear tests most probably underestimate the actual strength conditions, so that realistic $c_{u\ in\ situ}$ should be ~5 kPa at the Weggis and ~6 kPa at St. Niklausen site, as inferred from in situ CPT tests. Using these values for the model input reveal static FS between ~1.5 and 2 at Weggis and St. Niklausen, respectively. To trigger slope failure at the Weggis site, an additional pseudostatic seismic acceleration between 0.01 and 0.06 g (~0.04 g, if applying the estimated probable $c_{u\ in\ situ}$ value of ~5 kPa) is required, whereas the slope at St. Niklausen remains stable up to critical a_H values between 0.03 and 0.08 g (~0.07 g, if applying the estimated probable $c_{u\ in\ situ}$ value of ~6 kPa) (Fig. 11).

Leynaud et al. (2004) suggested that the pseudostatic horizontal seismic acceleration only represents about 50% of the effective earthquake peak ground acceleration (PGA). Results from slope stability back-calculations thus imply minimal PGA's of about 0.08 g (range of uncertainty ~0.02 to 0.12 g) and ~0.14 g (range of uncertainty ~0.06 to 0.16 g) during the 1601 A.D. and the 2220 cal yr B.P. earthquake, respectively. The result for the 1601 A.D. event from the Weggis site lies in the range of calculated values for PGA's deduced from predictive ground motion models for Central Switzerland (Bay et al., 2005), assuming a M_w 6.2 earthquake and an epicentral distance of 12 km (Fig. 1). The estimated PGA value for the prehistoric 2220 cal yr B.P earthquake in the order of 0.14 g, however, is slightly higher than the expected ground motion induced by low frequency (1 Hz) seismic

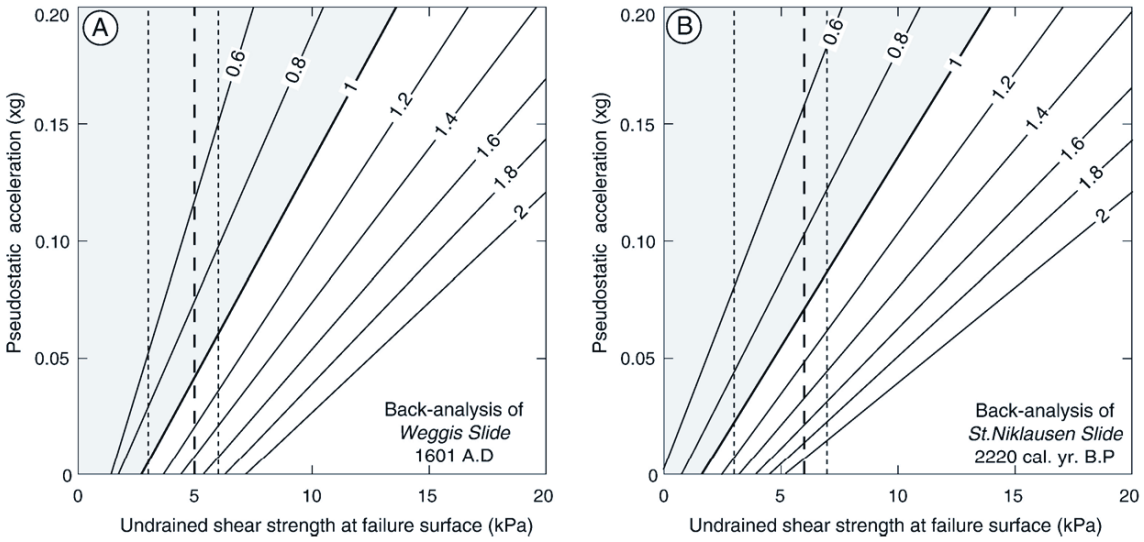

Fig. 10. Results of deterministic limit equilibrium slope stability back-analysis of Weggis (A) and St. Niklausen (B) Slides during the 1601 A.D. M_w ~6.2 earthquake and the 2220 cal yr B.P. earthquake (M_w>6.5), respectively. Contour plots show factor of safety (FS) as a function of the undrained shear strength at the failure surface and the pseudostatic acceleration (fraction of gravitational acceleration g). The gray shaded areas indicate solutions leading to instable conditions (FS<1). The range and reliable in situ values of measured undrained shear strength at the two study sites is shown as a fine dotted and bold dashed line, respectively. See Table 1 for model input data.

Table 2
Geotechnical material statistics used for probabilistic limit equilibrium slope stability analysis

	d (m)	γ (kN m^{-3})				c_u (kPa)				∇c_u (kPa m^{-1})			
		Mean	S.D.	Relative min	Relative max	Mean	S.D.	Relative min	Relative max	Mean	S.D.	Relative min	Relative max
Weggis site at 2220 cal yr B.P.													
Layer 1	1.5	13.3	0.3	0.5	0.5	1	0.5	0.5	0.5	1.75	0.5	0.75	0.5
Layer 2	1.25	14.7	0.5	0.5	0.5	5.4	3	3	3	–	–	–	
Layer 3	1	17.7	1	1	3	5.4	2.5	2.4	2	5	2	3	5
Chrüztrichter site at 2220 cal yr B.P.													
Layer 1	3.4	13.3	0.3	0.5	0.2	1	0.5	0.5	0.5	1.75	0.5	0.75	0.5
Layer 2	1.2	14.7	0.5	0.5	0.5	7.5	3	5	0.5	−2	0	1	2
Layer 3	1	20.6	1	3	1.5	8.5	2.5	4.5	2	5	2	3	3

Pseudostatic acceleration k_H during 2220 cal yr B.P earthquake ($\times g$)	Mean	S.D.	Relative min	Relative max
	0.07	0.03	0.012	0.023

waves with a return period of 2500 yr as estimated by probabilistic earthquake hazard assessment for the Lake Lucerne area (Giardini et al., 2004).

Although one would need to consider site effects that might amplify or attenuate seismic shaking and the fact that the accuracy of the used pseudostatic approach is governed by the simplification, with which the pseudostatic inertial forces represent the complex dynamic inertial forces during earthquake shaking (Kramer, 1996), the results from slope stability back-analysis suggest that during the prehistoric 2220 cal yr B.P earthquake that triggered the St. Niklausen Slide the Lake Lucerne area experienced significantly higher ground motions than during the historic 1601 A.D. M_w ~ 6.2 earthquake. This interpretation is supported by the fact that the 2220 cal yr BP earthquake also triggered subaqueous landslides in Lake Zurich at a distance of 40 km from Lake Lucerne, requiring a significantly larger magnitude (M_w > 6.5) than the historic 1601 A.D. earthquake (Strasser et al., 2006). However, the interpretation of higher ground motions during the 2220 cal yr B.P. event seems to contradict the observation that the Weggis and Chrüztrichter slopes remained stable during this stronger prehistoric event.

In order to investigate this apparent contradiction, the Weggis and Chrüztrichter slope stability conditions at 2220 cal yr B.P. were analyzed with a probabilistic limit equilibrium approach using the calculated critical horizontal seismic accelerations by the back-analysis described above (Table 2 summarizes the input parameters used). Both scenarios reveal mean FS values > 1 (1.03 and 1.14) and failure probability of < 50% (45.6 % and 43.7 %) for both the Weggis and Chrüztrichter slopes, respectively. Both slopes were relatively close to failure, but obviously remained stable during the 2220 cal yr B.P. event. These results indicate that the "charging" state of a submerged slope is a function of the sedimentation rate during the Holocene (i.e. the only parameter changing significantly from site to site), that controls the static weight of the slope-covering drape. Similar conclusions were drawn based on a significant increase in the frequency of lateral mass-movement deposits identified during Holocene times in other lakes (e.g. Waldmann et al., submitted for publication).

These observations further imply that ongoing sedimentation along the submerged slopes will continuously load the slopes so that the susceptibility for slope failure will increase in the future. As an end member scenario we investigated how long it would take to charge the Weggis slope (assuming constant sedimentation rates), so that the sediments acting on the critical surface would become unstable under static loading conditions. Solving the infinite slope equation (Morgenstern, 1967) for critical sediment thickness to initiate failure reveals as a first order assumption that the slopes only will become statically unstable in ~ 24 500 yr (input parameters: mean values for c_u, μ' and α as observed in the data described above). This is one order of magnitude longer than the time that separated the last two major earthquakes around Lake Lucerne implying that the occurrence of seismic events acts as main control on landslide triggering. Local differences in site-specific stability conditions, however, are governed by regional variations in sediment supply so that slope stability conditions may change locally over relative short geological time scales.

6. Summary and conclusions

This study presents the results from three comprehensive case studies of seismically-triggered, lateral non-deltaic subaqueous slope failures in perialpine, fjord-type

Lake Lucerne (Central Switzerland). The combined sedimentological, geophysical and in situ geotechnical approach provides a better understanding of the influence of the glacial-to-postglacial evolution in sedimentation processes along the investigated lateral slopes and their impact on the characteristic physical and geotechnical properties of the slope-covering sediments that control the stability condition and subaqueous slope failure initiation. On a larger scale, comparable slope stability conditions may evolve in fjords and high-latitude ocean margins, where glacially overconsolidated deposits are overlain by postglacial (glacio-) marine sediments accumulated during deglaciation periods and by pelagic and hemipelagic sedimentation deposited during interglacials (e.g. Boe et al., 2000; Locat et al., 2003; Boe et al., 2004). Our comprehensive lake study and resulting conceptual ideas thus also improve our understanding of larger slope instabilities occurring along formerly glaciated ocean margins.

A summary list of the main conclusions includes the following:

(1) Sedimentation dominated by suspension settling from meltwater plumes, slight overconsolidation by ice-grounding and postglacial draping lead to particular slope conditions characterized by: (i) fine-grained, thinly-laminated, slightly underconsolidated Late Glacial cyclic plume deposits with low undrained shear strength values overlying (ii) overconsolidated, glacially-deformed glacial deposits with overpressured formation pore pressure. This particular succession is overlain by a Holocene drape with variable thickness that acts as a surcharge on the lower sediment layers.
(2) During past earthquake shaking, slopes that were stable under static loading conditions (FS of 1.5–2) failed along glide planes that developed at this lithological boundary.
(3) This glide plane location is a consequence of the comparably low strength conditions within the overlying thinly-laminated Late Glacial clays and the additional excess in situ pore pressure in the underlying overconsolidated, low permeable material reducing effective strength at and below the zone of failure.
(4) Limit equilibrium back-analysis reveal seismic peak ground accelerations (PGA) at the study sites of ~0.08 g (range of uncertainty ~0.02 to 0.12 g) and ~0.14 g (range of uncertainty ~0.06 to 0.16 g) for the historical 1601 A.D. M_w ~6.2 earthquake and a prehistoric, 2220 cal yr B.P., M_w>6.5 northern alpine earthquake, respectively.
(5) The results thus pinpoint the potential of detailed subaqueous slope stability analysis as paleoseismological tool that allow for quantitative reconstruction of past earthquake shaking.
(6) Holocene sedimentation rates are a key parameter in "charging" subaqueous slopes susceptible for sliding. Stability conditions thus may change over relative short geological time scales.
(7) Lessons learned from the high-resolution case studies presented here should be implemented in future studies on a basinwide scale. In combination with more detailed analysis on the dynamic behavior of the material under cyclic loading these results eventually will yield strong arguments in identifying sites of potential slope instability in the future.

Acknowledgments

We thank B. Dürr, R. Hofmann and M. Lange as well as the whole ETH-Limnoteam and friends for technical support and assistance during the campaigns, respectively. Many thanks also to Urs Gerber for the core photographs. E. Button, E. Chapron, W. Haeberli, T. Mörz, A. Puzrin, M. Schnellmann, S. Springman and S. Wiemer, are acknowledged for the numerous discussions of the methods and data presented. We thank reviewers M. De Batist and N. Sultan for thoughtful comments that considerably improved the manuscript. Accommodations and harbour for field work were kindly provided by the Swiss EAWAG Limnological Research Center at Kastanienbaum. This study was supported by the Swiss National Science Foundation (Grant 620-066113) and the Deutsche Forschungsgemeinschaft (financial support to RCOM, project C8).

References

Aeschbach-Hertig, W., 1994. Helium und Tritium als Tracer für physikalische Prozesse in Seen. PhD Thesis, ETH Zurich Nr. 10714, 272 pp.
Andrews, D.C.A., Martin, G.R., 2000. Criteria for liquefaction of silty soils. 12th World Conference on Earthquake Engineering, Proceedings, Auckland, New Zealand.
Anselmetti, F.S., Bühler, R., Finger, D., Girardclos, S., Lancini, A., Rellstab, C., Sturm, M., in press. Effects of Alpine hydropower dams on particle transport and lacustrine sedimentation. Aquat. Sci. in press.
Azizian, A., Popescu, R., 2006. Three-dimensional seismic analysis of submarine slopes. Soil Dyn. Earthqu. Eng. 26, 870–887.
Bay, F., Wiemer, S., Fäh, D., Giardini, D., 2005. Predictive ground motion scaling in Switzerland: best estimates and uncertainties. J. Seismol. 9, 223–240.
Beck, C., Van Rensbergen, P., De Batist, M., Berthier, F., Lallier, S., Manalt, F., 2001. The Late Quaternary sedimentary infill of Lake

Annecy (northwestern Alps): an overview from two seismic-reflection surveys. J. Paleolimnol. 25, 149–161.
Biscontin, G., Pestana, J.M., Nadim, F., 2004. Seismic triggering of submarine slides in soft cohesive soil deposits. Mar. Geol. 203, 341–354.
Blass, A., Anselmetti, F.S., Ariztegui, D., 2003. 60 yr of glaciolacustrine sedimentation in Steinsee (Sustenpass, Switzerland) compared with historic events and instrumental meteorological data. Eclogae Geol. Helv. 96, 59–71.
Boe, R., Hovland, M., Instanes, A., Rise, L., Vasshus, S., 2000. Submarine slide scars and mass movements in Karmsundet and Skudenesfjorden, southwestern Norway: morphology and evolution. Mar. Geol. 167, 147–165.
Boe, R., Longva, O., Lepland, A., Blikra, L.H., Sonstegaard, E., Haflidason, H., Bryn, P., Lien, R., 2004. Postglacial mass movements and their causes in fjords and lakes in western Norway. Norw. J. Geol. 84, 35–55.
Bührer, H., Ambühl, H., 1996. Der Vierwaldstättersee 1961– 1992– Eine Dokumentation. Schriftenreihe der EAWAG, vol. 10. 54 pp.
Chapron, E., Beck, C., Pourchet, M., Deconinck, J.F., 1999. 1822 earthquake-triggered homogenite in Lake Le Bourget (NW Alps). Terra Nova 11, 86–92.
Cysat, R., 1601. Collectanea Chronica und denkwürdige Sachen pro Chronica Lucernensi et Helvetiae. In: Schid, J. (Ed.), Quellen und Forschungen zur Kulturgeschichte von Luzern und der Innerschweiz. Diebold Schilling Verlag, Luzern, pp. 882–888.
Duncan, J.M., 1996. State of the art: limit equilibrium and finite-element analysis of slopes. J. Geotech. Geoenviron. Eng. 122, 577–596.
Evans, J., Dowdeswell, J.A., Grobe, H., Niessen, F., Stein, R., Hubberten, H.W., Whittington, R.J., 2002. Later Quaternary sedimentation in Kejser Franz Joseph Fjjord and the continental margin of East Greenland. In: Dowdeswell, J.A., Cofaigh, C.O. (Eds.), Glacier-Influenced Sedimentation on High-Latitude Continental Margins. Geol. Soc. London, Special Publication. The Geol. Soc. London, London, pp. 149–179.
Eyles, N., Boyce, J.I., Halfman, J.D., Koseoglu, B., 2000. Seismic stratigraphy of Waterton Lake, a sediment-starved glaciated basin in the Rocky Mountains of Alberta, Canada and Montana, USA. Sediment. Geol. 130, 283–311.
Finckh, P., Kelts, K., Lambert, A., 1984. Seismic stratigraphy and bedrock forms in perialpine lakes. Geol. Soc. Amer. Bull. 95, 1118–1128.
Florineth, D., Schluchter, C., 1998. Reconstructing the Last Glacial Maximum (LGM) ice surface geometry and flowlines in the central Swiss Alps. Eclogae Geol. Helv. 91, 391–407.
Fredlund, D.G., Krahn, J., 1977. Comparison of slope stability methods of analysis. Can. Geotech. J. 14, 429–439.
Giardini, D., Wiemer, S., Fäh, D., Deichmann, N., 2004. Seismic Hazard Assessment of Switzerland, Swiss Seismological Service, ETH Zürich. http://www.earthquake.ethz.ch/research/Swiss_Hazard/Swiss_Hazard/downloads/Hazard_report_2004.pdf.
Gisler, M., Fäh, D., Kästli, P., 2004. Historical seismicity in Central Switzerland. Eclogae Geol. Helv. 97, 221–236.
Gyger, M., Mueller-VonMoos, M., Schindler, C., 1976. Untersuchungen zur Klassifikation spaet-und nacheiszeitlicher Sedimente aus dem Zuerichsee. Schweiz. Mineral. Petrogr. Mitt. 56, 387–406.
Haeberli, W., Schlüchter, C., 1987. Geological evidence to constrain modelling of the Late Pleistocene Rhonegletscher, Swiss Alps. The Physical Basis of Ice Sheet Modelling. Proc. of the Vancouver Symposium, Vancouver, pp. 333–346.
Hampton, M.A., Lee, H.J., Locat, J., 1996. Submarine landslides. Rev. Geophys. 34, 33–59.
Hantke, R., 2003. Unterseeische Moränen im Vierwaldstätter See. In: Lienert, S. (Ed.), Geologie und Geotope im Kanton Schwyz. Schwyzerische Naturforschende Gesellschaft, Einsiedeln, pp. 106–109.
Institute, B.S., 1977. Methods of testing soil for civil engineering purposes, BS 1377. BSI, London.
Ivy Ochs, S., Schafer, J., Kubik, P.W., Synal, H.A., Schlüchter, C., 2004. Timing of deglaciation on the northern Alpine foreland (Switzerland). Eclogae Geol. Helv. 97, 47–55.
Kelts, K., 1978. Geological and Sedimentary Evolution of Lake Zurich and Zug, Switzerland. PhD Thesis, ETH, Zurich, 224 pp.
Kelts, K., 1998. Components in Lake sediments: Smear Slide Identifications. http://lrc.geo.umn.edu/smears/smsl.html.
Kelts, K., Briegel, U., Ghilardi, K., Hsu, K., 1986. The Limnogeology–ETH Coring System. Swiss J. Hydrol. 48, 104–115.
Kopp, J., 1938. Der Einfluss des Kriensbaches auf die Gestaltung des Luzernersees und die Hebung des Seespiegels des Vierwaldstättersees. Eclogae Geol. Helv. 31, 376–378.
Kramer, S.L., 1996. Geotechnical Earthquake Engineering. Prentice Hall, New Jersey. 653 pp.
Lambe, T.W., Whitman, R.V., 1979. Soil Mechanics, SI Version. John Wiley & Sons, Singapore. 553 pp.
Lee, H.J., 2005. Undersea landslides: extent and significance in the Pacific Ocean, an update. Nat. Hazards Earth Syst. Sci. 5, 877–892.
Lee, H.J., Edwards, B.D., 1986. Regional method to assess offshore slope stability. J. Geotech. Geoenviron. Eng. 112, 486–509.
Lemcke, G., 1992. Ablagerungen aus Extremereignissen als Zeitmarker der Sedimentationsgeschichte im Becken von Vitznau/Weggis (Vierwaldstättersee, Schweiz). MS thesis Thesis, Georg-August-Universtität Götting, Götting, 154 pp.
Leroueil, S., Vaunat, J., Picarelli, L., Locat, J., Lee, H.J., Faure, R., 1996. Geotechnical characterization of slope movements. Proc. Int. Symposium on Landslides, Trondheim, pp. 53–74.
Leynaud, D., Mienert, J., Nadim, F., 2004. Slope stability assessment of the Helland Hansen area offshore the mid-Norwegian margin. Mar. Geol. 213, 457–480.
Lister, G.S., 1988. A 15,000-yr isotopic record from Lake Zuerich of deglaciation and climatic change in Switzerland. Quat. Res. 29, 129–141.
Lister, G.S., Giovanoli, F., Eberli, G., Finckh, P., Finger, W., He, Q., Heim, C., Hsu, K.J., Kelts, K., Peng, C., Sidler, C., Zhao, X., 1984. Late Quaternary sediments in Lake Zurich, Switzerland. Environ. Geol. 5, 191–205.
Locat, J., Lee, H.J., 2002. Submarine landslides: advances and challenges. Can. Geotech. J. 39, 193–212.
Locat, P., Leroueil, S., Locat, J., Duchesne, M.J., 2003. Characterisation of submarine flow-slide at Pointe-Du-Fort, Saguenay Fjord, Quebec, Canada. In: Locat, J., Mienert, J. (Eds.), Submarine Mass Movements and their Consequences, pp. 521–529.
Lu, T.S., Bryant, W.R., 1997. Comparison of vane shear and fall cone strengths of soft marine clay. Mar. Georesour. Geotechnol. 15, 67–82.
Lunne, T., Robertson, P.K., Powell, J.J.M., 1997. Cone Penetration Testing in Geotechnical Practice. Spon Press. 312 pp.
Lysa, A., Sejrup, H.P., Aarseth, I., 2004. The Late Glacial–Holocene seismic stratigraphy and sedimentary environment in Ranafjorden, northern Norway. Mar. Geol. 211, 45–78.
Mackiewicz, N.E., Powell, R.D., Carlson, P.R., Molnia, B.F., 1984. Interlaminated ice-proximal glacimarine sediments in muir inlet, Alaska. Mar. Geol. 57, 113–147.
Mienert, J., 2004. COSTA—continental slope stability: major aims and topics. Mar. Geol. 213, 1–7.

Morgenstern, N.R., 1967. In: Richards, A.F. (Ed.), Submarine Slumping and Initiation of Turbidity Currents. Marine Geotechnique UP, Urbana, IL, pp. 189–220.

Morgenstern, N.R., Price, V.E., 1965. Analysis of stability of general slip surfaces. Geotechnique 15, 79–93.

Nittrouer, C.A., 1999. STRATAFORM: overview of its design and synthesis of its results. Mar. Geol. 154, 3–12.

Plötze, M., Giudici Trausch, J., Messerklinger, S., Springman, S.M., 2003. Swiss Lacustrine clay: mineralogical and mechanical characteristics. In: Cudny, K.A. (Ed.), Int. Workshop on Geotechnics of Soft Soils— Theory and Practice, Noordwijkerhout, pp. 473–478.

Quigley, R.M., Ogunbadejo, T.A., 1972. Clay layer fabric and oedometer consolidation of soft varved clay. Can. Geotech. J. 9, 165–175.

Rothwell, R.G., 1989. Minerals and Mineraloids in Marine Sediments: An Optical Identification Guide. Elsevier Appl. Sci., London. 279 pp.

Schnellmann, M., Anselmetti, F.S., Giardini, D., McKenzie, J.A., Ward, S.N., 2002. Prehistoric earthquake history revealed by lacustrine slump deposits. Geology 30, 1131–1134.

Schnellmann, M., Anselmetti, F.S., McKenzie, J.A., Giardini, D., 2005. Mass movement-induced fold-and-thrust belt structures in unconsolidated sediments in Lake Lucerne (Switzerland). Sedimentology 52, 271–289.

Schnellmann, M., Anselmetti, F.S., McKenzie, J.A., Giardini, D., 2006. 15,000 yr of mass-movement history in Lake Lucerne: implications for seismic and tsunami hazards. Eclogae Geol. Helv. 99. doi:10.1007/s00015-006-1196-7.

Schwarz-Zanetti, G., Deichmann, N., Fäh, D., Giardini, D., Jimenez, M.J., Masciadri, V., Schibler, R., Schnellman, M., 2003. The earthquake in Unterwalden on September 18, 1601: a historic-critical macroseismic evaluation. Eclogae Geol. Helv. 96, 441–450.

Shilts, W.W., Clague, J.J., 1992. Documentation of earthquake-induced disturbance of lake-sediments using subbottom acoustic profiling. Can. J. Earth Sci. 29, 1018–1042.

Siegenthaler, C., Finger, W., Kelts, K., Wang, S., 1987. Earthquake and seiche deposits in Lake Lucerne, Switzerland. Eclogae Geol. Helv. 80, 241–260.

Stegmann, S., Villinger, H., Kopf, A., 2006. Design of a modular, marine free-fall cone penetrometer. Sea Technol. 47, 27–33.

Stegmann, S., Strasser, M., Anselmetti, F.S., Kopf A., in press. Geotechnical *in situ* characterisation of subaquatic slopes: the role of pore pressure transients versus frictional strength in landslide initiation. Geophys. Res. Lett.

Strasser, M., Anselmetti, F.S., Fäh, D., Giardini, D., Schnellman, M., 2006. Magnitudes and source areas of large prehistoric northern Alpine earthquakes revealed by slope failures in lakes. Geology 34, 1005–1008.

Sturm, M., Matter, A., 1978. Turbidites and varves in Lake Brienz (Switzerland); deposition of clastic detritus by density currents. In: Matter, A., Tucker, M.E. (Eds.), Modern and Ancient Lake Sediments; Proceedings of a Symposium. Oxford International, Blackwell, pp. 147–168.

Sultan, N., Cochonat, P., Canals, M., Cattaneo, A., Dennielou, B., Haflidason, H., Laberg, J.S., Long, D., Mienert, J., Trincardi, F., 2004. Triggering mechanisms of slope instability processes and sediment failures on continental margins: a geotechnical approach. Mar. Geol. 213, 291–321.

Terzaghi, K., 1925. Erdbaumechanik. Deuticke, Wien. 399 pp.

Terzaghi, K., Peck, R.B., Mesri, G., 1996. Soil Mechniscs in Engineering practice: Chapter 16: compressibility of confined layers of soil, Third ed. New York. 549 pp.

Thevenon, F., Anselmetti, F.S., Schnellmann, M., submitted for publication. 7200 yr of human impact evidenced by automated image analysis of pyrogenic products from Lake Lucerne sediments (Central Switzerland). Quat. Sci. Rev.

Urgeles, R., Leynaud, D., Lastras, G., Canals, M., Mienert, J., 2006. Back-analysis and failure mechanisms of a large submarine slide on the ebro slope, NW Mediterranean. Mar. Geol. 226, 185–206.

Van Rensbergen, P., De Batist, M., Beck, C., Chapron, E., 1999. High-resolution seismic stratigraphy of glacial to interglacial fill of a deep glacigenic lake: Lake Le Bourget, Northwestern Alps, France. Sediment. Geol. 128, 99–129.

Waldmann, N., Ariztegui, D., Anselmetti, F.S., Austin Jr., J.A., Dunbar, R., M. Moy, C.M., Recasens, C., submitted for publication. Lago Fagnano (Tierra del Fuego, Argentina) — a continuous archive of paleoclimatic change and tectonic activity since the Late Glacial. Geologica Acta.

Wessels, M., 1998. Natural environmental changes indicated by Late Glacial and Holocene sediments from Lake Constance, Germany. Palaeogeogr. Palaeoclimatol. Palaeoecol. 140, 421–432.

5.3. Marine deep-water Free-fall CPT measurements for landslide characterisation off Crete, Greece (Eastern Mediterranean Sea) - PART 2: initial data from the western Cretan Sea

Kopf, A., Stegmann, S., Krastel, S., Förster, A., Strasser, M., and Irving, M., In: Lykousis, V., Sakellariou, D., and Locat, J. (Eds.), Submarine Mass Movements and their Consequences, 3rd International Symposium, Springer, Netherlands, 199-208, published in 2007.

Marine deep-water Free-fall CPT measurements for landslide characterisation off Crete, Greece (Eastern Mediterranean Sea) - PART 2: initial data from the western Cretan Sea

A. Kopf, S. Stegmann, S. Krastel, A. Förster

Research Centre Ocean Margins, Bremen University, Leobener Strasse, 28359 Bremen, Germany

M. Strasser

Geological Institute, ETH Zurich, Universitätstrasse 16, CHN, 8092 Zurich, Switzerland

M. Irving

Picker Engineering Program, Smith College, 51 College Lane, Northampton, MA 01063, U.S.A.

Abstract

Pore pressure and shear strength are major controlling parameters for slope stability, which can be measured *in situ* using CPT (cone penetration testing) instruments. This paper presents results from initial tests with two free-fall CPT probes deployed in the neo-tectonically active submarine slope of northern Crete, Greece. Research expedition P336 investigated landslide-prone areas in the Cretan Sea using multibeam swathmapping, seismic reflection profiling, *in situ* CPT measurements, and gravity coring. Several large landslide complexes at the NE Cretan Margin as well as a small, but steep landslide scarp structure further east were identified on the seismic profiles. CPT devices were deployed in undisturbed slope sediments, across the slide scar, and in the main body of the slide, and remained stuck in the sediment for ~10 minutes to monitor pore pressure dissipation upon insertion. Excess pore pressure after insertion is in a range around 60 kPa in background sediment, and exceeds 80 kPa in the slide deposits. Cone resistance of the slope sediment ranges between 300 kPa and 500 kPa, corresponding to undrained shear strength of up to 40 kPa. The slid sediments (specifically the headwall material with <10 kPa strength) show velocity-weakening behaviour during ring shear experiments, indicating that those sediments are unlikely to show stable creep and instead may fail catastrophically.

KEYWORDS: CPT, LANDSLIDE, SHEAR STRENGTH, PORE PRESSURE

1. Introduction

Sediment stability at continental margins depends on given different soil mechanical conditions and a variety of trigger mechanisms (e.g. Hampton et al. 1996). This complexity demands a multi-disciplinary research approach, which has been achieved by several studies that combined geophysical, sedimentological and geotechnical methods (e.g. Storegga Landslide [Kvalstad et al. 2005]; Niger Delta [Sultan et al., 2007]). In these studies, the sediment physical properties were assigned a high priority, with shear strength and pore pressure playing a key-role in the assessment of sediment stability. Equally, there are several landslide occurrences north of Crete, an area that is regularly struck by neo-tectonic activity and earthquake tremors (Lykousis et al., 2002). During cruise P336 in April/May 2006 in the Cretan Sea, we studied landslide processes in two areas (here termed D and E). Bathymetric mapping and seismic profiling served to characterise the landslide-prone slopes. Subsequently, *in situ* CPT measurements were made in undisturbed slope sediments as well as in the mass wasting deposits and were complemented by geotechnical measurements on adjacent sediment cores.

2. Geological background of the Cretan Sea (Eastern Mediterranean)

The Cretan Sea represents the northernmost portion of the forearc region in the Hellenic subduction zone (HSZ) between Africa and Eurasia, which is well recorded over the past ca. 35 million years (Le Pichon and Angelier, 1979). It is sandwiched between the Aegean back-arc basin and island arc volcanoes (e.g. Santorini) in the north and the island of Crete, a prominent forearc-high, in the south (Fig. 1a). The island of Crete comprises a stack of nappes of variable lithologies (for details, see e.g. Fassoulas, 1999), parts of which got exhumed some 19 Ma ago and now are extending in both E-W- and N-S-direction. The main extensional phase of the Cretan Sea occurred between the Late Miocene and Pliocene however the Late Pleistocene experienced only minimal extension phenomena (Mascle and Martin, 1990). Tectonic movements still occur today, as indicated by recent seismicity and volcanic activity in the area (McKenzie, 1978). Landslides are one of the most immanent hazards in the Cretan Sea, being triggered by both the tectonic movements of the Cretan block in the south (e.g. Chronis et al., 2000a, b) and the flank collapse of volcanic islands in the north (e.g. Dominey-Howes et al., 2000). Although the inherent mechanisms and factors governing slope stability and submarine landslides are comprehensively studied, their temporal and spatial variability are poorly understood.

Geomorphologically, the Cretan Basin is an elongated depression, trending E–W; it is bounded to the north by the Cyclades Plateau, a relatively shallow (500 m) complex of islands, and has water depths no larger than 1000 m (with localized, ca. 2500 m deep sub-basins; see Kopf et al., 2006). Sediment accumulation processes at the southern margin of the Cretan Basin represent pro-delta deposition in the inner middle shelf, settling from bottom nepheloid layers in the shelf and upper slope, calcareous sediment formation due to settling from suspension, and re-deposition from suspension due to gravity processes and bottom currents (Chronis et al., 2000b). Hemipelagic sediments of the entire Cretan Sea are characterised by four different lithologies, regarded from top to bottom (Giresse et al., 2003):

(i) yellowish brown mud with bioturbation structures
(ii) grey mud mottled and moderate bioturbated with
(iii) brownish or olive black mud with >2% C_{org}, which represents sapropel S1 (9600-6400 yrs. BP)
(iv) yellowish, grey clay-rich mud.

Sedimentation rates in the Cretan trough are estimated to be 4.3-15 cm/ka (Giresse et al., 2003).

3. Methodology

Cruise P336 with the RV *Poseidon* focused on slope instability and sedimentation at the northern Cretan Margin (Fig. 1a). A variety of geophysical, sedimentological, and geotechnical methods were applied, of which only a few are relevant for this paper. A detailed report of this cruise is given in Kopf et al. (2006).

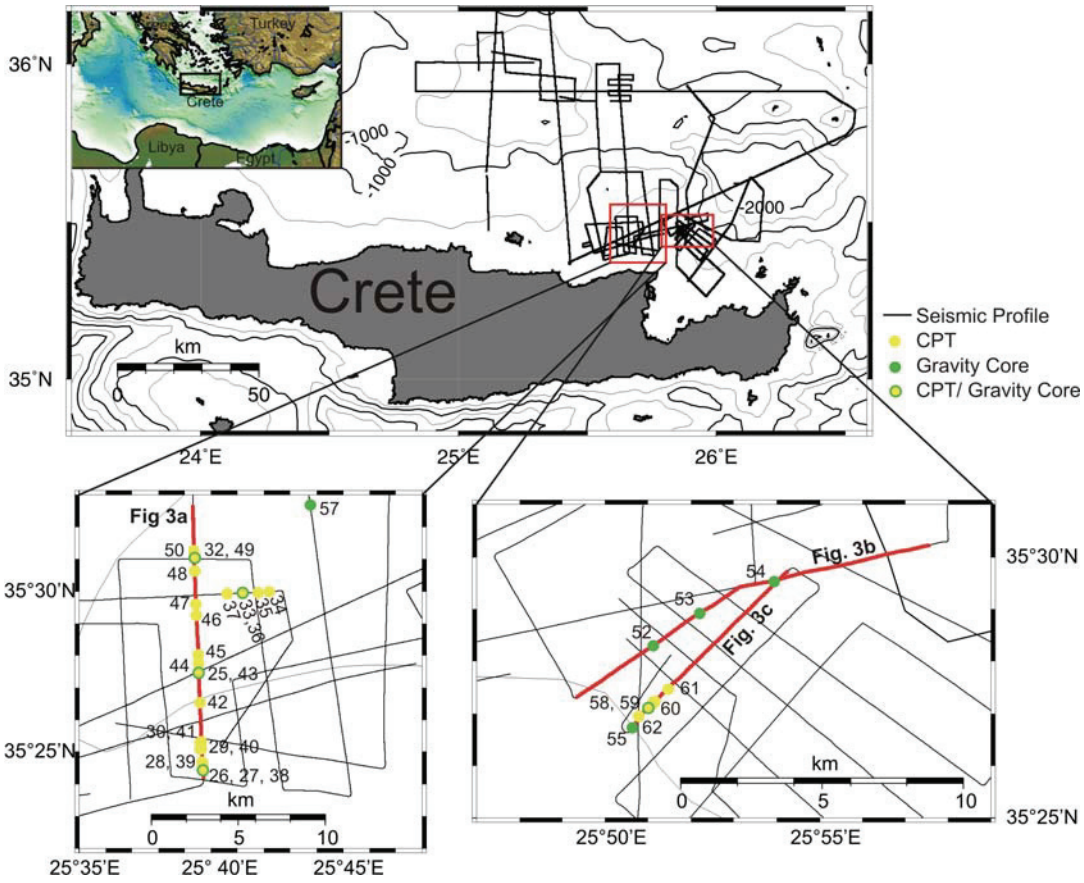

Figure 1: Map of the complete study area in the Eastern Mediterranean off Crete, Greece **(A)**. Mass wasting deposits at the Cretan Margin are identified in study area D **(B)** and study area E **(C, D)**. Numbers and lines represent the position of seismic profiles, gravity core stations and CPT locations.

3.1 Geophysical characterisation

Continuous seafloor mapping was routinely carried out with the multibeam echosounder ELAC SEABEAM 1050 in order to identify landslide scars. Seismic data were collected using a 3.5 kHz system and a high-resolution multi-channel system. The multi-channel seismic system consists of a Mini-Generator-Injector Airgun (frequency range 100-500Hz) and a 100-m-long 16 channel streamer. The presented seismic profiles (Fig. 1) are brute stacks generated by summing up the first three channels. The data were filtered with a wide bandpass (55/110-600/800 Hz). The combination of 3.5 kHz and seismic data were the basis for selecting coring and CPT-stations.

3.2 *in situ* Measurements

In situ measurements of sediment physical properties were carried out with two free-fall CPT devices. Their design and mode of deployment is described in the first part of this manuscript (see Stegmann and Kopf, this issue).

3.3 Sediment cores and physical properties

Sediment cores were taken with a 1.6 ton gravity corer. Cores were split and described on board including visual determination of lithological composition, colour and grain size classification. The mineralogy noted was based on a smear slide analysis. Shore-based work included logging of the archive half of each gravity core using a GEOTEK multi-sensor core logger (MSCL) at RCOM Bremen. Measured parameters included P-wave velocity, gamma ray attenuation (bulk density), and magnetic susceptibility.

In addition, preliminary sediment shear strength c_u was measured on board with a fall cone penetrometer. Based on its defined weight (80.51g) and geometry (30° cone), c_u was derived from the penetration depth following Hansbo (1957).

The rate-dependent shear behaviour of the disturbed and undisturbed sediments (see Fig. 2 for position of the samples) was measured using a Bromhead ring shear device. The specimen was placed into an annular chamber and loaded incrementally to normal stresses between 0.4 and 16 MPa. For each load increment, the sample was sheared at different rates (0.0005 mm/s, 0.001 mm/s, 0.01 mm/s and 0.1 mm/s). The friction coefficient, defined as the ratio of peak shear stress to normal stress, describes the strength of the material, whereas residual shear strength variations at different shear velocities (so called [*a-b*] parameter) define the frictional stability of the sediment (Scholz, 1998).

4. Results

4.1 Landslide targets

Based on the multibeam bathymetry and seismic data, two regions with characteristic mass wasting features were identified from their seafloor roughness and internal chaotic signatures (Fig. 2). Northeast of the island of Crete, area D shows a huge, roughly ~ 9 km long and 3-4 km wide lobe of displaced slope sediment consisting of two distinct slide units, with a relatively smooth surface (Fig. 2a). Some of the failed material seems to have slid as intact blocks while other portions appear to have been amalgamated. A headwall cannot be identified, but at the head of the slide body, the upper 20 m of sediments are missing and seem to be incorporated into the slide. Intact structures inside of the generally chaotic seismic facies of the slides suggest that the internal structure has not been totally destroyed and that the slide has not travelled very far.

Further east, in area E, a smaller slope failure event was identified based on its steep head scarp (Figs. 2b, c). Undisturbed, well-stratified sediments upslope are cut at the headwall, which has a height of ~50 m at this location. Directly adjacent to the headwall, a relatively

thin (< 50 m) chaotic unit overlies well-stratified sediments. Approximately 4 km down-slope of the headwall the chaotic unit thickens to roughly 100 m, which most likely represents the main depositional area of the slide. However, as this unit does not appear as a continuous feature, an estimation of the depositional area is difficult. It could be possible that the bulk part of the slide material is transported much further down-slope and was deposited in the deep basin.

In the two slides identified in areas D and E, a total of 11 gravity cores with lengths of 1-4.6 m were recovered (Figs. 2-3; Kopf et al., 2006). The sediment is generally comprised of four different lithologies: Yellowish brown bioturbated mud (Unit 1) is underlain by mottled and moderately bioturbated grey mud (Unit 2), sometimes containing a volcanic layer of the Thera eruption (3370 B.P.). Below that, greyish-brownish to olive grey mud with C_{org} >2% and no bioturbation has been identified as sapropel S1 (Unit 3). It is underlain by yellowish grey clayey mud, which is often slightly bioturbated (Unit 4).

Surprisingly, there is no significant difference between cores taken in the undisturbed slope and in the wasted mass below. In fact, all cores from the large slide complex D as well as area E show the four lithological units (Fig. 3). The only exception to this fact is core 52, where both Unit 2 and S1 are traceable only as remnants of mm-thicknesses (Fig. 3b). It appears from visual inspection that Unit 3 (S1) and parts (or all) of Unit 2 are missing. We will revisit this aspect when looking at the MSCL data (see below). Other than that, there are only minor differences between areas D and E regarding the thickness (and hence sedimentation rate) of the units. In area D, the landslide cores show condensed successions of Units 1 and 2 when compared to the undisturbed reference site. In contrast, area E shows no systematic relationship, with both the hangingwall and slid mass deposits showing both normal and condensed successions.

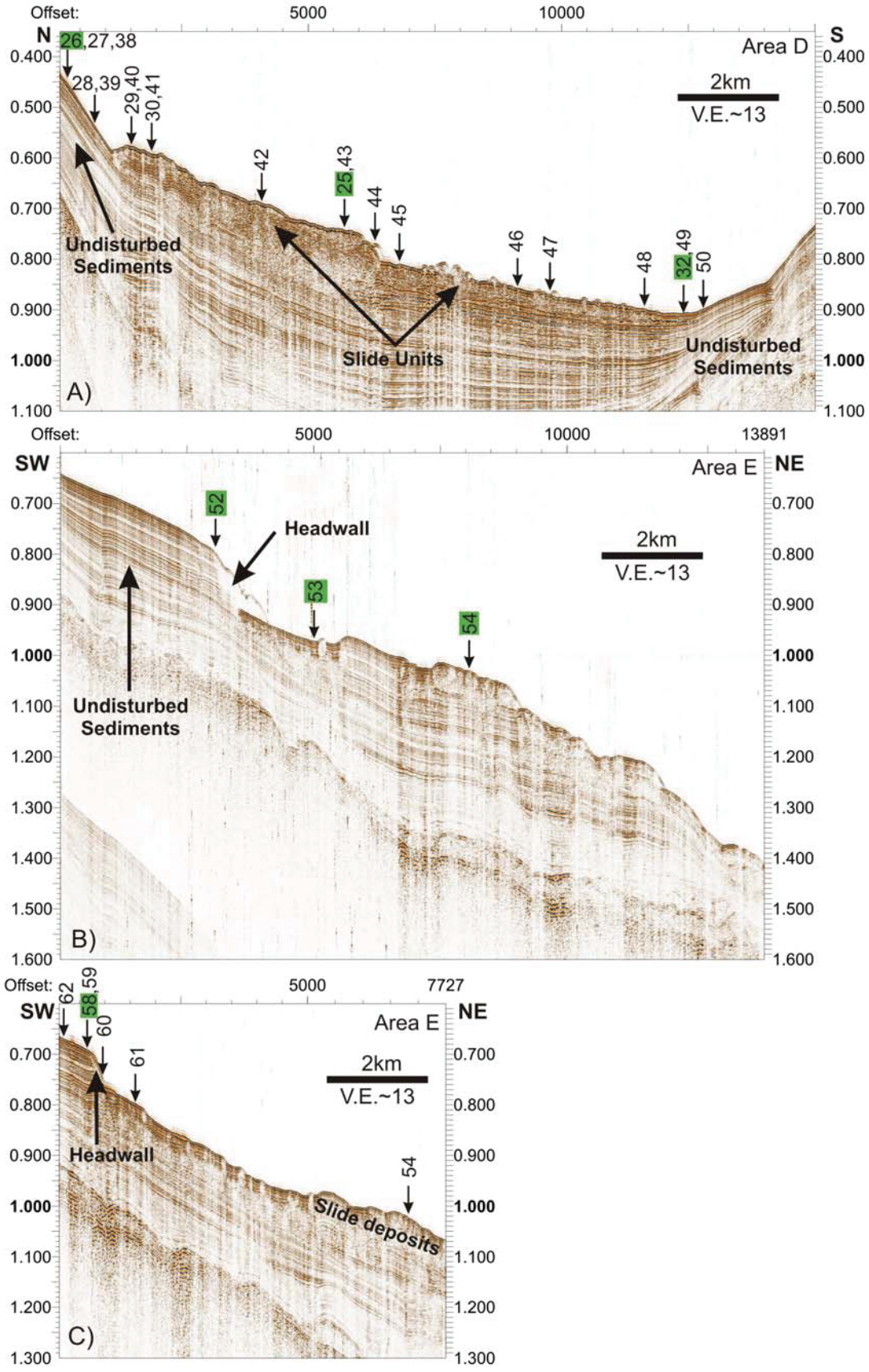

Figure 2: Airgun profile of mass wasting events at the Cretan Margin in area D **(A)** and area E **(B, C)** with the positions of the CPT and gravity cores (green marked signature).

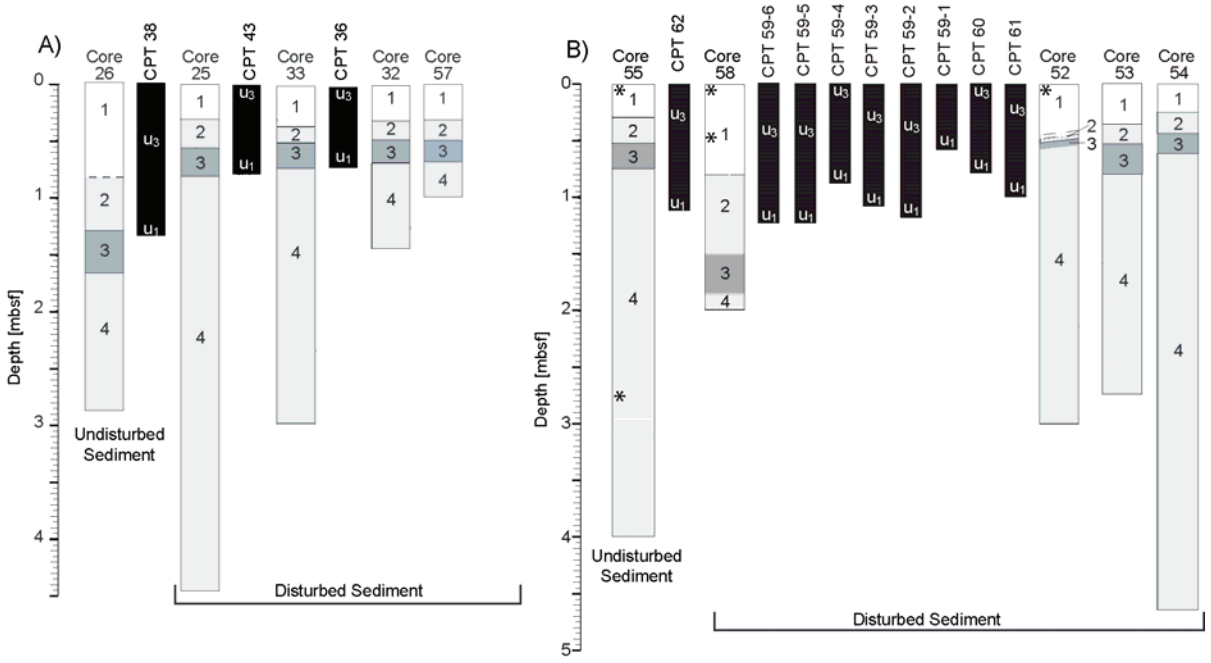

Figure 3: Lithology of cored sediments (see description in the text) and penetration depth of FF-CPT deployments in landslide sediments in areas D **(A)** and E **(B)**. The position of specimens, which have been tested in the ring shear device (see description in the text and Fig. 5), are marked by *.

4.2 *in situ* Physical properties

During the cruise, 26 FF-CPT deployments were carried out in areas D and E (Figs. 2-3). Unfortunately, the CPT cone failed during some of the deployments so that the strength parameters (q_c, f_s) could not be measured in each location. Consequently, we focus mainly on the differential pore pressure data in regions D and E. Initial penetration velocity of the complete CPT data set (derived from acceleration) ranged between 1.1 m/s and 1.8 m/s, which was mostly limited by winch speed (max. 2 m/s) and external conditions (waves, swell). Given the stiff nature of the sediments off Crete, total penetration depth was rather low. It appears as if the S1 layer, which has a higher strength than the surrounding sediments, is limiting the maximum penetration depth since it slows down the lance's momentum dramatically. In area D, penetration depth varied between 0.65 and 1.35 m (Fig. 3a), with the highest values in undisturbed sediments upslope of the scar, and between 0.6 and 1.25 m in area E (Fig. 3b). In nearly all measurements the tilt of the penetrated lance did not exceed ±9°. *In situ* measured cone resistance is limited to undisturbed and failed sediments of area D because of problems with the CPT probe at the tip of the lance. However, based on the results collected, we can show that the undisturbed section shows higher strength than the remobilised portion. This is reflected by maximum q_c plotting around 400-500 kPa upslope and 300-380 kPa on the landslide body. These findings correspond to the working hypothesis that the remobilised sediment has higher water content and lower strength, which is indicated

further by the MSCL data. These attest to lower p-wave velocities and bulk densities in the upper portion of cores in the landslide body (stations 25, 33, 32, 57), but higher p-wave velocities in Unit 4 in the lower part. Here, the undisturbed material ranges between 1575-1590 m/s while the landslide cores range from 1510 to 1560 m/s, possibly related to fluids trapped during remobilisation. Measured pore pressure response generally shows an insertion peak followed by a sudden drop. At the time, the lance is still penetrating the sediment (Stegmann and Kopf, this issue, red portion in their Fig. 3). Pore pressure then rises again to a second maximum, which in turn is followed by an exponential decay (Stegmann and Kopf, this issue, black portion in their Fig. 3). Unfortunately, several of our measurements exceeded the upper limit of the differential pore pressure sensor immediately after the impact of the probe (again, maybe as a result of high excess fluid pressures in Unit 4; see previous paragraph). For all landslide measurements of u_1, maximum excess pore pressure values after insertion ranged between 24 kPa to more than 82 kPa (this latter value being the upper range of the sensor). Pore pressure signals in area D show maximum insertion pore pressure (u_1) between 40 and 60 kPa for the sapropel unit of area D. The sediment in area E is found less dense and with higher porosities compared to area D. Accordingly, T_{50} values range between 1.9 and 4.2 mins. in the sapropel unit (60-80% porosity) compared to T_{50}=6 mins. in the muddy sediment (40-60% porosity). The u_3 pore pressure signal was measured in only 76 % (area D) and 33% (area E) of the measurements, because penetration depth did not exceed 80 cm (see instrument design, Stegmann and Kopf, this issue). When recorded, the u_3 signal often resembles that in u_1 position (see Stegmann and Kopf, this issue, Fig. 3d). The insertion pressure values are higher in area D, varying between 27 kPa (station 40) and 52 kPa (station 39), than in area E with a range between 9.5 kPa (station 62) and 28.6 kPa (station 59-4).

4.3 Lab-based physical properties

Data from the MSCL do not allow a clear distinction between cores taken in the undisturbed slope cover (reference core) and that in the landslide material. In general, area D cores show low p-wave velocities (1500-1550 m/s) and smaller bulk densities of approximately 1.85 g/cm^3 than area E. Values increase gradually down section in the reference core (core 26) (ca. 1600 m/s, ca. 2 g/cm^3), but decrease in each of the landslide cores in Unit 4. Lab-determined physical properties such as undrained shear strength c_u (determined with the fall cone penetrometer) mirror this trend. In the upper portion (i.e. unit 1-3) c_u increases with depth from 10 to 20 kPa. In the deeper section (2-2.9 m) of the

reference core, higher c_u (40 ±8 kPa) coincides with a significant jump to lower porosity (av. 40 %). Failed material of the Cretan Margin (stations 25, 32, 33, 57) can be different to very similar to the intact sediments located above the scarp. In contrast, the farthest removed deposits reveal a process of homogenisation as a result of displacement, expressed with a relatively high porosity of 60 % and a density in a range around 1.8 g/cm^3. c_u is more or less constant, which seems indicative of prograde consolidation history.

Although the scarp structure of the area E landslide is very recognisable in seismic data, landslide features are not very obvious to identify in the very homogeneous sediments with an average density of 1.8 g/cm^3. Upslope (station 55) and down-slope (station 54) materials are characterised by a linear increase of c_u from 20 to 40 kPa. Immediately near the scarp (station 52) and within the channel-like failure structure (stations 53, 58) a less pronounced linear trend of c_u is evinced.

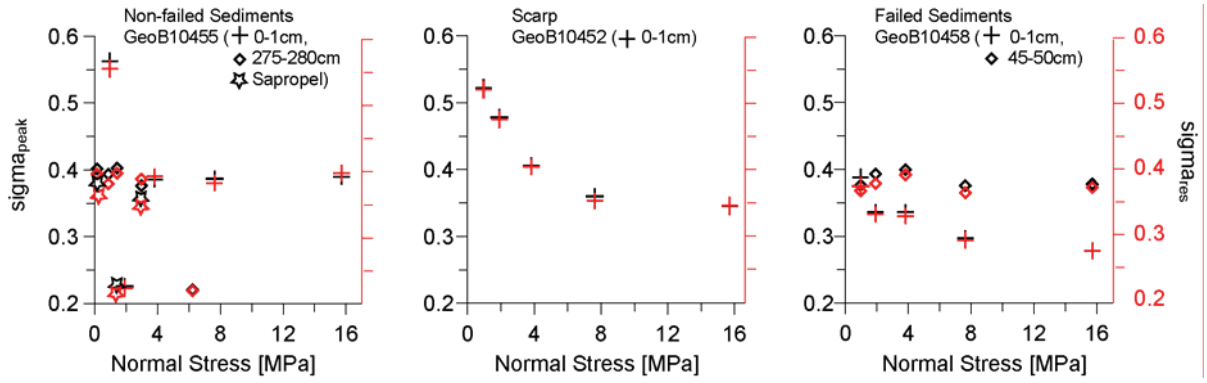

Figure 4: Frictional behaviour of undisturbed and disturbed superficial (crosses) and sediments from depth (lozenges) of the head scarp region in area E. The coefficient of friction is plotted vs. normal stress due to incremental loading during ring shear tests with a shear velocity of 0.01 mm/s. Black colours signify the coefficient of peak strength μ_{peak} while red colours show the coefficient of residual strength μ_{res}.

Ring shear data have only been collected in area E to characterise small-scale lateral variations across the headwall of the slide (Fig. 2b-c, 3b). The undisturbed sediments (station 55) indicate no significant difference between superficial (Unit 1) and deeper portion (Unit 4; 2.75-2.8 m) with an average μ_{peak} of 0.4 (Fig. 4a). Unit 3 (sapropel S1) shows a μ_{peak} range of 0.24-0.4, possibly reflecting a breakdown of the cohesive organic aggregates and fabric alignment. In contrast, μ_{peak} of the surface sediment from the headwall and landslide (stations 52, 58) are significantly lower, ranging around 0.35 (52; Fig. 4b) and 0.28 (58; Fig. 4c). Even the deeper portion of the landslide core 58 shows μ_{peak} ca. 0.36-0.4, which is slightly below that of the undisturbed core (Fig. 4a). This suggests to us that indeed some material is missing in the upper part of core 58 (see discussion below).

5. Discussion

Looking into the sedimentary and geotechnical results in more detail, we first revisit the seismic data. Despite the evidence for landslide features in area D with rough surface and internal features in the seismic images (Fig. 3), the gravity core description alone cannot unambiguously distinguish between the undisturbed vs. slid sediment. Based on sedimentological information, it can be speculated that:

(i) the lower part of the succession corresponds to amalgamated mud of the landslide body that would have occurred relatively shortly before the onset of sapropel deposition ~10 ka B.P., or that

(ii) the sedimentary succession represents primary sedimentary deposits and therefore, the landslide is either older and was not reached with coring, or all cores were recovered from an internally coherent slide, or out runner blocks. In case of the latter, the landslide can also be younger than S1 and the Thera volcanic deposit (3370 B.P.).

When further consulting the results from the MSCL and *in situ* measurements, we observe some variations that identify the landslide material. These include lower cone resistance in the remobilised section of landslide D, lower p-wave velocity in the deeper portion of cores from area D, and low frictional strength from ring shear tests at the head scarp materials and shallow landslide deposits in area E (cores 52 and 58; Fig. 4b, c). If we assume that these interpretations of the superficial measurements are correct, then the landslide should be relatively young. This is supported by the seismic reflection data where, despite lack of m-scale resolution, no seafloor-parallel, post-landslide reflections are found (Fig. 2). In study area E, the ~50 m high scarp is clearly visible in seismic reflection data (Fig. 2b, c). Apart from the low intrinsic friction (Fig. 4), mass wasting near the head scarp is confirmed by abundant clasts and carbonate concretions in core 58 immediately above sapropel S1 (see Kopf et al. [2006] for details). Also, sedimentation rates in that interval are roughly twice as high as in the other cores. However, given the overall lithostratigraphic similarities with S1 and other markers present, no final conclusion can be drawn on the timing and mechanism of scarp formation.

Since we were unable to perform long-term pore pressure dissipation experiments, we cannot safely propose the physical trigger mechanism of the two landslides. Neotectonic activity and regional seismicity make earthquake tremor a likely candidate. Earthquake magnitudes have been reported to be as high as M7.4 (e.g. in 1956; see Perissoratis and Papadopoulos, 1999), causing significant subsidence and sediment remobilisation. Excess pore pressures exceed

82 kPa, however, an unquantifiable portion of that number relates to the impact of the CPT instrument and is found to decrease rapidly (i.e. T_{50} values of several minutes only). In any case, pore pressures are believed to be lightly supra-hydrostatic because of the moderately high sedimentation rates. Hence, significant extra pore pressure from (pre-)seismic stress release is needed to cause landslide initiation. Sliding, however, is facilitated by friction coefficients of μ_{peak} ~0.3, or lower, as measured with the ring shear apparatus. Also, unstable sliding is likely given that these materials show velocity weakening behaviour when sheared at different rates, so that catastrophic mass wasting may occur.

6. Acknowledgements

We thank Master Michael Schneider and his crew for the friendly and efficient operations during cruise P336 with RV *Poseidon*. The manuscript benefited from constructive reviews and suggestions by Katrin Huhn and Nabil Sultan. Funding for this work was received by DFG through RCOM Bremen (project C8). This is RCOM publication #505.

7. References

Chronis, G., Lykousis, V., Georgopoulos, D., Poulos, M., Zervakis, V., Stavrakakis, S., 2000a. Suspended particulate matter and nepheloid layers in the southern margin of the Cretan Sea (NE Mediterranean): seasonal distribution and dynamics. Progress in Oceanography, 46, p.163–185.

Chronis, G., Lykousis, V., Anagnostou, C., Karageorgis, A., Stavrakakis, S., Poulos, S., 2000b. Sedimentological processes in the southern margin of the Cretan Sea (NE Mediterranean). Progress in Oceanography, 46, p.143-162.

Dominey-Howes, D., Cundy, A., Croudace, I., 2000. High energy marine flood deposits on Astypalaea Island, Greece: possible evidence for the AD 1956 southern Aegean tsunami. Mar. Geol., 163, p.303-315.

Fassoulas, C., 1999. The structural evolution of central Crete: insight into the tectonic evolution of south Aegean (Greece). Geodynamics, 27, p.23-43.

Giresse, P., Buscail, R., Charriere, B., 2003. Late Holocene multisource material input into the Aegean Sea: depositional and post-depositional processes. Oceanologica Acta, 26, p.675-673.

Hampton, M.A., Lee, H.J., Locat, J., 1996. Submarine Landslides. Reviews of Geophysics, 34/1, p.35-59.

Hansbo, S., 1957. A new approach to the determination of the shear strength of clay by the fall-cone test. Geotechnical Institute Proceedings, 14, p.50.

Kopf, A., Alves, T., Heesemann, B., Kaul., N.E., Kock, I., Krastel, S., Reichelt, M., Schäfer, R., Stegmann, S., Strasser, M., Thölen, M., 2006. Report and preliminary results of POSEIDON cruise P336: CRESTS - Cretan Sea Tectonics and Sedimentation. Berichte FB Geowiss., Univ. Bremen, No. 253: 140pp.

Kvalstad, T.J., Farrokh, N., Kaynia, A.M., Mokkelbost, K.H., Bryn, P., 2005. Soil conditions and slope stability in the Ormen Lange area. Marine and Petroleum Geology, 22, p.299-310.

Le Pichon, X., Angelier, J., 1979. The Hellenic Arc and Trench system: a key to the neotectonic evolution of the Eastern Mediterranean area. Technophysics, 6, p.1–42.

Lykousis, V., Roussakis, G., Alexandri, M., Pavlakis, P., Papoulia, I., 2002. Sliding and regional slope stability in active margins: North Aegean Trough (Mediterranean). Mar. Geol., 186, p.281-298.

Mascle, J., Martin, L., 1990. Shallow structure and recent evolution of the Aegean Sea: a synthesis based on continuous reflection profiles. Mar. Geol., 94, p.271–299.

McKenzie, D. P., 1978. Active tectonics of the Alpine–Himalayan belt: the Aegean Sea and surrounding regions. Geophysical Journal of the Royal Astrological Society, 55, p.217–254.

Perissoratis, C., Papadopoulos, G., 1999. Sediment instability and slumping in the southern Aegean Sea and the case history of the 1956 tsunami. Marine Geology, 161, p.287-305.

Scholz, C.H., 1998. Earthquakes and friction laws. Nature, 391, p.37-42.

Sultan, N., Voisset, M., Maresset, B., Marsset, T., Cauquil, E., Colliat, J.-L., 2007. Potential role of compressional structures in generating submarine slope failures in the Niger Delta. Mar. Geol., 237/3-4, p.169-190.

5.4. In situ pore pressure evolution during FF-CPT measurements in soft sediments of the western Baltic Sea

Seifert, A., Stegmann, S., Lange, M., Wever, T., and Kopf, A., Geo-Marine Letters under revision

Geo-Mar Lett
DOI 10.1007/s00367-008-0102-x

ORIGINAL

In situ pore-pressure evolution during dynamic CPT measurements in soft sediments of the western Baltic Sea

Annedore Seifert · Sylvia Stegmann · Tobias Mörz · Matthias Lange · Thomas Wever · Achim Kopf

Received: 3 May 2007 / Accepted: 21 January 2008

Abstract We present in situ strength and pore-pressure measurements from 57 dynamic cone penetration tests in sediments of Mecklenburg (n=51), Eckernförde (n=2) and Gelting (n=4) bays, western Baltic Sea, characterised by thick mud layers and partially free microbial gas resulting from the degradation of organic material. In Mecklenburg and Eckernförde bays, sediment sampling by nine gravity cores served sedimentological characterisation, analyses of geotechnical properties, and laboratory shear tests. At selected localities, high-resolution echo-sounder profiles were acquired. Our aim was to deploy a dynamic cone penetrometer (CPT) to infer sediment shear strength and cohesion of the sea bottom as a function of fluid saturation. The results show very variable changes in pore pressure and sediment strength during the CPT deployments. The majority of the CPT measurements (n=54) show initially negative pore-pressure values during penetration, and a delayed response towards positive pressures thereafter. This so-called type B pore-pressure signal was recorded in all three bays, and is typically found in soft muds with high water contents and undrained shear strengths of 1.6–6.4 kPa. The type B signal is further affected by displacement of sediment and fluid upon penetration of the lance, skin effects during dynamic profiling, enhanced consolidation and strength of individual horizons, the presence of free gas, and a dilatory response of the sediment. In Mecklenburg Bay, the remaining small number of CPT measurements (n=3) show a well-defined peak in both pore pressure and cone resistance during penetration, i.e. an initial marked increase which is followed by exponential pore-pressure decay during dissipation. This so-called type A pore-pressure signal is associated with normally consolidated mud, with indurated clay layers showing significantly higher undrained shear strength (up to 19 kPa). In Eckernförde and Gelting bays pore-pressure response type B is exclusively found, while in Mecklenburg Bay types A and B were detected. Despite the striking similarities in incremental density increase and shear strength behaviour with depth, gas occurrence and subtle variations in the coarse-grained fraction cause distinct pore-pressure curves. Gaseous muds interbedded with silty and sandy layers are most common in the three bays, and the potential effect of free gas (i.e. undersaturated pore space) on in situ strength has to be explored further.

A. Seifert (✉) · S. Stegmann · T. Mörz · M. Lange · A. Kopf
Research Centre Ocean Margins (RCOM), University of Bremen,
Leobener Strasse/MARUM,
28359 Bremen, Germany
e-mail: seifert@uni-bremen.de

T. Wever
Forschungsanstalt der Bundeswehr für Wasserschall und Geophysik (FWG),
Klausdorfer Weg 2–24,
24148 Kiel, Germany

Introduction

Ever increasing anthropogenic use of coastal areas and shallow seas—e.g. for the installation of wind power stations and gas pipelines, or the dredging of sediment to maintain navigable depth—requires in-depth knowledge of various processes operating in these regions, as well as the detailed characterisation of bottom sediments. The Baltic Sea is the biggest brackish sub-basin of the global ocean, and is intensively used for sea traffic, fishing, and the mining of resources such as Fe and Mn deposits, sand and gravel, or amber and industrial minerals (Harff et al. 2004). The sedimentary environment poses a particular challenge for such activities, because sediment physicochemical

properties show marked variations in both space and time, reflecting a complex postglacial development and the influence of multiple transgressions and regressions during the evolution of the Baltic Basin (Duphorn et al. 1995; Jensen et al. 1999). Sandy sediments are found mainly along the coastal fringes, whereas fine-grained mud dominates the deeper basins of the Baltic Sea (Lemke 1998). These soft muds commonly have high water contents (up to 500% relative water content at the seabed in Eckernförde Bay; Silva and Brandes 1998) and high organic matter contents (up to 10% in Mecklenburg Bay; Bobertz 2000), and reach thicknesses of 7 m in Mecklenburg Bay (Niedermeyer 1987) and even 8 m in Eckernförde Bay (Orsi et al. 1996). Remarkable for the western Baltic Sea is the occurrence of free gas in the shallow subsurface, where organic material undergoes degradation under anoxic conditions, thereby forming mainly methane (e.g. Duphorn et al. 1995; Wilkens and Richardson 1998; Albert et al. 1998; Wever et al. 1998, 2006).

Investigations of sediment properties in the western Baltic Sea have hitherto been carried out mainly by field sampling and subsequent laboratory analysis (e.g. Kolp 1966; Silva and Brandes 1998; Bohling 2003). For sediments containing free gas bubbles, such as occur in coastal seas including the Baltic Sea, North Sea and Black Sea, the recovery, storage and handling of sediment samples can cause disturbances due to degassing which, in turn, may affect measurements of physical properties. In order to overcome this problem in the case of the Baltic Sea, pressurised coring methods have been successfully used for a study of the microfabric of gassy sediments in Eckernförde Bay by Lavoie et al. (1996). If time and effort are to be reduced, however, in situ measurements of sediment physical properties are required.

Cone penetrometers (CPTs) are efficient instruments widely used for in situ determination of geotechnical properties of marine sediments (e.g. Lunne et al. 1997). For the Baltic Sea, Bennett et al. (1996) presented in situ pore-pressure response measurements in the course of six piezometer insertions into the fine-grained sediments of Eckernförde Bay. These tests were limited to the upper 100 cm, and further in situ investigations would therefore be necessary to determine sediment properties at greater depths in this region. In contrast to constant-rate CPT tests, which can result in considerable sediment disturbance because of the heavy rig, dynamic cone penetration tests show a response decelerating as the instrument impacts into the sediment, until it comes to a complete rest at a particular depth within a few seconds. During that period, very fast changes of pressure and deformation due to physical displacement of sediment and fluid are common (e.g. Schultheiss 1990a; Fang et al. 1993; Lee and Elsworth 2004; Stegmann et al. 2006a). Depending on properties such as the strength, density and permeability of the sediment, the induced pore pressure dissipates with time to reach its ambient equilibrium value.

Within this context, we present data from two research cruises carried out in 2006 to three muddy sub-basins of the western Baltic Sea, namely Mecklenburg Bay, Eckernförde Bay and Gelting Bay. The main aim of this paper is to relate differences in penetration resistance and pore-pressure evolution during and after CPT deployment to effects such as variability in the state of consolidation and degree of undersaturation (i.e. free gas in the mud). In addition to velocity-controlled, dynamic CPT measurements, we took gravity cores to determine various physicochemical sediment properties. Across some of the CPT and gravity core locations, we acquired high-resolution echo-sounder profiles to investigate the sub-bottom geological structures for data interpretation.

Materials and methods

Cruises to Mecklenburg, Eckernförde and Gelting bays (Fig. 1) were carried out aboard the R/V *Kronsort* in January 2006, and the R/V *Planet* in March 2006. Both cruises aimed at the characterisation of the shallow (<10 m below seafloor) sub-bottom sediment, and its stability and potential for remobilisation.

In all, 57 dynamic cone penetration tests were conducted in Mecklenburg ($n=51$, *Kronsort* and *Planet* cruises), Eckernförde ($n=2$, *Kronsort* cruise) and Gelting ($n=4$, *Kronsort* cruise) bays (Fig. 1), using a modular dynamic CPT lance designed at RCOM (Research Centre Ocean Margins), University of Bremen. It consists of a standard 15-cm^2 CPT probe to measure cone resistance (q_t), sleeve friction (f_s), and the tilt of the lance. Directly behind the cone, an absolute pore-pressure sensor (u_2) measures the pressure response during and after penetration. The pressure signal comprises the hydrostatic pressure, the ambient pore pressure, and a pore-pressure spike induced by the impact. For each CPT record, the excess pore pressure was determined as the difference between the measured absolute pressure and the hydrostatic pressure at a given depth during profiling. Any impact-induced pressure signal is given time to dissipate, so that measured pressure values are expected to approach ambient background values. A deceleration sensor, installed in the head, enables calculation of the penetration depth of the CPT via twofold integration of the deceleration. In the present case, the deceleration sensor sometimes reached the limit of its range, so that the penetration depth had to be estimated by correlating the length of the probe to which sediment had stuck with core and echo-sounding data (Table 1). The CPT raw data were further processed using MATLAB and

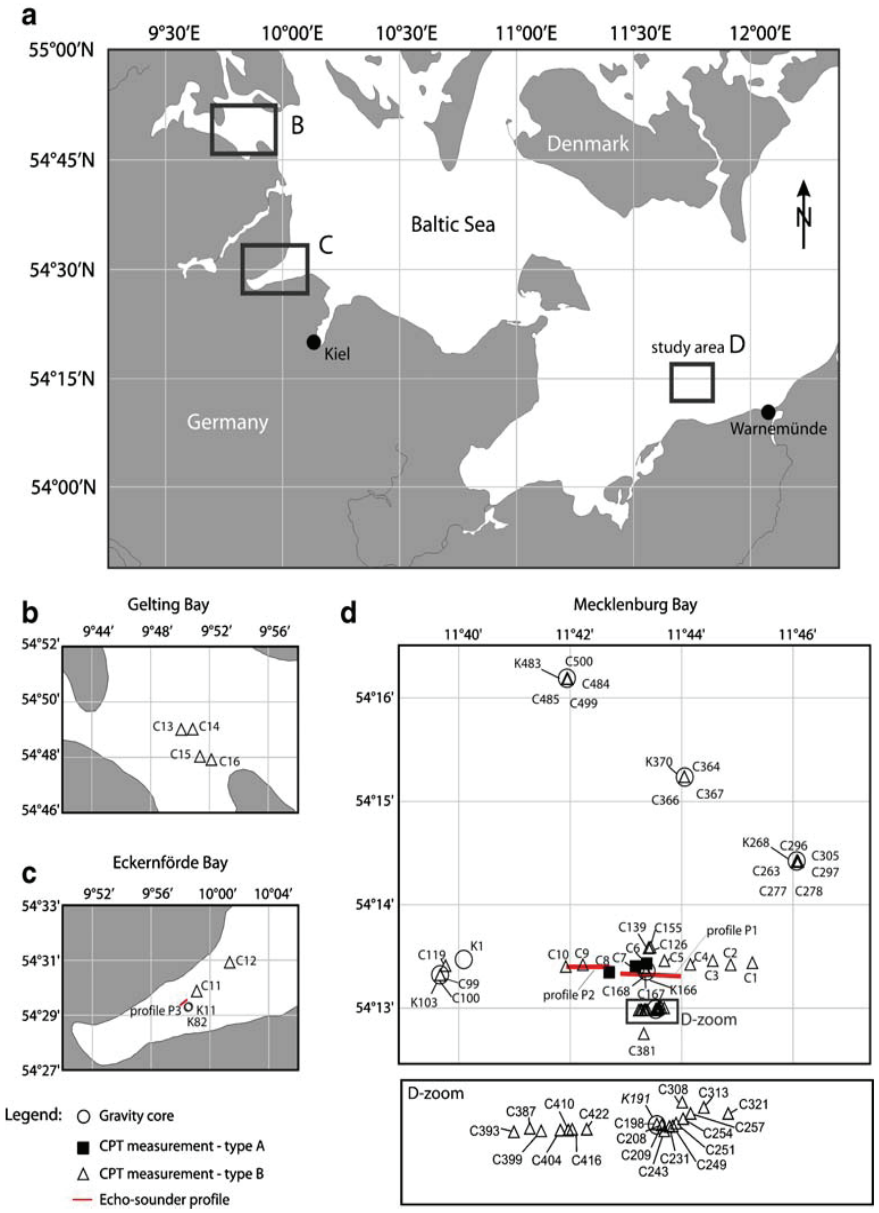

Fig. 1 **a** Map of the south-western Baltic Sea, with the locations of the study areas Gelting Bay, Eckernförde Bay and Mecklenburg Bay. **b** Map of the Gelting Bay study area, with the CPT locations C13–C16. **c** Map of the Eckernförde Bay study area, with the locations of CPT tests C11–C12, cores K11 and K82, and echo-sounder profile P3. **d** Locations of CPT tests C99–C500, cores K1, K103, K166, K191, K268, K370 and K483, and echo-sounder profiles P1 and P2 in Mecklenburg Bay (see Tables 1 and 2 for details)

LABVIEW routines. For further details regarding the device, the reader is referred to Stegmann et al. (2006b).

High-velocity dynamic CPT tests, in which the CPT is lowered at rates of 0.3 m/s up to free drop, differ significantly from standard cone penetrometer tests in which the lance is pushed into the sediment at a constant rate of 2 cm/s. The enhanced impact velocity affects both the initial peak of cone resistance, as well as the pore-pressure excursion. The former can be accounted for by introducing stress strain factors for different materials (e.g. Dayal and Allen 1975; Roy et al. 1982), while the latter requires time for the pore-pressure value to equilibrate to its ambient value. The advantage of the time-efficient dynamic procedure is that no hydraulic platform is needed on the seabed, which otherwise could disturb the sediments being investigated.

In Gelting and Eckernförde bays, the CPT lance was operated with 3-m-long extension rods and 60 kg extra weight, and lowered at a winch speed of around 1 m/s (0.6 1.2 m/s; Table 1), depending on winch configuration and handling. In Mecklenburg Bay, ten CPT deployments (C1 C10) were carried out using 3-m rods and 60 kg extra weight at a winch speed of around 1 m/s (0.7 1.2 m/s; Table 1). The other 41 deployments (C99 C500) had 2-m rods, 30 kg extra weight, and a winch speed of around 2 m/s (1.5 2.6 m/s; Table 1).

Apart from the primary CPT parameters mentioned above, a number of secondary parameters can also be derived. Most

Table 1 CPT code number, water depth, testing mode (velocity, duration of measurement), and penetration depth for excess pore-pressure types A and B

CPT	Location	Water depth (m)	Winch velocity (m/s)	Duration of measurement (min)	Penetration depth (m)
Type A, Mecklenburg Bay					
C6	011°43.380′ E/054°13.431′ N	25.5	1.1	4.5	1.77[a]
C7	011°43.178′ E/054°13.404′ N	25.5	1.1	2.8	2.27[a]
C8	011°42.708′ E/054°13.348′ N	25.7	0.7	9.5	2.30[a]
Type B, Mecklenburg Bay					
C1	011°45.277′ E/054°13.439′ N	25.3	1.1	2	2.00[a]
C2	011°44.887′ E/054°13.420′ N	25.2	1.2	2	3.40[a]
C3	011°44.567′ E/054°13.460′ N	25.3	1.1	2	2.00[a]
C4	011°44.163′ E/054°13.424′ N	25.3	1.1	1	2.00[a]
C5	011°43.698′ E/054°13.459′ N	25.4	0.9	2.5	*
C9	011°42.234′ E/054°13.420′ N	25.8	1.1	8.5	0.81[b]
C10	011°41.927′ E/054°13.403′ N	25.8	1.1	9	1.33[b]
C99	011°39.674′ E/054°13.322′ N	27.3	1.5	53	2.86[b]
C100	011°39.676′ E/054°13.324′ N	27.3	2.1	1	2.57[b]
C119	011°39.770′ E/054°13.412′ N	27.1	2.2	48.5	1.93[a]
C126	011°43.448′ E/054°13.589′ N	25.6	2.3	0.6	2.27[b]
C139	011°43.414′ E/054°13.582′ N	25.7	2.1	51.5	1.88[b]
C155	011°43.418′ E/054°13.586′ N	25.6	2.1	1.5	1.80[b]
C167	011°43.375′ E/054°13.362′ N	25.3	2.1	5	2.13[b]
C168	011°43.333′ E/054°13.393′ N	25.0	2.2	54	2.40[a]
C198	011°43.541′ E/054°12.991′ N	25.6	1.8	8.5	2.57[b]
C208	011°43.552′ E/054°12.990′ N	25.9	2.0	1.5	2.67[b]
C209	011°43.552′ E/054°12.990′ N	26.2	2.2	52	3.07[b]
C231	011°43.568′ E/054°12.988′ N	25.7	2.0	53.5	3.13[b]
C243	011°43.557′ E/054°12.983′ N	26.0	2.0	52	2.85[b]
C249	011°43.575′ E/054°12.989′ N	25.5	1.5	0.5	2.50[a]
C251	011°43.582′ E/054°12.992′ N	25.0	1.5	1	2.80[b]
C254	011°43.597′ E/054°12.997′ N	25.3	1.2	0.6	2.05[b]
C257	011°43.613′ E/054°13.003′ N	25.8	1.7	0.5	2.52[b]
C263	011°46.071′ E/054°14.422′ N	26.0	2.1	14.5	2.00[b]
C277	011°46.080′ E/054°14.425′ N	25.7	1.9	49	2.50[a]
C278	011°46.081′ E/054°14.424′ N	25.6	2.3	1	1.33[b]
C296	011°46.102′ E/054°14.417′ N	25.8	1.9	40	1.61[b]
C297	011°46.102′ E/054°14.418′ N	25.6	2.3	1	2.13[b]
C305	011°46.100′ E/054°14.421′ N	25.7	2.1	97	1.71[b]
C308	011°43.595′ E/054°13.016′ N	25.1	2.4	1	2.31[b]
C313	011°43.641′ E/054°13.010′ N	25.3	2.4	3	2.54[b]
C321	011°43.693′ E/054°13.003′ N	25.0	1.6	2.5	1.04[b]
C364	011°44.058′ E/054°15.237′ N	26.4	2.2	1.5	1.15[b]
C366	011°44.056′ E/054°15.237′ N	25.0	1.8	1	0.97[b]
C367	011°44.057′ E/054°15.237′ N	26.1	2.1	99	2.50[a]
C381	011°43.327′ E/054°12.754′ N	24.9	2.6	10	2.13[b]
C387	011°43.271′ E/054°12.986′ N	25.0	2.3	9.5	1.98[b]
C393	011°43.237′ E/054°12.982′ N	25.1	2.3	10	1.55[b]
C399	011°43.295′ E/054°12.983′ N	25.1	2.2	59	2.38[b]
C404	011°43.336′ E/054°12.984′ N	25.1	2.4	10.5	1.72[b]
C410	011°43.353′ E/054°12.984′ N	25.1	2.5	10	1.97[b]
C416	011°43.361′ E/054°12.985′ N	25.4	2.5	10	1.86[b]
C422	011°43.392′ E/054°12.985′ N	25.6	2.4	9.5	2.70[b]
C484	011°41.950′ E/054°16.187′ N	26.4	2.3	6	2.50[a]
C485	011°41.950′ E/054°16.187′ N	26.2	2.4	60	2.20[a]
C499	011°41.962′ E/054°16.185′ N	26.0	2.2	9.5	2.85[b]
C500	011°41.962′ E/054°16.185′ N	26.0	2.4	25	3.22[b]
Type B, Eckernförde Bay					
C11	009°59.100′ E/054°29.876′ N	29.1	1.1	6.5	3.28[b]

Table 1 (continued)

CPT	Location	Water depth (m)	Winch velocity (m/s)	Duration of measurement (min)	Penetration depth (m)
C12	010°01.340′ E/054°30.927′ N	29.6	0.6	2	*
Type B, Gelting Bay					
C13	009°50.080′ E/054°49.006′ N	25.7	0.7	11	3.66[b]
C14	009°50.866′ E/054°49.016′ N	24.4	1.1	7	3.00[b]
C15	009°51.354′ E/054°48.033′ N	23.1	1.1	10	1.98[b]
C16	009°52.133′ E/054°47.919′ N	21.5	1.0	3	2.39[b]

C1–C16: *Kronsort* cruise of January 2006; other CPT tests: *Planet* cruise of March 2006 (for details, see text and Fig. 1; *asterisk* poor data quality because of heave)

[a] Penetration depth measured onboard

[b] Penetration depth calculated from deceleration data

importantly, the undrained sediment shear strength (s_u) may be calculated by means of empirical equations proposed by Lunne et al. (1997), using the cone resistance $s_u = (q_t - \sigma_{v0})/N_{kt}$, where q_t is the cone resistance corrected for pore pressure, σ_{v0} the total overburden pressure, and N_{kt} a cone factor generally varying between 10 and 20 for normally consolidated clays. Such in situ strength measurements can be compared to those measured in the laboratory using a vane shear device for sediment cores (see below).

For ground-truthing purposes, several gravity cores were taken at selected CPT locations, i.e. seven in Mecklenburg Bay and two cores in Eckernförde Bay (Fig. 1 and Table 2). No cores could be taken in Gelting Bay due to rough weather conditions. Cores K103 and K166, both further analysed by T. Garlan and P. Guyomard (SHOM Institute, France), and K191 from Mecklenburg Bay were opened immediately after recovery in the shipboard laboratory to measure undrained shear strength. For this purpose, a motorized miniature vane shear apparatus (Wykeham Farrance Engineering Ltd., Tring, UK) with a constant rotation rate of 10°/min was used, following the ASTM D 4648-87 procedure (ASTM 1987).

At RCOM, the remaining gravity cores were analysed prior to splitting, using a non-destructive GEOTEK multi-sensor core logger (MSCL; Gunn and Best 1998) to determine wet bulk density and magnetic susceptibility. After core splitting, cores were described sedimentologically using the Munsell colour chart. Samples were then taken for measurement of water content and grain-size distribution. The former was done by freeze-drying, the latter by means of a Beckman Coulter Laser Particle Sizer LS200. Before measuring grain size, sodium pyrophosphate was added to the samples to prevent the formation of aggregates during analysis. Organic matter content was determined on selected samples by loss on ignition (LOI) at about 550°C, following the DIN 18128 procedure (DIN 1990). Undrained shear strength was measured using a four-blade vane viscometer (RotoVisco RV20 device, Haake, Germany) at a rotational rate of 30°/min until the peak shear strength was well exceeded.

Selected areas within Eckernförde and Mecklenburg bays were surveyed in March 2006 using a Parametric Sediment Echo Sounder SES-2000 (Innomar Technology GmbH, Rostock, Germany), in order to acquire high-resolution sub-bottom profiles. The system operates with a variable central frequency (4–15 kHz) for the detection of internal sediment layers, and also emits pulses at higher frequencies (100–500 kHz) for more precise detection of the sediment surface. The

Table 2 Gravity core code numbers, locations, lengths, and water depths (for details, see text and Fig. 1)

Core	RCOM identification	Date	Location	Water depth (m)	Core length (m)
Mecklenburg Bay					
K1	GeoB10501	23.01.2006	011°40.097′ E/054°13.471′ N	26.8	0.88
K103[a]		05.03.2006	011°39.672′ E/054°13.324′ N	26.8	3.36
K166[a]		08.03.2006	011°43.376′ E/054°13.361′ N	25.6	1.95
K191[a]		11.03.2006	011°43.541′ E/054°12.990′ N	25.8	2.40
K268	GeoB10502	12.03.2006	011°46.071′ E/054°14.423′ N	25.9	1.91
K370	GeoB10503	13.03.2006	011°44.063′ E/054°15.234′ N	25.5	2.06
K483	GeoB10504	16.03.2006	011°41.948′ E/054°16.189′ N	26.2	4.03
Eckernförde Bay					
K11	GeoB10505	28.02.2006	009°58.559′ E/054°29.309′ N	27.1	1.00
K82	GeoB10507	04.03.2006	009°58.498′ E/054°29.287′ N	27.8	0.95

[a] Cores were opened and analysed in the shipboard laboratory

penetration depth can reach 50 m, depending on sediment type, water depth, and the frequency selected.

Results

In this section, we first present the overall geological background. This includes seismic reflection profiles typical for the study area, and results from representative gravity cores nearby. For clarity, this subsection is subdivided into the three areas of interest, i.e. Mecklenburg, Eckernförde and Gelting bays. In a second subsection, we present the main in situ results, and relate these to sedimentary conditions and the presence of microbial gas within the strata.

Sediment geotechnical properties and echo-soundings

Mecklenburg Bay

A total of seven gravity cores were taken for ground-truthing purposes. The longest core, K483 in the northern part of the study area (Fig. 1d), has a length of 4 m and provided us with the most comprehensive record. Regardless of small-scale regional differences in composition or thickness of particular horizons, three lithological units can be distinguished. We present data from three gravity cores of different length and at different locations within Mecklenburg Bay to illustrate the overall lithostratigraphy (Fig. 2). The uppermost unit I is greenish black to olive grey mud or clayey silt. Fine sand is found occasionally, and often coincides with areas of slightly elevated shear strength (Fig. 2). The average wet bulk density of this unit ranges from 1.21 to 1.31 g/cm^3 (Fig. 2 and Table 3). Contents in organic material (LOI) vary moderately between 5.8 and 10.5 wt%, underlining the organic richness of the fine-grained sediments. The boundary to the underlying unit II is characterised by a stepwise increase in both wet bulk density and magnetic susceptibility. The silt is of grey to olive grey colour, containing layers of fine sand, plant debris or peat, the latter indicating a terrestrial influence. Such horizons are considerably stronger than the

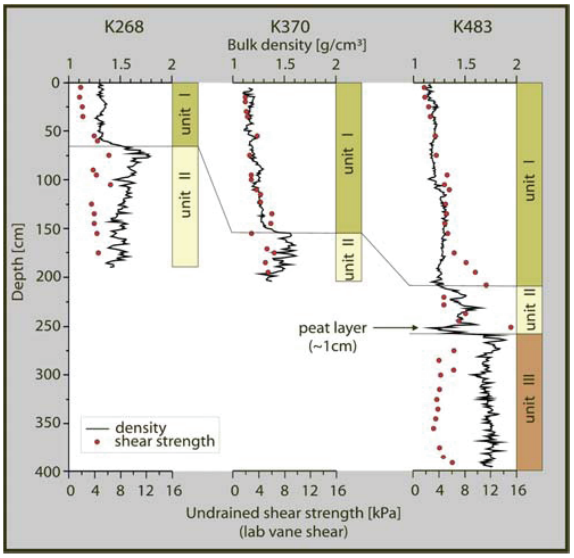

Fig. 2 Lithologs showing bulk density and undrained shear strength of cores K268, K370 and K483 in Mecklenburg Bay

Table 3 Summary of the sediment properties from gravity cores (for details, see text)

Sediment properties		Unit I		Unit II	Unit III	Comments
		Mecklenburg Bay	Eckernförde Bay			
Clay	(%, <2 μm)	5.8–12.2	5.4–7.3	5.1–12.5	11.5–15.1	Occasionally sandy beds in unit I and II: ~3%
Silt	(%)	73.0–83.2	76.5–85.8	68.2–80.2	74.6–81.6	Occasionally sandy beds in unit I and II: 54–57%
Sand	(%)	4.6–21.2	6.9–16.4	8.5–26.7	3.3–13.8	Occasionally sandy beds in unit I and II: ~40%
Water content	(%)	112.2–176.9	186.3–250.6	37.4–72.7	34.1–49.5	K483 peat layer (unit II): 225.6%
Wet bulk density	(g/cm^3)	1.21–1.31	1.05–1.20	1.38–1.46	1.57–1.89	
Organic matter	(%)	5.8–10.5	10.6–15.5	–	–	
Magnetic susceptibility	(×10^{-5} SI)	1–10	1–4	15–40	50–95	
Undrained shear strength	(kPa)	1.7–6.4	1.6–3.1	2.9–8.2	3.2–6.3	Occasionally in unit I: sandy beds up to 11.3 kPa (K483) and in clayey beds up to 19 kPa (K166) K483 peat layer (unit II): 15.2 kPa

hyphen not analysed

rest of the unit (see, e.g. the outlier of unit II at core K483; Fig. 2). The average wet bulk density in this unit ranges from 1.38 to 1.46 g/cm^3 (Fig. 2 and Table 3).

At the boundary between units II and III, a sharp increase in wet bulk density and decrease in water content are found, while grain-size distribution and colour remain very similar (Table 3). Bulk densities scatter around 1.73 g/cm^3; however, one has to acknowledge that unit III was recovered only in two gravity cores (e.g. core K483; Fig. 2). Within unit III, magnetic susceptibility increases again from values around 15 40×10^{-5} SI (unit II) to values between 50 and 95×10^{-5} SI (the horizons with high clay-size contents marking the higher end of the spectrum; Table 3). Within the succession of the three units, the shear strength roughly mirrors the incremental increase in bulk density (Fig. 2). In unit I, strength is about 2 kPa in the very soupy bottom layer, and then increases gradually to about 5 6 kPa (e.g. cores K268, K370 in Fig. 2) or even 11 kPa (K483 in Fig. 2). Unit II is marked by a slight drop in shear strength in each of the cores, and shows an average value of 5 6 kPa (see summary in Table 3). Surprisingly, the sharp increase in density when looking at unit III is not reflected in the vane shear data. In fact, average strength in unit III is only about 5 kPa, which represents a slight decrease.

If we regard echo-sounder profiles in the areas where long cores were taken, the discontinuities in density and other parameters at the unit I/II as well as unit II/III boundary seem to coincide with a high-amplitude reflector (e.g. Fig. 3a). Typical seismic records from Mecklenburg Bay show seafloor-parallel reflectors indicating sedimentary layering. In places, coarser-grained sub-bottom units show bodies with inclined reflectors and cross-bedding (see left portion of Fig. 3a). Lithological unit I is characterised by seafloor-parallel reflectors (i.e. bedding) and a typical downward increase in undrained shear strength (see core K166 data, Figs. 2 and 3a). At a depth of about 2 mbsf (meters below seafloor), a prominent orange reflector is most likely related to contrasts in strength or density. This depth coincides with the location of the unit I/II boundary in many of the shorter cores (e.g. K370; Fig. 2). Unit II is characterised by a somewhat chaotic signature with inclined reflectors. Changes in amplitude may stand in line with variable sand contents observed in the gravity cores. Further below, another strong green-to-orange reflector indicates the top of unit III, which shows characteristic bodies of cross-bedding and an overall increase in density below approximately 2.5 3 m (for example, see core K483, Fig. 2).

While geophysical images across Mecklenburg Bay generally show undisturbed sections of seafloor-parallel bedding throughout, there are a few discrete zones which show unusual blanking behaviour (Fig. 3b). These are vertical features of only a few meters to tens of meters in diameter, with no internal reflectors visible. This observation is typical for the presence of free gas, which adsorbs much of the seismic energy at shallow levels. The fact that gas hinders saturation of the pore volume has repercussions for the in situ CPT measurements (see next section).

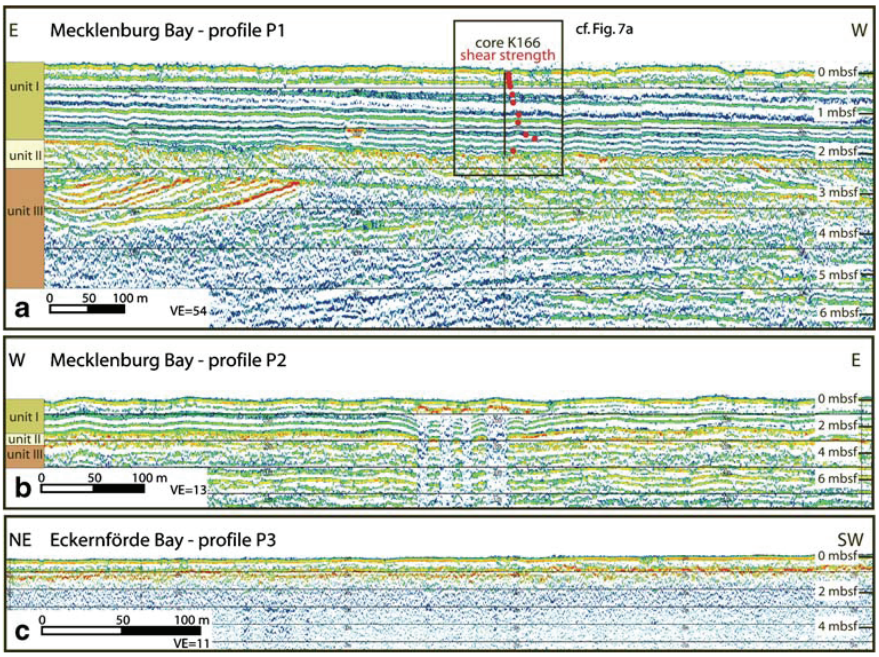

Fig. 3 Echo-sounder profiles of Mecklenburg (P1 and P2) and Eckernförde (P3) bays with lithostratigraphic units. **a** E–W profile P1 [length 1.1 km, vertical exaggeration (VE)=54], adjacent to core K166, with corresponding undrained shear strength measurements. **b** W–E profile P2 (length 846 m, VE=13). **c** NE–SW profile P3 (length 550 m, VE=11). Note different scale in P1–P3 (see Fig. 1 for locations and text)

Eckernförde Bay

In Eckernförde Bay, only two gravity cores were taken, each yielding only about 1 m of sediment recovery (cores K11 and K82, Fig. 1, Table 2). The dominant lithology is greenish black to olive grey mud throughout, which stratigraphically represents unit I. In comparison to that of Mecklenburg Bay, however, it is much softer, with a fluffy texture, a pungent smell of H_2S, higher LOI values (10.6 15.5%), and higher relative water contents (186 250%; Table 3). Bulk density is only about 1.1 g/cm^3. Grain-size distribution shows little down-core variation, being dominated by silt (about 82%), and lesser amounts of sand (about 11%) and clay (7%). The undrained shear strength in the upper 50 cm in Eckernförde Bay is 1.6 2.4 kPa, and increases up to 3.1 kPa at 50 100 cm depth. These values agree well with those measured in unit I of the Mecklenburg cores (e.g. Fig. 2 and Table 3).

Echo-soundings at the locations of cores K11 and K82 exhibit widespread sub-bottom zones of acoustic turbidity, i.e. evidence of gas bubbles at sediment depths as shallow as 65 100 cm (Fig. 3c). In fact, no coherent reflectors can be seen below approximately 1 mbsf beneath the lower yellowish red reflection. This observation is similar in seismic signature to the rather narrow zones seen in some areas in Mecklenburg Bay (Fig. 3b). The Eckernförde area, however, is seismically opaque and must hence be regarded as much more gaseous than is the case for the Mecklenburg area.

Gelting Bay

Owing to rough weather, no gravity cores were collected in Gelting Bay. However, the sediment recovered on board after retrieval of the CPT lance consisted of a very soft, olive black mud with a strong smell of H_2S. Similarly to Eckernförde Bay, this suggests the occurrence of free microbial gas.

Excess pore-pressure profiles

For all three bays combined, two very different signals of excess pore pressure were identified for the dissipation period after penetration, from the wealth of short-term (<15 min) CPT deployments (Fig. 4). After an initial spike, type A shows an exponential decay (Fig. 4a) of induced positive excess pore pressures, commonly reaching negligible values within a few minutes. By contrast, type B shows sub-hydrostatic values upon insertion and then increases slowly with time until a constant value is reached (Fig. 4b). In places, longer deployments (30 100 min) served to shed light on the ambient pore-pressure values. It was found that the background pore pressure was somewhat lower than the initial excursion (see test C305 in Fig. 5, Table 1).

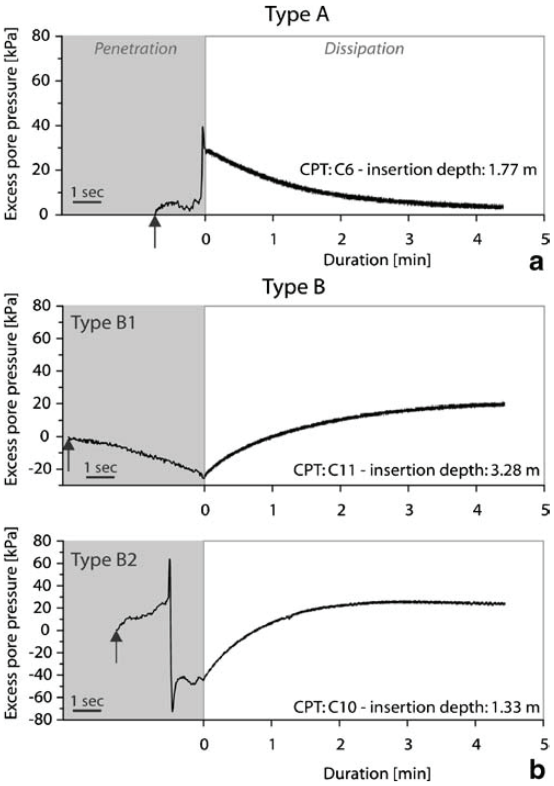

Fig. 4 Classification of excess pore-pressure evolution during and after penetration of the CPT lance in the three study areas. **a** Type A. **b** Type B1 and B2. As examples, C6, C10 and C11 are shown, all veered with winch speed of around 1.1 m/s. *Arrows* mark the first contact with the seafloor. Note the different timescale for the penetration and dissipation periods (for details, see text and Table 1)

In terms of penetration period, the two different pore-pressure signals (types A and B) can be further divided into subgroups. In order to illustrate the consistent trends but local variations, three examples are provided for each group (Fig. 6). Type A always shows an induced increase in excess pore pressure (Figs. 4a, 6a). For type B, pore pressure in some cases decreases to sub-hydrostatic values upon penetration of the CPT, this trend being classified as type B1 (Figs. 4b, 6b). In other cases, there is a sharp increase in excess pore pressure upon penetration, which is followed by a dramatic decrease to sub-hydrostatic pressures, this trend being classified as type B2 (Figs. 4b, 6c).

Taking all results together, type B pore-pressure curves are by far the most abundant. All CPT deployments in Gelting (n=4) and Eckernförde bays (n=2), as well as 48 of 51 deployments in Mecklenburg Bay show type B response (Fig. 1 and Table 1). Only three experiments showed type A responses (C6 C8, Table 1). In order to place these observations into a geological context, we next compare

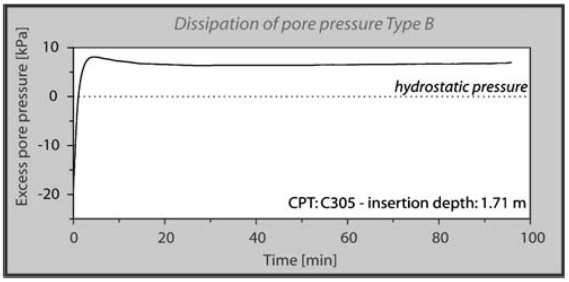

Fig. 5 Dissipation of excess pore pressure of type B (CPT test C305) after penetration of the lance

the in situ pore-pressure results with data obtained on the sediment cores in the laboratory.

Pore-pressure signal type A

If we regard the pore-pressure response of CPT tests C6, C7 and C8 (Fig. 6a), striking similarities can be seen. At depths between 1.5 and 2.1 mbsf, a sharp increase in excess pore pressure is observed. This increase coincides with a density increase at the unit I/II boundary, which is also characterised by a change in shear strength (Fig. 2). Below, the pore-pressure spike dissipates again. The degree of pore-pressure drop is variable (15 35 kPa), and is likely a function of the lithology of unit II. When further comparing data from CPT deployment C6 (type A) with sediments of the adjacent core K166 (Figs. 3a and 7), cone resistance and pore pressure explicitly increase at 160 cm depth where a greenish clay layer reveals s_u values of up to 19 kPa. Both shear strength and the distinct pore-pressure maximum of 39 kPa and higher are significantly different from those for other measurements nearby (notably type B2 curves; compare Figs. 2, 6c, 7 and Table 3). Also, shear strength derived from the CPT deployment (Fig. 7a, diamonds) overestimates that from vane shear testing of the core (Fig. 7a, circles), most likely being a result of the dynamic penetration of the former.

Pore-pressure signal type B

A similar agreement between core data and CPT results can be made between data from core K268 and CPT C263, again in Mecklenburg Bay (Figs. 1 and 8). Pore pressure shows a type B2 evolution, while cone resistance increases at 40 60 cm depth (Fig. 8b). This is related to an increase in undrained shear strength (6.2 kPa; Fig. 8a), most likely reflecting an increase in sand content. At the same depth, the pore pressure drops rapidly (Δu ~66 kPa; Fig. 8b).

The excess pore-pressure evolution of type B2 during penetration, especially the absolute difference between the penetration peak and the pressure minimum from 15 kPa (C305) to 136 kPa (C10), is highly variable within the wealth of CPT deployments during this study. Each of the pressure drops is mirrored by a sharp increase in cone resistance (e.g. 180 kPa for C305, and 701 kPa for C10). Compared to the B2 pore-pressure response (see Figs. 6c and 8b), type B1 curves show a steady decrease to sub-hydrostatic values (Fig. 6b). This observation is unexpected, given total penetration depths of >3 mbsf (e.g. C11, C13; Fig. 6b). At such depths, the CPT probe already passed the unit I/II boundary (and thus the density increase) without any noticeable deviation in pore-pressure trend. On the other hand, the unit boundary may be blurred, given the poor resolution in some of the seismic lines, especially in Eckernförde Bay (see Fig. 3c). Some uncertainty remains at this point, because the observed increase in density at the two unit boundaries is not reflected by shear strength (core data) and cone resistance (CPT data).

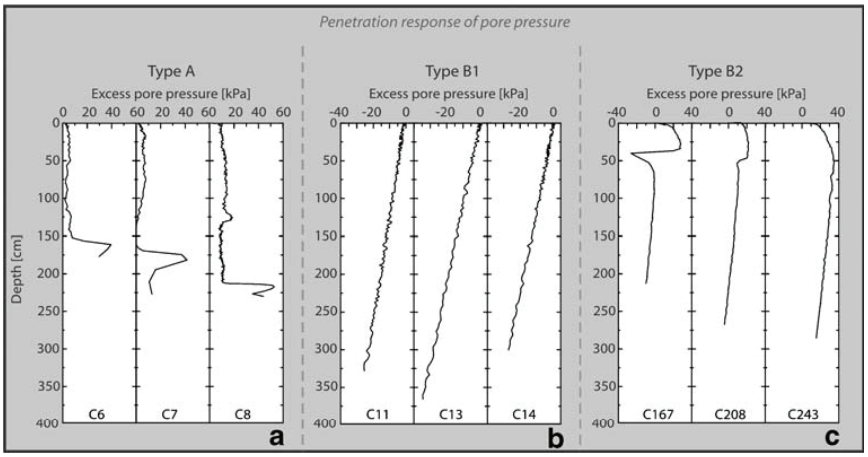

Fig. 6 Different excess pore-pressure response during the penetration periods of various CPT tests. **a** Type A: C6, C7, C8. **b** Type B1: C11, C13, C14. **c** Type B2: C167, C208, C243. For details, see Fig. 1 and Table 1

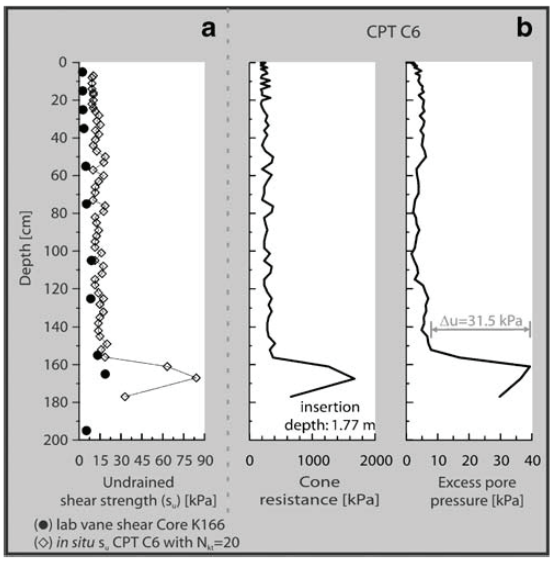

Fig. 7 Comparison of sediment properties and CPT measurements, type A, versus depth. **a** Undrained shear strength (core K166 and in situ CPT test C6 calculated from corrected cone resistance) **b** C6 parameters during penetration: cone resistance (uncorrected) and excess pore-pressure evolution (type A); C6 veered with winch speed of 1.1 m/s (see Fig. 1 for locations and text)

Discussion and conclusions

The discussion is split into two subsections. First, we interpret the in situ CPT results by utilising the information from echo-sounder profiles and ground-truthing (especially data on discrete core samples). Here, we focus on the pore-pressure evolution and follow the distinction into three types of responses, i.e. A, B1 and B2. In the second part of the discussion, we then use the wealth of CPT data to carry out a sediment classification. Given the relatively small number of cores (n=9) relative to the CPT deployments (n=57), this type of sediment characterisation without sampling may prove a versatile approach in future surveys.

Pore-pressure evolution

In general, the penetration process of a dynamic CPT device is more complex than that of standard, quasi-static CPT deployments at constant rates of 2 cm/s. Penetration at high rates causes significant disturbance of the sediment in the vicinity of the lance and, as a result, changes of the stress regime of the soil and the pore fluid. Theoretical considerations describe the excess pore pressure in two different zones surrounding the cone penetrometer during penetration (e.g. Teh 1987; Burns and Mayne 2002): (1) a plastically deformed region around the cone, influenced by normal stress-induced pore pressure, and (2) a zone along the penetrometer soil interface, in which intense shear stresses are generated (shear-induced pore pressure). In addition, factors related to sediment physical properties (coefficient of consolidation, etc.), the interaction of sediment with the lance, the configuration of the lance (e.g. the position of the pressure sensor), the mode of deployment (e.g. penetration velocity) and, last but not least, the presence of free gas and already elevated in situ pore pressure may cause severe difficulty in interpreting the measured data. We take all those factors into account when discussing the three types of pressure responses seen in the Baltic Sea.

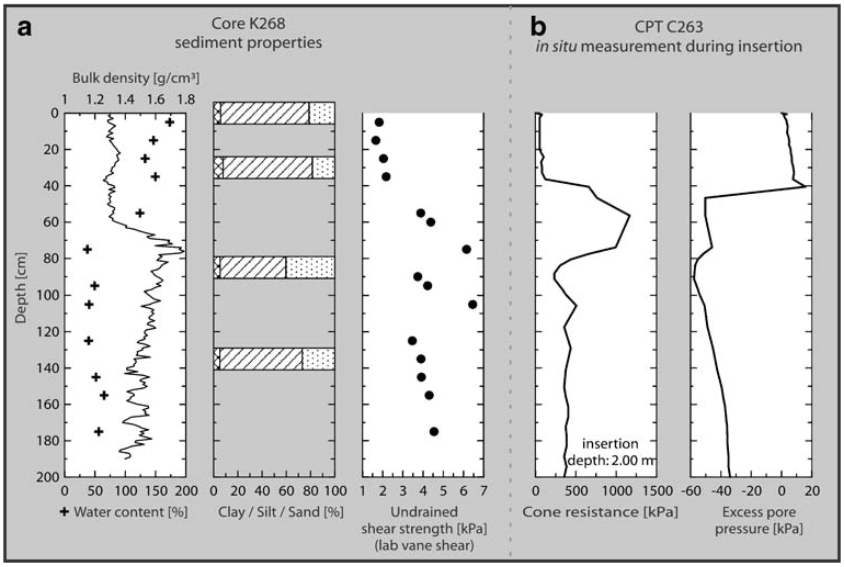

Fig. 8 Comparison of sediment properties and CPT measurements, type B2. **a** Bulk density, grain-size distribution, and undrained shear strength, core K268. **b** C263 cone resistance (uncorrected) and excess pore-pressure evolution (type B2) with penetration depth; C263 veered with winch speed of 2.1 m/s (see Fig. 1 for locations)

Pore-pressure signal type A

The consistent type A response is an induced spike in excess pore pressure upon penetration of the CPT, followed by a progressive decline during the dissipation period (Figs. 4a, 6a, 7b). Pore-pressure records similar to type A have been measured using dynamic pressure instruments in marine sediments (Schultheiss 1990b; Fang et al. 1993). The initial positive pressure rise is particularly difficult to interpret, because a likely artefact from the impact of the probe may overprint positive pressures occurring in situ due to clay compaction, layers of high sedimentation rates, or absence of gas in the pore volume (e.g. Wichman 2000). In Mecklenburg Bay, we are in favour of the first possibility because, at the depth of the 39-kPa pore-pressure spike, cone resistance of the CPT as well as shear strength in the corresponding core rise to unusually high values (1,675 and 19 kPa respectively). In the deeper part of the CPT profiles and core (Fig. 7), the shear strength is lower and the pore pressure can dissipate, so excess pore pressure decreases rapidly (cf. Bennett et al. 1989).

Pore-pressure signal type B1

All measurements of type B1 exhibit a delayed pore-pressure increase after penetration, which is typical for Eckernförde and Gelting bays (Figs. 1, 4b, 6b). There is a number of potential explanations for such a pore-pressure response, involving either lightly consolidated sediment or undersaturated pore space (i.e. free gas attenuating the pressure signal by the profiling lance).

Initial sub-hydrostatic pressures followed by a delayed increase to ambient values occur in overconsolidated or fissured sediments due to dilatory sediment behaviour and local redistribution around the cone tip (see similar examples in Lunne et al. 1997; Burns and Mayne 1998, 2002). In isotropic sediments where the vertical coefficient of consolidation (c_v) is equal to its horizontal counterpart (c_h), pore-pressure gradients between the cone and shaft might induce vertical fluid flow, whereas a reduction of the vertical coefficient of consolidation could impede it (Teh 1987). Since the soft muds of type B1 are homogeneous, highly compressible, and have a high plasticity index (Eckernförde mud: average plasticity index of 163%; Silva and Brandes 1998), the difference between c_v and c_h, is small, and vertical flow feasible. The two different pore-pressure zones around the CPT (see above) are interacting to achieve equilibrium and, thus, effectively delay the dissipation. Additionally, the pore pressure from the far-surrounding field flows to the zone near the penetrometer and, therefore, pore-pressure responses might be further delayed before approaching ambient pressure (Song and Voyiadjis 2005; Elsworth et al. 2006).

Although normally consolidated surficial sediments throughout the sub-basins in the Baltic Sea would be expected based on the geological history, light overconsolidation was detected in the upper 2.5 m in Eckernförde Bay by Brandes et al. (1996). The surface sediments exhibit high average organic contents of 12% dry weight (Silva et al. 1996), with overconsolidation ratios between 1.2 and 12.7 (Brandes et al. 1996) related to this. In deeper sections of their cores, the material approaches normally consolidated conditions. This phenomenon is referred to as apparent overconsolidation, and is considered to be due to inter-particle physicochemical bonding or cementation (Silva and Brandes 1998; Anandarajah and Lavoie 2002). This has been observed also at other locations, e.g. in the organic-rich sediments on the continental slope off Peru (Keller 1982), or in Sagueny Fjord sediments (Urgeles et al. 2002). Apparent overconsolidation could have an influence on the type B1 pore-pressure dissipation, but it is unlikely to be the main reason for this signal.

In Eckernförde and Gelting bays, type B1 trends dominate with an obvious similarity in sub-hydrostatic response during penetration, while cone resistance does not show a pronounced increase upon penetration. This has been explained by low bulk densities of 1.1 g/cm^3, high water contents of 250%, low shear strength of 3 kPa (for details, see "Results" above), and the high permeability (Bennett et al. 1996) and high compressibility of the mud (Silva and Brandes 1998). The initially loose, open microfabric with large channels and voids (Lavoie et al. 1996) collapses during the high loading impulse upon CPT impact. The mud will be displaced, and any initially induced pore pressure will dissipate very rapidly. A net pore water flow away from the pressure sensor, nearly unrestrained throughout the highly permeable sedimentary network, causes negative pressures.

Another important aspect in understanding the negative response is the occurrence of free gas. There are three potential scenarios: (1) gas in the filter of the CPT causing artefacts, (2) microbial gas causing overpressures and variations in shear strength, and (3) 'skin effects' related to rapid CPT penetration.

1. It is known that an unsaturated filter of the pressure sensor can also cause delayed pore-pressure response (e.g. May 1987; Burns and Mayne 1998; Strout and Tjelta 2005). However, we detected very fast pore-pressure changes during penetration (e.g. type B2 response), so we are confident that partially saturated sediment due to free gas, rather than an unsaturated filter, caused a delayed response. Also, we tried to saturate the filter on deck when preparing the instrument, and additionally allowed it to equilibrate in the water column for 5 min prior to each deployment.

2. Free gas in the sediment pore volume may be held responsible for the type B1 pore-pressure response in Mecklenburg, Eckernförde and Gelting bays. As shown above (Fig. 3b, c), opaque acoustic signatures in the echo-soundings hint to the presence of free gas. This observation reconfirms earlier work in Eckernförde and Gelting bays, where free gas was related to the degradation of organic material under anoxic conditions (Abegg and Anderson 1997; Richardson and Davis 1998; Wilkens and Richardson 1998; Albert et al. 1998; Wever et al. 1998, 2006). Free gas in the pore space influences sediment properties such as shear strength (Wheeler 1988; Wilkens and Fu 1994; Briggs and Richardson 1996; Fu et al. 1996; Grozic et al. 2005), mainly because voids partially filled with gas, rather than seawater, have a different compressibility than fully saturated pores. Therefore, free gas dramatically influences sediment deformation, although it appears ambiguous whether shear strength is increasing or decreasing with increasing gas content (e.g. Wheeler 1988; Brandes 1999). Wichman (2000) tested the consolidation of soft gassy mud in a settling tube and could show that gas significantly retards the consolidation process. Compressible gas bubbles in the fluids of the pores can attenuate pore-pressure propagation (Köhler and Schwab 2005), and also cause a decrease in permeability (Wichman 2000). After a rapid external pressure change, such as after penetration of the CPT lance, the pore pressure will need a longer time to adapt to the change and might cause the observed delayed response in our type B sediments (e.g. C10 and C11 in Fig. 4, C305 in Fig. 5).
3. Skin effects during measurement have to be taken into account. In general, gas may cause elevated pore pressure and, therefore, the formation of cracks can be induced (van Kesteren and van Kessel 2002), rendering the sediment unstable. Given the buoyancy of the gas, bubbles of variable size naturally escape upwards (see in situ tests in Eckernförde Bay by Anderson et al. 1998). A further disruption, such as the penetration of the CPT probe, could release free gas along the shaft of the lance, or could generate cavities into which fluid escapes. Equally, a thin adhesive layer of pore water and sediment suspension may be formed along the interface between the probe and the sediment body, like a skin. During penetration, this layer moves opposite to the lance penetration, thereby causing suction at the filter covering the pore-pressure port, and thus negative pressure excursions are measured. These so-called skin effects appear related to the rate with which the CPT hits the sediment. In an earlier study, Bennett et al. (1996) measured ambient and dynamic pore pressure in Eckernförde Bay with a piezoprobe. Their measurements in the uppermost meter bsf suggest a pore-pressure behaviour of type A, whereas our data show type B1. The different pore-pressure response might be caused by the different design of the lances (their probe is almost half the diameter of ours), the different penetration depth and, most importantly, the different penetration rate. The piezoprobe of Bennett et al. (1996) was lowered slowly into the sediment, while our probe was lowered at around 1 m/s. The fragile microstructure of the aggregates and large pores in the mud of Eckernförde Bay is very sensitive to disturbance (Bennett et al. 1996; Lavoie et al. 1996), and this may have been destroyed instantaneously with the RCOM CPT. The penetration rate may thus have affected all our deployments (see penetration rates in Table 1), e.g. causing an increase in cone resistance and a higher induced initial penetration pressure with an increasing rate of penetration in clayey sediments (Lunne et al. 1997; Finke et al. 2001). Stoll and Sun (2005) and Stoll et al. (2007) compared results of quasi-static and dynamic penetrometers, and concluded that the latter accentuates excursions in the data profile. However, the results of Roy et al. (1982) indicate insignificant differences in pore-pressure profiles for variable rates of penetration (3–240 cm/min). Unfortunately, no comparative data for high penetration rates are available to further evaluate our results.

Pore-pressure signal type B2

Pore-pressure type B2 somehow presents a mixture of type A and type B1, and its evolution can be variable (Fig. 6c). We suggest that the response of type B2 is associated with indurated or even overconsolidated layers of silt containing a considerable amount of sand, which are interbedded in softer mud (Milkert 1994). Silts may show a partially drained behaviour during penetration (Lunne et al. 1997), and a rapid drop in pore pressure, even to negative values. Robertson (1990) as well as Song and Voyiadjis (2005) found silty sediments with negative excess pore pressures during penetration. Schneider et al. (2001) made similar observations in residual soils of Singapore, and Finke et al. (2001) reported the same for residual silts and fine sands of the US Atlantic Piedmont geologic province. Similar observations were reported by Baltzer et al. (1994) when using a cone penetrometer to characterise sediments from the Nova Scotian Slope on the eastern Canadian continental margin. The authors concluded that the presence of stronger sandy layers caused a peak in cone resistance associated with a drop in pressure when penetrating these sediments. Recently, two different types of pore-pressure evolution, similar to the ones of types A and B2, were observed with

2. Free gas in the sediment pore volume may be held responsible for the type B1 pore-pressure response in Mecklenburg, Eckernförde and Gelting bays. As shown above (Fig. 3b, c), opaque acoustic signatures in the echo-soundings hint to the presence of free gas. This observation reconfirms earlier work in Eckernförde and Gelting bays, where free gas was related to the degradation of organic material under anoxic conditions (Abegg and Anderson 1997; Richardson and Davis 1998; Wilkens and Richardson 1998; Albert et al. 1998; Wever et al. 1998, 2006). Free gas in the pore space influences sediment properties such as shear strength (Wheeler 1988; Wilkens and Fu 1994; Briggs and Richardson 1996; Fu et al. 1996; Grozic et al. 2005), mainly because voids partially filled with gas, rather than seawater, have a different compressibility than fully saturated pores. Therefore, free gas dramatically influences sediment deformation, although it appears ambiguous whether shear strength is increasing or decreasing with increasing gas content (e.g. Wheeler 1988; Brandes 1999). Wichman (2000) tested the consolidation of soft gassy mud in a settling tube and could show that gas significantly retards the consolidation process. Compressible gas bubbles in the fluids of the pores can attenuate pore-pressure propagation (Köhler and Schwab 2005), and also cause a decrease in permeability (Wichman 2000). After a rapid external pressure change, such as after penetration of the CPT lance, the pore pressure will need a longer time to adapt to the change and might cause the observed delayed response in our type B sediments (e.g. C10 and C11 in Fig. 4, C305 in Fig. 5).
3. Skin effects during measurement have to be taken into account. In general, gas may cause elevated pore pressure and, therefore, the formation of cracks can be induced (van Kesteren and van Kessel 2002), rendering the sediment unstable. Given the buoyancy of the gas, bubbles of variable size naturally escape upwards (see in situ tests in Eckernförde Bay by Anderson et al. 1998). A further disruption, such as the penetration of the CPT probe, could release free gas along the shaft of the lance, or could generate cavities into which fluid escapes. Equally, a thin adhesive layer of pore water and sediment suspension may be formed along the interface between the probe and the sediment body, like a skin. During penetration, this layer moves opposite to the lance penetration, thereby causing suction at the filter covering the pore-pressure port, and thus negative pressure excursions are measured. These so-called skin effects appear related to the rate with which the CPT hits the sediment. In an earlier study, Bennett et al. (1996) measured ambient and dynamic pore pressure in Eckernförde Bay with a piezoprobe. Their measurements in the uppermost meter bsf suggest a pore-pressure behaviour of type A, whereas our data show type B1. The different pore-pressure response might be caused by the different design of the lances (their probe is almost half the diameter of ours), the different penetration depth and, most importantly, the different penetration rate. The piezoprobe of Bennett et al. (1996) was lowered slowly into the sediment, while our probe was lowered at around 1 m/s. The fragile microstructure of the aggregates and large pores in the mud of Eckernförde Bay is very sensitive to disturbance (Bennett et al. 1996; Lavoie et al. 1996), and this may have been destroyed instantaneously with the RCOM CPT. The penetration rate may thus have affected all our deployments (see penetration rates in Table 1), e.g. causing an increase in cone resistance and a higher induced initial penetration pressure with an increasing rate of penetration in clayey sediments (Lunne et al. 1997; Finke et al. 2001). Stoll and Sun (2005) and Stoll et al. (2007) compared results of quasi-static and dynamic penetrometers, and concluded that the latter accentuates excursions in the data profile. However, the results of Roy et al. (1982) indicate insignificant differences in pore-pressure profiles for variable rates of penetration (3–240 cm/min). Unfortunately, no comparative data for high penetration rates are available to further evaluate our results.

Pore-pressure signal type B2

Pore-pressure type B2 somehow presents a mixture of type A and type B1, and its evolution can be variable (Fig. 6c). We suggest that the response of type B2 is associated with indurated or even overconsolidated layers of silt containing a considerable amount of sand, which are interbedded in softer mud (Milkert 1994). Silts may show a partially drained behaviour during penetration (Lunne et al. 1997), and a rapid drop in pore pressure, even to negative values. Robertson (1990) as well as Song and Voyiadjis (2005) found silty sediments with negative excess pore pressures during penetration. Schneider et al. (2001) made similar observations in residual soils of Singapore, and Finke et al. (2001) reported the same for residual silts and fine sands of the US Atlantic Piedmont geologic province. Similar observations were reported by Baltzer et al. (1994) when using a cone penetrometer to characterise sediments from the Nova Scotian Slope on the eastern Canadian continental margin. The authors concluded that the presence of stronger sandy layers caused a peak in cone resistance associated with a drop in pressure when penetrating these sediments. Recently, two different types of pore-pressure evolution, similar to the ones of types A and B2, were observed with

resistance and excess pore pressure (Fig. 7b). Compared with the type B data (Fig. 9), this sediment shows the highest consistency, which is in agreement with the elevated undrained shear strength in core K166 at 160–180 cm (Fig. 7a).

Since higher penetration rates may increase cone resistance and induced initial pore pressure and, thus, accentuate lithological variations, our dynamic CPT measurements showing higher penetration velocity than for the standard CPT (2 cm/s) may overestimate the soil stiffness (for example, the identified classification of silty sand in the C6 data could be pure silt). However, given the overall good agreement between the soil classification data and ground-truthing evidence we gathered from the gravity cores, we propose that the time- and cost-efficient dynamic CPT device represents a versatile approach in muddy sediments. This is particularly true in gas-rich muds on which, for stability reasons, standard CPT rigs cannot be deployed.

Acknowledgements We thank the captains and crews of the German Navy vessels *Kronsort* and *Planet* for their support during our study. Innomar Technology GmbH, in particular J. Lowag, is acknowledged for providing the sediment echo-sounding data from SES-2000. We also thank T. Garlan and P. Guyomard (SHOM, France) for kindly providing shear strength data of cores K166 and K103. S. Kreiter, R. Lühder, B. Schlue and J.B. Stuut are acknowledged for interesting discussions, and shipboard and lab support. The paper benefited from suggestions by two anonymous referees as well as the superb editorial handling by M. Delafontaine and B. Flemming. Funding was granted by DFG (via RCOM). This is RCOM publication no. 0545.

References

Abegg F, Anderson AL (1997) The acoustic turbid layer in muddy sediments of Eckernfoerde Bay, Western Baltic: methane concentration, saturation and bubble characteristics. Mar Geol 137:137–147

Albert DB, Martens CS, Alperin MJ (1998) Biogeochemical processes controlling methane in gassy coastal sediments. Part 2. Groundwater flow control of acoustic turbidity in Eckernförde Bay sediments. Cont Shelf Res 18:1771–1793

Anandarajah A, Lavoie D (2002) Numerical simulation of the microstructure and compression behavior of Eckernförde Bay sediments. Mar Geol 182:3–27

Anderson AL, Abegg F, Hawkins JA, Duncan ME, Lyons AP (1998) Bubble populations and acoustic interaction with the gassy floor of Eckernförde Bay. Cont Shelf Res 18:1807–1838

ASTM (1987) Standard test method for laboratory miniature vane shear test for saturated fine-grained clayey soil. ASTM D 4648–87. ASTM International, West Conshohocken, PA, Annual Book ASTM Standards 04.08:868–873

Baltzer A, Cochonat P, Piper DJW (1994) In situ geotechnical characterization of sediments on the Nova Scotian Slope, eastern Canadian continental margin. Mar Geol 120:291–308

Bennett RH, Li H, Burns JT, Percival CM, Lipkin J (1989) Application of piezometer probes to determine engineering properties and geological processes in marine sediments. Appl Clay Sci 4:337–355

Bennett RH, Hulbert MH, Meyer MM, Lavoie DM, Briggs KB, Lavoie DL, Baerwald RJ, Chiou WA (1996) Fundamental response of pore-water pressure to microfabric and permeability characteristics: Eckernförde Bay. Geo-Mar Lett 16:182–188

Bobertz B (2000) Regionalisierung der sedimentären Fazies der südwestlichen Ostsee. PhD Thesis, Ernst-Moritz-Arndt-Universität, Greifswald

Bohling B (2003) Untersuchungen zur Mobilität natürlicher und anthropogener Sedimente in der Mecklenburger Bucht. PhD Thesis, Ernst-Moritz-Arndt-Universität, Greifswald

Brandes HG (1999) Predicted and measured geotechnical properties of gas-charged sediments. International Journal of Offshore and Polar Engineering 9(3):219–225

Brandes HG, Silva AJ, Ag A, Veyera GE (1996) Consolidation and permeability characteristics of high-porosity surficial sediments in Eckernförde Bay. Geo-Mar Lett 16:175–181

Briggs KB, Richardson MD (1996) Variability in in situ shear strength of gassy muds. Geo-Mar Lett 16:189–195

Burns SE, Mayne PW (1998) Monotonic and dilatory pore-pressure decay during piezocone tests in clay. Can Geotech J 35:1063–1073

Burns SE, Mayne PW (2002) Analytical cavity expansion-critical state model for piezocone dissipation in fine-grained soils. Soils and Foundations Japanese Geotechnical Society 42:131–137

Dayal U, Allen JH (1975) The effect of penetration rate on the strength of remolded clay and sand samples. Can Geotech J 12:336–348

DIN (1990) Baugrund, Versuche und Versuchsgeräte—Bestimmung des Glühverlustes. DIN 18128 (November 1990). Deutsches Institut für Normung, Berlin

Duphorn K, Kliewe H, Niedermeyer RO, Janke W, Werner F (eds) (1995) Die deutsche Ostseeküste. Gebrüder Borntraeger, Berlin, Sammlung geologischer Führer 88

Elsworth D, Lee DS, Hryciw R, Shin S (2006) Pore pressure response following undrained uCPT sounding in a dilating soil. ASCE, J Geotech Geoenviron Eng 132:1485–1495

Fang WW, Langseth MG, Schultheiss PJ (1993) Analysis and application of in situ pore pressure measurements in marine sediments. J Geophys Res 98:7921–7938

Finke KA, Mayne PW, Klopp RA (2001) Piezocone penetration testing in Atlantic piedmont residuum. ASCE, J Geotech Geoenviron Eng 127:48–54

Fu SS, Wilkens RH, Frazer LN (1996) In situ velocity profiles in gassy sediments: Kiel Bay. Geo-Mar Lett 16:249–253

Grozic JLH, Nadim F, Kvalstad TJ (2005) On the undrained shear strength of gassy clays. Comput Geotech 32:483–490

Gunn DE, Best AI (1998) A new automated nondestructive system for high resolution multi-sensor core logging of open sediment cores. Geo-Mar Lett 18:70–77

Harff J (ed) (2003) Projekt DYNAS—Dynamik natürlicher und anthropogener Sedimentation; Vorhaben: Sedimentationsprozesse in der Mecklenburger Bucht; Laufzeit/Berichtszeitraum: 01.06.2000–31.05.2003. Forschungsvorhaben des Bundesministeriums für Bildung und Forschung, Institut für Ostseeforschung Warnemünde, Abschlußbericht (Meilenstein 6). http://www.io-warnemuende.de/projects/dynas/dynas2/db/data/pub/dynas_I_abschlussbericht_2seitig.pdf, accessed 11 Apr 2007

Harff J, Emelyanov EM, Schmidt-Thome M, Spiridonov M (eds) (2004) Mineral resources of the Baltic Sea. Exploration, exploitation and sustainable development, Special Issue 2:1–227

Jensen JB, Bennike O, Witkowski A, Lemke W, Kuijpers A (1999) Early Holocene history of the southwestern Baltic Sea: the Ancylus Lake stage. Boreas 28:437–453

Keller GH (1982) Organic matter and the geotechnical properties of submarine sediments. Geo-Mar Lett 2:191–198
Köhler H-J, Schwab R (2005) Fluidisierungsphänomene unter Wellenbelastung. HANSA Int Maritime J 142:49–59
Kolp O (1966) Die Sedimente der westlichen und südlichen Ostsee und ihre Darstellung. Akademie, Berlin, Beiträge zur Meereskunde 17/18:9–60
Lavoie DM, Lavoie DL, Pittenger HA, Bennett RH (1996) Bulk sediment properties interpreted in light of qualitative and quantitative microfabric analysis. Geo-Mar Lett 16:226–231
Lee DS, Elsworth D (2004) Indentation of a free-falling sharp penetrometer into a poroelastic seabed. J Eng Mech 130:170–179
Lemke W (1998) Sedimentation und paläogeographische Entwicklung im westlichen Ostseeraum (Mecklenburger Bucht bis Arkonabecken) vom Ende der Weichelvereisung bis zur Litorinatransgression. Institut für Ostseeforschung, Warnemünde, Meereswissen Ber Mar Sci Rep 31
Lunne T, Robertson PK, Powell JJM (1997) Cone penetration testing in geotechnical practice. Spon Press, London
May RE (1987) A study of the piezocone penetrometer in normally consolidated clay. DPhil Thesis, University of Oxford, Oxford
Milkert D (1994) Auswirkungen von Stürmen auf die Schlicksedimente der westlichen Ostsee (Influences of storms on muddy sediments in the western Baltic Sea). Universität Kiel, Kiel, Ber/Rep Geol-Paläontologisches Institut no 66
Niedermeyer RO (1987) Beiträge zur komplexen Untersuchung von rezenten Sedimentationsprozessen in Schlickgebieten der westlichen und mittleren Ostsee. PhD Thesis, Ernst-Moritz-Arndt-Universität, Greifswald
Orsi TH, Werner F, Milkert D, Anderson AL, Bryant WR (1996) Environmental overview of Eckernförde Bay, northern Germany. Geo-Mar Lett 16:140–147
Richardson MD, Davis AM (1998) Modelling methane-rich sediments of Eckernförde Bay. Cont Shelf Res 18:1671–1688
Robertson PK (1990) Soil classification using the cone penetration test. Can Geotech J 27:151–158
Roy M, Tremblay M, Tavenas F, La Rochelle P (1982) Development of pore pressures in quasi-static penetration tests in sensitive clay. Can Geotech J 19:124–138
Schneider JA, Peuchen J, Mayne PW, McGillivray AV (2001) Piezocone profiling of residual soils. Proceedings of the International Conference In Situ Measurements of Soil Properties and Case Histories, 21–24 May 2001, Bali, Indonesia, pp 593–598
Schultheiss PJ (1990a) Pore pressures in marine sediments: an overview of measurement techniques and some geological and engineering applications. Mar Geophys Res 12:153–168
Schultheiss PJ (1990b) In-situ pore-pressure measurements for a detailed geotechnical assessment of marine sediments: state of the art. In: Demars KR, Chaney RC (eds) Geotechnical engineering of ocean waste disposal, ASTM STP 1087. American Society for Testing and Materials, Philadelphia, PA, pp 190–205
Silva AJ, Brandes HG (1998) Geotechnical properties and behavior of high-porosity, organic-rich sediments in Eckernförde Bay, Germany. Cont Shelf Res 18:1917–1938
Silva AJ, Brandes HG, Veyera GE (1996) Geotechnical characterization of surficial high-porosity sediments in Eckernförde Bay. Geo-Mar Lett 16:167–174
Song CR, Voyiadjis GZ (2005) Pore pressure response of saturated soils around a penetrating object. Comput Geotech 32:37–46
Stegmann S, Mörz T, Kopf A (2006a) Initial results of a new free fall-cone penetrometer (FF-CPT) for geotechnical in situ characterisation of soft marine sediments. Norwegian J Geol 86:199–208
Stegmann S, Villinger H, Kopf A (2006b) Design of a modular, marine free-fall cone penetrometer. Sea Technol 47:27–33
Stegmann S, Strasser M, Anselmetti F, Kopf A (2007) Geotechnical in situ characterization of subaquatic slopes: the role of pore pressure transients versus frictional strength in landslide initiation. Geophys Res Lett 34:L07607
Stoll RD, Sun Y-F (2005) Using penetrometer to measure sea bed properties. Office of Naval Research, Arlington, VA, Science & Technology, Ocean Battlespace Sensing (32), Coastal Geosci Annu Rep FY05:1–5
Stoll RD, Sun Y-F, Bitte I (2007) Seafloor properties from penetrometers tests. IEEE J Oceanic Eng 32:57–63
Strout JM, Tjelta TI (2005) In situ pore pressures: what is their significance and how can they be reliably measured? Mar Petrol Geol 22:275–285
Teh CI (1987) An analytical study of the cone penetration test. DPhil Thesis, University of Oxford, Oxford
Urgeles R, Locat J, Lee HJ, Martin F (2002) The Saguenay Fjord, Quebec, Canada: integrating marine geotechnical and geophysical data for spatial seismic slope stability and hazard assessment. Mar Geol 185:319–340
van Kesteren W, van Kessel T (2002) Gas bubble nucleation and growth in cohesive sediments. In: Winterwerp JC, Kranenburg C (eds) Fine sediment dynamics in the marine environment. Proc Marine Science 5. Elsevier, Amsterdam, pp 329–341
Vermeulen N, Rust E (1995) CPTU profiling: a numerical method. Proceedings of the International Symposium on Cone Penetration Testing, CPT 95, 4–5 October 1995, Linköping, Sweden. Swedish Geotechnical Institute, SGI, Rep 3:95, vol 2, pp 343–350
Wever T, Abegg F, Fiedler HM, Fechner G, Stender IH (1998) Shallow gas in the muddy sediments of Eckernförde Bay, Germany. Cont Shelf Res 18:1715–1739
Wever TF, Lühder R, Voß H, Knispel U (2006) Potential environmental control of free shallow gas in the seafloor of Eckernförde Bay, Germany. Mar Geol 225:1–4
Wheeler SJ (1988) The undrained shear strength of soils containing large gas bubbles. Géotechnique 38:399–413
Wichman BGHM (2000) A finite strain theory for gassy sludge. Géotechnique 50:35–41
Wilkens RH, Fu SS (1994) Acoustic lance operations in Eckernförde Bay. In: Wever TF (ed) Proc Gassy Mud Worksh, 11–12 July 1994, Forschungsanstalt der Bundeswehr für Wasserschall und Geophysik, Kiel, FWG Rep 14:34–38
Wilkens RH, Richardson MD (1998) The influence of gas bubbles on sediment acoustic properties: in situ, laboratory, and theoretical results from Eckernförde Bay, Baltic Sea. Cont Shelf Res 18:1859–1892

5.5. *In situ* experiments at active Dashgil mud volcano: Evidence for excess fluid pressure, updoming, and future violent eruption

Kopf , A., Stegmann, S., Delisle, G., Panahi, B., Aliyev, C.S., Guliyev, I., submitted to Marine and Petroleum Geology

In situ CPTU experiments at active Dashgil mud volcano, Azerbaijan: Evidence for excess fluid pressure, updoming, and possible future violent eruption

Achim Kopf (1), Sylvia Stegmann (1), Georg Delisle (2), Behrouz Panahi (3), Chingiz S. Aliyev (3), Ibrahim Guliyev (3)

(1) Research Centre Ocean Margins, University of Bremen, Leobener Strasse, 28359 Bremen, Germany

(2) Bundesanstalt für Geowissenschaften und Rohstoffe, Stilleweg 2, 30561 Hannover, Germany

(3) Geological Institute, Azerbaijan National Academy of Sciences, H. David Ave. 29A, 370143 Baku, Azerbaijan

ABSTRACT

Active mud volcanism is a global phenomenon that represents a natural hazard, both by self-igniting eruptions and the continuous emission of methane gas in both marine and continental settings. Mud domes are most common in compressional tectonic settings such as the Caucasus orogenic wedge. Dashgil mud volcano, the most prominent of >200 features in Azerbaijan, has erupted vigorously in historic times. For several years, we observe variations in the activity of Dashgil dome, including transients in methane flux, build-up of extrusive mud cones on the main feature, and flexural polygonal cracks adjacent to the main crater-lake and new mud cones. In spring 2007, we carried out *in situ* CPT (Cone Penetration Testing) experiments in the crestal area of Dashgil. Our data suggest that the central portion of the crater-lake, which hosts the conduit for gas (and possible mud) ascend, shows both low sediment shear strength and the maximum excess pore fluid pressures (up to ca. 30 kPa suprahydrostatic at 1m subbottom depth). *In situ* cone resistance as a measure for undrained shear strength is as low as 150 kPa in the conduit, whereas the mud is found rather stiff in all other testing locations (300-700 kPa, probably a result of deeply buried shales of the Maikop formation parts of which now liquefy and ascend). Pore pressure decreases upslope in the lake and reaches hydrostatic values at the crater rim. The overpressured region beneath the fluid-filled crest of Dashgil dome, combined with the other observations, suggest an ongoing period of updoming. The presence of sintered mudstones from explosive eruptions in 1908 and 1928 (and most likely before) suggests that a similar violent activity may occur in the near future.

INTRODUCTION

Mud volcanism and diapirism are well-known phenomena that occur predominantly in collisional tectonic areas (see reviews by Higgins and Saunders, 1974; Kopf, 2002). The presence of mud domes and ridges is most abundant in areas with rapid sedimentation rate,

active compressional tectonics, and the formation of hydrocarbons at depth. Mud volcano (MV) eruptive mechanism and evolution seem strongly dependent on state of consolidation and gas content of fine-grained sediments at depth. A model concerning the formation of mud volcanoes and sedimentary diatremes following gas expansion in the pore space has been proposed by Brown (1990). Since it has long been known that the strength of a soil is mainly controlled by both mineralogical composition and pore pressure (Hubbert and Rubey, 1959), it is crucial to separate the effects of the two, ideally by *in situ* measurement rather than laboratory testing. Cone penetration testing (CPT) is a versatile, time efficient method to geotechnically characterize sediment strength and pore pressure (see summary in Lunne et al., 1997). Here, a free-fall CPT probe was used to monitor a suite of critical physical parameters while vertically profiling the sediment.

In this paper we present the first *in situ* CPT data across the crest and crater lake of one of the most active mud domes on Earth, Dashgil MV in Azerbaijan (e.g. Jakubov et al., 1971; Guliyev, 1992; Aliyev et al., 2002). Mapping and structural observations complement the *in situ* strength and pore pressure data collected with a new free fall-cone penetrometer for shallow water application (Stegmann et al. 2006). Of particular interest is the observed increase in fluid flow out of the crater-lake into a morphologically deeper reservoir, and a small number of cm-wide fissures and grabens in the crestal rim that assist draining the lake. Also, the estimated flow of methane through the central crater area is high, and may compare to that of Lokhbatan MV, which had burst into flames at least 23 times since 1829 when methane-rich muds self-ignited during extrusion to the Earth's surface (Aliyev et al., 2002). Similarly, so called "everlasting fires" have been reported to show ignition of methane over many decades (e.g. in Romania or Azerbaijan; Aliyev et al., 2002; Baciu and Etiope, 2005). Also, man-made "Lusi" mud volcano near Surabaya, Java/Indonesia (Davies et al., 2007) represents a considerable hazard given millions of m^3 of mud having extruded within almost a year, with several villages abandoned as a consequence. The 2004 great Sumatra-Andaman EQ caused mud eruptions several meters in height on the island of Baratang (Geol. Survey India, 2005), and a large number of similar instances with mud volcanic activity and large EQs has recently been compiled by Mellors et al. (2007).

GEOLOGICAL SETTING

During Eocene times, the Arabian block collided with Eurasia and narrowed wide portions of the Tethyan Ocean (Dercourt et al. 1986). After its closure (~20 Ma), subduction shifted to the north. As a result of the indentation of the Arabian block, the continuous Tethyan back-arc basin was separated, and oceanic crust remained only in the Black Sea

and southern Caspian Sea (Philip et al. 1989). The collision itself formed a massive orogenic wedge comprising the Greater and Lesser Caucasus, with km-thick marine, rapidly deposited sequences being incorporated. Those thick clastic, clay mineral-rich rocks, known as the Oligocene-Miocene Maikop Formation, have been suggested to be the source layer for mud volcanism (e.g. Lavrushin et al. 1996). As a function of complex folding and faulting, the Maikop shales occur at depths of 4 to more than 10 km below the surface. Faults and mud conduits are well imaged by industry seismic reflection data and provide the pathways for the buoyant clay-bearing sequence (Cooper, 2001).

In the Greater Caucasus, which extends from the Taman Peninsula and northern Black Sea all the way through Georgia and Azerbaijan to the western border of the Caspian Sea, MVism has long been recognized. Detailed reports on violent eruptions accompanied by gas dissipation and self-ignition date back many decades (e.g. Abriutski, 1853; Sjogren, 1887). It was noted already in the early days that earthquake activity preceded such eruptions (Abich, 1869), and that there is a clear relationship between petroleum and mud extrusion (e.g. Jakubov et al., 1971) (see also Fig. 1A-B from Dashgil MV). For comprehensive studies on MVism in the Caucasus area, refer to Jakubov et al. (1971), Guliyev (1992), and Aliyev (2002).More than 60 MVs floor the southwestern Caspian Sea (Soloviev and Ginsburg, 1994), with something in the order of 220 MVs in Azerbaijan along its western coastline. The size of the MVs is variable (up to 400 m height and 10 km^2 area), and so is the occurrence of gryphons (up to > 30 on Dashgil) the amount of clasts in the clayey matrix (see example in Fig. 1C), salses (small lakes of 30-75 m diameter), sinter mounds (aligned near the crest in case of Dashgil; Fig. 1D), and the ejection of oil (Fig. 1B), water, or gas (Fig. 1A). New gryphons, or even mud cones of >10 m height (Fig. 1E) form in areas where mud ascent is facilitated by fractures or conduits. For Dashgil MV, emission of methane has been tentatively estimated to be around 15 x 10^6 m^3/a (Jakubov et al., 1971), 800 m^3/a (Hovland et al., 1997), and 630 m^3/a (this latter value being measured at a small salse, not the main crater lake; Delisle et al., 2005). Given the fact that - based on visual observation - gas emission during the last five years from the crater lake exceeded significantly the emission from the small (monitored) salse, a gas output on the order of 10^4 m^3/a from both lakes appears to be a more realistic estimate. We will revisit the amount of gas flux when discussing our pore pressure measurements (see below).

Fig. 1: (**A**) Violent bubbling of methane escaping from the central crater lake on Dashgil (see also pulley on wire where CPT is deployed); (**B**) oil seep at the base of the western flank of Dashgil; (**C**) sheared, foliated clasts of the Maikop formation, which were brought up from > 5 km depth; (**D**) burnt and sintered mudstone showing red and dark gray colors; these rocks build the SE' ridge bordering the crater-lake region. They are interpreted as relics from a violent, methane-combusting eruption in historic times (caterpillar for scale); (**E**) Mud cone NW of the crater-lake. Refer to Fig. 3 for locations of the features.

METHODS

Apart from topographic mapping and general observations regarding the structural setting of the various small domes (or gryphons) and tiny lakes, we used a free-fall CPT lance (FF-CPT) within the crestal lake of Dashgil MV. In addition, basic sediment characterization was carried out. Grain size analysis followed the Atterberg settling method to determine the fine-grained fraction of the mud matrix. Samples were scraped off the CPT probe after deployment at various depth levels, because gravity coring was impossible in this setting. The FF-CPT is a modular, lightweight design that can be extended in length depending on the anticipated penetration. On Dashgil MV, we deployed a 2 m-long configuration with a total weight of 50 kg (Fig. 1A). The probe consists of an industrial 15cm^2 piezocone (ca. 25 mm diameter; Fig. 1B) and a water-proof housing containing a microprocessor, volatile memory, battery, and accelerometer. Strain gauges inside the probe measure the cone resistance and sleeve friction (subtraction method; see Lunne et al., 1997) and allow a first-order estimate of the sediment strength. A single pore pressure port (u_2) is equipped with an absolute 2 MPa pressure sensor. An inclinometer is installed to monitor the penetration angle at +/-30° relative to vertical, while temperature is monitored via a thermistor. Three accelerometers (provide information about the descent velocities and deceleration behavior of the instrument upon penetration. Its data serve to calculate penetration rate (1st integration) and penetration depth (2nd integration). For details on the instrument design, refer to Stegmann et al. (2006a). Seven FF-CPT measurements yielded a NNW-SSE transect across the Dashgil crater-lake (Fig. 3A-C). The probe was generally deployed in free drop from a wire spanning the lake near the water level.

The instrument entered the ground at rates of ca. 5 m/s and remained in one location for 30-240 mins. to allow the pore pressure to climb towards its ambient value. One penetration at the crater rim (test #6) was done by pushing the device into the mud above the lake level at a rate of 3 cm/s (Fig. 1A). Tests #1 and #2 were carried out in the same location to monitor reproducibility of results.

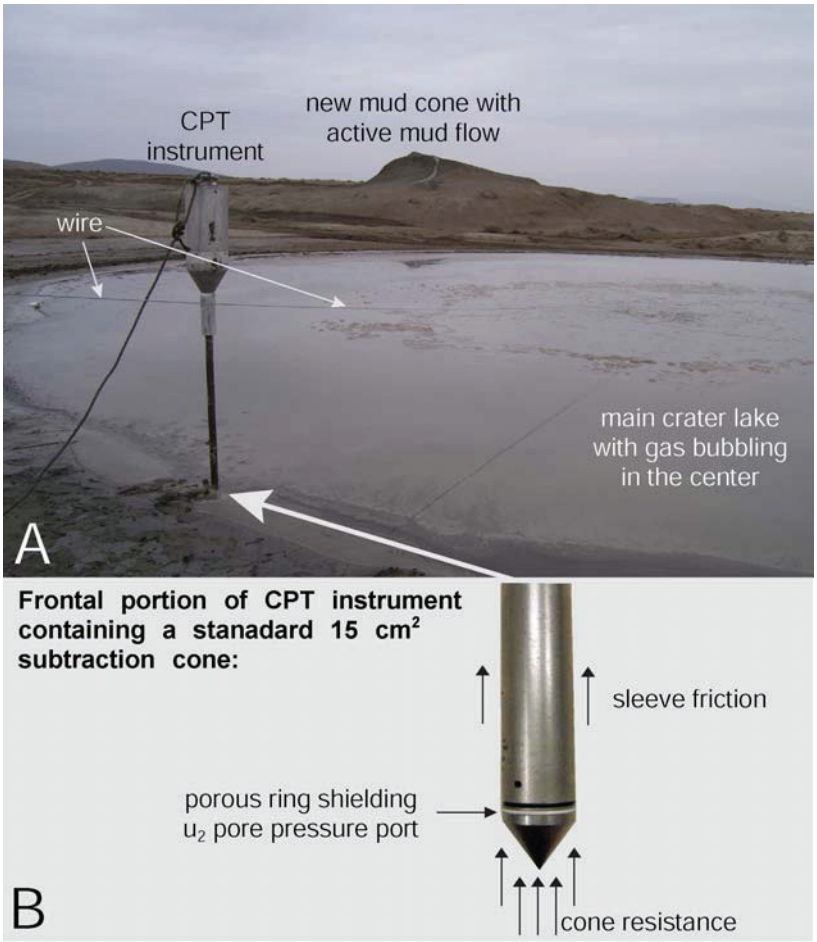

Fig. 2: (**A**) Photograph of the setup of a wire supported by steel poles along which the free fall-CPT was pulled into the position of deployment. Note the instrument while collecting data at the first point of the measurement transect at the rim of the crater-lake (left); (**B**) Schematic of frontal portion of the instrument. See text.

RESULTS

CPT measurements

The number of CPT measurements is shown in map view in Figure 3C. In all crater-lake locations, the device was deployed in free drop from a wire across the lake using a pulley.

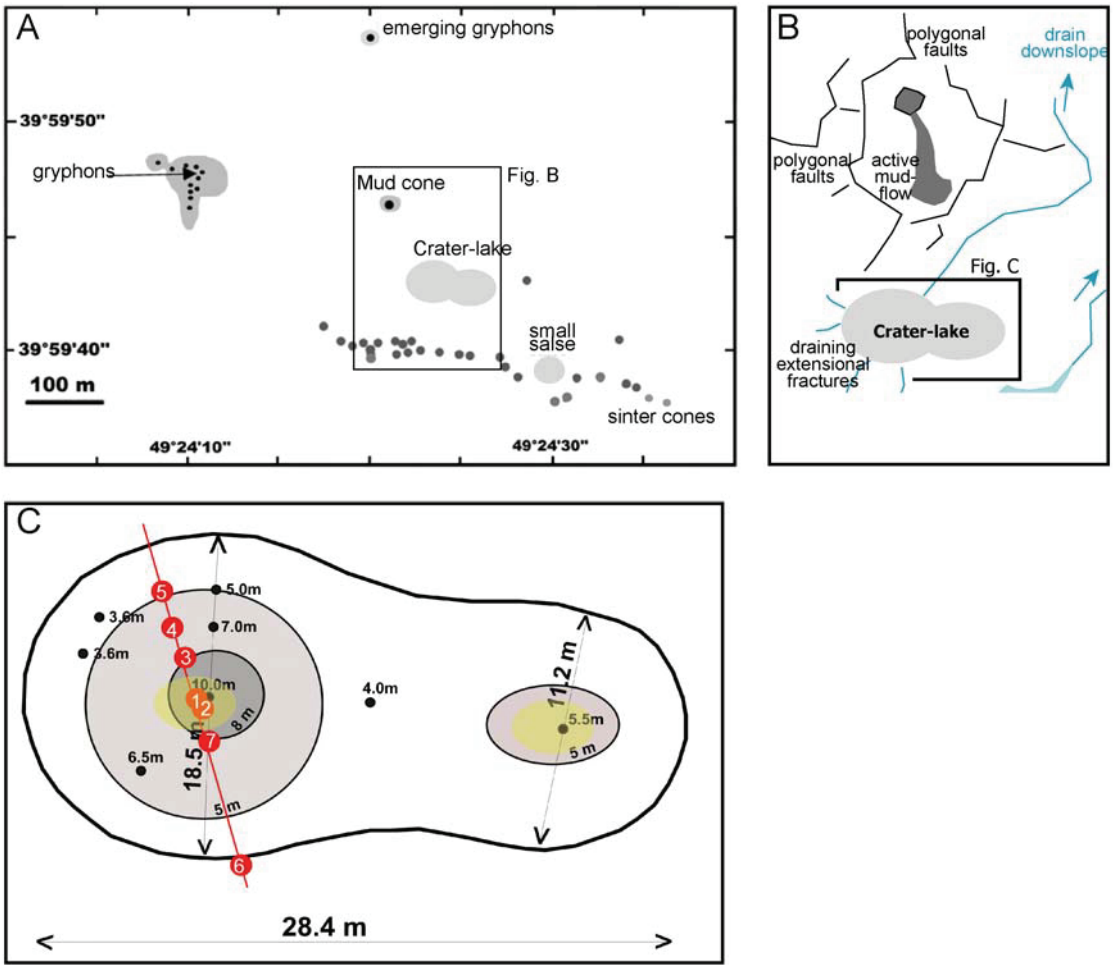

Fig. 3: (A) Dashgil MV in map view including all features relevant in this study; (B) Central part of Dashgil MV, showing new mud cone north of crater-lake, which overflows to the south towards a sintered mudstone ridge. Black lines repesent extensional features from updoming of the lake area and adjacent mud cone over the last couple of years; (C) Bathymetric chart of the central crater lake showing its two "sub-basins". Dots with numbers (#1-#7) represent points of CPT deployment, 6 of which gained satisfying results (see Fig. 5B).

Figure 4 shows a typical protocol of a CPT deployment in free drop, exhibiting an exponential decrease in penetration velocity with depth (1st integration of acceleration), cone resistance, and sleeve friction during profiling the sediment until the probe comes to halt.
In contrast, the pore pressure signal shows a characteristic decrease to sub-hydrostatic values, and subsequently rises slowly towards the ambient pore pressure value with time (Fig. 5A). It is obvious from the *in situ* records that measured pore pressure exceeds the hydrostatic values significantly. High pore pressures are maintained by the low permeability of the sediment with high clay content (41%).

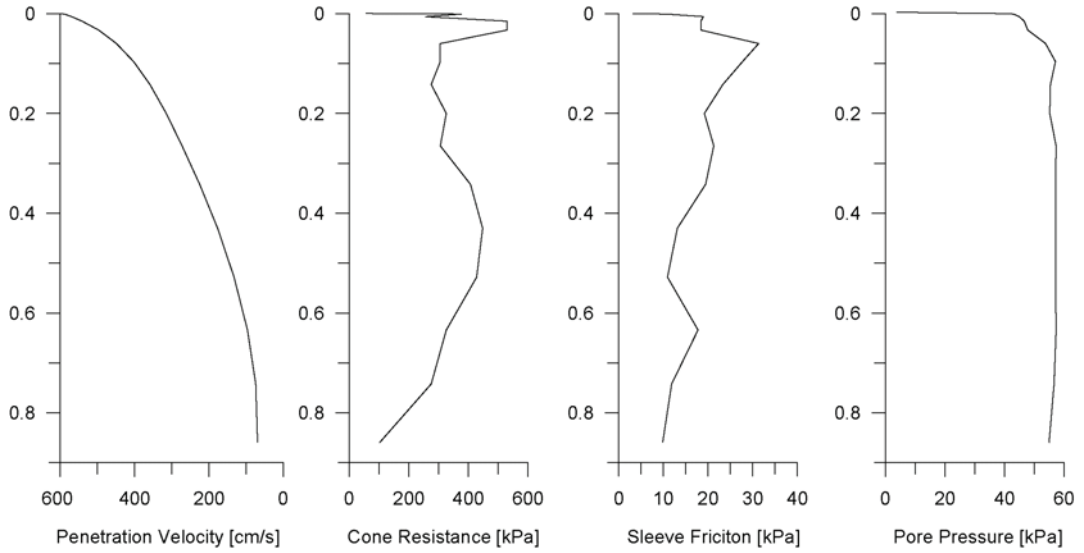

Fig. 4: Typical test protocol of a free-fall CPT test in Dashgil crater lake. Please note that velocity (left-hand panel) is calculated from first integration of the deceleration. See text.

From the CPT deployments (Fig. 3C), we gathered a transect of 6 tests that pinpoint the shear strength and pore pressure state from the crater rim to the bubbling central domain (Fig. 5B, lower part). Both of these primary parameters (as well as penetration depth or derived parameters such as undrained shear strength [Lunne et al., 1997; their eq. 5.16]) show characteristic trends. When regarding cone resistance, it can be seen that the crater-lake's slope and rim show a more competent response than the central area hosting the conduit. In contrast, a prominent increase is observed when excess pore pressure (P_{fluid}) is plotted from the crater rim (= hydrostatic condition, P_{hyd}) towards the central termination the transect where values exceed 30 kPa (Fig. 5B). Since the density of free methane gas is lower than that of water by more than 3 orders of magnitude, and given further that estimated degassing rates (see above) produce a constant stream of bubbles in the water column of the crater-lake (Fig. 1A), excess pore pressure values may be considerably higher relative to the *in situ* (gas-bearing) hydrostat.

STRUCTURAL AND GEODYNAMIC OBSERVATIONS

Since the new CPT data are part of a longstanding investigation, they can be placed in context of recent structural observations that are related to the excess pore pressure development. Compared to the morphological situation on Dashgil MV in the past, a prominent mud cone has grown during the last decade 100m NW of the crater-lake. It is characterized by recent and ongoing mud extrusion, which is forming a 25 m-long lobe at the southern flank. The flanks of the mud cone are bordered by a network of polygonal faults whose surface outcrop represents anastomosing, dm-wide extensional fissures. In the crater-

lake area, the rim is intersected by several fractures of 5-15 cm width and similar depth. Most prominently, two N-S-striking fractures serve to drain the overflowing lake (Fig. 3B) to the N and S; the southern branch forms a small puddle of several meters in diameter before flowing counter-clockwise around the central portion, draining northward.

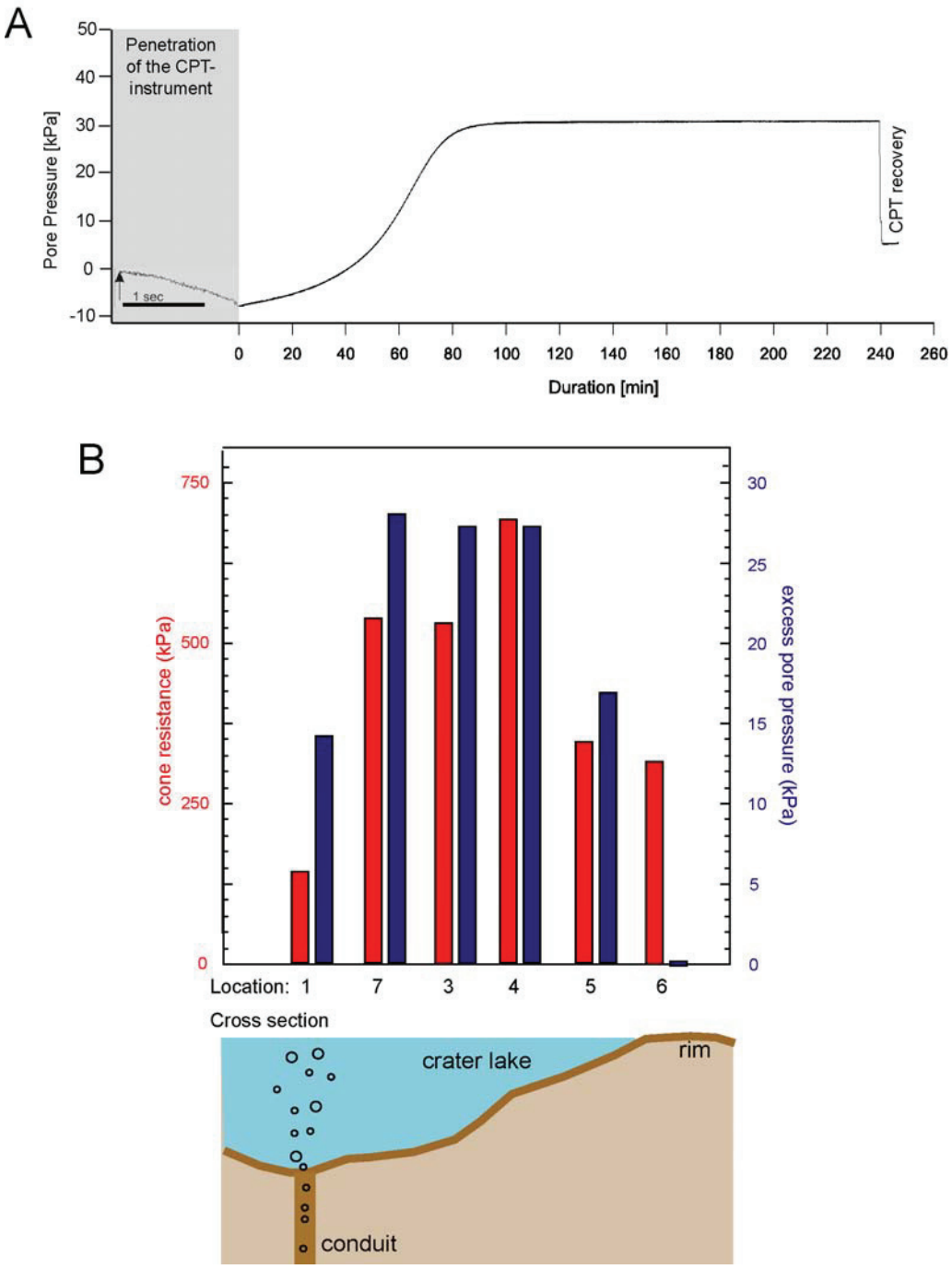

Fig. 5: CPT results showing cone resistance and pore pressure. (**A**) Pore pressure evolution during insertion (grey shading) and long-term at location #7 (see Fig. 3B). Arrow marks impact of instrument; (**B**) histogram of cone resistance upon insertion and excess pore pressure taken 30 mins. after deployment at each location. Note variable x-axis in (A) and different y-axes (left: cone resistance, right: excess pore pressure) in (B).

Older observations include a several 100 m-long, arcuate ridge of burnt and sintered, red mudstones along the southern margin of the central dome (see Figs. 1D, 3A-B). This feature is believed to have resulted from a violent, self-igniting eruption where methane-rich clayey paste produced frictional heat when ascending along a fault. The timing of this eruption, which stands in a line with the regular outbursts of Dashgil (6-37 yrs. recurrence time; Aliyev et al., 2002), is not known with any certainty, but occurred most likely not later than 1928 according to historical records.

DISCUSSION AND CONCLUSIONS

If we first regard our geomorphodynamic observations, it is noteworthy that the fault patterns we observe in the crestal area and around the mud cone are very similar to those shown by Cartwright et al. (2003; see their Fig. 6), Nicol et al. (2003; see their Fig. 1A), or Stuerold et al. (2003; see their Fig. 7A-B). These and other studies describe polygonal fault systems as connected, layer-bound normal faults with diverse fault strike, moderate throw, and a variably large coverage in map view. The faulting seems to occur predominantly in fine-grained sediments, which fail due to density-inversion of an overpressured unit sealed by finer material (see pioneering model by Henriet et al., 1989). These workers termed them "clay tectonic structures', and although they are found mostly at passive margins and in sedimentary basins, they exhibit a number of similarities to the emplacement of mud domes at convergent margins. These include (i) high clay mineral contents, (ii) *in situ* formation overpressures leading to density inversion and potentially liquefaction (Watterson et al., 2000), (iii) collapse after rapid fluid escape (Cartwright et al., 2003), and (iv) irregular patterns of fractures owing to extension and/or relaxation (Nicol et al., 2003). In addition to the parallels to polygonal faults, the geometry of our findings closely resembles that of hydraulic failure from analog experiments. Using a simple laboratory setup with pore water being forced through a large sediment cylinder by incrementally increasing the hydraulic head, geotechnical researchers have charged fine-grained granular media and observed a polygonal pattern of extensional fracturing (e.g. Wilhelm and Wilmanski, 2001; Mörz et al., 2007). In these experiments, the formation of small-scale (mm- to dm-diameter) sediment mounds occur at the sediment-water interface, but are immediately connected to permeable normal faults once the hydraulic gradient is risen. As soon as faulting becomes pervasive, the strike of the evolving features grows a random pattern. If the pressure gradient is increased further, the fault trace may actually start to migrate, and piping (i.e. the formation of mm- to cm-wide conduits for transfer of sediment and fluid) is also observed (see Mörz et al. [2007]

for details). Given the similarities of the Dashgil mud volcanic features and the polygonal fault patterns from the hydraulic failure experiments, we propose that stress conditions similar to those in areas of active polygonal faulting may have caused recent updoming and extensional fault formation due to subsurface overpressures. Taken the evidence of the highly active mud cone, the evolution of active polygonal fissures and small grabens around it (Fig. 1E, foreground), and recently formed cracks causing the crater-lake to overflow, we suspect a pressure build-up at depth. This inference is supported by transients in methane emission rates from long-term gas monitoring since 2003 (Delisle et al., 2005). During the observation period, a slow overall decrease in natural methane output has been recorded, which points towards an increasingly effective blockage of gas flow from depth. This progressive decrease in permeability of the conduit adds to the overall overpressure, as measured by the CPT probe (Fig. 5B). If we now relate the values to earlier work (e.g. in the Baltic Sea: Stegmann et al., 2006b; Seifert et al., in press), we find similarities in the drop to subhydrostatic pore pressures followed by a steady increase to excess pore pressures. While the first is typical for the displacement of fluids during CPT impact (Fig. 5A, grey shading), the latter demonstrates overpressuring (Fig. 5A, long-term curve). In addition, Stegmann et al. (2007) found an identical pore pressure response in overconsolidated glacial clays on a landslide-prone slope. At Dashgil MV, there is an increase in excess pore pressure from the slope to the actively degassing central portion of the crater-lake (i.e. from hydrostatic pressure to >100 kPa above P_{hyd}; Fig. 5B). Even at shallow sub-surface depths (ca. 100 cm penetration into mud of 2.2 g/cm^3 bulk density at location #7; Fig. 3C), P_{fluid} (28 kPa) ranges in the same order of magnitude as the geostatic stress (22 kPa). As a consequence, the stress conditions presently encountered on Dashgil MV suggest that a minor transient increase may push the system “over the cliff”, i.e. towards excess pore pressures which cannot be supported by the flexed, overflowing central area. Such an increase may either be triggered by an earthquake (see Mellors et al., 2007) or, more likely, by increasing buoyancy due to hindered gas flux (Delisle et al., 2005). Either way, the anticipated net result may be a self-igniting, violent eruption similar to the ones that caused the reddish sinter mud ridge south of the crater-lake (Fig. 3) and that were reported in 1902 and 1928 (Aliyev et al., 2002). Given the average recurrence intervals of 6-37 yrs., quiescence for almost 80 yrs. argues further for the likelihood of a violent eruption in the near future.

ACKNOWLEDGMENTS

The authors thank Matthias Lange (RCOM Bremen) for assisting with the *in situ* CPT measurements in Azerbaijan. BGR is acknowledged for providing funding for this study.

REFERENCES CITED

Abich, O.W.H., 1869. Mittheilungen über Erdbeben, vulcanische Erscheinungen (Schlammvulkane?) u.s.w. in den Caucasus-Ländern. *Mitth. k.-k. Geogr. Ges. Wien*, XII: 166-175

Abriutski, V., 1853. Eruption of mud volcanoes in the Taman Peninsula, in August 1853. *Gorn. Jurn*., 4: 271-277 (in Russian)

Aliyev, A.A., Guliyev, I.S., Belov, I.S., 2002. Catalogue of recorded eruptions of mud volcanoes of Azerbaijan for period of years 1810-2001. Nafta, Baku/Azerbaijan, 88 p.

Baciu, C., Etiope, G., 2005. Mud volcanism and seismicity in Romania. In: Martinelli, G., Panahi, B. (eds.), Mud volcanism, Geodynamics and Seismicity. *NATO Earth Env. Sci. Ser.,* 51: 77-88.

Brown, K.M., 1990. The nature and hydrogeologic significance of mud diapirs and diatremes for accretionary systems. *J. Geophys. Res.*, 95: 8969–8982.

Cartwright, J., James, D., Bolton, A., 2003. The genesis of polygonal fault systems: A review. *Geol. Soc. London, Spec. Publ.*, 216: 223-244.

Cooper, C., 2001. Mud volcanoes of Azerbaijan visualized using 3D seismic depth cubes: The importance of overpressured fluid and gas instead of non-existent diapers. *Proc. EAGE Conf. "Subsurface Sediment Mobilisation"*, Gent, Belgium (Sept. 2001): 71.

Davies, R.J., Swarbrick, R.E., Evans, R.J. and Huuse, M., 2007. Development of a pioneer mud volcano (East Java, May 2006): Implications for mud volcano system studies. *GSA Today*, 17/2: 4-9

Delisle G., Teschner M., Panahi B., Guliyev I., Aliev C., Faber E., 2005. On preliminary monitoring results of methane flux from the Dashgil mud volcano (Azerbaijan). *Proceedings of Azerbaijan National Academy of Sciences*, Earth Sciences Series, 4: 11-23.

Dercourt, J., Zonenshain, L.P., Ricou, L.E., Kazmin, V.G., Le Pichon, X., Knipper, A.L., Grandjaquet C., Sbortshikov, I.M., Geyssant, J., Lepvrier, C., Pechersky, D.H., Boulin, J., Sibuet, J.-C., Savostin, L.A., Sorokhtin, O., Westphal, M., Bazhenov, M.L., Lauer, J.P., Biju-Duval, B., 1986. Geological evolution of the Tethys belt from the Atlantic to the Pamirs since the Lias. *Tectonophysics* 123: 241-315

Geological Survey of India, 2005. http://www.gsi.gov.in/mudvol.htm

Guliyev, I.S., 1992. *A review of mud volcanism*. Azerbaijan Academy of Sciences, Inst. Geology, Report, 65pp, 1992.

Henriet, J.P., De Batist, M., Van Vaerenbergh, W., Verschuren, M., 1989. Seismic facies and clay tectonic features in the Southern North Sea. *Bull. Belgian Geol. Soc.,* 97: 457-472.

Higgins, G.E., Saunders, J.B., 1974. Mud volcanoes – Their nature and origin. *Verh. Naturf. Ges. Basel,* 84: 101–152.

Hovland, M., A. Hill, D. Stokes, (1997), The structure and geomorphology of the Dashgil mud volcano, Azerbaijan, *Geomorphology*, 21, 1-15.

Hubbert, M.K., Rubey, W.W., 1959. Role of fluid pressure in the mechanics of overthrust faulting. I: mechanics of fluid filled porous solids and its applications to overthrust faulting. *GSA Bulletin*, 70, 115-166.

Jakubov, A.A., Ali-Zade, A.A., Zeinalov, M.M., 1971. *Mud volcanoes of the Azerbaijan SSR*. Publishing house of the Academy of Sciences of the Azerbaijan SSR, Baku: 257 p.

Kopf, A.J., 2002. Significance of mud volcanism. *Reviews of Geophysics*, 40/2, 52 p. [DOI 10.1029/2000RG000093].

Lavrushin V.U., Polyak B.G., Prasolov R.M. and Kamenskii I.L. (1996) Sources of material in mud volcano products (based on isotopic, hydrochemical, and geological data). *Lith Min Resources*, 31/6:557-578

Lunne, T., Robertson, P.K., Powell, J.J.M., 1997. *Cone Penetration Testing in Geotechnical Practice*, Spon Press, 312 p.

Mellors, R, Kilb, D., Aliyev, A., Gasanov, A., and Yetirmishli, G., 2007. Correlations between earthquakes and large mud volcano eruptions. *J. Geophys. Res*., 112, B04304, doi:10.1029/2006JB004489, 11 p.

Nicol, A., Walsh, J.J., Watterson, J., Nell, P.A.R., Bretan, P., 2003. The geometry, growth, and linkage of faults within a polygonal faut system from South Australia. *Geol. Soc. London, Spec. Publ.*, 216:245-262.

Philip, H., Cisternas, A., Gvishiani, A., Gorshkov, A., 1989. The Caucasus: an actual example of the initial stages of continental collsion. *Tectonophysics*, 191: 1-21.

Seifert, A., Stegmann, S., Lange, M., Wever, T., Kopf, A., in press. *In situ* pore pressure evolution during FF-CPT measurements in soft sediments of the western Baltic Sea. *Geo-Marine Letters*.

Soloviev, V., Ginsburg, G.D., 1994. Formation of submarine gas hydrates. *Bull.Geol. Soc. Denmark*, 41: 86-94.

Stegmann, S., Villinger, H., Kopf, A., 2006a. Design of a modular, marine free-fall cone penetrometer. *Sea Technology*, 47/02, 27-33.

Stegmann, S., Moerz, T., Kopf, A., 2006b. Initial Results of a new Free Fall-Cone Penetrometer (FF-CPT) for geotechnical *in situ* characterisation of soft marine sediments. *Norwegian Journal of Geology*, 86/3: 199-208.

Stegmann, S., Strasser, M., Anselmetti, F.S., Kopf, A., 2007. Geotechnical *in situ* characterisation of subaquatic slopes: The role of pore pressure transients versus frictional strength in landslide initiation. *Geophysical Research Letts.*, 34/7, doi:10.1029/2006GL029122.

Stuevold, L.M., Faerseth, R.B., Arnsen, L., Cartwright, J., Moeller, N., 2003. Polygonal faults in the Ormen Lange field, More Basin, offshore Mid Norway. *Geol. Soc. London, Spec. Publ.*, 216: 263-282.

Watterson, J., Walsh, J.J., Nicol, A., Nell, P.A.R., Bretan, P.G., 2000. Geometry and origin of a polygonal fault system. *J. Geol. Soc. London,* 157: 151-162.

Wilhelm, T., Wilmanski, K., 2001. On the onset of flow instabilities in granular media due to porosity inhomogeneities. *Int. Journal of Multiphase Flow*, 28: 1929-1944.

6. Conclusions

During this study, a marine cone penetrometer system, containing a shallow-water (200 m max. depth) and deep-water probe (4000 m max. depth), was developed for geotechnical sediment characterisation. It was deployed 338-times in a variety of operation modes, configurations, and geological settings. When compiling overarching similarities from the two blocks of manuscripts (five on CPT performance, five on its geological application) presented as main portion of this dissertation, a number of conclusions can be drawn. They are summarised below as a series of bullets:

- Both instruments, the SW-probe more than the DW-probe, were designed to provide the user with maximum flexibility concerning operations. First of all, either CPT probe can be deployed at very low rates to free drop (i.e. several hundred cm/s). With a custom-built adapter, the SW-CPT was even used on a hydraulic stamp to perform pushed "standard" CPT tests (2 cm/s) for reconnaissance purposes (see Chapter 4.3). Both instruments are also fully self-contained so that long-term deployments with the lance on a buoy or mooring can easily be carried out (as done in Lake Lucerne or the Ligurian margin, where the probe stayed in the sediment overnight for pore pressure dissipation while the ship went elsewhere). Other features handy for the user are the modular weight sets and cable-bearing extension rods realised in the SW-instrument. Depending on the anticipated sediment stiffness and penetration depth, weights and/or rods may be added. Also, the length can be tailored to the vessel's specifications; in Lake Lucerne, we once used 5 extension rods since the length of the small aluminium boat was only 6 m (see Chapter 3.1, Fig. 1). In deed, the design of the RCOM probes does not restrict the user by any means since the SW-CPT was used from vessel's of all sizes, from bridges (in streams and rivers), from the pier (harbours), or from improvised constructions in onshore settings (e.g. mud volcano crater-lake; see Chapter 5.5, Figs. 1 and 2).
- In case of the SW-FF-CPT, a comprehensive study comparing pushed constant rate test results with dynamic ones carried out at a range of winch speeds typical for research vessels gained overwhelming reproducibility and consistency (see Chapter 4.3). In fact, strain-rate effects could be shown to largely follow an earlier relationship postulated by Dayal and Allen (1975). Also, we could reconfirm that dynamic deployments give higher readings for f_s, q_c, and - to a lesser extent - u when compared to pushed 2 cm/s deployments; this was also observed recently by Stoll et al. (2007).

- Another conclusion to be drawn from the velocity-controlled dynamic versus pushed quasi-static CPT experiments is the whole suit of data is indicative of an undrained sediment response. This is certainly obvious for the faster tests (17 cm/s to free drop; see individual papers above), but also applies to the constant rate deployments at 2cm/s. This finding is in line with a study by Campanella et al. (1982) who proposed that penetration is essentially undrained down to rates as low as 2 mm/s.
- The results from dynamic CPT deployments may also be used for a first order soil classification. In two of the studies, we applied existing classification methods and validated them by coring. In sediments studied near Bremen, the model relying in the friction ratio F (see Douglas and Olsen 1981) provided good agreement with ground-truthing using gravity cores (see Chapter 4.2). Similarly, the method plotting pore pressure versus q_c (Vermeulen and Rust 1995) gave excellent agreement for the fine-grained sediments in the Baltic Sea (see Chapter 5.4). It can hence be deduced that dynamic CPT tests are, at least within the range of deployment rates tested, a suitable method to classify sediments following those methods.
- When reviewing the observations in the various geological settings, it is astonishing that the wealth of data collected can be subdivided into three typical pore pressure responses. Type I occurs in granular, normally consolidated material where a pore pressure spike upon impact is followed by an exponential decay back to ambient values. In contrast, Type II exhibits a negative (i.e. sub-hydrostatic) pressure spike followed by an increase to ambient pore pressure values. The sub-hydrostatic signal is caused by displacement of pore fluid by the profiling CPT probe, usually only found in highly permeable, coarse-grained deposits. Type III signals generally show supra-hydrostatic pressures upon impact and during profiling, but then approach even higher pressures versus time. Graphs like this are found in sediments of variable grain size distribution, are related to fluid overpressures, and are found in the majority of the geological settings studied in this thesis: Lake Lucerne, Baltic and Cretan Seas, or Azerbaijan.
- In Lake Lucerne, Switzerland, landslide events on the subaquatic slopes have been related to earthquake tremor. Our *in situ* CPT profiling attests that glacial clays beneath a Holocene cover show excess pore pressures up to 70 kPa and likely require only a minor trigger event to exceed their stability field (Chapters 5.1, 5.2). The findings from this thesis were condensed into two manuscripts and a conceptual model for the effective stress state at such slopes. This model was adopted for ocean margin landslide failure in EQ-prone

areas, and already got incorporated into the recently compiled white paper on "Deep Sea-Floor Frontiers" by the European Community.

- As in Lake Lucerne, Type III pore pressure responses were seen in fine-grained muds in the Baltic Sea (Chapter 5.4). Measured excess pore pressure may rise up to 40 kPa, however, the reason for those excursions is microbial rather than tectonic. With CPT profiling, it was easily possible to identify the areas where gas-rich, overpressured sediment is encountered.
- Even more remarkable are recent observations from a CPT study in an active mud volcano in Azerbaijan, located close to the Caspian Sea coastline. Here, Type III pore pressure graphs look similar to those in the earlier deployments. However, Δu is exceeding ~30 kPa in the central part of the crest where methane-rich mud is expelled through the clays. In contrast, q_c drops by a factor of 3 in the vicinity of the mud volcano conduit.
- From the 50 CPT deployments carried out at the landslide-prone Ligurian slope, Western Mediterranean Sea, a first glance at the raw data suggests again excess pore water pressures. Of particular interest are groundwater-charged coarse-grained sediments in which both short-term profiles and mid-term tests were recorded. These data will illuminate an alternative trigger mechanism for slope instability in the near future.
- In summary, the learning experience when developing and utilising this first RCOM penetrometer system shows promising, reproducible and geologically interesting results. Refinements are underway, and some experience gathered may be beneficially extended towards equipping the seafloor-based drill MeBo with a CPT probe.

7. Supplementary Material

7.1. List of FF-CPT deployments

Date	Location	Tool	Number of Profiles	Kind of Test	Platform	Geological Background	Test	Processing & Interpretating
09.05.05	Kuhgraben	SW	1	cable-lowered, midterm test	Bridge	Instrument test	x	x
10.05.05	Kuhgraben	SW	1	free-drop, longterm test	Bridge	Instrument test	x	x
13.05.05	Bremerhaven / Harbour	SW	1	winch-controlled, longterm test	Pier	Investigation of muddy sediments, Instrument test	x	x
20.05.05	Kuhgraben	SW	1	cable-controlled, longterm tests	Bridge	Instrument test	x	x
24.05.05	Kuhgraben	SW	1	cable-controlled, longterm tests	Bridge	Instrument test	x	x
26.05.05	Lake Hemelingen	SW	5	velocity-controlled, short- and longterm tests with variable weights	Pier, Pontoon	Instrument test	x	x
07.06.05	Kuhgraben	SW	2	free-drop and winch-controlled, shortterm tests	Bridge	Instrument test	x	x
09.06.05	Bremerhaven / Harbour	SW	1	winch-controlled, longterm test	Pier	Investigation of muddy sediments, Instrument test	x	x
17.06. 05	Lake Hemelingen	SW	1	pushed, longterm test	Pier, Pontoon	Instrument test	x	x
21.06.05	Wilhemshaven / Harbour	DW	1	winch-controlled, longterm test	Pier	Investigation of muddy sediments, Instrument test	x	x
13.07.05	Wilhemshaven / Harbour	SW	2	winch-controlled, longterm test	Pier	Investigation of muddy sediments, Instrument test	x	x
01.08.05	Kuhgraben	SW	4	cable-controlled, midterm test with different velocities	Bridge	Instrument test	x	x
13.08.05	Kuhgraben	SW	4	winch-lowered, shortterm tests with variable weight	Bridge	Instrument test	x	x
20.09.05	Bremerhaven / Harbour	SW	2	free-drop and winch-lowered, midterm tests	Pontoon	Investigation of muddy sediments, Instrument test	x	x
03.10.05	Kuhgraben	SW	1	winch-controlled test	Bridge	Instruments test	x	x
06.-08.10.05	Lake Lucerne	SW	6	winch-controlled, stepwise-testing, short- and longterm tests	Float	Slope Stability	x	x
09.-10.11. 05	North Sea / Helgoland	SW	13	winch-controlled, mid- and longterm tests	RV Planet	Investigation of gassy sediments	x	x
20.12. 05	M66/4b Continental Slope Chile	DW	7	winch-controlled, midterm tests	RV Meteor	Slope Stability	x	x
18.01. 05	Kuhgraben	SW	1	cable-controlled, midterm test	Bridge	Instrument test	x	x

24.-26.01.06	Baltic Sea	SW	49	winch-controlled, short- to longterm tests	RV Kronsort	Investigation of gassy sediments		partly
10.-17.03.06	Baltic Sea / Mecklenburg Bay	SW	96	winch-controlled, short- to longterm tests	RV Planet	Investigation of gassy sediments	x	
		DW	2				x	
03-16.05.06	POS 336 / Cretan Sea	DW	40	winch-controlled, short- to midterm tests	RV Poseidon	Slope Stability	x	x
		SW	5				x	x
19.01.07	Kuhgraben	SW	1	cable-controlled, midterm test	Bridge	Instrument test	x	x
16./17.02.07	Azerbaijan / Mud Volcano	SW	7	free-drop, cable-controlled, longterm test	Wire-rope	Pore pressure regime in mud volcano		x
01.03.07	Lake Hemelingen	SW	13	velocity-controlled short- to longterm tests	Pier	Instrument test	x	x
		DW	4				x	x
09.03.07	Lake Hemelingen	SW	12	velocity-controlled short- to longterm tests	Pier	Instrument test	x	x
		DW	4				x	x
15.03.07	Lake Hemelingen	SW	15	velocity-controlled short- to longterm tests	Pier	Instrument test	x	x
		DW	4				x	x
23.03.07	Kuhgraben	SW	1	cable-controlled, midterm test	Bridge	Instrument test	x	x
29.03.07	Lake Hemelingen	SW	20	velocity-controlled short- to longterm tests	Pier	Instrument test	x	x
		DW	4				x	x
29.06.07	Lake Hemelingen	SW	1	pushed, shortterm test Test	Pontoon	Instrument test	x	x
21.07.-30.07.07	M73/1 Ligurian Sea	SW	16	winch-controlled, mid- and longterm tests	RV Meteor	Slope Stability	x	x
		DW	7				x	x
31.07.-30.07.07	M73/1 Ligurian Sea	SW	25	winch-controlled, mid- and longterm tests	RV Meteor	Slope Stability		x
		DW	2					x

7.2. Role of candidate

Sea Technology journal article (revised by editor)

This article summarises the concept and design of the shallow-water FF-CPT developed during the course of my Ph.D. project at RCOM Bremen. It exemplifies some of the advantages in cone penetration testing at variable rate using geological data, but otherwise focuses on introducing the instrument to a broader, technically oriented community. I assisted in designing the SW-instrument and did a lot of research to select sensors, etc. I have further acquired all the data presented in this paper, processed them, and then wrote the manuscript.

IGCP Submarine Landslides (Kluwer) book chapter (peer-reviewed)

As an analogue to the *Sea Technology* article, this short paper mainly serves to introduce the design of the deep-water FF-CPT developed during year 2 of my Ph.D. project. The paper, presented at the second IGCP Submarine landslides conference (Santorini/Greece, Sept. 2007), is part of a two-part publication on initial CPT results from Poseidon cruise Pos336 in the Cretan Sea, Greece. I have helped with the design and construction of the DW-instrument

and carried out all the initial testing (on RV *Meteor* M66/4b off Chile). Pos336 with an improved version of the DW-FF-CPT delivered the first reliable data set, which partly went into the generic paper (Ch. 3.2), partly dwelled on geological data and interpretation (Ch. 5.3). I wrote both papers jointly with Achim Kopf.

EuroGoos book chapter (peer-reviewed)

This article summarises some of our initial data collected with the SW-FF-CPT at the ports of Bremerhaven, Wilhelmshaven, and a small stream called Kuhgraben near Bremen. All testing and data processing were carried out by myself. I also presented a poster at the 5th EuroGOOS conference, Brest/France (June 2005) and wrote the summary article for the conference proceedings, which were published as a book chapter.

Norwegian Journal of Geology journal article (peer-reviewed)

This manuscript represents the second set of data with the SW-FF-instrument, which also serves as a "proof-of-concept". The paper was presented at the IGCP meeting at Oslo in September 2005, and was then condensed into an article in the Norwegian Journal of Geology, where it got published in 2006. In addition to the earlier manuscript in the EuroGOOS book, it adds systematic data when varying the weight and length of the instrument, and also contains data from deployments in the Baltic Sea and Lake Hemelingen. I carried out the majority of the deployments and all the data processing and wrote the manuscript, which was seconded by two co-authors.

Canadian Geotechnical Journal journal article (under peer-review)

This article presents one of the key papers in my thesis. It consists of a comprehensive literature review on CPT testing and further incorporates the biggest data set acquired in one location. It compares data from 32 velocity-controlled free-fall tests and 6 constant rate tests (pushed at a standard 2 cm/s) at Lake Hemelingen and tries to outline the pros and cons of our instrument and testing procedure. I compiled the testing strategy (which also included DW-FF-CPT tests, which are so far unpublished), carried out all of the experiments and data processing afterwards, and condensed everything into a long manuscript. This work is currently under review.

Geophysical Research Letters journal article (peer-reviewed)

This article is part of a bigger campaign conducted at Lake Lucerne, Switzerland. It focuses on SW cone penetration tests in a step-like fashion to study pore pressure dissipation at various depth levels. Results gain insight into different states of consolidation of the landslide-prone slope sediments. I conducted all the tests and data processing, and developed a model how the effective stress patterns observed in Lake Lucerne may be adopted to marine continental slopes. The manuscript was written by myself and got immediately published in *GRL* early in 2007.

Marine Geology journal article (peer reviewed)

In a second article, which was recently printed in *Marine Geology*, the Lake Lucerne working group tried to sketch the bigger picture of the earthquake-induced landslides in the area. The article led by Michi Strasser summarises *in situ* as well as laboratory data and ties it to regional and historical geology. My contribution was to supply the CPT data and write and revise part of the manuscript text, as is reflected by the second author position.

IGCP Submarine landslides (Kluwer) book chapter (peer-reviewed)

This paper is the second part of the Cretan Sea results, concentrating on the geological application of the CPT in a small-scale landslide deposit off NW Crete. I participated in the cruise, carried out the deployments and data processing, and assisted in writing the manuscript text. My contribution is acknowledged by the second author position.

Marine and Petroleum Geology journal article (under peer-review)

In a joint project between RCOM Bremen, Bundesanstalt für Geowissenschaften und Rohstoffe (BGR) Hannover and the Academy of Sciences in Baku, Azerbaijan, Dashgil mud volcano is currently instrumented with long-term pore pressure and gas flux instruments. In a pilot study, Achim Kopf and Matthias Lange collected SW-FF-CPT data along a transect through the crater lake of the active dome. My contribution was the data processing, interpretation, and help with the manuscript text submitted to *Marine and Petroleum Geology*.

Geo-Marine Letters journal article (under peer-review)

The manuscript presently being revised by the first author Annedore Seifert aims to identify characteristic pore pressure signals in gas-charged versus normal soft marine mud in the Baltic Sea. Data were collected on three campaigns on three cruises on German navy vessels *Kronsort* (1) and *Planet* (2). I participated in two of the three cruises and helped with data processing, interpretation and preparing the text.

In addition to the abovementioned papers, I contributed to two cruise reports on expeditions carried out by RCOM Bremen. Both cruises were largely focusing on sub-project C8, which is dedicated to study the stability of ocean margin slopes. I also participated in the two cruises in question: Pos 336 on RV *Poseidon* in the Cretan Sea, Eastern Mediterranean (April/May 2006), and M73/1 on RV *Meteor* at the Ligurian Margin, Western Mediterranean. Both cruises were making use of Cone Penetration Testing with both the SW- and DW free-fall instrument.

Kopf, A., Alves, T., Heesemann, B., Kaul., N.E., Kock, I., Krastel, S., Reichelt, M., Schäfer, R., Stegmann, S., Strasser, M., Thölen, M., 2006. REPORT AND PRELIMINARY RESULTS OF POSEIDON CRUISE Pos336: CRESTS - Cretan Sea Tectonics and Sedimentation. *Berichte aus dem Fachbereich Geowissenschaften der Univ. Bremen,* No. 253: 140pp.

Kopf, A., Alexandrakis, E.C.C., Blees, J., Bogus, K., Dennielou, B., Förster, A., Girault, F.E., Haarmann, T., Hanff, H., Hentscher, M., Kaul., N.E., Klar, S., Krastel, S., Lange, M., Meier, M.-A., Metzen, J.F., Spiess, V., Stegmann, S., Strozyk., F., Volen Krumova, T., 2007. REPORT AND PRELIMINARY RESULTS OF METEOR CRUISE M73/1: LIMA-LAMO *(Ligurian Margin Landslide Measurements & Observatory)*, in preparation.

8. Literature (not cited in manuscripts)

Baligh, M.M. 1985. The strain path methods. Journal of the Geotechnical Engineering, ASCE, 111, 9, 1108-1136.

Baligh, M.M. 1986a. Undrained deep penetration, I: shear stress. Geotechnique, 36, 4, 471-458.

Baligh, M.M. 1986b. Undrained deep penetration, II: pore pressures. Geotechnique, 36, 4, 487-501.

Baltzer, A., Cochonat, P., and Piper, D.J.W., 1994. *In situ* geotechnical characterization of sediments on the Nova Scotian Slope, eastern Canadian continental margin. Marine Geology, 120, 291-308.

Becker, K., Fisher, A.T., and Davis, E.E., 1997. The CORK experiment in hole 949C: Long-term observations of pressure and temperature in the Barbados accretionary prism, in T.H. Shipley et al., Proc. ODP, Sci. Results, 156, 247-252.

Bennett, R.H., Li, H, Valent, P.J., Lipkin, J., and Esrig, M.I., 1985. In-Situ Undrained Shear Strengths and Permiabilities Derived from Piezometer Measurements. Strength Testing of Marine Sediments: Laboratory and In-Situ Measurements, ASTM STP 883, Chany, R.C., and Demars, K.R., (Ed.), American Society for Testing and Materials, Philadelphia, 83-100.

Bishop, R.F., Hill, R., and Mott, N.F., 1945. "The theory of indentation and hardness tests.", Proc. Phys. Soc., 57, 147-159.

Burns, P.E., and Mayne, P.W., 1998a. Penetrometers for Soil Permeability and Chemical Detection. Report No. GIT-CEEGEO-98-1, July 1998, School of Environmental Engineering, Georgia Institute of Technology, 144.

Burns, S.E., and Mayne, P.W. 1998b. Monotonic and dilatory pore-pressure decay during piezocone test in clay. Canadian Geotechnical Journal, 35, 1063-1073.

Burns, S.E., and Mayne, P., 2002. Analytical Cavity Expansion-Critical State Model for Piezocone Dissipation in Fine-Grained Soils. Soils and Foundation, 42, 2, 131-137.

Campanella, R.G., Gillespie, D., and Robertson, P.K., 1982. Pore pressure during cone penetration testing. *Procs. 2nd European Symposium on Penetration Testing*, ESOPT-II, Amsterdam (Balkema Pub.) 1, 507-512.

Chari, T.R., and Abdel-Gawad, S.M., 1981. Static Penetration resistance of Soils. In: POAC 81: The 6th International Conference on Port and Ocean Engineering under Arctic Conditions, Quebec, Canada, July 27-31, 1981: Proceedings, 1981, 2, 717-725.

Dayal, U., Allen, J.H., and Jones, J.M., 1973. Marine Impact Cone Penetrometer. Proc. Conf. Int. Ocean '73, Düsseldorf, West Germany, 912-923.

Dayal, U., 1978. Recent Trends in Underwater In-Situ Soil Testing. IEEE Journal of Oceanic Engineering, OE-3, 4, 176-186.

Douglas, B.J., and Olsen, R.S., 1981. Soil classification using electric cone penetrometer. American Society of Civil Engineers (ASCE). Proceedings of Seminar on Cone Penetration Testing and Experience, St.Louis, 209-227.

Fang, W.W., Langseth, M.G., and Schultheiss, P.J., 1993. Analysis and Application of in Situ Pore Pressure Measurements in Marine Sediments, Journal of Geophysical Research, 98, 5, 7921-7938.

Ferguson, G.H., McClelland, B., and Bell, W.D, 1977. Seafloor cone penetrometer for deep penetration measurements of ocean sediment strength. In: Proc. 9th Offshore Technological Conf. OTC 2787, 471-480.

Hampton, M.A., and Lee, J.L., 1996. Submarine Landslides. Review of Geophysics, 34, 1, 33-59.

Hubbert, M.K., and Rubey, W.W., 1959. Role of Fluid Pressure in Mechanics of Overthrusting Faulting, I. Mechanics of Fluid-Filled Porous Solids And Its Application To Overthrust Faulting, Bulletin of the Geological Society of America, 70, 115-166.

Jeng, D.-S., and Cha, D.H., 2003. Effects of dynamic soil behaviour on the wave-induced pore pressure and effective stresses in porous seabed. Ocean Engineering, 30, 2065-2089.

Kim, D.-K. and Tumay, M.T., 2004, Miniature Piezocone Test Results in Cohesive Soils. The Electronical Journal of Geotechnical Engineering, 9/E, Ppr0441.

Kiousis, P.D., Vayiadjis, G.Z., and Tumay, M.T., 1988. A Large Strain Theory and its Application on the Analysis of the Cone Penetration Mechanism. International Journal for Numerical and Analytical Methods in Geomechanics, 12, 45-60.

Kleven, A., Lacasse, S., and Anderson, K.H., 1986. Soil parameters for offshore foundation design. N61 Report No. 40013-34, dated 9 April 1986.

Kjestad, O., Lunne, T., and Clausen, C.J.F., 1978. Comparison between *in situ* resistance and loboratory strength for overconsolidated North Sea clays. Marine Geotechnology, 3, 1, 23-36.

Lunne, T., Robertson, P.K., and Powell, J.J.M., 1997. Cone Penetration Testing in Geotechnical Practice, Spon Press, London, 312.

Mahmoud, M., Woeller, D., and Robertson, P.K., 2000. Detection of shear zones in a natural clay slope using the cone penetration test and continuous dynamic sampling. Canadian Geotechnical Journal, 37, 3, 652-661.

Maltman, A. (editor). 1994. The Geological Deformation of Sediments. Chapman & Hall, London, pp.363.

Meyerhoff, G.G., 1961. The ultimate bearing capacity of wedge-shaped foundations. Proc. 5th ICSMFE; Moscow, 2, 103-109.

Mienert, J., 2004. COSTA—continental slope stability: major aims and topics. Marine Geology 213, 1–7.

Mitchell, J.K, and Durgunoglu, H.T, 1973. In situ strength of static cone penetration test. Proc 8th ICSMFE, Moscow, 1, 279-286.

Moore, J.C., and Vrolijk, P.J., 1992. Fluids in accretionary prisms. Rev. Geophys., 30, 113-135.

Randolph, M.F., Carter, J.P., and Wroth, C.P., 1979. Driven Piles in Clay – The Effects of Installation and Subsequent Consolidation, Geotechnique, 29, 4, 361-393.

Roy, M., Tremblay, M., Tavenas, F., and La Rochelle, P., 1980. Induced pore pressures in static penetration tests in sensitive clays. Procs. of the 33rd Canadian Geotechnical Conference, Calgary, 11.3.1 – 11.3.13.

Ruiter, J.D., and Fox, D.A., 1975. Site investigation for North Sea forties fold, Proc. 7th Offshore Technological Conference, OTC 2246, 21-36.

Salgado, R., Mitchell, J.K., and Jamiolkowski, M., 1997. Cavity expansion and penetration resistance in sand. Journal of Geotechnical and Geoenvironmental Engineering, 123, 344-354.

Sanglerat, G., 1972. The penetrometer and soil exploration, Elsevier, Amsterdam, 464.

Schultheiss, P.J., 1990. Pore Pressures in Marine Sediments: An Overview of Measurement Techniques and Some Geological Engineering Applications. Marine Geophysical Researches, 12, 153-168.

Silva, M.F., White, D.J., and Bolton, M.D., 2006. An analytical study of the effect of penetration rate on piezocone tests in clay. International Journal for Numerical and Analytical Methods in Geomechanics, 30, 501-527.

Song, C.R., Voyiadjis, G.Z., and Tumay, M.T., 1999. Determination of permeability of soil using the multiple piezo-element penetrometer. International Journal for Numerical and Analytical Methods in Geomechanics, 23, 1609-1629.

Song, C.R., and Voyiadjis, G.Z., 2005. Pore pressure response of saturated soils around a enetrating object. Computers and Geotechnics, 32, 37-46.

Stegmann, S., Strasser, Michael, Anselmetti, F., and Kopf, A., 2006. Geophys. Res. Lett., 34, L07607, doi:10.1029/2006GL029122.

Strout, J..M., and Tjelta, T.I., 2005. In situ pore pressure: What is their significance and how can they be reliably measured. Marine and Petroleum Geology, 22, 275-285.

Sully, J.P., Robertson, P.K., Campanella, R.G., and D.J. Woeller, 1999. Canadian Geotechnical Journal, 36, 369-381.

Sultan, N., Gaudin, M., Berne, S., Canals, M., Urgeles, R., and Lafuerza, S. 2007a. Analysis of slope failure in submarine canyon heads: An example from the Gulf of Lions. Journal of Geophysical Research, 112, F01009, doi: 10.1029/2005JF000408.

Sultan, N., Voisset, M., Marsset, B., Marsset, T., Cauquil, E., and Colliat, J.-L., 2007b. Potential role of compressional structures in generating submarine slope failures in the Niger Delta. Marine Geology, 237(3-4), 169-190, doi: 10.1016/j.margeo.2006.11.002.

Teh, C.I., and Houlsby, G.T., 1991. An analytical study of the cone penetration test in clay. Geotechnique, 41/1, 17-34.

Terzaghi, K., 1946. Theoretical Soil Mechanics, John Wiley & Sons, Inc., New York, 510.

Vermeulen N, Rust, E., 1995. CPTU profiling: A numerical method. In: Proc Int Symp Cone Penetration Testing, CPT 95, 4-5 October 1995, Linköping, Sweden. Swedish Geotechnical Institute, SGI, Report 3:95, vol. 2, pp 343-350.

Yu, H.S, and Mitchell, J.K, 1998. Analysis of Cone Resistance: Review of Methods. Journal of Geotechnical and Geoenvironemntal Engineering, 124, 140-149.

Yu, H.S., Herrmann, L.R., and Boulanger, R.W., 2000. Analysis of steady Cone Penetration in Clay. Journal of Geotechnical and Geoenvironmental Engineering, 127, 7, 594-604.

Acknowledgments - Danksagung

Zum Gelingen meiner Arbeit haben eine Vielzahl von Personen beigetragen, denen ich an dieser Stelle ein aufrichtiges Dankeschön sagen möchte.

CPT-TEAM

Achim Kopf gab mir die Möglichkeit, an seiner Idee, eine marine Frei-Fall-Lanze zu konstruieren, im Rahmen meiner Dissertation mitzuwirken. Für diese spannende, vielseitige und abwechslungsreiche Aufgabe möchte ich mich, ebenso für zahlreiche lebendige und kreative Diskussionen bedanken, die mir verschiedenste geologische und wissenschaftliche Einblicke schenkten.

Matthias Lange möchte ich für die Umsetzung der wissenschaftlichen Ideen in Hardware mit innovativen und improvisierten Lösungen bedanken. Besonders wertvoll war für mich seine ständige über die normale Arbeitszeit hinausreichende Hilfestellung und die Versorgung mit leckerem Kuchen in intensiven Arbeitsphasen.

GUTACHTER

Ich möchte mich bei Tobias Mörz und Heinrich Villinger für die Begutachtung meiner Dissertation sowie für manche kritische Impulse bedanken.

ARBEITSGRUPPE

Ein herzliches Dankeschön an meine Zimmergenossin Anne Seifert für das wohltuende Zusammensein, für die zahlreichen Diskussionen und das gemeinsame Zähneausbeissen an CPT-Daten und anderen geotechnischen Rätseln.

Ein großer Dank gilt auch Hendrik Hanff und Wolfgang Schunn für die Unterstützung bei der Wartung der Geräte und Hilfe bei diversen Messeinsätzen.

Annika Förster gebührt mein Dank für die Unterstützung in zeitaufwendiger Laborarbeit, sowie Tobias Mörz und Stefan Kreiter für die Assistenz bei Ödometer-Tests.

MARUM-CLAN

Ein herzliches Dankeschön möchte ich der MARUM-Arbeitsgruppe aussprechen, deren HiWi-Jobs mich während meines Studiums an marine Technologien herangeführt haben.

RETTER

Thorsten Klein, ein großes Dankeschön für den Software-Support und für die schnelle und effektive Rettungsaktion der Daten meiner Festplatte, die in der finalen Phase dieser Arbeit das Zeitliche gesegnet hatte.

Weiteren Rettern soll gedankt werden. In einer kühnen Tauchaktion haben Bela Buck, Alex Schröder, Susanne Spahic, Markus Geisen (AWI) den beim Hieven abgebrochenen vorderen Teil der Flachwasser-Lanze aus den schlickigen Tiefen des Hafenbeckens in Bremerhaven geborgen.

ZUSAMMENARBEIT

Ein großer Dank gilt Wilfried Conrades und seinem Team (Atlas Elektronik), das uns die Infrastruktur (Kran, hydraulischer Stempel, Ponton) für zahlreiche CPT-Tests im Hemelinger See (Bremen) bereitwillig zur Verfügung stellten und mich in mehrtägigen CPT-Tests mit wertvollem Arbeitseinsatz unterstützen.

Ebenso möchte ich mich bei Thomas Wever (FWG) bedanken, der uns immer wieder auf der *FS Planet* die Möglichkeit gab, unsere Geräte einzusetzen, sowie in diversen Diskussionen konstruktive Impulse gab.

Ich möchte mich bei Flavio Anselmetti und Michi Strasser für die äußerst unkomplizierte und angenehme Zusammenarbeit mit der ETH Zürich bedanken.

Dank auch allen Kapitänen und Schiffsbesatzungen, die mir mit den CPTs auf *Meteor* und *Poseidon* hilfreich zur Seite standen.

FREUNDE

Meinen Eltern und meiner Oma, die immer mit großem Interesse meine Arbeit verfolgt haben und die mir Neugier lehrten.

Für meine Schwester Rike und all meine Freunde, die es mir verziehen haben, wenn ich dann & wann in geologische Welten abgetaucht bin und für eine Weile nicht mehr gesehen ward.

Mein inniger Dank gilt Achim, der mir mit großem Vertrauen die Möglichkeit gab, an der Sache zu wachsen und Grenzen zu verschieben.

Le FIN

Erklärung

Hiermit versichere ich, dass ich

1. **die Arbeit ohne unerlaubte fremde Hilfe angefertigt habe,**

2. **keine anderen als die von mir angegebenen Quellen und Hilfsmittel benutzt habe und**

3. **die den benutzten Werken wörtlich oder inhaltlich entnommenen Stellen als solche kenntlich gemacht habe.**

Bremen, im September 2007

(Sylvia Stegmann)